2015

Developing composite membranes for desalination

Ahmed Ali Alshahrani
University of Wollongong

UNIVERSITY OF WOLLONGONG

Developing Composite Membranes for Desalination

A thesis submitted in fulfilment of the requirements for the degree of

Doctor of Philosophy

From

University of Wollongong

By

Ahmed Ali Alshahrani

Faculty of Science, Medicine and Health

January 2015

Certification

I, Ahmed Ali Al Shahrani, declare that this thesis, submitted in fulfilment of the requirements for the degree of Doctor of Philosophy, in the School of Chemistry, University of Wollongong, is wholly my own work unless otherwise referenced or acknowledged. This document has not been submitted for qualifications at any other academic institution.

Ahmed Ali Al Shahrani

January 2015

ABSTRACT

The survival of living things largely depends on unpolluted pure and palatable water. A major portion (about 97.5%) of Earth is covered with oceans containing mostly saline water, with the remaining 2.5% comprising fresh water. Unfortunately, fresh water is being depleted from these sources with the growth of the world's population, enormous climate changes and contamination by agricultural and industrial effluents. As a result, people are constantly in search of fresh water sources. Many physical-chemical methods have been developed, such as chemical and heat treatments, to obtain fresh water. Sadly, these methods are typically uneconomical, time-consuming and environmentally hazardous or unfriendly. However, one of these techniques, the filtration of ocean water through membranes of different types, shows promise as a sustainable method. The present work focuses on developing a suitable chemical membrane with carbon nanotubes (CNT) incorporating chitosan surfactants and other dispersant additives. Such a CNT membrane (buckypaper [BP]) could be used in the desalination process because it has a uniquely high internal mechanical strength, thermal stability, uniform pore distribution and is easily handled.

In this study, CNT buckypaper membranes were successfully fabricated by a vacuum-filtration method using well-dispersed multi-walled (MWNTs) CNTs and carboxyl functionalised multi-walled carbon nanotubes (MWNT-COOH and MWNT-NH_2) MWNTs in the presence of different surfactants, such as chitosan (both non-functionalised and functionalised) and Triton X-100 (Trix). The optimal sonification time, stability and homogeneity of different CNTs (i.e. MWNT, MWNT-COOH and MWNT-NH_2) dispersion solutions were first evaluated. The synthesised CNT BP membrane was then characterised using different tools. The functionalised MWNT-COOH and MWNT-NH_2 membranes were highly dispersed in solution but possessed relatively decreased electric conductivity (7 ± 1 S/cm and 1 ± 0.3 S/cm respectively) compared to that of the BP membrane made with unfunctionalised MWNTs (70 ± 1 S/cm). Improved mechanical properties were obtained with the BP membranes prepared with unfunctionalised and functionalised MWNTs in the presence of chitosan and crosslinked chitosan. The value of these properties of the BP membranes significantly decreased when Trix dispersant was used instead of chitosan and crosslinked chitosan. Moreover, scanning electron microscope (SEM) and Brunauer-Emmett-Teller (BET) analysis showed that the surface morphologies, internal pore structures and porosities of several BP membranes were improved when both unfunctionalised and

functionalised MWNTs were used with a low concentration of chitosan 0.1% (w/v) and Trix (range 114 ± 2 m^2/g and 89 ± 6 m^2/g). The value of these properties decreased when a concentration of chitosan > 0.1% (w/v) and crosslinked chitosan were used (range 0.07 ± 0.01 m^2/g and 45 ± 5 m^2/g). Water permeability and salt-rejection capacity of the synthesised BP membranes were investigated using laboratory-scale tests with crossflow-cell and dead-end stirred-cell filtration techniques. The water permeability of BP membranes was mostly related to other physicochemical properties, such as hydrophobicity, surface area and pore size. However, water permeability of BP membranes made with MWNT-COOH/chitosan was considerably higher than that of BP membranes made with MWNT-NH_2/chitosan. The rejection of salts by BP membranes was dominated by adsorption mechanisms, and both electrostatic repulsion and size exclusion were related to the rejection of positively charged salts. The BP membranes with lower surface area and porosity were more capable of rejecting lower than higher molecular weight salts. In addition, an acidic feed solution (i.e. decrease in pH from 10 to 3) resulted in an increased rejection of salt molecules. Further research is required, particularly in selectivity studies, as these experiments showed that buckypaper membranes successfully rejected the salt from solution and are very promising in the area of desalination.

ACKNOWLEDGEMENTS

First, I am very grateful to my supervisor, Associate Professor Marc, in het Panhuis, who has encouraged, supported and guided me from the beginning to the end of my thesis. He has always been a source of encouragement and knowledge.

I would also like to thank the King Abdulaziz City for Science and Technology in Saudi Arabia for providing me with a postgraduate scholarship.

I express deep gratitude to all the members of the research group at the Soft Materials and Intelligent Polymer Research Institute (IPRI) at the University of Wollongong for their help and guidance in carrying out this research.

I am also deeply grateful to the staff and students in Environmental Engineering at the University of Wollongong for all their support, willingness to exchange knowledge, for helping with the membrane-filtration experiments and for creating a very friendly environment. I offer special thanks to the students and colleagues in the lab who have supported me in this research: Hamad Altalyan, Ziuad Alrowaili, Kha and Luke Sweetman.

I extend great thanks to Dr Tony, who helped me with my SEM images, and to the technical staff, Mick, Bob, Frank and Linda, for their support and patience during my experimental study.

I offer thanks to my colleagues at the King Abdulaziz City for Science and Technology Prof Ahmed Basfer, Salah Mufti, Fadhl Alfadhl, Abdulrahman Aldurahim and Raed bin Khnin, who have supported me in this research. I wholeheartedly thank all my friends who have not been mentioned but who have supported me and prayed for me to achieve my goals.

I also offer my blessings and regards to my parents, brothers and sisters for their moral support during the difficult times.

A very special thanks and expression of respect to my wife, who was my real supporter during the hard times, especially while I was spending most of my time at the University of Wollongong while she was looking after our children.

A very special thanks also to my four children, Ali, Rowa, Anas and Yizan, for their help and understanding, particularly when I left them at home for a long time while I was doing my experiments.

CONTENTS

LIST OF FIGURES

LIST OF TABLES

LIST OF ABBREVIATIONS

3-D	three-dimensional
Å	Angstrom
AFM	atomic-forces microscopy
APS	Asia Pacific Specialty
ATRP	atom-transfer radical polymerisation
BET	Brunauer-Emmett-Teller
BJH	Barret, Joyner and Halenda
BP	Buckypaper
BSA	bovine serum albumin
C6S	4-sulphonic calix-6-arene hydrate
CA	cellulose acetate
cipro	ciprofloxacin hydrogen chloride
CNT	carbon nanotube
CVD	chemical vapour deposition
DCMD	direct contact membrane distillation
DI	deionised
DNA	deoxyribonucleic acid
DSI	Desalination Systems Inc.
DWNT	double-walled nanotubes
ENP	extended Nernst-Planck
GMA	glycerin monomethacrylate
H	hexagonal
HBAB	2-(4'-hydroxybenzeneazo) benzoic acid
HiPco	high-pressure carbon monoxide
HK	Horvath-Kawazoe
HMWC	high-molecular-weight component
HPN	hybrid polymer network
I	discontinuous cubic
IPN	interpenetrating polymer network
IPRI	Intelligent Polymer Research Institute
I–V	current–voltage
KACST	King Abdul Aziz City for Science and Technology

L	lamellar
LLC	lyotropic liquid crystals
LMWC	low-molecular-weight component
MD	membrane distillation
MF	microfiltration
MFI-ZM	MFI-type zeolite membrane
MPD	*m*-phenylenediamine
MWNT	multi-walled carbon nanotube
MWNT-COOH	carboxyl functionalised multi-walled carbon nanotubes
MWNT-NH_2	amine functionalised multi-walled carbon nanotubes
NF	nano-filtration
P/P_o	relative pressure
PALS	positron annihilation lifetime spectroscopy
PC	personal computer
PEDGE	poly (ethylene glycol) diglycidyl ether PEG
PEO	poly (ethylene oxide)
PMMA	poly (methyl methacrylate)
polyGMA	poly (glycerin monomethacrylate)
PS-*b*-PLA	polystyrene-*block*-poly (lactic acid)
PS-*b*-PMMA	polystyrene-*block*-poly (methyl methacrylate) copolymer
PS-*b*-PVP	polystyrene-*block*-poly (4-vinylpyridine)
TSP	meso-tetra(4-sulfonatophe- nyl)porphyrin dihydrogenchloride
PSO	polysulphone (polyethersulphone or polyarylethersulphone)
PTFE	polytetrafluorethylene
PTS	phthalocyaninetetrasulfonic aci
PVA	polyvinyl alcohol
PVDF	polyvinylidene fluoride
PVP	poly (vinylpyridine)
QI (or V)	bicontinuous cubic
RO	reverse osmosis
S-D	solution-diffusion
SDBS	sodium dodecyl benzene sulphonate
SDS	sodium dodecyl sulphate

SEM	scanning electron microscope
SWNT	single-walled nanotube
TFC	thin-film composite
TGA	thermogravimetric analysis
TMS	trimesoyl chloride
Trix	Triton X-100
UF	ultrafiltration
UV	ultraviolet
UV-vis	ultraviolet visible
UV-vis-NIR	ultraviolet-visible-near infrared

1. INTRODUCTION

Chapter 1: Introduction

Most of Earth is covered in water, yet over a billion people worldwide have no access to reliable, fresh drinking water, and more than 2 billion people are suffering acute shortages of drinkable water [1, 2]. This figure will continue to grow with time, as approximately 97.5% of Earth's water is within the oceans and is unsuitable for human consumption [3]. Only 2.5% of the planet's water is fresh, but only 0.5% of this is easily accessible and suitable for human consumption [4], as a significant amount is trapped in polar ice caps and glaciers [5]. This 0.5% of fresh water is available from very limited sources, such as rivers, canals, ponds, lakes and underground reservoirs, compared to the vast quantities of saline waters available in our oceans.

The supply of fresh water is expected to decrease in the near future, as fresh water sources are continuously depleted through contamination by natural biodegradation, anthropogenic pollution and agricultural and industrial effluents containing biologics, pesticides, fertilizers, metals, dyes and so on [6-8]. These contaminated waters must be treated by physical, chemical or by both methods to remove contaminations and render them suitable for regular usage. Demand for clean water will continuously increase with the rate of population growth and the modernisation of human society. Thus, it is imperative to create clean water supplies to meet the ever-increasing demand.

Sufficient clean water can be obtained through decontamination of polluted water as well as the desalination of ocean water. Whereas the decontamination of polluted waters by chemical methods is expensive, time-consuming and environmentally hazardous and unfriendly, the desalination process of ocean water is relatively clean, cost-effective and environmental friendly. Thus, desalination is generally acceptable and commonly used. One such desalination process is shown schematically in Figure 1.1.

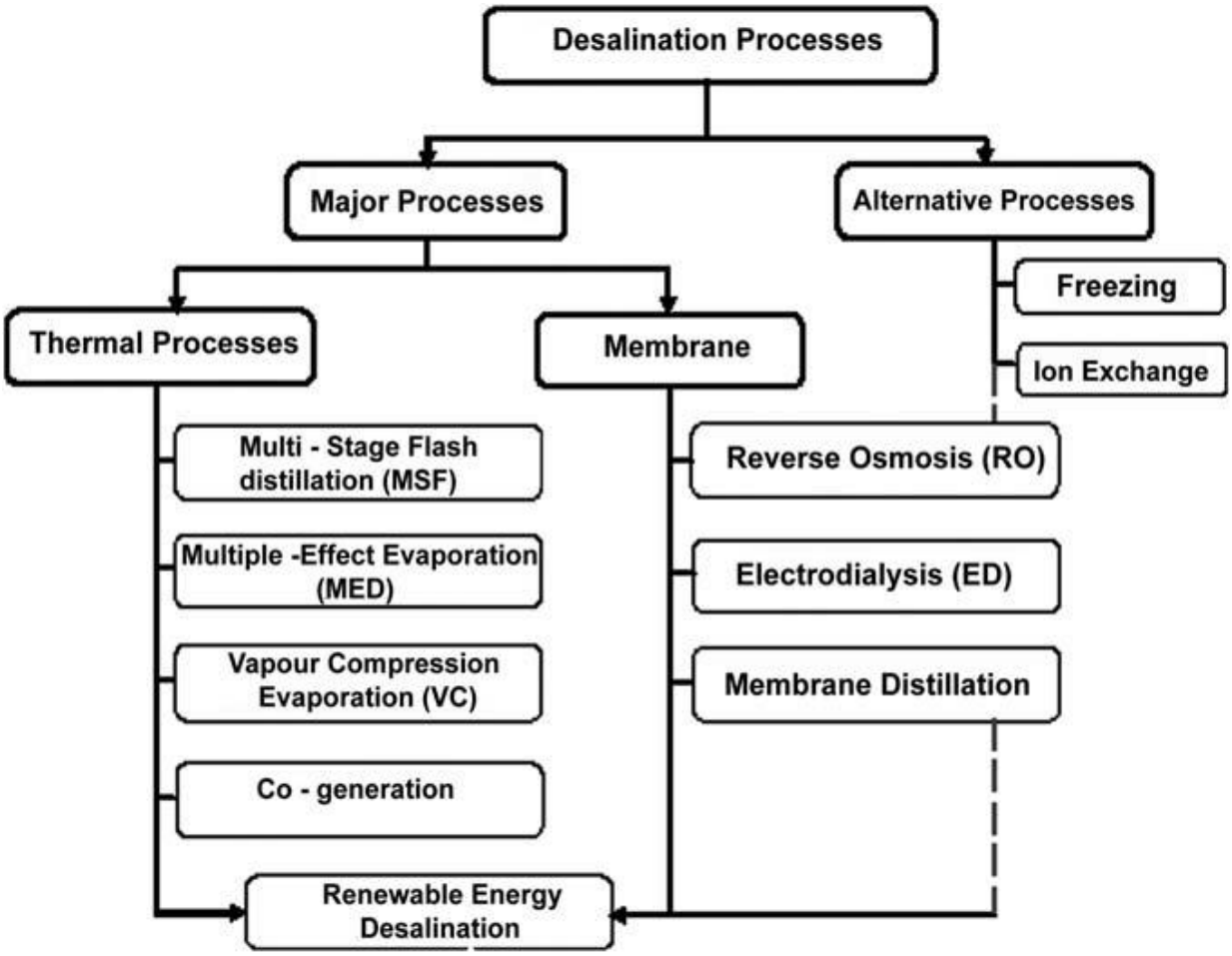

Figure1.1. Schematic desalination process (reproduced from reference [3])

The aim of the present work was to design and fabricate polymer membranes using different polymers and additives, including carbon nanotubes (CNTs). In polymer-membrane processes water is forced from a region of high dissolved-solute concentration through the active layers and pores of membranes to reach a region of low solute concentration using a pressure that exceeds the osmotic pressure. A skin layer of membrane allows water to pass through while retaining or removing salts and contaminants. A schematic diagram of a typical polymer-membrane process is presented in Figure 1.2.

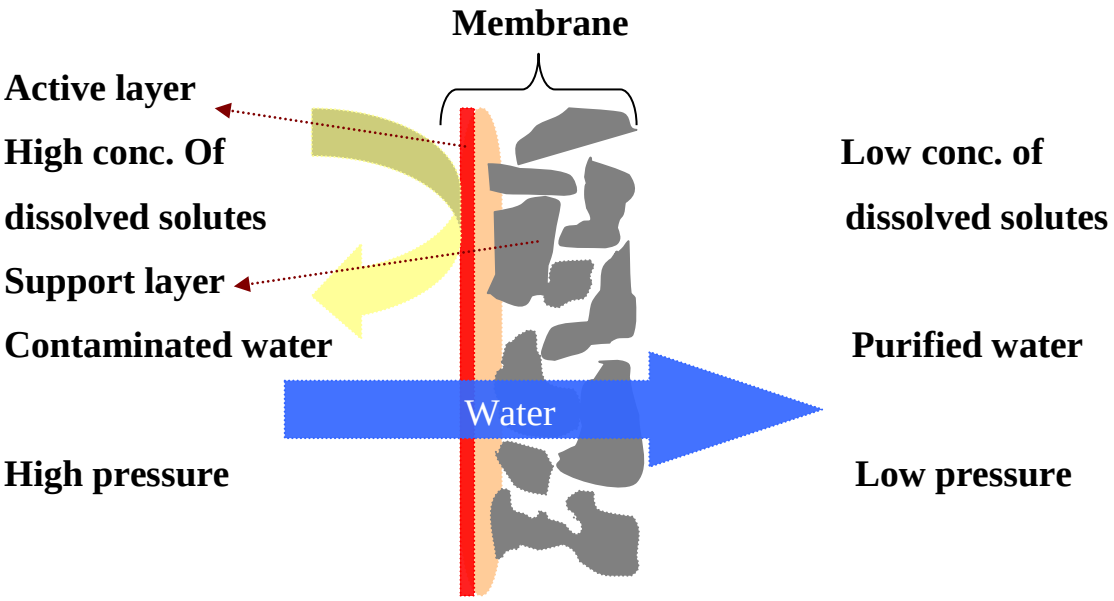

Figure1.2. General membrane process

1. 1 Seawater Desalination Technologies

The process of seawater desalination involves the separation of seawater into a stream of brine with high salt content and fresh water with negligible salt content. The desalination process involves energy and technology; over the years, several desalination techniques have been developed, such as freezing, membrane separation, distillation and electrodialysis [4, 9-11]. Of these, the most commercially used processes are Multi-Stage Flash (MSF) and reverse osmosis (RO). Experts believe that in the future, these processes, along with Multiple Effect Distillation (MED), will be dominantly and competitively used [3, 12]. In 1999, MSF technology was being used for nearly 78% and RO technology for 10% of seawater desalination capacity [4, 13]. Some of the technologies employed for desalination are discussed below.

1.1.1 Vapour-compression distillation

In the vapour-compression distillation (VCD) desalination process (Fig. 1.3), the compression of vapour provides the heat for seawater evaporation [4, 10, 14]. The boiling point temperature is reduced by pressure in VCD processes, and the production of the heat required for the evaporation of seawater feed for the condensation of the water vapour is achieved using either a steam jet or mechanical compressor.

VCD using a steam jet, known as thermo-compressor, consists of a venturi orifice at the steam jet, which is used in the creation and extraction of water vapour from evaporator, resulting in a lower ambient pressure. The steam jet compresses the extracted water vapour, and the condensation of this mixture on the tubing wall provides the condensation heat and thermal energy required for the evaporation of seawater flowing through the alternate side of the tubing wall inside the evaporator.

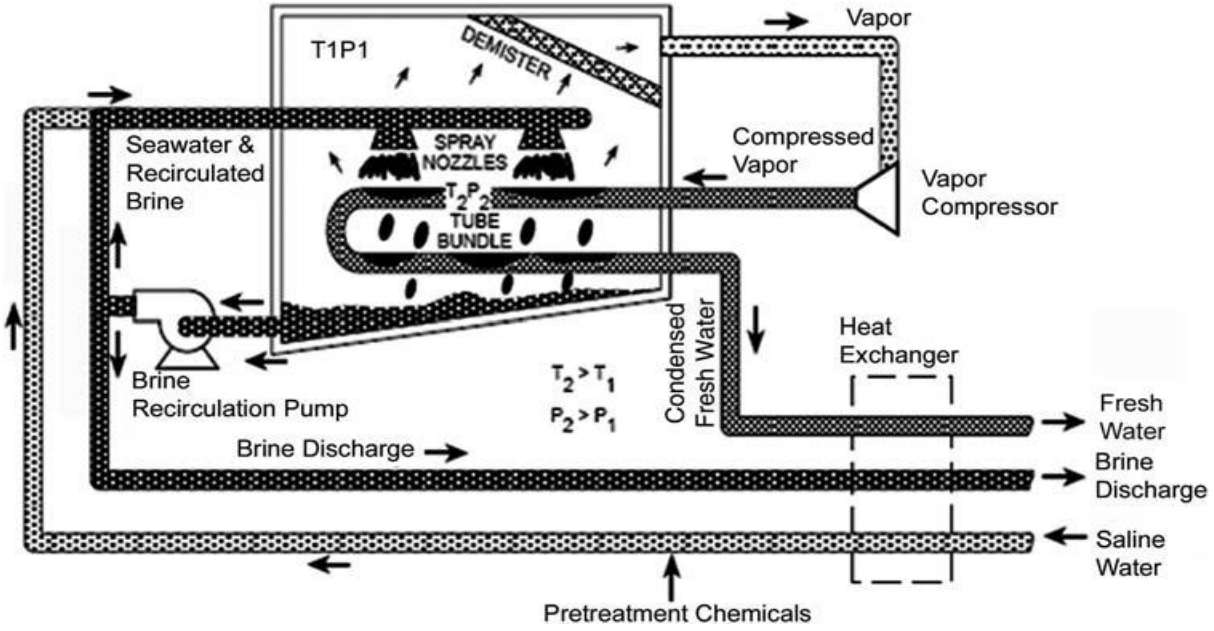

Figure1.3. Vapour-compression evaporation [3].

Electricity is used to drive the mechanical compressor-type VCD, which is designed in various formations for promoting heat exchange and seawater evaporation. A vacuum is created in the evaporator, and the vapour is compressed and removed from the evaporator and condensed inside the tubing bundle. A spray of seawater on the outside of the heated tubing bundle boils the seawater, resulting in partial evaporation and production of more vapour.

VCD desalination processes operating at low temperatures are reliable, simple and effective and have low power requirements. Temperatures below 70°C can be achieved using compressors with large capacities, resulting in a reduced risk of scale formation and corrosion. VCD processes are typically used in small-scale desalination plants, with usual capacities of 3000 m^3/day, requiring power of 7–12 kWh/ m^3 of water production. VCD units find application in contexts such as drilling sites, remote locations and resorts, where fresh water is hard to access [14].

1.1.2 Multi-stage flash (MSF) distillation

The principle of flash evaporation is used in the process of MSF distillation, as shown in Figure 1.4. The process involves evaporation of seawater by subjection to reduced pressure rather than increased temperature. The MSF process comprises a heat input, heat recovery unit and heat rejection sections. Regenerative heating is used in this method, with the seawater flash transferring some heat to the seawater headed for flashing in each flash chamber. At every stage, heat is released due to condensation of water vapour, and this heat is used to increase the temperature of the incoming seawater. Scale control is achieved by high temperature additives or by acid dosage [15].

A gas turbine, steam turbine or heat recovery steam generator supplies steam at low pressure, which is used to heat the seawater in the brine heater [4, 16, 17]. The seawater is fed into the brine heater, which consists of a heat exchanger at the top portion of the evaporator. The seawater flows into the heat exchanger tubes, gains heat and is passed into the evaporation flash chambers. The evaporation typically has 19–28 stages in any modern MSF desalination plant [4, 15, 18, 19]. The operating temperature of top brine is 90–120°C and is dependent on the scale control methodology being employed [4, 20-23]. A plant operating at a higher temperature range of 120°C typically increases the efficiency, but also increases the rate of scale formation [20, 23] and metal surface corrosion.

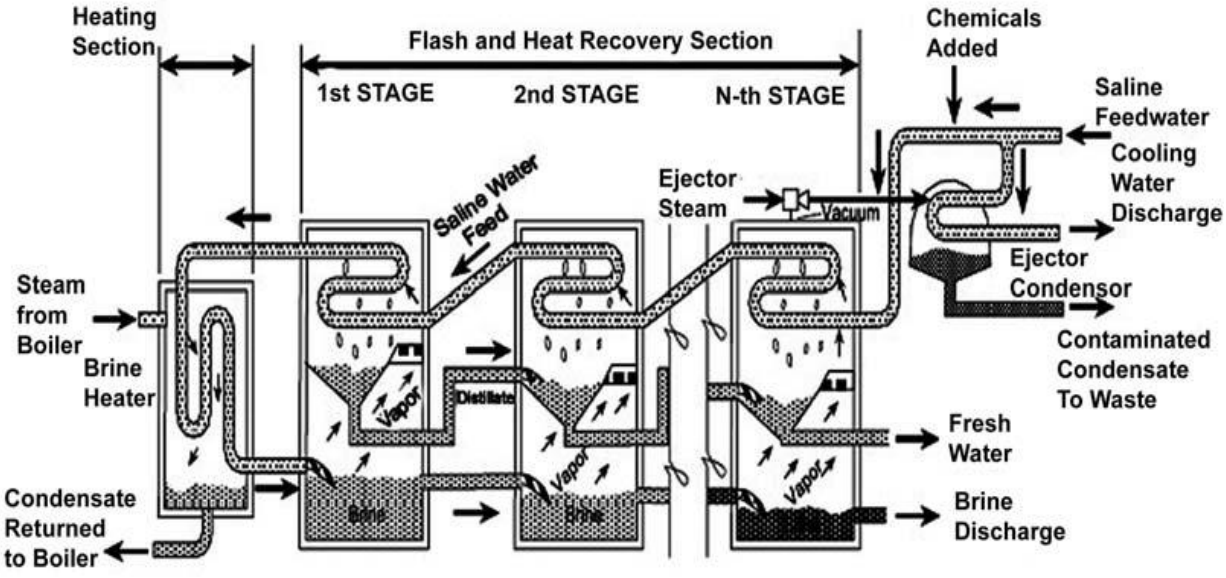

Figure1.4. Multi-stage flashing process (MSF) [3].

The pressure at every stage is maintained below the saturation pressure of the heated seawater, which flows into the stage. Introducing the seawater inside the flash chamber would cause it to boil quickly and vigorously due to flashing. The pressure of the brine is reduced using baffles and orifices located in between the stages, to a level equal to the vapour pressure necessary for boiling at the temperature of the brine solution at equilibrium. The seawater is boiled until it reaches its boiling point at the flash chamber. Flash distillation is achieved by gradually producing water vapour by controlled pressure reduction of hot seawater in a sequential manner. The un-flashed brine is passed on to the next stage with a further reduced pressure for flashing in subsequent stages. Therefore, the seawater could be subject to evaporation without the need to add more heat.

Demisters are integrated in each stage design to minimise the carryover of brine droplets into the distillate. The evaporator design also consists of a vacuum deaerator, which is used to remove gases dissolved in the brine, and a de-carbonator, in case acid is used to control scales. Air and flashed vapour are used as stripping media for the deaerator and de-carbonator. Carbon dioxide produced by a reaction of seawater bicarbonates with sulphuric acid is removed using the de-carbonator [20, 23]. Alkaline scale formation is mainly due to the presence of bicarbonates in seawater [4, 23]. To maintain a vacuum inside the evaporator stage, there is a mechanism consisting of a steam jet ejector along with an inter-condenser, vent-condenser, after-condenser and so on. During the flashing process, the mechanism extracts non-condensable gases, such as oxygen, nitrogen and carbon dioxide. The flashed water vapour is cooled and condensed using cold seawater, which flows inside the condenser tubing, to produce distillate. The vapour condensation releases latent heat, which is used to heat the inflowing brine in the tubes. The produced distillate at every stage is collected and flows in a parallel line along with brine from stage to stage, and is finally pumped to a storage tank. Typically, the desalinated water produced using this MSF technique consist of 2–10 ppm dissolved solids, and is therefore re-mineralised using the post-treatment or potabilisation process [24-29].

The water vapour quantity depends on the pressure maintained at every stage, where the flash results in a 2–5°C drop. The distillate production rate varies with the seawater temperature, as the range of flash (usually 50–75°C) tends to vary inversely with the seawater temperature. The number of stages in the MSF plant also affects the productivity level due to scale economics. The process efficiency increases with the number of stages, but this also

increases the capital plant costs. To evaluate the water production economies of cost, the performance ratio (PR) is determined, with modern MSF having typical PR values in the range of 6.5–10.5 pounds per 1000 BTU heat supplied [20]. The heat rejection segment, typically comprising 2–4 stages, is used to reject the input energy of the brine heater by cooling the flowing seawater [4, 18, 19]. A part of the warmed, cooling seawater undergoes diversion for utilisation as the makeup stream of the process, which will replace part of recirculating brine lost in vapour formation. The makeup stream is mixed with part of the brine that emerges from the last stage of the heat recovery mechanism and is recirculated to the brine heater through tube side of the condenser. This brine undergoes heating and flashing through the different stages. This process is known as recirculation MSF and is different from the once-through processes. Cold seawater is primarily used as a cooling medium in the heat rejection mechanism, and a major portion is returned back to the sea along the blowdown stream. This has been used for scale control to prevent the excessive concentration of brine, which would result in an increased boiling point temperature. Consecutive evaporation of brine results in increased salt concentrations and subsequent scale formation and corrosion.

The equipment used to supply seawater for desalination and cooling includes a submarine pipe (open intake channel), sodium hypochlorite generator, pump house and return and distribution piping or channels. Moving screens and traversing trash rakes are used in the pump house to separate debris. The spent hot brine is discharged into the sea through the outfall channel from the heat rejection section.

MSF plants have been in operation from the 1950s and have been built in units of about 4,000–57,000 m3/d [14]. In 1953, the US Navy built an MSF plant with five stages, having a total capacity of 189m^3/day. The year 1957 saw the establishment of four plants in Kuwait, with a capacity of 2,271m^3/day [9]. The world's largest desalination plant is the Saline Water Conversion Corporation, located at Al-Jubail, KSA, with a capacity of 815,120m^3/day [4]. The largest MSF plant is located at Shuweiat, United Arab Emirates (UAE), with a capacity of 75,700m^3/day [4, 30].

1.1.3 Multiple effect distillation

MED is the oldest desalination method [31] and also has thermodynamic efficiency, as demonstrated in Figure 1.5 [32]. The process of MED is based on the principle of ambient pressure reduction using a series of evaporators known as effects. In this process, the seawater

feed undergoes multiple boiling processes without any supplementary heat apart from the first effect. Seawater entering the first effect is raised to its boiling point through pre-heating in the tubing. A spray of seawater on the surface of the evaporator tubing promotes faster evaporation. A dual-purpose power plant supplies external steam that heats the tubing. Steam condensation takes place on the opposite side of the tubing and is recycled for use in the boiler of the power plant. The steam economics of the MED plant varies with the number of effects, which is restricted by the available range of total temperature and minimal difference in temperature allowed between two consecutive effects.

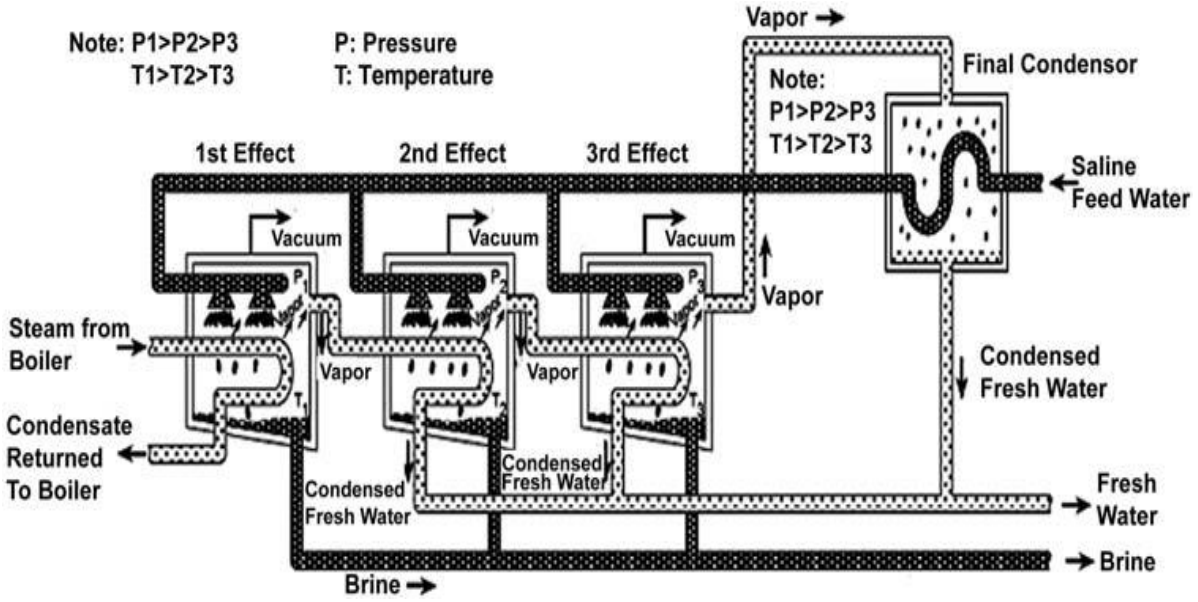

Figure1.5. Multi-effect distillation plant [3].

Evaporation of only a proportion of supplied seawater takes place in the first effect. The remaining seawater feed is passed on to the next effect, where it is fed into a bundle of tubes heated by the vapours generated in the previous effect. Condensation of the vapour results in fresh water production and heat, which is then used in the evaporation of the residual seawater in the consequent effect. This process of evaporation and condensation is repeated in consecutive effects at lower temperatures and pressures, continuing over several effects ranging from 4–21, with typical PR ranging from 10–18 in large plants [33]. Few plants have been designed to function at initial top brine temperatures (TBTs) of around 70°C, which results in a decreased risk of scale formation [4] but requires more area for heat transfer and, thus, extra tubing. MED plants typically consume significantly lower power and have higher PRs than MSF plants; therefore, they are more efficient in terms of heat transfer and

thermodynamics [34]. Even though there are much fewer MED plants than MSF plants, MED plants have seen a steady growth, with a majority of the large capacity MED plants located in the Arabian Gulf region. MED plants with capacities of 45,400 m^3/day have been designed and demonstrated [4, 35]. Sharjah, UAE has two MED plants, each with a capacity of 22,700m^3/day [35].

1.1.4 Reverse osmosis (RO)

The last 2 decades have seen significant developments in the reverse osmosis (RO) process, resulting in drastic falls in capital and operational expenses. Major membrane improvements have resulted in improved compression resistance, extended life, greater efficiency, better flux and better passage of salts. In the RO process, the osmotic pressure of the seawater is overcome through the application of higher external pressure, which results in water flow across the membrane in the direction opposite to the natural flow. The dissolved salts are left behind on the side with increasing salt concentration. As no heating or phase change is required, the energy is used only for pressurising the seawater feed. Typically, an RO plant [36-39] has four major parts: the seawater feed pre-treatment, high-pressure pump, separation membrane and permeate post-treatment, as shown in Figure 1.6.

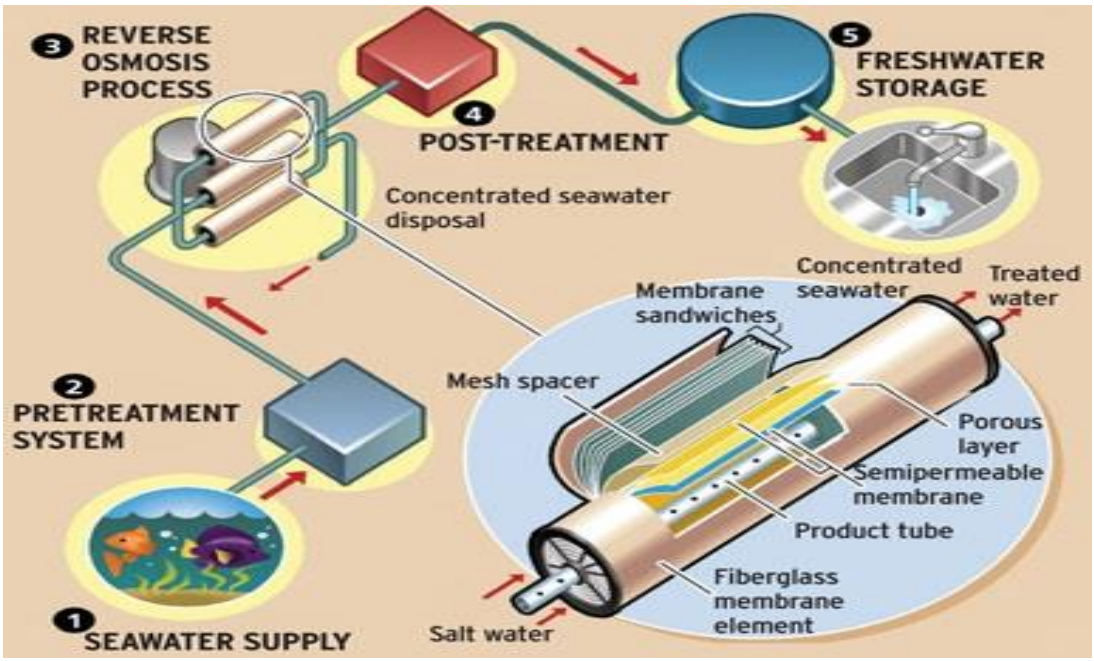

Figure1.6. RO processes [40].

Seawater is fed through trash racks and moving screens to eliminate rubbish, and is further cleaned using a multimedia gravity filter made of silica, sand, granite or anthracite to eliminate suspended objects. The feed is then passed into the micron cartridge filter to remove particles larger than 10 microns. Seawater filtration ensures that high-pressure pumping equipment and the RO plant are not damaged. The pressure of the pre-treated feed is increased to the optimal level required for the membrane using high-pressure pumping. The dissolved salts are unable to pass through the semi-permeable membrane, but pure water flows through. The concentrated brine solution is released into the seas.

To prevent fouling the membrane, it is essential to remove unwanted elements of seawater by pre-treatment [41-46]. Pre-treatment generally involves chlorination, acidulation, coagulation, de-chlorination and filtration using multimedia and micron cartridge filters. The pre-treatment method varies according to the properties of feed, configuration, type of membrane, water quality and recovery ratio. Other chemical additives, such as sulphuric acid to adjust water pH and to control scale formation and hydrolysis, sodium hypo-chlorite for preventing micro-organism growth, sodium bisulphite for de-chlorination and ferric chloride as flocculant, are added at different stages [36-39].

Stainless steel pumps increase the pressure of the pre-treated feed to a level optimal for the RO membrane, thereby allowing only water pass through and leaving salt impurities behind. Generally, centrifugal pumps are used to increase pressure in the range of 50–80 bar in seawater, but the pressure is affected by the salt content in the feed. The membrane is designed to bear the huge pressure drop across it, with the latest membranes designed to suit pump operations of 84kg/cm^2. Still, a small amount of salt can pass through the membrane and is present in the permeate. The two most common commercial configurations for RO membranes are hallow fine fibre (HFF) and spiral wound [4, 47-49]. The HFF configuration has a u-shaped membrane made of cellulose, polyamide and triacetate, and is contained inside a pressure vessel [4].

1.1.5 Solar evaporation

Extensive investigations have been done on the use of solar energy for seawater desalination [4]. The principle behind the method is similar to the natural hydro-logic cycle, wherein sunlight heats the seawater and produces water vapour, whose condensate is fresh water. The green-house, where salt water placed inside is heated and the resulting vapour

condenses on the sloping glass roof, serves as a basic example [14]. Many modifications have increased the effectiveness of this method; however, they all face the drawbacks of requiring large areas for the collection of solar energy (typically 25 hectares of land per 1000m^3/day of water production), high capital expenditures and increased risk of weather damage [14]. Although the thermal energy is freely supplied by solar energy, additional power is required for pumping the water.

1.1.6 Freezing

In the freezing method of desalination, freezing under controlled conditions allows pure ice crystals to form, leaving behind the dissolved salt. Prior to freezing the whole mass of water, the mixture is subjected to washing and rinsing to separate the salt attached to the ice and present in the remaining water. The separated ice is melted to form fresh water. The process involves cooling the feed, partial crystallisation of the ice, removing the ice from the feed, melting the ice, refrigeration and heat rejection. Several processes, such as indirect, triple point, hydrate process, eutectic and secondary refrigerant, have been developed to the pilot plant state [14, 50]. In theory, desalination by freezing requires low energy and causes minimal corrosion, scaling and precipitation. However, handling ice blocks and water requires complicated mechanisms. An experimental desalination plant using the freezing method was constructed in 1985 in Saudi Arabia [4], and a few other freezing desalination plants have been built in the last 4 decades, but the process has not seen commercial success in fresh water production for civic supplies.

Though many processes, such as solar evaporation and freezing, have been designed for desalination, they have not been able to operate as economically as MED, MSF and RO. They might still be used under certain situations or with further improvement; however, membrane technology is simpler and cheaper and has therefore seen greater use and advancements. The membrane technologies used for water filtration are discussed below.

1. 2 Membrane Separation Technology for Water Filtration

The membrane process has been used over the past 40 years to achieve a 44% share in the world's desalting production processes. It is the primary choice for 80% of all desalination plants worldwide because it requires less energy than thermal desalination [51, 52].

In the late 1950s, Reid proved that salt could be separated from water using cellulose acetate (CA) membranes, although the resulting water fluxes were miniscule in practical

terms [53, 54]. Loeb and Sourirajan designed a technique in 1959 for constructing asymmetric CA membranes with higher water fluxes and separations than those Reid obtained [54]. They developed a phase-inversion process where viscous CA polymer solutions were cast onto the membrane supports and immersed in a non-solvent of the polymer (water), resulting in a semi-porous polymer membrane. The resulting polymer membrane comprised a relatively dense 'skin' on the surface, with a porous network support [55]. The Loeb-Sourirajan CA-modified membrane led to an economical membrane desalination process, which is still used today in updated form [56].

Cadotte developed a type of membrane called a thin-film composite (TFC) for desalination in the mid-1960s. These are used in interfacial-condensation polymerisations to create thin films (<1 μm) of crosslinked polyamides on a porous support [57]. TFC membranes have high fluxes and high salt-rejection capacity, while being relatively simple to manufacture. Currently, TFC membranes are used in the membrane desalination process. Polyamides are sensitive to degradation by oxidative compounds, such as chlorine-based substances used to control biological contamination, as they have the amide group in their structure. Sulphonated polysulphone (PSF) membranes were recently investigated as an alternative for desalination applications because they are resistant to degradation by chlorine compounds [58-60]. Generally, the thickness of the skin layer is approximately ≤ 0.1 μm, whereas the total thickness of the membrane is 150–250 μm [61]. The skin layer also functions to protect the pores of the membrane from fouling that occurs within, having a minor effect by reducing the pore size [62]. This also helps keep salt and pollutants from crossing the membrane. Recent developments have facilitated extensive membrane-technology applications in the production of high-quality pure water, as well as addressed a variety of contaminated waters. One such process is shown schematically in Figure 1.7.

.

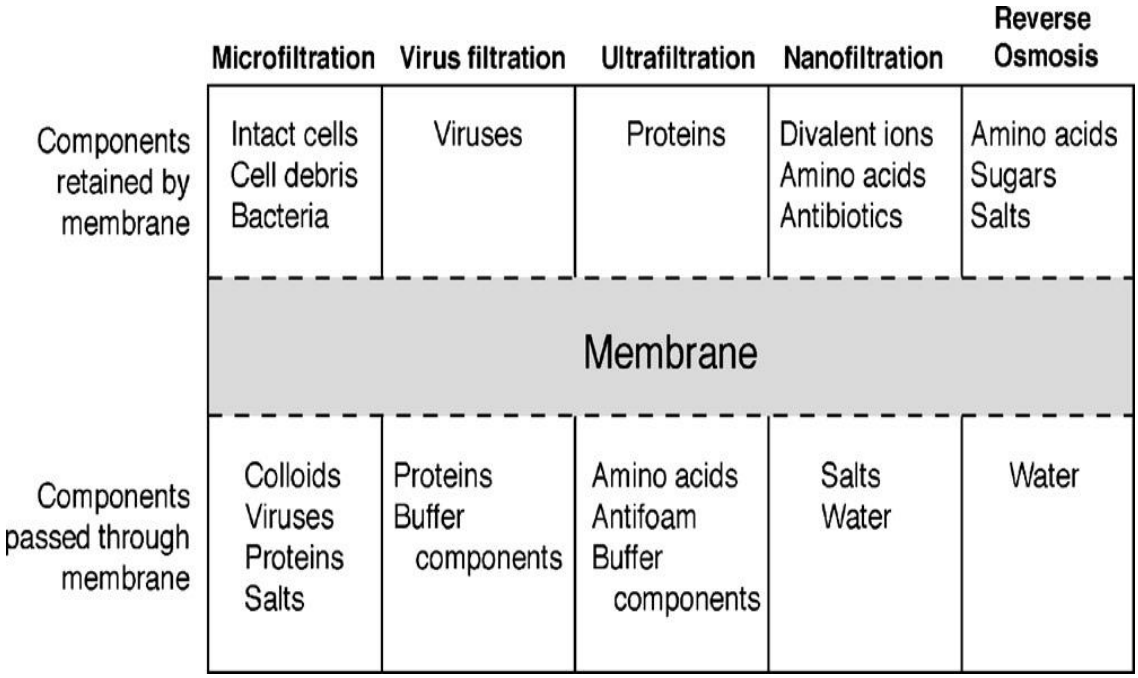

Figure 1.7. Schematic diagram of different types of membrane-filtration systems to remove contaminants from water (Reproduced from reference [62]).

There are many ways to categorise membranes, as shown in Table 1. In these processes, membranes are characterised according to their material compositions, for example, polymeric, ceramic, metallic and supported liquid membranes. Membranes are also classified as symmetrical or asymmetrical, depending on their modes of construction or according to their pore sizes. A symmetrical membrane has a uniform morphology throughout its entire membrane thickness [63]. Ion-exchange, electrodialysis and microporous membranes are examples of symmetrical membranes. An asymmetrical membrane, such as the Polyamide TFC or Loeb-Sourirajan-type CA membrane, has a heterogeneous morphology and with a dense skin layer on top of a thick, porous support layer**.**

Table 1. Membrane categories (Reproduced from reference [61])

	RO	NF	UF	MF
Membrane	Asymmetrical	Asymmetrical	Asymmetrical	Symmetrical Asymmetrical
Thickness **Thin film**	150 µm 1 µm	150 µm 1 µm	150 µm 1 µm	150 µm 1 µm
Reject	HMWC, LMWC salt (i.e. NaCl) Glucose Amino acid	HMWC Mono-,di-and oligosaccharides polyvalent neg. Ions	Macromolecules, Proteins, polysaccharides vira	clay, and bacteria
Membrane **Materials**	CA Thin film	CA Thin film	Ceramic, PSO, PVDF, CA Thin film	Ceramic, PSO, and PVDF
Membrane **Model**	Tubular, spiral wound, plate-and-frame	Tubular, spiral wound, plate-and-frame	Tubular, hollow-fibre spiral wound, plate-and-frame	Tubular, hollow-fibre
Operating **Pressure**	15–150 bar	5–35 bar	1–10 bar	<2 bar

As shown in Figure 1.8, membranes are also categorised as nonporous and porous depending on their pore sizes [52]. Gas-separation and RO membranes are nonporous membranes and do not contain discrete pores. Conventional filtrations separate macroscopic pieces using membranes with pore sizes from 0.001–1 mm for many applications. Water-filtration membranes are typically classified by the sizes of the solutes they can remove from water (i.e. by their filtration-rejection performance). Microfiltration (MF) is employed in the separation of suspended particles and colloids from 0.1–10 µm [52]. Other types are termed ultrafiltration (UF) membranes and typically have small pore sizes in the range 0.01–0.1 µm [52]. UF membranes are usually used to reject the high-molecular-weight component (HMWC), such as proteins and suspended solids, while the low-molecular-weight component (LMWC), such as mono- and di-saccharides, salts, amino acids, organics, inorganic acids and sodium hydroxide, are allowed to pass through the membrane. Nano-filtration (NF) membranes have pore sizes ranging 1–10 nm. These membranes are only used to reject ions

with more than one negative charge (e.g. sulphate or phosphate); that is, they allow monovalent ions to pass. NF membranes also have the capacity to reject uncharged, dissolved materials and positively charged ions according to the size and shape of the molecule in question. In addition, NF membranes are used for the pre-treatment of water. These membranes require low pressure, whereas RO is a high-pressure method [64]. Membranes for RO usually have pore sizes ranging 0.5–10 nm.

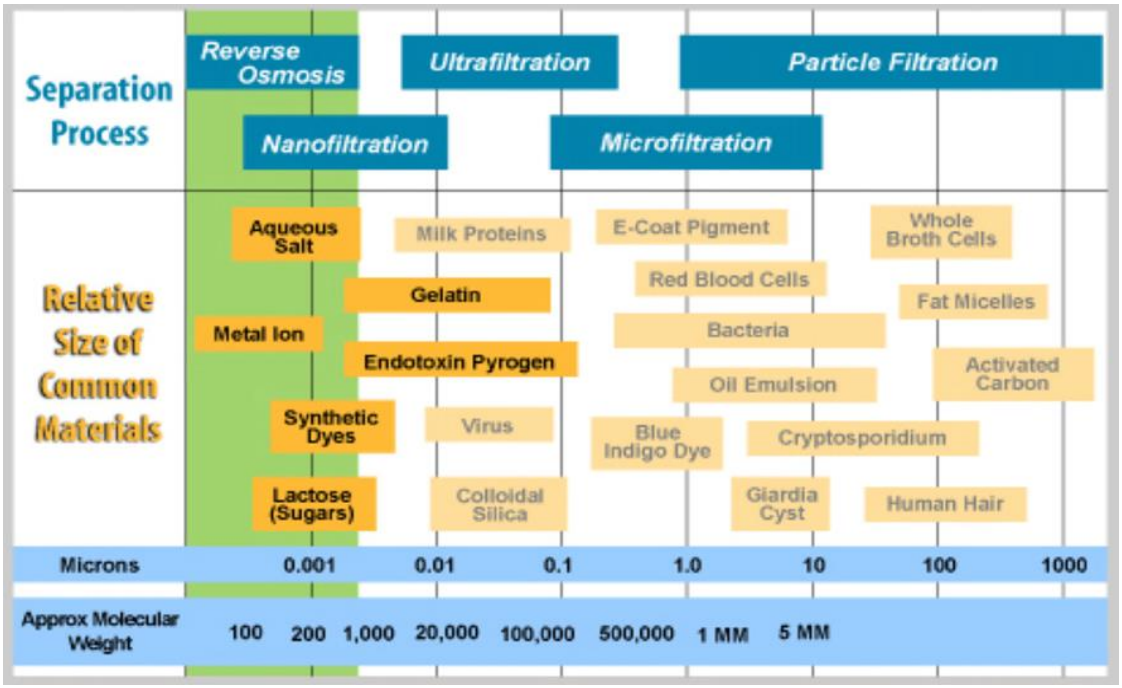

Figure1.8. Effect of pore size polymer membranes and corresponding solute sizes (Reproduced from reference [52]).

1.2.1 Microfiltration (MF) and ultrafiltration (UF) membranes

MF membranes are employed to remove bacteria and various colloids from water [65]. They require low transmembrane pressure drops at high fluxes. MF membranes are extensively used for the pre-treatment of water in desalination processes, cold sterilisation of beverages and sterile filtration of pharmaceuticals. UF membranes can eliminate bacteria, viruses and some dissolved solutes with high molecular weights, including larger proteins. UF membranes have been widely used in the treatment of surface water, oil–water emulsion waste treatment (producing water and grey water) and various food-processing procedures (e.g. cheese production, other protein concentration processes and fruit juice clarification) [66]. Owing to their pore size ranges, MF and UF membranes do not reject small salt ions, mono- and di-saccharides, amino acids, organics, inorganic acids or sodium hydroxide. These

materials must be extracted from contaminated water for safe consumption. Therefore, these membranes are usually employed as filters in pre-treatment steps to increase the lifetime and the performance efficiency of NF and RO membranes.

1.2.2 Reverse osmosis (RO) membranes

RO membranes can be divided into three types: 1) high-pressure RO, 2) low-pressure RO and 3) NF or 'loose-RO', as described in Table 2. Moreover, RO membranes are asymmetric with skin layers that donate selective properties to the membrane. They are efficient at removing most of the ions and organic molecules from water [67]. While they do not have distinct pore sizes, NF membranes have 'effective' pore sizes ranging 0.001–0.01 µm in the form interstitial voids between the polymer chains that make up the membrane film. They remove >99.5% of all salts from seawater and completely exclude all organic molecules except those with molecular weight <100 Da [52, 63]. RO membranes are used in several water-purification processes to supply drinking water from surface water, brackish water, seawater and other contaminated water sources.

Table 2. Different types of RO membranes and their applications [63].

RO membrane	Pressure range (MPa)	Salt rejection (%)	Application
High-pressure	5.6–10.5	95–99.9	Seawater desalination
Low-pressure	1.4–4.2	95–99.9	Brackish water desalination
NF or loose-RO	0.3–1.4	0-20	Pre-treatment of seawater for RO desalination (i.e. high pressure)

In general, RO membranes are manufactured using either phase-inversion or interfacial-condensation polymerisation [63]. Phase-inversion membranes are made by taking a viscous polymer solution (usually CA blends in organic solvents), casting it onto an

appropriate support and immersing it into a non-solvent, such as water. The polymer solution phase separates into a solid, polymer-rich phase and a liquid, polymer-poor phase. The polymer-rich phase forms the solid structure of the polymer membrane. The polymer-poor phase forms the pore structure of the membrane. The resulting membrane has a thick, macroporous layer supporting a thin, denser skin layer on the surface, which contacted the non-solvent. The dense skin layer is responsible for the extremely fine sieving properties of the RO membrane. In the mid-1980s, Desalination Systems Inc. (DSI) manufactured three-layer composite membranes. Today they are the only producer of these membranes, which are more stable and less prone to fouling than conventional RO membranes and are still the membrane of choice for managing a common array of difficult processes.

In both categories of RO membranes, the dense, thin skin layer (sometimes referred to as the 'active layer') acts as a semi-permeable barrier that selectively allows water molecules to pass through when a driving force is applied. The mechanism of the water transport and solute rejection through the RO membrane's active layer is still a matter of debate between the solution–diffusion (S–D) and preferential sorption-capillary flow models. The S–D model, originally developed by Lonsdale, Merten and Riley, stipulates that water and solutes dissolve in the dense and homogeneous surface layer of the RO membrane [68]. The components diffuse through the surface layer by their own chemical potential gradient (the sum of transmembrane pressure and concentration gradient). Differences in the solubilities and diffusivities of the solvent and solute in the active layer govern the rejection. In the preferential sorption-capillary flow model originally developed by Sourirajan, water molecules preferentially sorb to (or solute molecules are preferentially repelled by) the surface of the membrane. This leads to a water-rich layer at the surface and pore walls of the membrane. The enriched water layer then flows through the discrete pores of the membrane when a pressure gradient is applied, while solutes are repelled or refused because of the preferential sorption of water and the size-exclusion effects of the pores [69]. Current reports using atomic-forces microscopy (AFM) and positron annihilation lifetime spectroscopy (PALS) support this model because they have demonstrated proof of clarified pores in RO membranes [70].

1.2.3 Nano-filtration (NF) membranes

NF membranes, occasionally referred to as 'loose-RO' membranes, are relatively new in membrane processes. Typically, NF membranes have high rejection of larger ions (e.g. SO_4^{2-}, Ca^{2+}), low rejection of smaller ions (e.g. Cl^-) and rejection of mainly organic molecules [63]. NF membranes conventionally exhibit lower rejection than RO membranes, but they are attractive due to their lower pressure requirements. The lower pressure allows more energy-efficient water-purification processes. However, achieving rejection of small, uncharged organic compounds, such as methanol and formaldehyde, can be quite difficult with RO and NF membranes. Nevertheless, they are used in several water-purification processes for human consumption or reuse, such as treatment of low brackish water, municipal wastewater [71], contaminated well or ground water [72], paper-mill process water [73] and pre-treatment of seawater for RO desalination [74].

NF membranes are also used to concentrate products, such as whey protein and lactose in the dairy industry [75]. They are fabricated similarly to RO membranes (Loeb-Sourirajan and TFC) and processing parameters are in need of greater pore sizes. Solvents and solutes are transported through the membrane by a combination of convection and diffusion through electric forces and the well-defined pores. Models describing this transport are generally based on the extended Nernst-Planck (ENP) equations [76, 77]. Further details of the model are discussed later. Mechanisms of membrane separation commonly used for separating the components of a mixture from water are discussed below.

1.2.4 Mechanisms of membrane separation

Membrane separation mechanisms often include adsorption and exclusion by size or electrostatic interaction [78]. Exclusion by size is a common technique for molecular removal and takes place when the structural size of the analyte is too large to channel through the membrane pores. The degree of removal depends on the size, structure, hydro-dynamic radius and geometry of the component [79]. A great deal of modelling has been done based on these physical characteristics, along with membrane pore sizes, to predict the filterability of the membrane [80, 81]. Still, experimental models are often much more complex as a result of the variability of the membrane pores and component shapes and sizes.

Although exclusion by size is the principle mechanism of membrane separation, other factors influence the process. One of these is adsorption, which is the level of hydrogen

bonding, hydrophobicity and relative hydrophilicity of the membrane's surface and other reactions between the membrane and the solutes. For instance, adsorption of the hydrophobic components of the mixture occurs through the internal pore structure of the conventional hydrophobic polymer membrane at the surface, when compared to other hydrophilic components. The adsorption continues until the membrane pores are saturated with hydrophobic components of the mixture, and is followed by a low rejection level of hydrophobic components [82]. A similar effect can be produced as a result of hydrogen bonding of the hydrophilic membrane and the hydrophilic components, which occurs due to competition between hydrophilic analytes and water molecules for hydrogen bonding space on the surface of the membrane [83].

Electrostatic interaction is the primary factor that inhibits the membrane's ability to separate charged solutes of a mixture. The levels of these interactions are influenced by the positive and negative charge sizes of the analytes, which are dependent on the ion concentration and pH of the solution. The feed solution pH can also alter the surface charge of the membrane by affecting retention characteristics [84, 85]. Research has also indicated repulsive electrostatic interactions with the surface of the negatively charged membrane, which results in an increased rejection level of negatively charged organic solutes [85, 86]. Vice versa, solutes carrying a positive charge have lower rejection levels because the negatively charged membrane attracts these solutes.

Another common mechanism is the adsorption of ions or tiny molecules within the chemical separations sector. Activated carbon was initially used in the United States as an adsorbent material to eliminate undesirable odour and taste from polluted water [87]. The production of various types of activated carbon is done using lignite, peat, petroleum coke, coconut shells, wood charcoal, coal and so on to produce porous materials of varying diameters and molecular dimensions [87, 88]. Activated carbon remains the most widely used material for water purification because of its high surface area (nearly 2000m^2/g), capability to eliminate a large variety of pollutants, high removal capacity and rapid uptake kinetics. Unfortunately, active carbon is expensive, becomes useless after reaching capacity and is non-selective. Therefore, the industry is moving towards molecular sieves, bio-absorbents, such as bacteria, algae and chitosan, and clay minerals and zeolites [87, 89, 90]. The capability of analyte adsorption is not restricted to microporous material but also covers many conventional polymer membranes. For instance, some nano-filter membranes can utilise hydrophobic

adsorption properties to remove traces of organic contaminants that other membranes are unable to remove due to unfavourable electrostatic interactions [82, 85].

Chlorine degradation and biological fouling can significantly affect membranes' performance and shorten their lifespans. The next section provides information about these issues.

1. 3 Current Issues with Membranes for Water-Filtration Applications

Membrane technology has contributed to the provision of safe drinking water for several decades [91, 92]. Despite this, a number of issues limit its usage. These issues decrease membrane performance by affecting pore size and pore-size distribution control, chlorine degradation [93, 94] and biological fouling [69, 95, 96]. This section focuses on these issues, which have significant effects on the performance and lifespans of membranes.

1.3.1 Pore size and pore-size distribution control

Traditional membrane fabrication methods offer little control over the average size, size distribution and morphology of the effective pores in NF and RO membranes [63, 92, 97]. A broad pore-size distribution allows solutes considerably larger than the effective average pore size to pass through the membrane. This behaviour can prevent the high rejection that is desirable for certain applications, such as the rejection of monovalent ions and cations [63]. In addition, many studies have reported that the rejection of small, uncharged organic compounds, such as urea, methanol and formaldehyde, can also be difficult to achieve with RO or NF membranes [71]. A narrower pore-size distribution allows better overall rejection and more predictable separation performance [71].

The non-uniform, poor alignment and discontinuous nature of the pores in traditional RO and NF membranes lead to lowered water fluxes [93]. The lower fluxes require more membrane surface area and/or higher pressures to assess the effect of pore size for the permeability and rejection of solutes. This results in lower process efficiencies and higher costs due to increased energy consumption. New membrane materials with more controlled pore nanostructures may allow for better and more predictable rejections, higher permeability and lower costs.

1.3.2 Chlorine degradation

Commercial RO membranes are typically based on poly-aryl amide and suffer from low resistance to chlorine (in the form of hypochlorite ClO^-, ion). Chlorine is added to municipal water and desalination processes for disinfection purposes [93, 94]. Extra chemicals and processing are often required to prevent chlorine exposure to the membrane. This results in a much more complex and expensive system that is difficult to implement. Chlorine concentrations as low as 0.1 ppm initially reduce the flux of the membrane and, over time, reduce its ability to reject salts [93, 98]. Poly-aryl amide TFC membranes are chemically modified by the chlorination of the aromatic rings and amide linkages [93, 98]. Whereas the mechanism for this reaction is not well understood, it eventually leads to the degradation of the polymer matrix and a reduction in rejection. Chlorine degradation is a limiting factor in the lifespan of RO and NF membranes.

1.3.3 Biological/protein fouling

Most UF membranes are easily fouled by biological contaminants in water and demand constant cleaning and/or replacement [96, 99]. Biomacromolecules and other organic compounds in water can adsorb onto the surface of a membrane [95, 100]. This generates a reduction in water flux [101]. Bacteria and micro-organisms can then expand and build on the membrane surface, resulting in further loss of flux.

There are specific fouling mechanisms used for a number of relevant aqueous solution separation processes, including proteins and other bio-organic solutes (e.g. dialysis, breakwater purification, membrane bioreactors and bioseparations). The porous polymer membranes used in these water-purification operations are exposed to high concentrations of proteins. Adsorption and accumulation or collection of proteins on the membrane surface reduce water flux and can limit the membrane's useable lifetime [102-104]. To overcome difficulties associated with protein fouling, a number of studies have been carried out to evaluate the surface chemistries that intrinsically resist the non-specific adsorption of proteins [105-108]. For example, a category of poly (ethylene glycol) (PEG)-based substances has been labelled protein resistant in the form of blended polymers, copolymers, grafted polymers and crosslinked films [107, 109]. However, crosslinked or chemical modifications by PEG or other materials have not been used at the industrial scale. This may be for several reasons, including that (1) the adsorption capacity might be reduced by increases in crosslinking [110-

112]; (2) crosslinking may lead to changes in the physical properties and thermal transition characteristics of the polymer [112, 113]; (3) the crosslinking agent has lower swelling capacities, has a strong effect on the sturdiness of the materials and reduces polymer chain flexibility [112]; (4) increasing the crosslinking density reduces the diffusion of pollutants into the polymer matrix; and (5) the number of free function groups (i.e. amine groups) can be decreased by crosslinking agents.

Researchers are continuously devising and fabricating new suitable membranes with narrow pore size, uniform pore distribution and resistance to chlorine degradation and biological fouling while maintaining a good combination of flux and solute rejection capacity. These monodisperse pore size membranes include track-etched [114], gold nanotube [115-117], thermotropic liquid crystal [118, 119], molecular square [120] and organic lithography-based [121, 122]. Unfortunately, these technologies suffer from a combination of high cost, low porosity, low flux, impractical processing and/or low solute rejections, which make them less effective. However, the following alternative technology for membrane fabrication seems more promising.

1. 4 Materials Used for Water Filtration Membranes

As previously mentioned, traditional membrane technology for water filtration is well developed and has been successful. However, it is difficult to control membrane pore size and pore-size distribution due to material properties and fabrication processes. The development of new membrane materials or new membrane types with narrower pore-size distributions, resistance to chlorine degradation and/or biological fouling, with good combinations of flux and rejection would be a step forward in meeting the increasing demand for clean water [8].

1.4.1 Polymer membranes

The chlorine degradation process can be substantially reduced on polyamide polymer membranes of asymmetric hollow-fibres treated with hypochlorous acid [123]. Forming a thin polyamide film on the porous surface of a polysulphone-supported membrane through an interfacial reaction between trimesoyl chloride (TMS) and *m*-phenylenediamine (MPD) can result in further improvement. Polysulphone membranes are more durable than sulphur-containing hydrophobic thermoplastic membranes and are not susceptible to chlorination [124]. However, the desalination process is slowed in these membranes due to their hydrophobic natures. This problem was partially addressed by reducing the hydrophobicity

without affecting other chemical and physical properties of the membrane. This was done by attaching additional charged sulfonic acid groups to the polysulphone membrane. The sulfonic acid groups can be co-grafted onto the polysulfonated membrane by radiation or chemical means. Other improvements to the membrane included simultaneous polymerisations of a disulphonate monomer containing two hydrophilic sulfonic acid groups and another type of monomer, such as the polyamide polymer. The hydrophobic and hydrophilic characteristics of this membrane can be controlled by altering the number of charged hydrophilic sulfonic acid groups on the polymer chain. Grafting hydrophilic groups onto polymer chains increases the wet-ability of the membrane, creating a reduced pore size in the polymer matrix. As a route to decrease biofouling and other impurities, an ultraviolet (UV)-assisted photochemical graft-polymerisation technique was used to produce a modified polyethersulphone (PES) UF membrane, which reduced interaction with natural organic matter [125, 126]. Similarly, an NF membrane was developed by UV photografting of sodium *p*-styrene sulphone [125, 126]. A polyacrylamide membrane was further enhanced by several researchers through radiation-induced graft polymerisation of acryl amide on low-density polyethylene [127]. An RO membrane was also developed by post-radiation grafting of vinyl acetate onto low-density polyethylene films [128].

Occasionally, polymers of different backbones and functional groups may contribute excellent characteristics to membranes. Thus, block copolymers can be used as tools to produce nanoscopic materials. In some cases, the differences in the polymer chemistries between the blocks cause microphase separations where the polymer self-organises into micellar, columnar, lamellar and/or bicontinuous cubic structures with uniform and distinct spacing between features [121, 129, 130]. Several researchers have used the self-assembly properties of block copolymers to form membranes with distinct and relatively monodisperse pores [131-134]. For example, a polystyrene-*block*-poly (methyl methacrylate) (PMMA) copolymer (PS-*b*-PMMA) was used to form a crosslinked polymer membrane with regular 17-nm diameter cylindrical pores. After annealing the copolymer to 170°C for 60 h under vacuum, the PMMA block phase segregated into regular columns perpendicular to the membrane surface while the polystyrene block surrounded these domains [3]. Subsequently, UV light was used to crosslink the polystyrene block sections to provide mechanical strength and prevent membrane swelling upon exposure to solvents. Uniform columnar pores, devoid of any polymeric materials, were then made by removing the PMMA block via irradiation

with UV light (254 nm) and washing with acetic acid. The pore diameter was reduced by chemically grafting short poly (ethylene oxide) (PEO) to the inner pore walls. Water-transport studies demonstrated that the membrane could remove ions based on size exclusion [132]. In a similar study, a polystyrene-*block*-poly (lactic acid) (PS-*b*-PLA) polymer was used to form membranes with aligned columnar pores with diameters of 20 nm. Similarly, a polystyrene-*block*-poly (4-vinylpyridine) (PS-*b*-PVP) copolymer was mixed with a low-molecular-weight molecule, 2-(4'-hydroxybenzeneazo) benzoic acid (HBAB). The HBAB and poly (vinylpyridine) (PVP) block phase separated into columnar domains surrounded by the polystyrene block. The HBAB was then removed from the columnar domains by a water wash. The resulting membrane contained columnar pores with diameters of 8 nm. Unfortunately, no water-filtration study was conducted on this material [135]. In a similar study, PS-*b*-PMMA was mixed with PMMA to form 10–40-nm diameter pores. Water-filtration studies demonstrated that smaller protein molecules passing through this material allowed bovine serum albumin (BSA) while larger viruses were retained.

Block copolymers are a promising platform for water-filtration membranes with relatively monodisperse pores because pore morphology and size can be controlled by changing block sizes, block chemistries and a variety of processing conditions, allowing for a high degree of customisability in membrane performance. Unfortunately, the pores sizes are too large to perform separations for RO and NF applications. In most cases, it is not possible to obtain pore sizes below 10 nm. This makes block copolymer membranes unsuitable for RO and NF applications.

1.4.2 Thin-film composite (TFC) membranes

TFC can be used to fabricate polymer membranes. Interfacial polymerisation is a process wherein a rich porous membrane, such as a polysulphone membrane, is coated with a monomer or polymer, followed by a reaction with a crosslinking agent that leads to the formation of a crosslinked high-density polymer layer at the solution interface [136]. TFC membranes are constructed using an interfacial-condensation polymerisation technique to cast an ultrathin film of polymer onto a highly porous UF membrane [92]. The interfacial-condensation polymerisation conventionally appears between a diamine, such as MPD, and a multi-functional acid chloride, such as trimethyl chloride. Typically, the diamine is dissolved in a solvent (usually water) and then coated onto the UF membrane. The diamine-coated

membrane is then immersed in a multi-functional acid chloride solution using a solvent hexane that is immiscible with the diamine solution [137]. A condensation or step-growth polymerisation reaction between the diamine and multi-functional acid chloride occurs only at the solvent–solvent interface near the surface of the membrane, resulting in a highly crosslinked polyamide film [137, 138]. This thin film, reinforced by the UF membrane or active layer, supplies the transport properties of the TFC membrane [137]. Compared to the asymmetric membranes, these thin, highly crosslinked polymer membranes demonstrate higher water fluxes and selectivity. This is because the surface layers of composite membranes are thinner than asymmetric membranes. The surface layer comprising crosslinked aromatic polyamide and supported by a polysulphone sublayer is one of the most widely used TFC membranes.

1.4.3 Zeolite membranes

Generally, crystalline aluminosilicate materials with highly ordered three-dimensional (3-D) pores are used to prepare zeolite membranes with pore sizes from <1 nm to several nanometers in diameter, depending on composition and processing conditions. These membranes have been used extensively for gas and vapour separations, catalysis and chemical sensing processes [139]. In the past 5 years, they have also been tested for water filtration [140, 141]. Zeolite membranes are promising because of their monodisperse and tunable pore sizes. The pore size can be varied by changing the ratio of aluminium and silicon in the zeolite. This system is highly customisable (in terms of pore size and charge control) and allows the manufacture of membranes for precise separation applications. Zeolite membranes have additional properties to overcome problems that plague traditional polymer membranes. For example, zeolites are stable in a wider range of solvents and at higher temperatures and are generally more inert to microbiological degradation than are conventional polymer membranes [142]. Interest in zeolites as water-filtration membranes gained momentum after computer modelling studies, which demonstrated that a zeolite could potentially reject Na^+ ions completely in an aqueous solution [143]. More recently, initial experimental research on zeolite membranes showed their water-filtration capabilities. In an early example, a zeolite (pore size 0.56 nm) was coated on a 28-mm diameter porous aluminium substrate and was used to filter 0.1-M NaCl solution, rejecting 77% of the Na^+ ions with a water flux of 0.12 $kgm^{-2}\ h^{-1}$ [144]. Using a different processing procedure, an MFI with the same composition

had a rejection rate of 21.6%, with a flux of 0.162 kgm^{-2} h^{-1}. More recently, an MFI-type zeolite membrane (MFI-ZM) improved this performance with a rejection rate of 98% ions (solutes) at a water flux of ~0.34 kg m^{-2} h^{-1} [145]. Other studies have demonstrated that organic solutes can also be removed from water using MFI-ZMs. For example, 99.5% of toluene was rejected with a flux of 0.03 kg m^{-2} h^{-1} and a transmembrane pressure of 2.76 MPa [140]. Despite these promising results, several issues related to these membranes, including low flux compared to current NF and RO membranes, make this technology less useable. Processing zeolite membranes with minimal defects is problematic. In addition, their long-term stability in an RO process is questionable because they are susceptible to degradation under slightly acidic aqueous conditions [146].

1.4.4 Polymerisable lyotropic liquid crystals (LLCs)

LLCs, which are used in the preparation of nonporous membranes [147-150], are composed of amphiphilic (surfactant) molecules that self-organise into ordered, phase-separated assemblies (aqueous and organic regions) creating uniform aqueous domains in the <1–5 nm range when mixed with a solvent, such as water [151]. The geometry of the resulting LLC phase depends on several factors, including composition, temperature and pressure.

Recently, LLCs demonstrated an excellent improvement in the separation process through the S–D and porous transport mechanisms. The amphiphilic characteristics of these molecules play an important role in enhancing phase separation. This is achieved through the production of tails with fused hydrophobic areas and hydrophilic head-groups and characterise interfaces of ordered domains enclosing the water component, as shown in Figure 1.9.

Separate aggregate structures of LLCs are usually made by surfactants and lipids (e.g. vesicles, microtubules) that lack periodic order and can be extended to include water areas with uniform feature sizes in the range of 1–10 nm [152]. LLC phases are normally categorised according to the packing symmetry of the ordered domains, termed as lamellar (L), hexagonal (H), bicontinuous cubic (Q or V) and discontinuous cubic (I) phases. In addition, LLC phases are classified as water excessive (type I) and water deficient (type II); all LLC phases are presented in Figure 1.9. LLCs were improved by crosslinking and could be useful as NF membranes. The LLC membrane (supported H_{II} membrane, Fig. 6) was fabricated using LLC, which was cast and supported by a commercial ultraporous

polysulphone to increase the mechanical strength and viable water permeation. These membranes completely rejected most molecules larger than 1 diameter of nanopore (1.2 nm). The salt-rejection performance was 7–37%. Moreover, bicontinuous cubic (QI) phase membranes were developed by crosslinking the LLC monomer. QI membranes were evaluated using a dead-end NF system under 400 psi applied pressure and 2,000 ppm aqueous feed solutions. As a result, the membrane exhibited an ability to transport water and reject salts (NaCl, $MgCl_2$ and $CaCl_2$) from feed solution, as shown in Table 3.

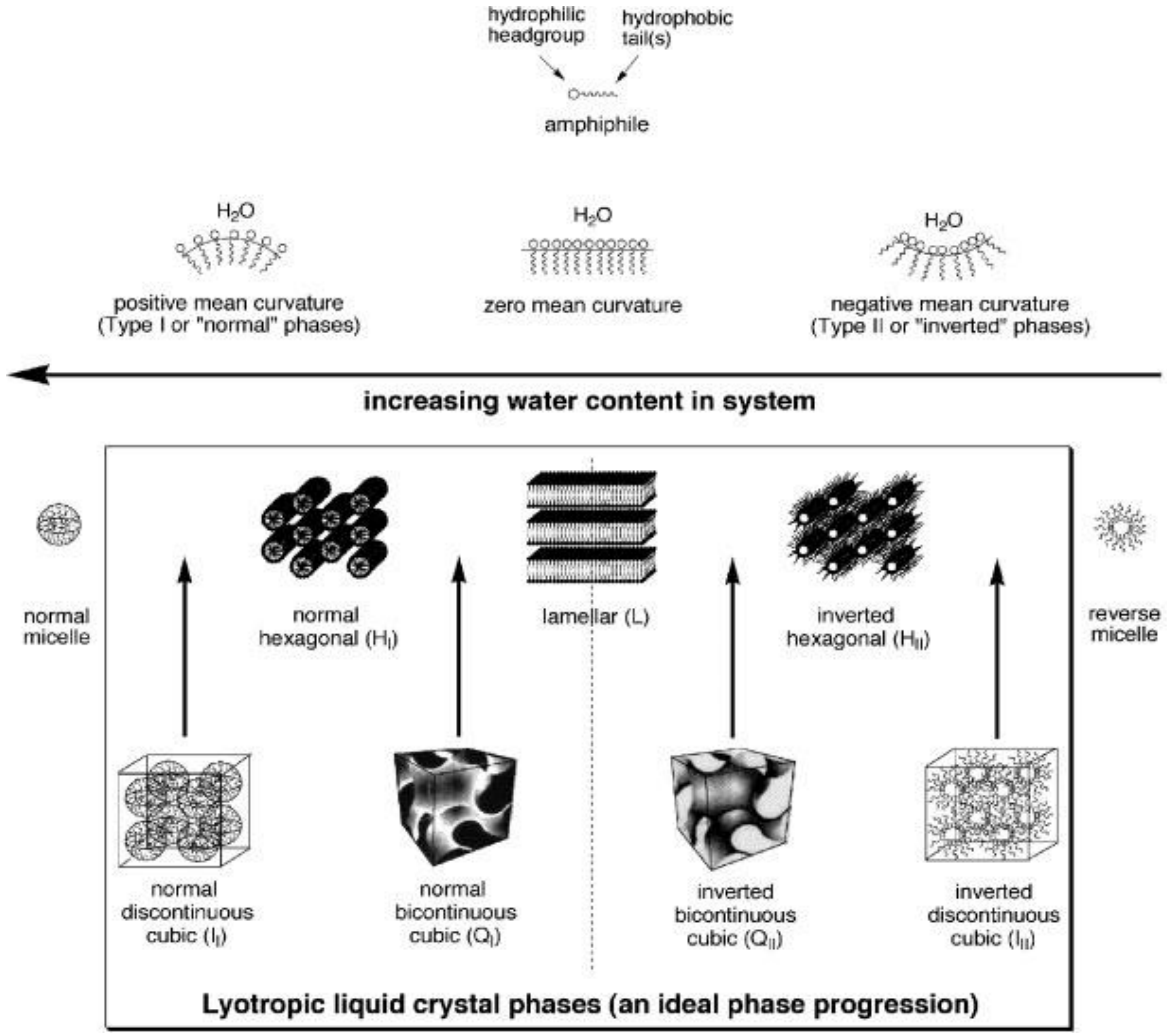

Figure1.9. LLC phase progression and common LLC phase designations (Reproduced from reference [152]).

Table 3. Water desalination and NF performance of the QI membranes of dead-end method (400 psi; 0.45-mm pre-filtered 2,000 ppm [152].

Solute	Diameter (nm)	Pressure (psi)	Rejection (%)	Flux $L.M^{-2}\,h^{-1}$
NaCl	$Cl^{-}_{(aq)}$ 0.66 $Na^{+}_{(aq)}$ 0.72	400	95–99.9	$5.1 \pm 0.1 \times 10^{-2}$
$MgCl_2$	$Mg^{+2}_{(aq)}$ 0.86	400	95–99.9	$5.2 \pm 0.6 \times 10^{-2}$
$CaCl_2$	$Ca^{+2}_{(aq)}$ 0.82	400	20	$5.1 \pm 0.4 \times 10^{-2}$
Glycerin	0.36	400	53 ± 1	$5.1 \pm 0.6 \times 10^{-2}$
Ethylene glycol	0.32	400	38 ± 4	$5.2 \pm 0.1 \times 10^{-2}$

The advantages, disadvantages and preparations of different membranes and their processing systems have so far been discussed in relation to their base material compositions, including polymers, block copolymers, zeolites and LLCs. Pore sizes and pore distributions, separation efficiency and rejection of different solutes under different conditions, chlorine degradation and biological fouling have also been considered. The following section discusses membranes made in conjunction with CNTs, beginning with a description of CNTs and their unique properties.

1.4.5 Carbon nanotubes membranes

Iijima [153] discovered carbon nanotubes (CNTs) in 1991. Since then, their unique electronic, thermal, optical and mechanical properties have attracted worldwide attention for the development of a wide range of materials for various purposes [154, 155]. CNT materials can be produced using four methods that result in unique yields and purities. These are arc discharge, laser ablation, chemical vapour deposition (CVD) and high-pressure carbon monoxide (HiPco) [156]. CNTs are classified as single-walled nanotubes (SWNTs), which consist of seamless cylinders made of a single atomic layer of graphene, double-walled nanotubes (DWNTs), which contain two seamless cylinders made of two atomic layers, and multi-walled carbon nanotubes (MWNTs), which consist of several concentric nanotube shells, as shown in Figure 1.10.

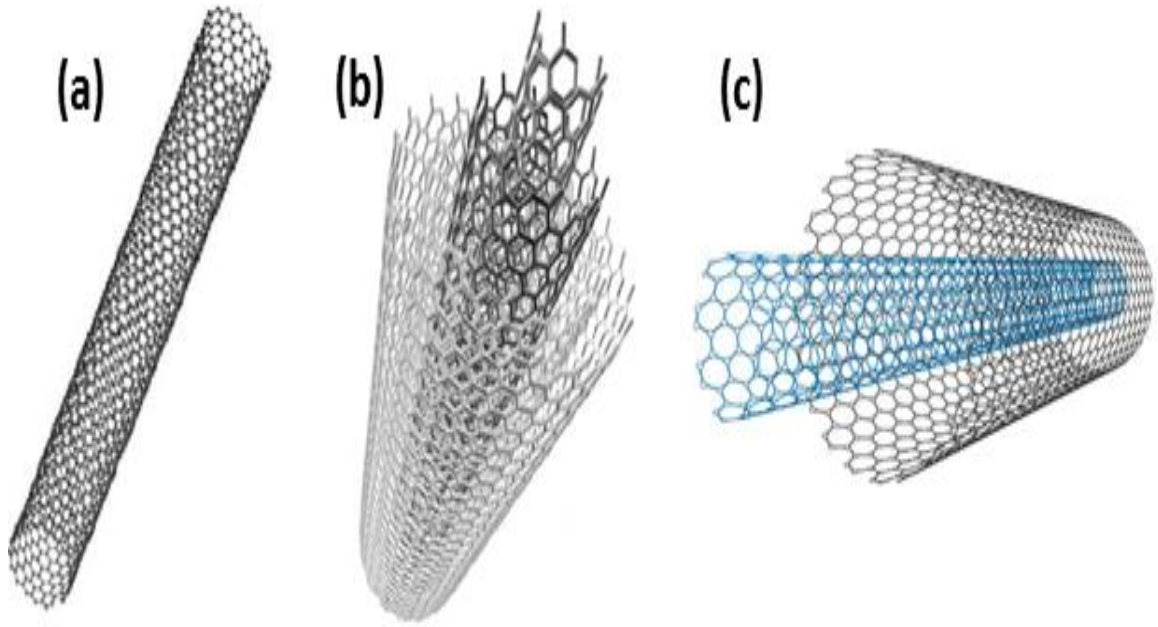

Figure1.10. Schematic illustrations of a) SWNT; b) MWNT and c) DWNT (Reproduced from reference [157, 158]).

The diameter of an SWNT ranges 0.7–5 nm, though most SWNTs have a diameter of <2 nm. SWNTs are present in various geometric forms (chirality and diameter) that determine their electronic properties. The usual way to define the chirality of a single CNT cylinder is to use the chiral vector of the H network of a graphene sheet (Fig. 1.11) [159]. The chiral vector is defined as

$$\hat{C}_h = n\,\hat{a}_1 + m\,\hat{a}_2 \qquad (1)$$

where $\hat{a}_1$ and $\hat{a}_2$ are unit vectors, and n and m are integers. There are three types of cylinders: 1) armchair-form cylinders, $m = n$; 2) zigzag when '$n = 0$'; and 3) chiral, all other values of n and m as presented in Figure 1.12.

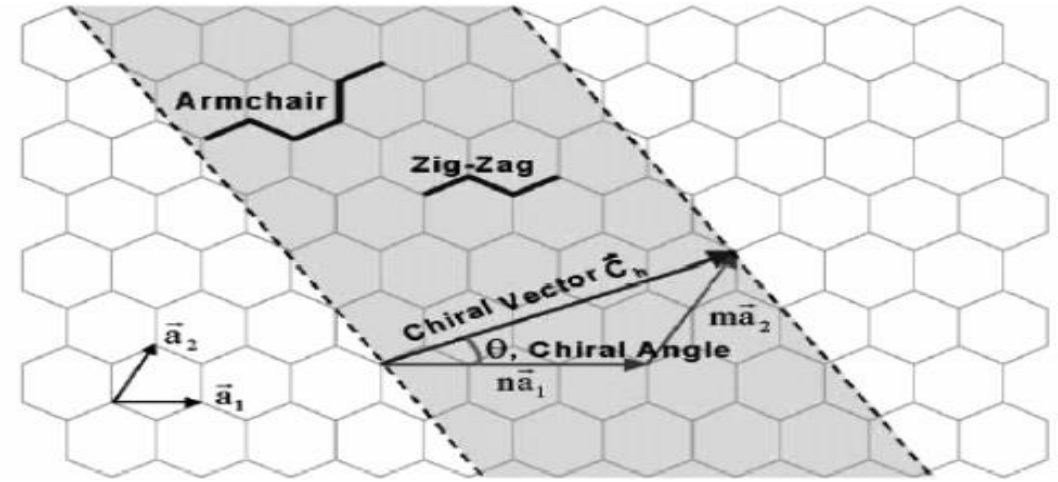

Figure1.11. Schematic diagram demonstrating how an H sheet of graphene is 'rolled' to form a CNT; the rolling presented in the diagram will form a (3,2) nanotube (Reproduced from reference [160]).

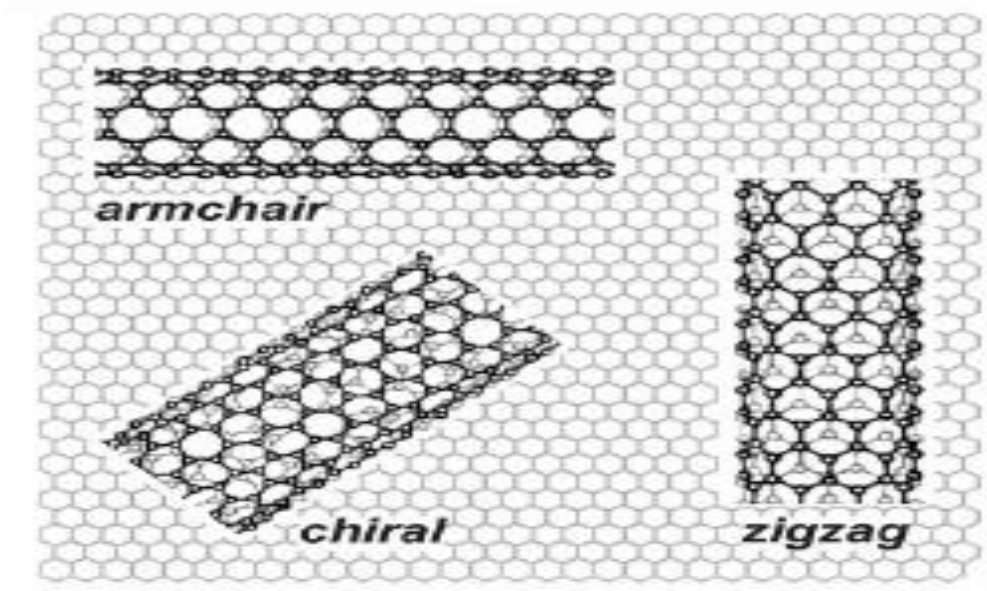

Figure1.12. Molecular models of SWNTs offering various chiralities: armchair configuration; zigzag arrangement and chiral conformation (Reproduced from reference [157]).

The mechanical character originates in the strength of the C-C bonds in the graphene sheets and is about ~53 GPa for SWNT [154, 161]. This is evident in Young's moduli for SWNTs up to 1470 GPa, whereas MWNTs reach as high as 950 GPa.

Small-diameter CNTs, such as SWNTs, are also considered superconductors at low temperatures. For example, a 1.4-nm-diameter SWNT exhibits a transition temperature at

0.55 K [154, 162], whereas a 0.5-nm-diameter SWNT harvested in zeolites exhibits a transition temperature at 5 K [154, 163]. MWNTs are also excellent thermal conductors, displaying values greater than 3000 W/m.K, which is higher than both natural diamond and planes of graphite (2000 W/m.K) at room temperature but lower than SWNTs (6600 W/m.K) [164]. The latter value is close to the thermal conductivity value of a single layer of graphene. The surface area of individual CNTs and bundles is established by considering the number of walls in the bundle, tube diameter and/or the number of tubes in the bundle. For example, the surface area can range 50–1315 m^2/g of SWNT for a very large bundle [165]. The surface area of SWNT is usually higher than that of MWNT; that is, the total surface area of SWNTs (as-grown SWNTs) are from 400–900 m^2/g, whereas the surface-area values for MWNTs are from 200–400 m^2/g [166, 167].

These distinctive properties make CNTs extremely useful for many applications [154, 168]. Examples include field-emission displays, high strength and conductive composites, sensors [169, 170], composites [171], catalytic supports [172] and membrane materials [173, 174]. More specifically, CNTs with core diameters as small as 0.4 nm [175, 176] also have potential for use as nanopores in membrane materials [177, 178]. This suggests that these nanotubes make ideal membranes because they display unprecedented selectivity and flux properties rarely seen in other materials. These properties can be further enhanced if CNT materials can be functionalised.

1.4.5.1 Functionalisation of CNTs

CNTs generally exist in agglomerated form due to van der Waals interactions and are consequently difficult to disperse in aqueous polymer solutions. Functionalisation of CNT is one of the most effective methods for stabilising CNTs in a solution [179]. CNTs can be functionalised through covalent or non-covalent bonding.

1.4.5.1.1 Non-covalent functionalisation

Non-covalent functionalisation of CNTs does not make or break bonds, but involves van der Waals interactions. Examples of non-covalent functionalisation of CNTs using surfactants, biomacromolecules and polymers are listed in Table 4. The non-ionic surfactant octylphenol ethoxylate (Triton X-100 [Trix]) is a commonly used surfactant for dispersing SWNT and MWNT. Trix produces a stable dispersion solution of CNTs due to π-stack on the surface of the CNTs, as illustrated in Figure 1.13[179-181].

Table 4. Functionalisation of CNTs by non-covalent bonding.

Polymer or surfactant	CNT type	Preparation method	Reference
1: Surfactant			
Cationic(CTAB)	SWNT	Microemulsion	[179]
Cationic (CTAB)	SWNT	Ultrasonication	[179, 180]
Cationic (CTVB)	SWNT	Sonication	[179]
Cationic (MATMAC)	MWNT	Emulsion polymerisation	[179]
Anionic (SDS)	MWNT	Ultrasonication	[179]
Anionic (SDBS)	SWNT	Ultrasonication	[179]
Anionic (SDBS)	SWNT	Bath sonication	[179]
Non-ionic (Triton X-100)	MWNT & SWNT	Ultrasonication	[179-181]
B-cyclodextrin sulphated sodium salt *meso-tetra*(4-sulfonatophenyl)	SWNT	Ultrasonication	[179]
Porphyrin dihydrogen chloride	SWNT	Ultrasonication	[179]
Phthalocyanine tetrasulfonic acid			
2: Biomacromolecules			
Proteins/DNA	SWNT	Ultrasonication	[179]
Glucose (Dextran)	SWNT	Mobilisation Dialysis	[179]
β-1,3-glucans	SWNT	Electroactive interaction	[179]
chitosan	SWNT	Ultrasonication	[180]
Gellan gum	SWNT	Ultrasonication	[180]
Carrageenan	SWNT & MWNT	Ultrasonication	[182]
Lysozume	SWNT	Ultrasonication	[180]
Enzymes	SWNT	Ultrasonication	[180]
3: Polymers			
Poly (4-vinyl pyridine)	SWNT	Ultrasonication	[179]
Poly (phenyl acetylene)	MWNT	Sol–gel chemistry	[179]
Poly (m-phenylenevinylene-co2,5-dioctoxy-p phenylenevinylene acid)	MWNT & SWNT	Solution mixing	[179]

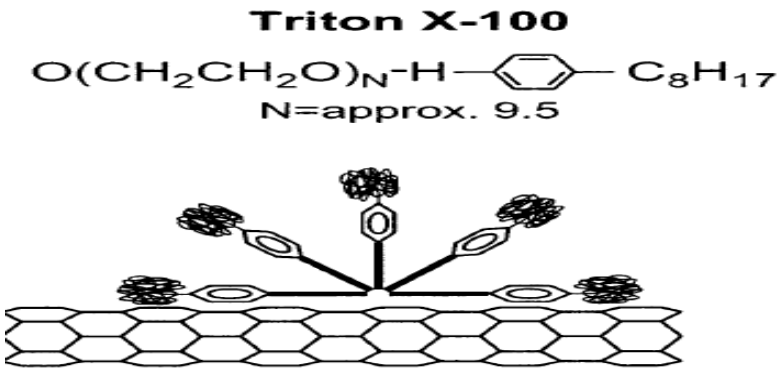

Figure1.13. Schematic representation of how surfactants may adsorb onto the nanotube surface (Reproduced from reference [183]).

Polysaccharide gellan gum is a good material to disperse CNTs for non-covalent functionalisation because it can do so even at concentrations as low as 0.0001% (w/v). Self-supporting optically transparent films are formed and are highly sensitive to water vapour [184]. Polysaccharide chitosan is also used to prepare non-covalent functionalisation because it conveniently separates SWNTs by sizes, since SWNTs are the smallest tubes and easily dispersed in aqueous media [185]. Fubing Peng et al. [186] reported that the polymer chain of chitosan can be wrapped along the nanotube axis, which substantially enhances the distribution of CNT in chitosan aqueous solution, as shown Figure 1.14 chitosan is discussed in detail later in section 1.4.6 .

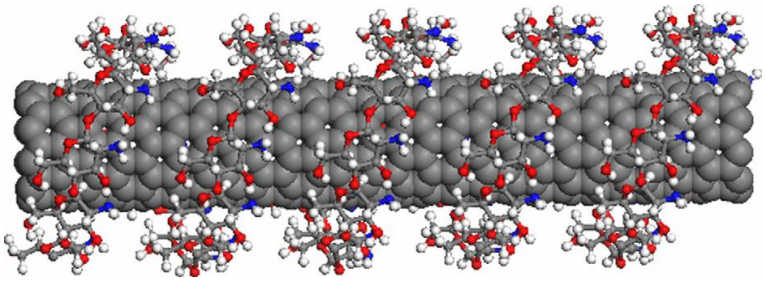

Figure1.14. CNT wrapping by a polymer chain of chitosan (Reproduced from reference [186]).

1.4.5.1.2 Covalent functionalisation of CNTs

In addition, a CNT can be functionalised or its surface modified by attaching various functional groups, such as -COOH, –COH, NH_2 and hydroxyl (–OH), onto the sidewalls

and/or terminal ends of CNTs by covalent bonds [187]. The carboxylic acid groups are widely used on the nanotube surfaces in a variety of chemical reactions. CNTs functionalised with the –COOH and –OH groups allow the attachment of both organic and inorganic materials, which is a key in the stabilisation of nanotubes. Moreover, carboxylic groups and other oxygen-bearing groups, such as hydroxyl, carbonyl ester and nitro, can also be directly attached to ends and/or defect sites in the sidewalls of CNTs using an oxidative treatment process, as shown in Figure 1.15.

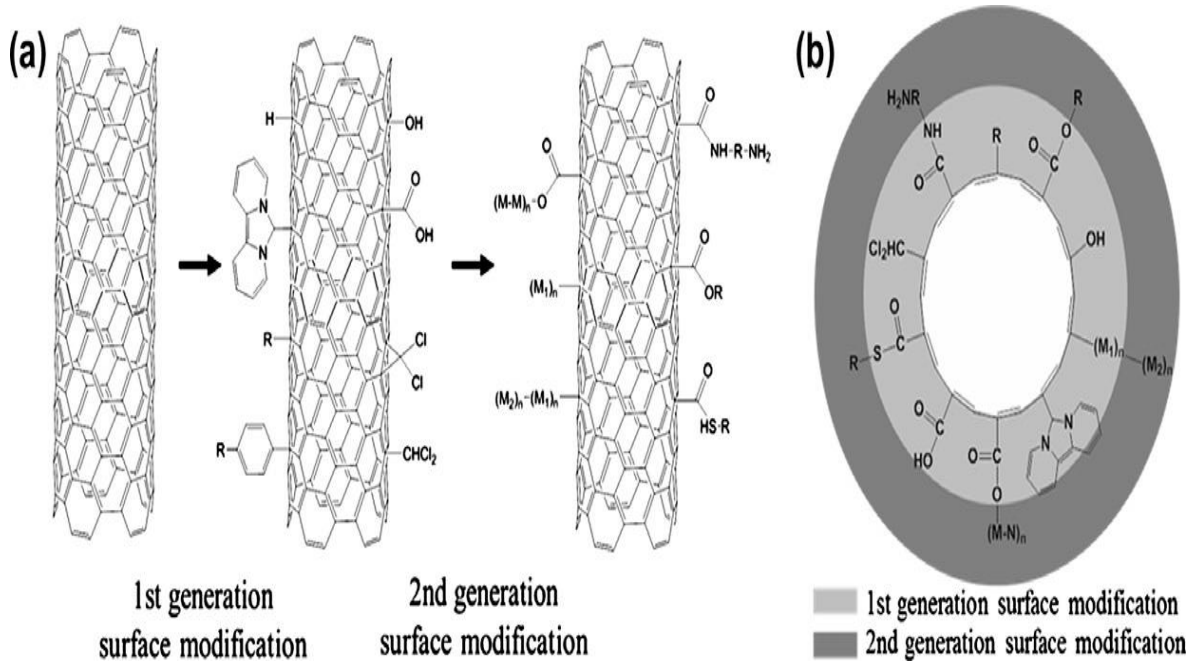

Figure1.15. Schematic diagram of functional groups or modifier molecules that are attached to CNTs by covalent bonds; these are shown from a) side view and b) top view (Reproduced from reference [187]).

Some polymers can be hooked to the CNT surface through in situ polymerisation of monomeric polymers in the presence of reactive CNTs or CNT-supported initiators. The resulting polymer-CNT composites have high grafting density and can graft many polymers. Gao et al. [188] reported the functionalisation of MWNTs with a hydrophilic polymer glycerin monomethacrylate (GMA) using the grafting technique. The MWNTs were treated with thionyl chloride, glycol and 2 bromo-2-methylpropionyl bromide to create MWNT-Br macroinitiators to create atom-transfer radical polymerisation (ATRP) of GMA, as demonstrated in Figure 1.16.

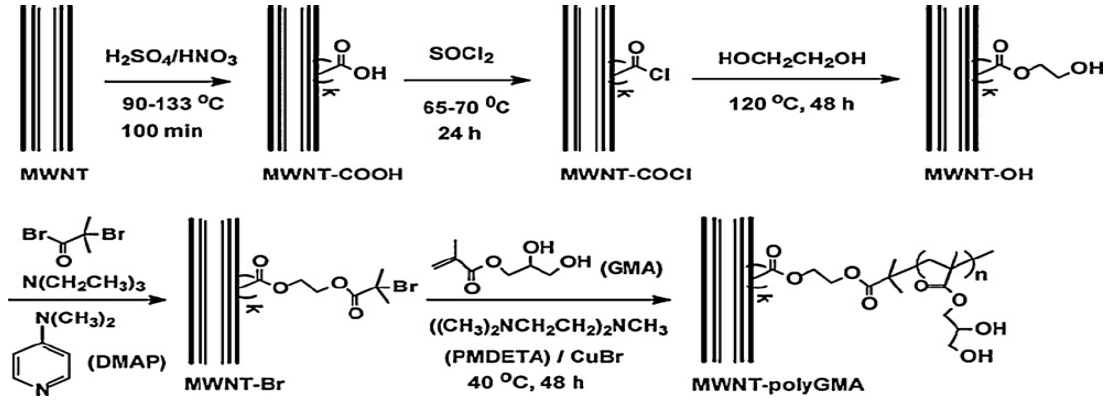

Figure1.16. Covalent functionalisation of MWNTs with poly (glycerin monomethacrylate) (polyGMA) by ATRP and esterification of the hydroxyl groups of MWNT-polyGMA by ATRP (Reproduced from reference [179]).

1.4.5.2 Non-aligned CNTs BP membranes

A thin sheet of non-aligned CNTs, called buckypaper (BP), are normally prepared by filtering a dispersion of CNTs [189]. These are often fairly disordered because of the randomly dispersed nature of the CNT solution and the presence of van der Waals interactions [190], which can 'glue' the CNT aggregates together, as shown in Figure 1.17.

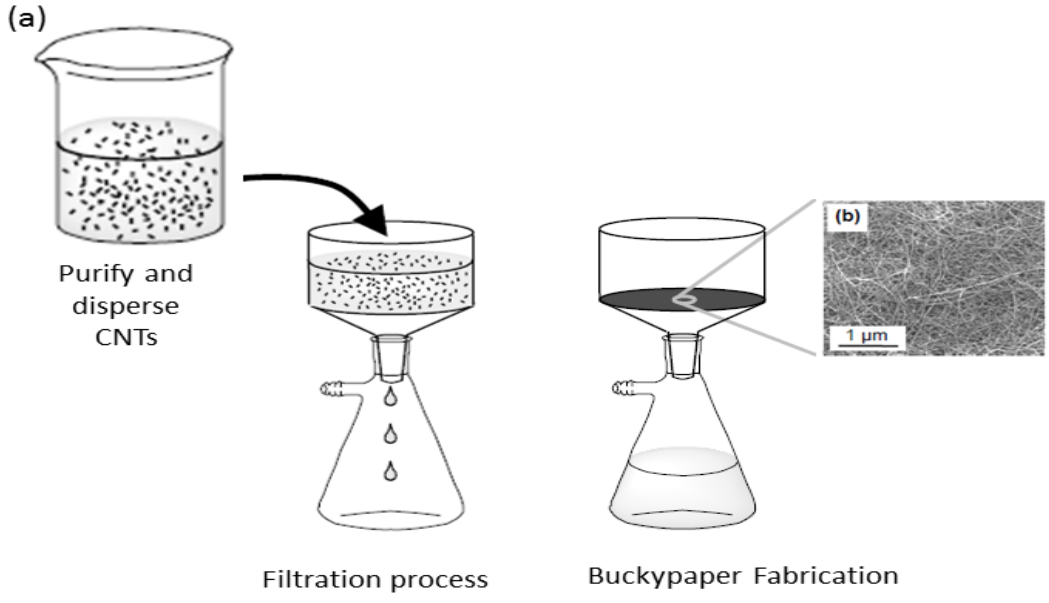

Figure1.17. BP membrane preparation process: b) SEM image of BP membrane surfaces (Reproduced from reference [191]).

As mentioned, BPs have unique thermal, optical, electrical and mechanical properties that enable the use of CNTs (BP) in the development of materials including cold field-emission cathodes, strain sensors, nano-actuators, antimicrobial coatings and radio-frequency filters [189, 190, 192-197]. The sizes of the BP pores are wholly dependent on the arrangements and sizes of the CNTs. However, BPs can absorb 60–70% of their volume in gases and liquids because of intrabundle pores and interbundle gaps. This porosity, coupled with high strength, rigidity and exceptional flow rates, suggests that BPs could make outstanding filter membranes [194]. The porosities were reported at 91% for fine and 87% for coarse CNTs through helium pycnometer calculations. Specific surface area, as reported by Cinke et al., was as high as 1587 m^2/g for BPs made from SWNTs [198]. The high surface area was attributed to the preparation method, which involved two-way steps of the purification process. It also revealed that CNTs were de-bundled and could be purified.

Transporting gas through BPs is highly dependent on pressure. At low pressures, BPs have been proven to maintain their strength and filtration abilities over time when transporting liquids. This is particularly useful for removing bacteria from water for extended periods.

Polysaccharides and deoxyribonucleic acid (DNA) are also effective dispersants because of their amphiphilic molecular structures [199]. For example, gellan gum (an anionic polysaccharide) and chitosan (cationic polysaccharides) were employed as dispersants to improve the mechanical properties of BPs and can thus be used for filtration under a wide range of temperatures, pressures and flow rates. BPs are also useful in many other applications involving the processes of filtration, membrane distillation (MD) and water purification. BP membranes have many physical and surface properties that favour the MD process, for example, BP membranes demonstrated a high degree of contact angle (~113°), greater porosities (90%) and a thermal conductivity of 2.7 kW/m^2 h [200]. These characteristics are superior to those of other polymeric membranes used conventionally in MD processes and are more comparable to polytetrafluorethylene (PTFE) membranes. In direct contact membrane distillation (DCMD), the CNT BP membranes demonstrated high salt (NaCl) rejection (99%) at low pressure (22.7 kPa) and a flux rate of 12 kg/m^2 h. Mechanical properties of BPs, such as Young's modulus, tensile strength and toughness, can be improved using adhesives, by polymer intercalation or by soaking in polymer solutions, such as polyvinyl pyrrolidone, polystyrene and polyvinyl alcohols [201].

1.4.5.3 Aligned CNT membranes

Membranes from aligned CNTs feature cylindrical pores across a thick, impermeable film in a structure different from BP membranes (Fig. 1.18).

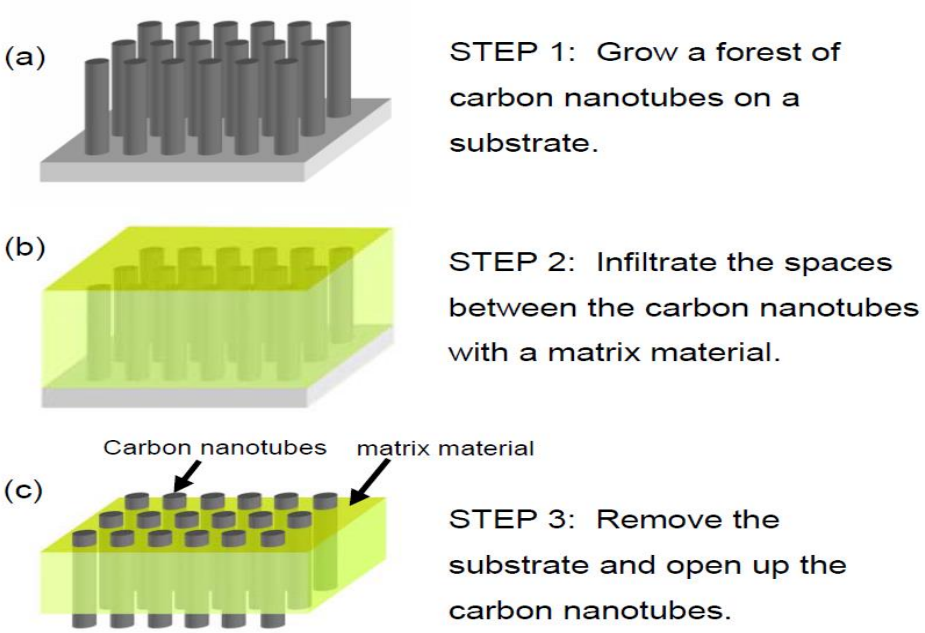

Figure1.18. Preparation of aligned CNT membrane (Reproduced from reference [191]).

MWNTs were first produced by Ren et al. as aligned bundles using an enhanced carbon-vapour-deposition method wherein a plasma generator was employed during the CNT synthesis stage [202, 203]. Newer methods no longer require the use of plasma generators to produce aligned CNTs. For example, freestanding CNT-membrane structures are easily prepared using nanoparticles of a structured transition metal catalyst on a suitable substrate material using the CVD method. In an argon-hydrogen-reducing atmosphere, this has resulted in the formation of aligned SWNT [204]. Aligned CNT membranes can also be fabricated using quartz and/or silicon as support material. Subsequently, suitable catalyst particles, such as Co or Ni, can be deposited in regular arrays to serve as growth sites for the CNTs, as shown in Figure 1.19. CVD is then employed to grow CNTs using gaseous ethylene, which is passed across the support material at a flow rate of 50–150 mL/min and decomposition at 750°C [205]. During the production process, the outermost walls of the growing nanotubes interact with one another via van der Waals forces to produce rigid bundles of tubes aligned perpendicularly to the substrate. The length of the nanotubes can be controlled to remain

within a range of 10–240 μm [206]. CNTs can be opened using oxidation with water plasma to expose their interior to gas or solvent molecules.

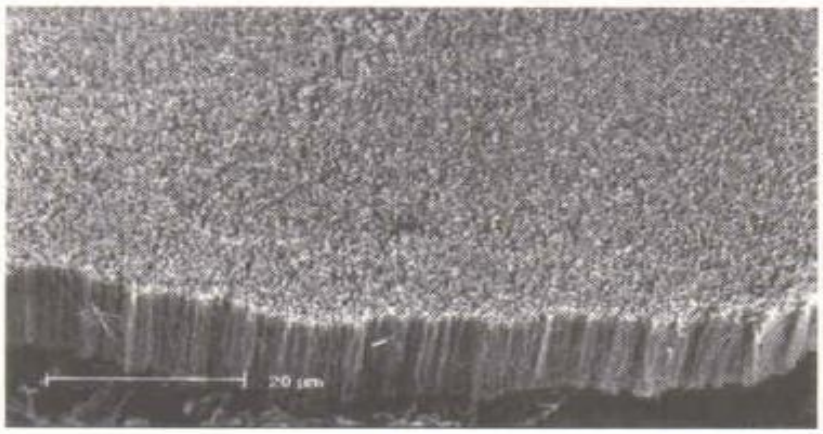

Figure1.19. SEM image of an array of MWNTs grown as a CNT forest (Reproduced from reference [154]).

Since CNTs have finite pore sizes, it should be expected that aligned CNT membranes would effectively separate particles of different sizes by allowing smaller particles to pass through and excluding particles that exceed the pore diameter. DWNT membranes have been prepared by methods similar to those described above [174]. A DWNT membrane was employed to investigate molecular transport across the membrane; specifically, $[Ru(bpy)_3]^{2+}$ ions and gold nanoparticles (diameter 2 nm). The average pore size of this membrane (1.65 ± 0.35 nm) allowed the ruthenium-bipyridyl complex ions but not the 2-nm gold particles to pass through the membrane. A similar study using an aligned MWNT membrane (average pore size 6.5 ± 0.5 nm) demonstrated that gold particles with diameters of 5 nm passed through the membrane but those with 10 nm did not.

Srivastava et al. fabricated a material with aligned MWNT that produced cylindrical pore structures with closed ends [207]. This ensured that pore size was not determined by the internal cavity size of the CNTs, but by the presence of the pores surrounded by the MWNT. The resulting membrane was tested for its ability to separate mixtures of hydrocarbons. Accordingly, a petroleum sample containing a variety of hydrocarbons of different chain lengths passed through the membrane and the materials were identified by gas chromatography. The lighter components with shorter chain lengths were readily separated from the mixtures. When combinations of naphthalene and benzene passed through, the two components were well separated; naphthalene being selectively adsorbed on the carbonaceous

material. Further testing of the membrane using water containing *Escherichia coli* bacteria and Sabin poliovirus, which is approximately 25 nm in size, demonstrated that both organisms were removed from the water passing through the membrane.

It is clear from these studies that membranes prepared from aligned CNTs may have broad applications for filtration purposes; however, these membranes have a low rejection ability of concentrated salt solutions and an inability to reject monovalent salts, such as NaC, which limits their usefulness in desalination processes [208]. In addition, the brittle and rigid silicon substrate required for the growth of aligned CNT membranes is not compatible with high surface-area water-filtration models used in industrial applications. Despite the high flux of each individual CNT, the low porosity of CNT membranes results in a low overall permeate flux. Further, processing methods for aligned CNT membranes, as described above, are complex, expensive and impractical for the production of commercially viable membranes. However, computer simulation studies in water transportation through an individual CNT was faster than expected [209]. It was proposed that the orientation of water confined within the narrow, smooth and hydrophobic CNT walls allowed the rapid transportation of water [210, 211]. Vertically aligned DWNT membranes were fabricated with pore sizes below 2 nm using a catalytic CVD process. The DWNTs were then encapsulated in a silicon nitride (Si_3N_4) matrix to fill the gaps between the pores. Finally, an etching process was used to open the ends of the DWNTs, rendering them available for water-filtration experiments. Initial water-filtration studies demonstrated that gold particles with diameters of 2 nm were completely rejected, while small gold particles with diameters of 1.3 nm were allowed to pass through. A review of recent literature and a detailed discussion of flow in nanotubes can be found in reference [212]. Water structure in nanotubes has been studied extensively using molecular-dynamics simulations [213-217]. Recently, similar DWNT membranes were functionalised with –COOH groups at the pore entrance. These membranes rejected dilute solutions (1 mM) of inorganic salts, such as $K_3Fe(CN)_6$, $K2SO_4$, $CaSO_4$, and KCl, at low pressures (0.69 bar) on a level comparable to an NF membrane (NF90, Dow Filmtec™). However, salt rejections dropped off significantly as salt concentrations were increased to 10 mM [208]. A further reduction in CNT pore diameter was required to achieve higher rejections of inorganic salts.

Kalra et al. examined water transportation through CNT (SWNT) membranes using two self-assembled chambers of hexagonally packed CNTs separated in two compartments:

one filled with pure water and the other with an aqueous solution of NaCl. The NaCl began with a concentration of 5.8 M. The sub-nanometer pores of the CNTs permitted transport of water molecules between the two compartments, but not those of hydrated Na^+ or Cl^- ions [211]. Similar processes occur in living organisms, where lipid membranes separate compartments of different osmolarity, thereby driving the transport of water and solutes through membrane-inserted pores. The resulting osmotic imbalance drives water to flow from the pure water to the salt-solution compartment, thus gradually draining the pure water compartment. The nature of specific osmotic pressure allowed not only the passing of water through molecule-sized pores but also the structural and thermodynamic aspects of water layers sandwiched among the CNT membranes [211]. The membranes, consisting of open-ended (uncapped) CNTs, appear to be useful for water-filtration with their relatively monodispersed pores.

1.4.6 Biopolymer Materials as Membranes

The natural polymers/biopolymers produced using living organisms and plants are biodegradable and suitable as membranes despite their poor mechanical characteristics. Cellulose, chitin, alginate and chitosan are examples of biopolymers that have the potential to develop membrane structures [218]. Among these biopolymers, only chitosan will be discussed in detail hereunder.

1.4.6.1 Structure and properties of chitosan

Chitosan consists of a linear polysaccharide chain containing a 1, 4-glycosidic linkage whose structure is generated by a partial deacetylation of chitin, which is a key component of crustacean shells (e.g. crab, shrimp and crawfish). Owing to partial deacetylation, repeated units of chitosan consist of glucosamine and *N*-acetylglucosamine. This molecule is of considerable significance because of its characteristic chemical and biological properties [219]. It has high reactivity because chitosan has abundant amino ($–NH_2$) and –OH functional groups in its structure, as shown in Figure 1.20.

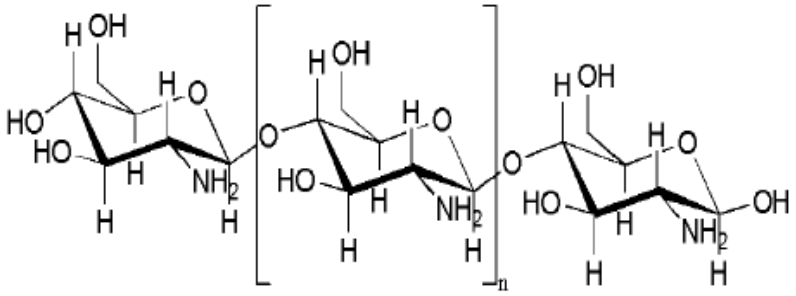

Figure1.20. Structure of fully deacetylated chitosan (Reproduced from reference [220]).

Chitosan is soluble in aqueous acids but insoluble in organic solvents [221, 222]. Therefore, when the pH is <7, the amino groups can be protonated, forming a water-soluble substance called chitosan, which is a cationic polyelectrolyte. However, chitosan's amino groups can be deprotonated and insoluble when their pH >7. The addition of various functional groups that can link themselves to chitosan through covalent bonding can reform the properties of chitosan (i.e. the degree of hydrophobicity can be altered). Similarly, chitosan can be processed into gels, films, scaffolds, beads and fibres [223].

1.4.6.2 Crosslinking chitosan

In addition to the properties of chitosan mentioned above, it has high hydrophilicity, yields increased water flow and exhibits good chelating properties with heavy metals, including lead and mercury, providing high binding affinity without adsorbing on the membrane's surface. It has anti-bacterial efficiency, which prevents biofouling and facilitates the formation of ultrathin yet strong films [110, 220, 224].

When attached to chitosan, two distinct functional groups ($–NH_2$ and –OH) facilitate the formation of crosslinking in the polymeric chain structure [225], which enhances chemical stability, mechanical strength, biocompatibility and so on. Hydrogels formed by crosslinking chitosan can be grouped into four distinct types based on structural features: 1) self-crosslinked chitosan (Fig. 1.21a); 2) hybrid polymer network (HPN) (Fig. 1.21b); 3) semi-interpenetrating polymer network (IPN) (Fig. 1.21c); and 4) ionic crosslinking (Fig. 1.21d). Highly crosslinked chitosan is very stable and insoluble in an acidic environment. This means that modified chitosan polymer can be used as an adsorbent in a low-pH environment. The crystalline nature of chitosan can also be altered to improve its sorption ability.

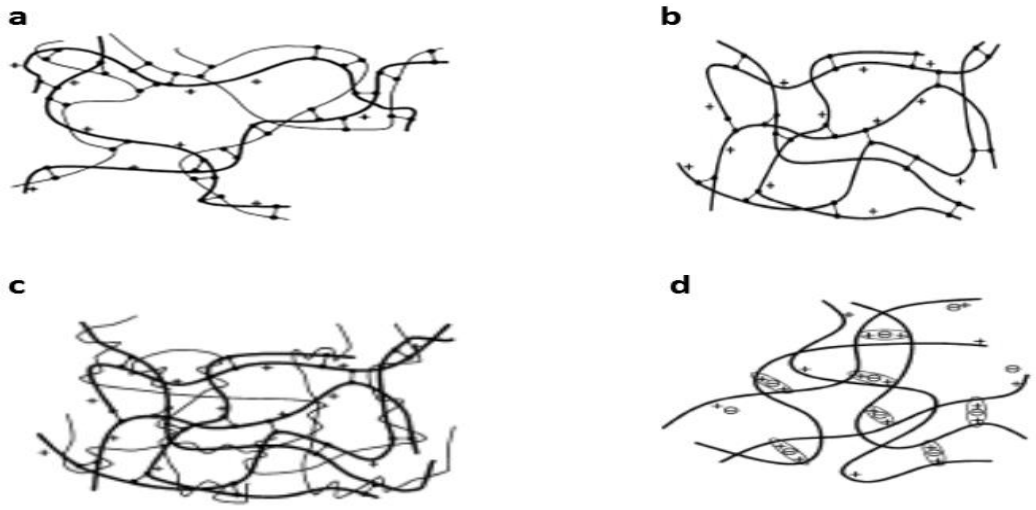

Figure1.21. Structure of typical chitosan hydrogels produced by a) self-crosslinking; b) HPN; c) semi-interpenetrating network; and d) ionic crosslinking; ⊷ covalent crosslinker; + positive charge of chitosan; ▬ chitosan; ——— additional polymer; Θ charge ionic crosslinked; ⬭ ionic interaction (Reproduced from reference [220]).

Bio-functional ethylene glycol-diglycidyl ether (EGDE) was grafted/crosslinked to chitosan by heat treatment [226]. Its utilisation is generally determined by the reactivity of two epoxide groups with free amine groups in chitosan. EGDE-modified chitosan prevents swelling and delamination of the coating layer used in composite membranes. Aldehyde groups interact with chitosan's amino groups to form imine bonds [227, 228]. This helps resonate double-adjacent ethylenic bonds through a Schiff-based reaction and is associated with the hydroxyl group of chitosan.

Chitosan was first crosslinked with glutaraldehyde, and MWNTs were then introduced into the reaction [229, 230] to produce a crosslinked chitosan-MWNT composite. Two principal hindrances limit ideal CNT dispersion in the chitosan polymer matrix: 1) aggregation, which makes manipulation and incorporation in the polymeric matrix difficult and 2) its hydrophobic nature, which has a considerable effect on membrane permeability. CNT can be modified by hydrophilic characteristics (e.g. of chitosan), which can be introduced by providing good membrane selectivity features (Fig. 1.22). Significant improvement in CNT dispersion and solubility can be achieved via chitosan based on its emulsifying properties. The lack of solubility of CNTs in aqueous solution is related to its hydrophobicity solubility, which can be enhanced by acid treatment. This results in the functionalisation of the CNT surface with the –OH and –COOH groups, which are

hydrophilic in nature. Three types of functional groups (amino, primary and secondary) and hydroxyl embedded in the glucosamine matrix are present in the chitosan, which is a hydrophilic biopolymer with the ability to attach or interact with CNT through carboxylic and hydroxyl groups present in acid-treated CNT. The strength and reduction of damage to CNT can be reduced by attaching chitosan to CNT.

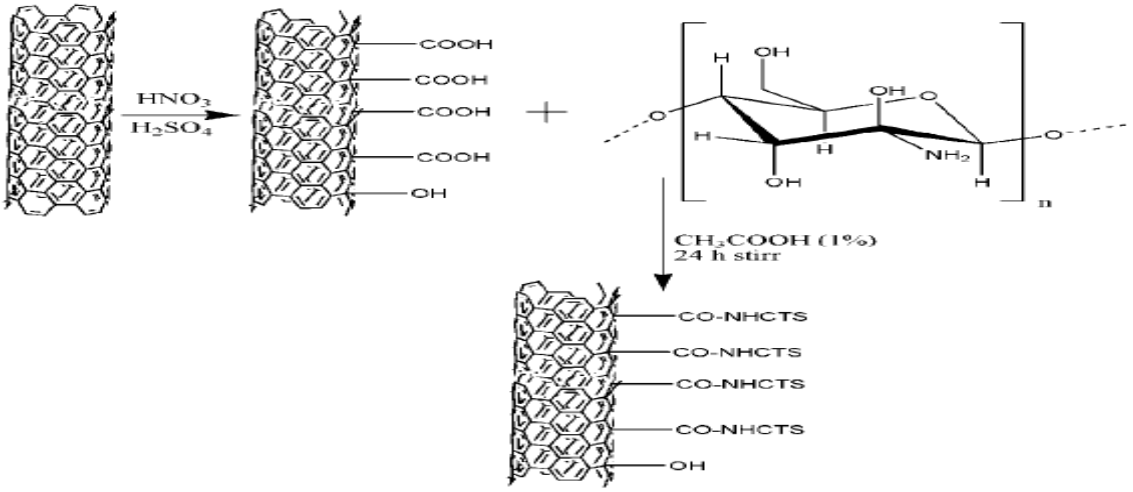

Figure1.22. Chemical interactions between chitosan and CNT (Reproduced from reference [220]).

1. 5 Thesis Objectives

The main objective of this thesis work is to design and fabricate composite BP membranes incorporated polymer matrix in the presence of different additives (i.e. Triton X-100, chitosan, chitosan cross-linked), surfactants and dispersants for the desalination of seawater. The present study also evaluated the ability of these BP membranes to separate salts from an aqueous solution. The specific objectives (used to evaluate the membranes' capabilities) are as follows:

1- Investigate a variety of surfactants for their abilities to maintain stable dispersions of CNTs using as-received (unfunctionalised) and functionalised MWNTs, and then characterise the produced dispersions by ultraviolet-visible-near infrared (UV-vis-NIR) spectrophotometry and optical microscopy.

2- Synthesise BP membranes with MWNTs using covalently functionalised MWNT-COOH and MWNT-NH_2, characterise the fabricated BP membranes and finally compare these BP membranes with previously produced BPs in terms of their physical and morphological properties and pore structures.

3- Evaluate the permeate flux through different BP membranes by investigating their behaviours towards water using a custom-built filtration-cell (dead-end cell and crossflow filtration cell), and then compare the water permeability of CNTs/biopolymer BP membranes with those of MWNT/Trix BP membranes.

4- Evaluate the ability of BP membranes fabricated using as-received (unfunctionalised) MWNTs, chitosan and cross-linked chitosan to reject salts from aqueous solutions.

5- Compare the abilities of BP membranes fabricated using MWNT-COOH and MWNT-NH_2 to reject salts from aqueous solutions with those BPs prepared using as-received (unfunctionalised MWNTs).

6- Explore the effects of changing the pH solution on salt rejection, permeability towards water and charge of the surface of membrane.

2. EXPERIMENTAL

Chapter 2: Experimental

This chapter presents general experimental information about the materials, methods and instrumentation used for this thesis. The details of particular techniques are demonstrated in the experimental section of each relevant chapter. All the experiments were carried out at room temperature (21°C) in the laboratories of the Soft Materials Group, School of Chemistry, the IPRI and the School of Civil Mining and Environmental Engineering at the University of Wollongong. Other experiments using nitrogen adsorption-desorption analysis and thermogravimetric analysis (TGA) were done at King Abdul Aziz City for Science and Technology, Saudi Arabia (KACST).

2. 1 Materials

The following materials were used to prepare the BP membranes. The unfunctionalised thin multi-walled carbon nanotubes (MWNT) (Nanocyl™ 3100, batch no. 110303 P1), functionalised thin multi-walled carbon nanotubes (e.g. MWNT-COOH) (Nanocyl 3101, batch no. mel 091216) and thin MWNTs-NH_2 (Nanocyl, lot no. NFL6.3) were obtained from Nanocyl, Belgium. MWNTs with diameter ranging 10–15 nm (lot no. 08052310) were procured from Hanwha Nanotech Corporation, Let, Korea. All the MWNT samples had 95% purity and were used without further purification.

The non-ionic surfactant Trix (TX, $M_w \approx 625$ Da; USA) and chitosan (batch no. MKBB4232) with low molecular weight, a degree of deacetylation (82%) and a viscosity 200–800 cP (1% in 1% acetic acid) were obtained from Sigma-Aldrich Chemicals, China. Glacial acetic acid with 99.7% purity was purchased from Asia Pacific Specialty (APS) Chemicals Limited, Australia.

NaCl 99% (batch no. 048K0041) was purchased from Sigma-Aldrich Chemicals, China. Anhydrous magnesium sulphate ($MgSO_4$) 98% was purchased from Scharlau, Spain. $MgCl_2$ 99% (batch no. (10)247452) was purchased from Supply, Australia. HCl 32%, methanol 99.8% (batch no. 1206323) and ethanol 96% (batch no. 1110137) were bought from Ajax Finechem Pty Ltd., Australia. Glycerin was obtained from Sigma, United States (batch no. 033k009), and polyethylene glycol-diglycidyl ether (PEGDGE) (Mn ~*526*) was obtained from Aldrich, Japan (batch no. MKBC9721). These were used for crosslinking chitosan.

The filter for MWNT dispersions comprised rectangular pieces of polyvinylidene fluoride (PVDF), which were purchased from Millipore (Ireland) in the form of a hydrophobic commercial membrane measuring ca. 142 × 75 mm^2 with a pore size 0.22 μm. A hydrophilic nylon membrane filter with a pore size 0.45 μm and a hydrophobic PVDF membrane filter with a pore size 0.45 μm were also purchased from Millipore. The hydrophobic PTFE membrane filters with pore sizes 5.0 μm were purchased from Ireland and were used as filtration membranes for chitosan solution to remove any residual chitosan particles. All the solutions and dilutions in this study were prepared using Milli-Q® water (resistivity 18.2 MΩ cm).

2. 2 Methods

The following experimental methods were used to prepare different solutions, dispersions, materials and BP membranes.

2.2.1 Preparation of dispersion solutions

A dispersant solution was prepared by mixing Trix (1%, w/v), chitosan (0.1–0.6% w/v), or chitosan (0.2% w/v) with glycerin polyethylene glycol diglycidyl ether (PEGDE), 20% of chitosan mass. It was then used for stabilisation of CNTs (MWNT, MWNT-COOH and MWNT-NH_2) in aqueous solution. CNT was added to a dispersant solution at 1:1, w/v and was mixed by sonication for 20 min for Trix solution and 30 min for chitosan, chitosan-glyceine and chitosan-PEDGE solutions. The sonication parameters of the Sonifier® (Branson Digital 400W) were ~16 w power output and pulses of 0.5 sec 'on' and 0.5 sec 'off'. The sample vial (2.5 cm in diameter) containing the MWNT and dispersant solution was placed in an ice water bath to maintain its temperature at approximately 6°C.

2.2.2 Preparation of MWNT/Trix buckypaper membranes

A schematic diagram of the preparation of a circular small buckypaper (BP) membrane of nearly 3.7 cm in diameter is shown in Figure 2.1. Here, MWNT (15 mg, diameter 10–15 nm) was dispersed in aqueous Trix surfactant solution and sonicated as above for about 20 min with gaps in between. The solution was then diluted to 0.5 L and filtered through polytetrafluoroethylene (pore size 0.45 μm) under vacuum at 30–40 mbar. The filtering funnel was kept covered with a petri dish to prevent evaporation during filtration.

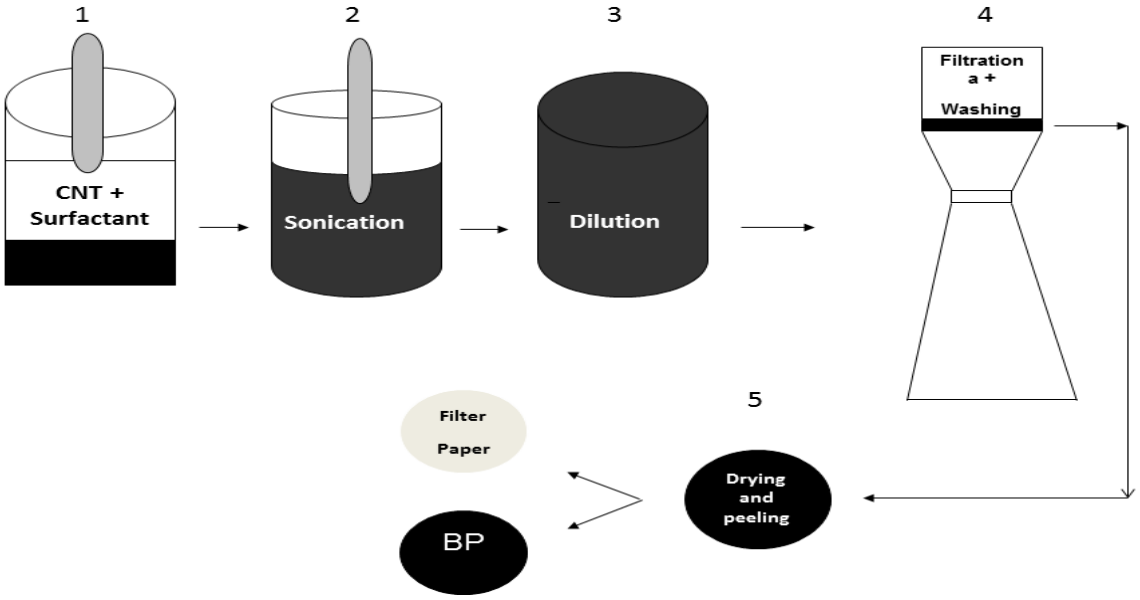

Figure 2.1. Schematic diagram of five steps involved in making small circular BP membranes.

The resulting circular BP membranes were then washed with 250 mL of Milli-Q water and 10 mL of methanol and left to dry for 24 h at 21°C. After the drying process, the BP membranes were peeled from the commercial attachment. The membranes were then annealed at 500°C for 2 h using Carbolite® horizontal tube furnace at heated up to 1800°C, under argon gas, to remove any residual surfactant and contaminants. The BP sheet was then soaked in low-molecular-weight chitosan solution (0.1% w/v; see section 2.3.1). Thus, four different BP composites were prepared: 1) MWNT BP with Trix dried at 21°C; 2) MWNT BP annealed at 500°C for 2 h; 3) MWNT BP annealed and soaked for 24 h in low-molecular-weight chitosan 0.1% (w/v); and 4) MWNT BP annealed and soaked for 96 h in low-molecular-weight chitosan 0.1% (w/v).

2.2.3 Preparation of BP-coated membranes

Different amounts (5, 15, 30 and 60 mg) of MWNTs (Nanocyl 3100, batch no. 110303 P1, Nanocyl, Belgium), were dispersed in 30 mL of Milli-Q water containing surfactant (Trix, 0.6% w/v) using an ultrasonicator for 24 min. Each mixture was diluted up to 0.5 L and then filtered through a hydrophilic nylon membrane filter (diameter 47 mm; pore size 0.45 μm) using a simple filtration vacuum pump (CVC2 Vacuubrand®, University of Wollongong). After filtration, a thin MWNT coating-like membrane was found on the surface of the hydrophilic filter and was dried at room temperature (21°C) for 24 h. The membranes before

and after coating with MWNTs are shown in Figure 2.2. The preparation steps for the circular membrane are shown in Figure 2.2.

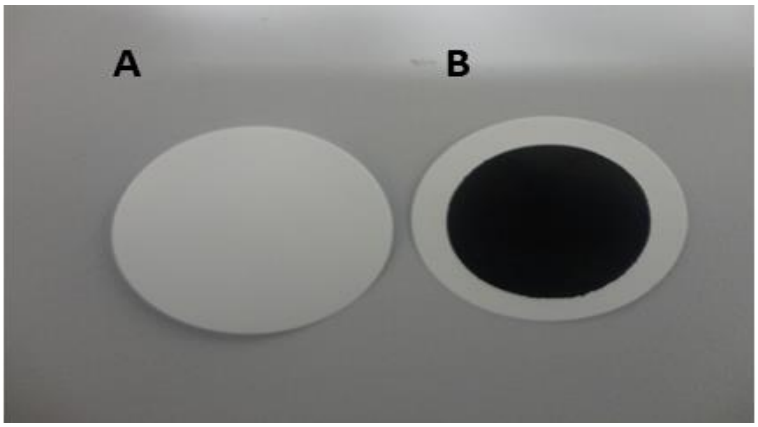

Figure 2.2. Photo of A) commercial membrane and B) commercial membrane coated with MWNTs.

2.2.4 Preparation of MWNT/chitosan large BP membranes

Large, rectangular BP membranes (6 × 12 cm^2) were prepared using a custom-built transport cell unit following the same procedure used for circular BP membranes shown in Figure 2.3, and were divided into three groups as follows.

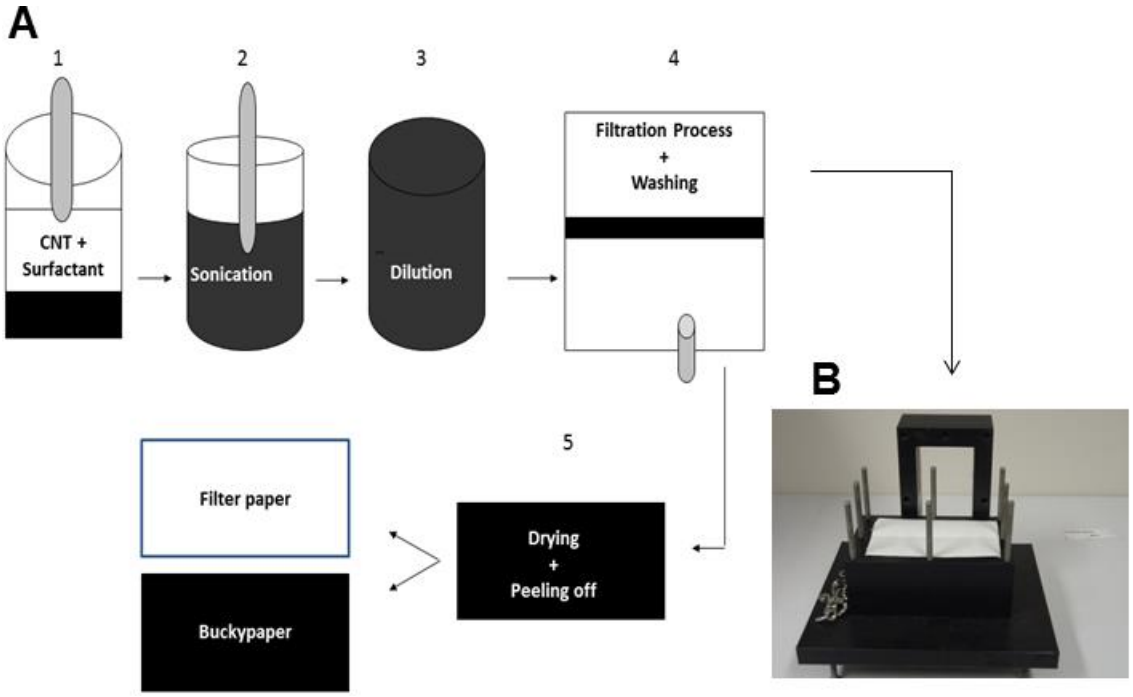

Figure 2.3. A) Schematic diagram of five steps for large, rectangular BP membranes (6 × 12 cm^2) prepared using the filtration method and B) a custom-built transport cell unit.

2.2.4.1 MWNT and chitosan BP membranes

Four chitosan surfactant solutions were prepared by dissolving 1 g (0.1% w/v), 2 g (0.2% w/v), 3 g (0.3% w/v) and 4 g (0.4% w/v) in 1 L of Milli-Q water containing 1% (v/v) acetic-acid solution. All these solutions were heated for 3 h at 80°C and stirred for 24 h until most of the chitosan particles were dissolved. They were then left overnight to cool at 21°C. All resulting homogenous solutions were successively filtered using hydrophobic PTFE membrane filters with pore size 5.0 µm to remove any undissolved particles.

Using 30 min of sonication, 15 mg of MWNTs (Nanocyl 3100, batch no. 110303 P1, Nanocyl, Belgium) was dispersed in 15 mL of the above surfactant (chitosan solution). This procedure was repeated 10 times to produce 150 mL of dispersion containing 150 mg of MWNTs. Each dispersion solution was diluted up to 250 mL and filtrated through hydrophobic PVDF filter paper (142 mm; pore size 0.22 µm) under vacuum suction. The filtration funnel/unit was covered with aluminium foil to avoid evaporative loss. The large BP membrane obtained on the surface of the filtrating sheet/membrane was placed between absorbent paper sheets, and flat glass sheets were placed on top of the absorbent paper sheets and left to dry for 24 h at 21°C. The dry BP membrane was then peeled from the filtrating membrane. The preparation steps for the BP membranes were same as those shown in Figure 2.3.

2.2.4.2 MWNT and chitosan crosslinking BP membranes

The chitosan solutions were prepared by dissolving 4 g of chitosan (0.2% w/v) in 2 L of Milli-Q water containing 1% (v/v) acetic-acid solution. The solutions were heated for 3 h at 80°C and stirred for 24 h until the chitosan particles dissolved. The solutions were then left overnight to cool at 21°C. The homogenous solution was successfully filtered through hydrophobic PTFE membrane filters with pore size 5.0 µm to remove any undissolved particles. The final homogenous solution after filtration was divided into two groups.

1) chitosan-glycerne: This was prepared with the above chitosan solution (0.2% w/v) and 0.8 g of glycerine (20% chitosan mass).

2) chitosan-PEGDGE: This was prepared with chitosan (0.2%w/v) and 0.8 g of PEGDGE (20% chitosan mass). Each of the two solutions was heated for 2 h at 50–70°C, stirred 24 h and left overnight to cool at 21°C.

MWNT (15 mg) (Nanocyl 3100, batch no. 110303 P1, Nanocyl, Belgium) was added to 15 ml each of chitosan-glycerne and chitosan-PEGDGE solutions and mixed by sonication for 30 min. The above procedure was repeated 10 times to produce 150 mL of MWNT dispersion solution. Each dispersion solution was diluted up to 250 mL and then filtrated through hydrophobic PVDF filter paper (142 mm, pore size 0.22 μm) using a vacuum pump at 30–40 mbar. The top of the filtration system (custom-built transport cell unit) was covered with aluminium foil to avoid evaporative loss. The large BP membrane produced on the filtration sheet was placed to dry between absorbent paper sheets with small, flat glasses at the top and left for 24 h at 21°C. The dry BP membrane was then peeled from the filtration sheet. The preparation steps for the BP membranes were the same as those in Figure 2.3.

2.2.4.3 Functionalised CNTs (MWNT-COOH and MWNT-NH_2) and chitosan BP membranes

Chitosan solutions were prepared by dissolving 4 g (0.2% w/v) in 2 L of Milli-Q water containing 1% (v/v) acetic-acid solution and were heated for 3 h at 80°C and stirred for 24 h until the chitosan particles dissolved. This solution was then left overnight to cool at 21°C. The final homogenous solution was successfully filtered through hydrophobic PTFE membrane filters with pore size 5.0 μm to remove any undissolved particles.

MWNT-COOH or MWNT-NH_2 (15 mg) was added to 15 mL of the chitosan 0.2% (w/v) solution and mixed by sonication for 30 min. The above procedure was repeated 10 times to produce 150 mL of solution (chitosan), which contained 150 mg of MWNT-COOH or MWNT-NH_2. Each dispersion solution was diluted to 250 mL and then filtrated through hydrophobic PVDF filter paper (142 mm, pore size 0.22 μm) using a vacuum pump at 30–40 mbar. The top of the filtration system was covered with aluminium foil to avoid evaporative loss. The large BP membrane produced on the filtration sheet/membrane was placed to dry between absorbent paper sheets with flat glasses at the top and left for 24 h at 21°C. The dry BP membrane was then peeled from the filtrating membrane. The preparation steps for the BP membranes were the same as Figure 2.3.

2. 3 Characterisation and Instrumentation

The following instrumentation methods were adopted to analyse and characterise different properties of the BP membranes.

2.3.1 UV-vis-NIR spectroscopy

The absorption behaviour of all dispersion solutions was measured from 300–1000 nm using a Cary® 500 UV-vis-NIR spectrophotometer. Each dispersion solution (0.1 ml) was diluted in a small vial (20 mL) by adding 15 mL of Milli-Q water and mixing manually for 1 min. The dispersion solution was taken into a quartz cuvette (1-cm path length) and spectra were obtained at room temperature (around 21°C).

2.3.2 Electrical conductivity

The electrical resistance of the BP membranes was estimated at 21°C and 45% RH using the two-point probe method [231]. BP samples were prepared by cutting them into thin strips (typically 4 × 30 mm). Thickness was measured with a Mitutoyo Digital Micrometer, and width was determined by optical microscope. The sample was then placed on glass slides using double-sided tape. Silver paint (SPI-paint 05002-AB) and copper tape (3M #1181 electrical tape) were used to obtain low resistance contact. The sample-electrode contacts were placed under standard compression (10^5 Pa) using bull clips prior to measurement. A second glass slide was fastened over the membrane using bull clips to guarantee continuous connection during the testing (Fig. 2.4).

An arbitrary waveform generator (Agilent 33220A) was used to apply a stepwise DC-voltage ramp (voltages between –0.1 V and +0.1 V). The current (I) and voltage (V) response were measured using a digital multimeter (Agilent 34410A). Measurements were repeated for a minimum of five channel lengths from 0.5–3 cm. Electrical resistance as a function of changed length was calculated using Ohm's law. This was repeated for at least five different lengths for each sample to determine resistance.

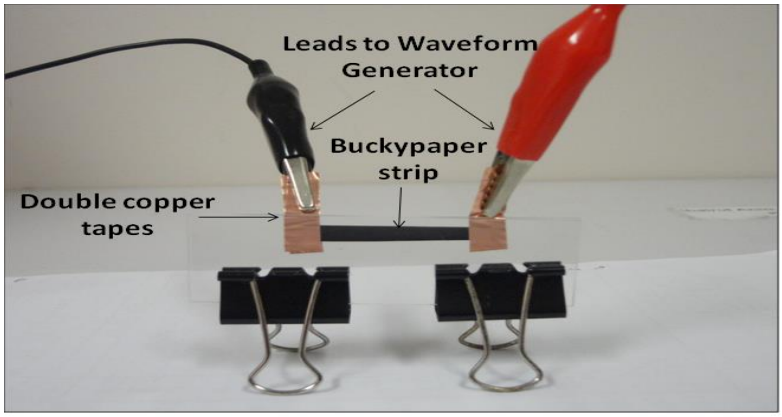

Figure 2.4. Schematic diagram of a conductivity measurement apparatus.

2.3.3 Hydrophobicity and contact-angle measurement

The hydrophobicity of the BP membranes was determined using the sessile drop method and a DataPhysics® SCA20 Goniometer fitted with a digital camera. BP samples measuring 4 × 35 mm were clamped flat on a glass microscope slide, and 2-µL water (Milli-Q, Millipore) droplets were placed on the surface of the membranes. Measurements were immediately taken using the goniometer. The contact angle can also be calculated using Young's equation [218]:

$$\gamma L\ COS\ \theta = \gamma S - \gamma SL, \quad (2)$$

where γL is the liquid vapour, γS the solid vapour, and γSL the solid–liquid interfacial tension, respectively, and θ is the measured angle with respect to the surface, as demonstrated schematically in Figure 2.5. The mean contact angle was determined from at least 10 measurements.

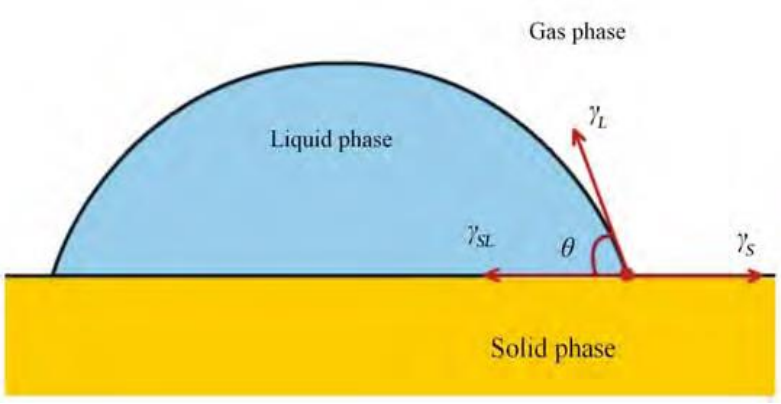

Figure 2.5. Diagram illustrating the contact point of a solid and liquid surface to determine the value of the contact angle [218].

2.3.4 Swelling measurements

Dried BP samples were cut into thin strips (typically 4 × 10 mm) and their thicknesses were measured with a Mitutoyo Digital Micrometer. The weight of each sample was determined using a digital balance (Mettler XS 64). The samples were immersed and kept for 24 h at 21°C in different solutions (water/acetic acid at 1, 3 and 5 w/v) and 3 M of sodium hydroxide solution. The strips were taken out at regular intervals, blotted to remove excess liquid and weighed. The percentage degree of swelling (SW) was calculated using:

$$SW = \frac{W_S - W_o}{W_o}\ X\ 100\%, \quad (3)$$

where W_s is the weight of swollen BP membrane and W_o is the weight of dry membrane.

2.3.5 Porosity measurements

The porosities of the MWNT-chitosan and MWNT-chitosan-crosslinked BP membranes were determined by dry-wet method using the following expression [232]:

$$Porosity\ (\%) = \left\{\frac{W_2 - W_1}{d_{water}}\right\} 100/V \qquad (4)$$

where W_1 and W_2 stand for the weights of the BP membranes in the wet and dry states respectively, d_{water} is the density of pure water at 21°C and V is the BP-membrane volume in the wet state.

2.3.6 Thermogravimetric analysis (TGA)

A TGA instrument from Perkin Elmer at KACST was employed to determine the thermal stability of the BP membranes. The sample's mass ranged 3–5 mg, and it was heated under nitrogen flow at temperatures from ambient to 1000°C with a heating rate of 10°C/min.

2.3.7 Scanning electron microscope (SEM)

BP membrane (20 × 4 mm^2) morphology was investigated using a JEOL JSM-7500FA SEM at the Electron Microscopy Centre of Wollongong University. All the samples were dried in an oven (Binder) at 50°C for 24 h, and the non-conductive material was coated with gold to improve imaging. They were then mounted onto an 11 × 5 mm brass stub using conductive carbon tape under the SEM's vacuum system. A 5-kV electric field was created prior to striking the BP target. To investigate the cross-sectional images, the samples were soaked in liquid nitrogen and carefully snapped open to expose the interior.

2.3.8 Mechanical testing

Tensile testing was carried out using a Shimadzu EZ-S tensile tester. Five strips (4 × 10 mm^2) of a BP-membrane sample were taken, and their thicknesses were measured using a Mitutoyo IP65 Digital Micrometer. The membrane samples were then placed between two parallel plates at room temperature (21°C and 45% RH). The percentage elongation (γ) of each BP membrane was calculated using the following equation:

$$\gamma = \frac{l - l_o}{l_o} \times 100\%, \qquad (5)$$

where l is the distance at break and l_0 is the initial distance [233]. Young's modulus of a BP-membrane strip was determined using the relationship between the strain and the stress:

$$E = \frac{\sigma}{\varepsilon}, \quad (6)$$

where σ is the stress, ε is the strain and E is Young's modulus (MPa) [233]. The tensile strength is the stress (σ_{max}) at the maximum on the engineering stress–strain curve, and the toughness is calculated from the area under the strain curve.

2.3.9 Surface areas and pore-size distributions of membranes

The surface areas and pore-size distributions of the BP membranes were estimated using a Micrometric ASAP-2020 analyser at KACST, Saudi Arabia, Quantachrome Instruments, Qi, at the University of Wollongong, and a Micrometric ASAP-2020 analyser at Particle & Surface Sciences Pty Ltd., Australia. The BP samples were cut into small pieces (2 × 2 mm^2) and then de-gassed at 80°C for 16 h under vacuum before being tested. The surface areas and pore volumes were determined for all BP membranes by nitrogen adsorption/desorption technique at 77 K. Nitrogen adsorption/desorption isotherms were performed using the BET method to determine the sample surface areas [234]. The N_2 isotherms were employed to calculate both small and large pore sizes of the sample using the Barret, Joyner and Halenda (BJH) [235] and Horvath-Kawazoe (HK) [236] methods.

2.3.10 Permeability and salt-rejection behaviours of membranes

Two different instrumental custom-built filtration-cell (dead-end cell) and crossflow-cell (RO/NF system) units were used to investigate (a) the permeability to water and (b) the salt-rejection capability of BP membranes. These units were (1) custom-built filtration cells unit used, for example, for MWNT/Trix buckypaper membranes and commercial membranes coated by MWNT/Trix. These membranes have large pore-size distribution, brittle (low mechanical properties), high porosity and require low pressure <6 bar, and (2) crossflow-cells unit used, for buckypaper membranes (MWNT/chitosan, MWNT/chitosan-glycerine and MWNT/chitosan- PEGDGE), strong mechanical properties, small pore-size distribution and low porosity, which require high pressure > 6 bar. These investigations were performed as follows.

2.3.10.1 Custom-built filtration-cell unit

2.3.10.1.1 Permeability

A cylindrical dead-end cell unit (Fig. 2.6A) with a custom-built filtration cell (Fig. 2.6B) and an effective area of 4.68 cm^2 was used to determine the permeability of a small BP membrane to water. BP membranes were cut into small rectangular strips measuring 3 × 2.5 cm^2, which were carefully placed between two layers of the filtration cell. A compressed air cylinder was used to force water from a feed tank through the filtration cell via a pressure regulator. Initially, pressure was applied at a slowly increasing rate of 10 kPa/min to guide water transport across the membranes. The mass of water permeating through the BP membranes was measured as a function of time after every 30 sec over a total time interval of 6 min using an electronic balance (Mettler-Toledo AB2) connected to a personal computer (PC) via Balance link software at pressures from 5–600 kPa.

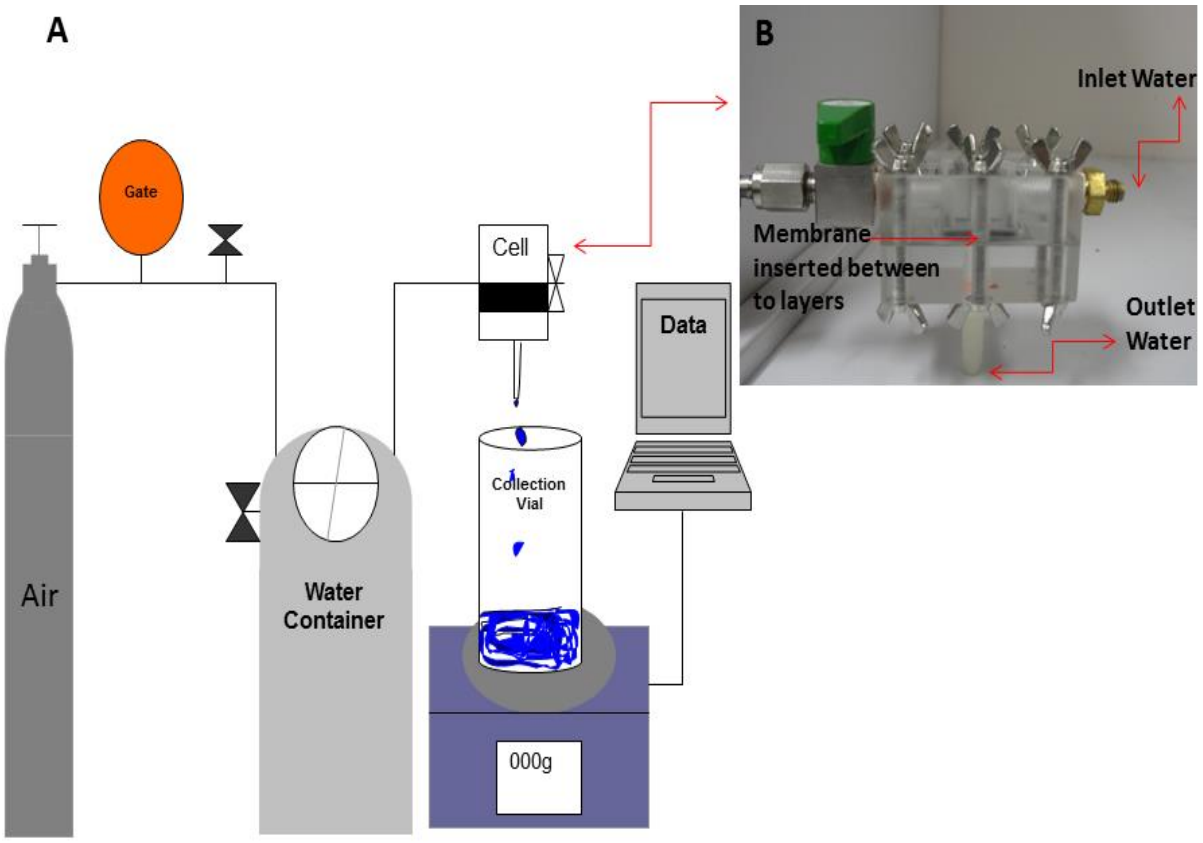

Figure 2.6. A) Schematic illustration of a cylindrical stirred dead-end cell used with thin-film samples to determine the water permeability and salt rejection of the thin membranes and B) custom-built filtration cell.

2.3.10.1.2 Salt-rejection ability

For salt-rejection experiments, the membrane-performance tests were conducted in the 1–6 bar range using 2000 mg/L NaCl and $MgSO_4$ solutions at room temperature with the small, custom-built filtration cell (Fig. 2.6B). Small, rectangular membrane samples (3 × 2.5 cm^2) were placed between two layers of the custom-built filtration-cell apparatus facing the feed solution. The effective membrane area was approximately 4.68 cm^2. The permeating volume collected for 30 min was used to describe flux (in units of cm^3/cm^2 sec). A standardised conductivity meter (Thermo Scientific™ conductivity meter Orion 4-Star™, Singapore, as presented in Fig. 2.7) was used to estimate the salt concentrations in the feed and permeate water. The rejection of the salts (R_O) was determined from the permeate and feed samples using the following equation [237]:

$$R_o = \left(1 - \frac{C_p}{C_f}\right) 100\%, \qquad (7)$$

where C_p and C_f are salt concentrations on the permeate and the feed water respectively.

Figure 2.7. Photo of the conductivity meter used to measure pH and salt rejection.

2.4.10.2 Crossflow-Cell Unit (RO/NF system)

2.4.10.2.1 Permeability and salt rejection

Measurements of water permeability and salt-rejection rate by different BP membranes were carried out using a laboratory-scale crossflow RO/NF system at the School of Civil, Mining and Environmental Engineering, University of Wollongong, Australia, as illustrated in Figure 2.8.

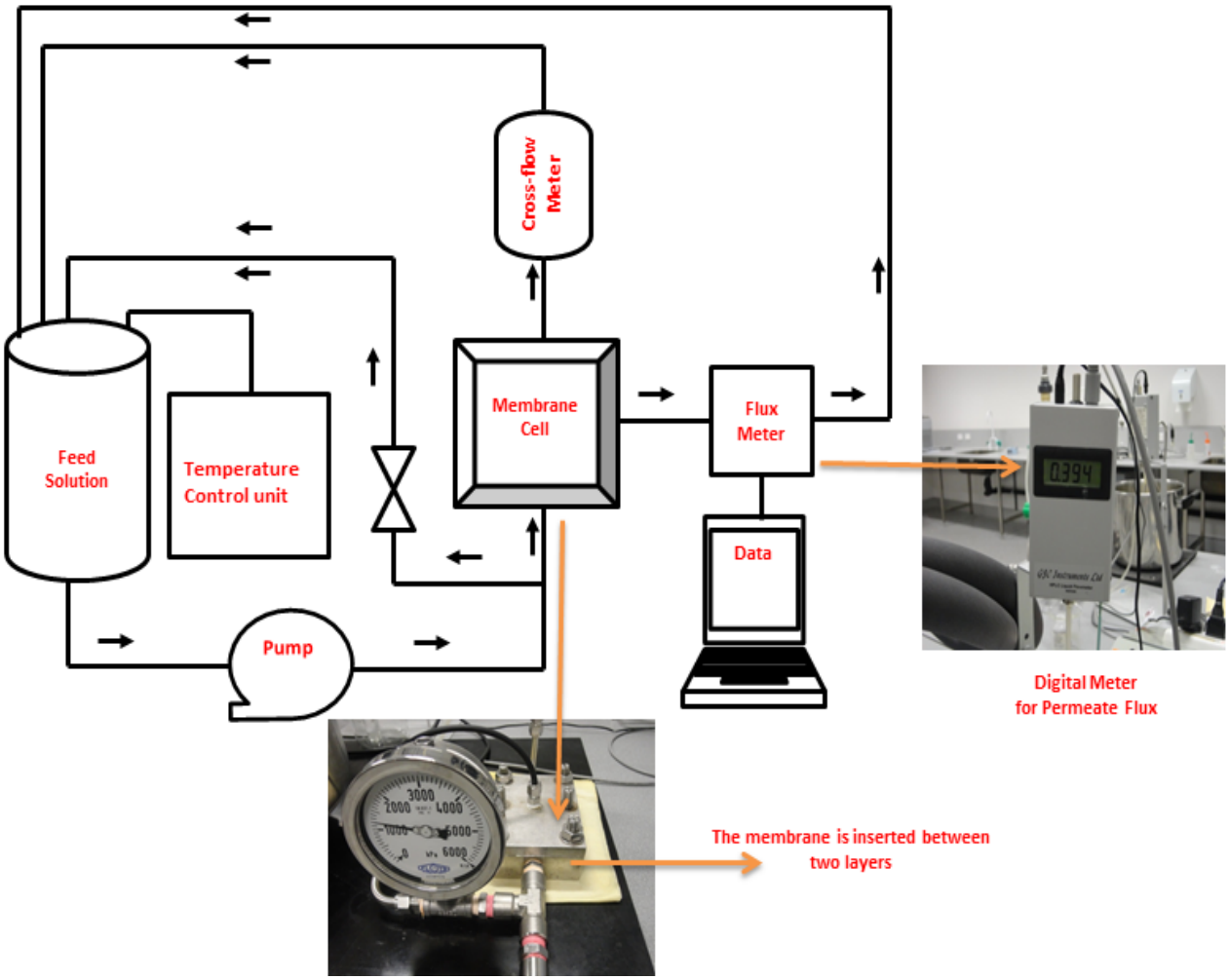

Figure 2.8. Schematic diagram of a crossflow unit (RO/NF system).

Deionised (DI) water was applied to all membranes at a pressure of 22 bar to compress or compact the membranes before conducting the RO experiments. Compression of the membranes was carried out for almost 1 h until a steady baseline flux was attained. After the compacting process, permeate flux of pure water (DI-water) was determined at different applied pressures to calculate the water permeability of the membranes. Salts (e.g. NaCl,

$MgSO_4$, $MgCl_2$, and Na2SO4) were added into the feed reservoir at 2g/L each salt to compose a feed solution (16g/L). The crossflow velocity was carried out at 34.7 cm/sec (100 L/h). The temperature of the feed solution was maintained at 20 ± 2°C throughout the experiment with the help of a chiller (Series Water Chiller 001-D081 ISS E, Aquacooler, Australia).

The real rejection *(R_r)* can be determined from the knowledge of salt-permeate concentration at the surface of a BP membrane, which is expected to be different from the bulk salt concentration (related to concentration polarisation). The relation between the observed rejection (R_O) and the real rejection can be calculated as follows [237]:

$$In\ \frac{(1-R_r)}{R_r} = In\frac{(1-R_o)}{R_0} - \frac{J_v}{k_f}, \quad (8)$$

where R_r is the real rejection expression that relates to the solute permeate concentration at the membrane surface and is different from the bulk concentration due to concentration polarisation, R_O is observed rejection expression, J_v is a permeate flux and k_f is the mass transfer coefficient that can be estimated by the following equation, which is also explained by Sutzkover et al. [238]:

$$k_f = \frac{(Jv)_{salt}}{In\left\{\frac{\Delta P}{\pi_b - \pi_p}\left[1 - \frac{(Jv)_{salt}}{(Jv)_{H_2O}}\right]\right\}}, \quad (9)$$

where k_f is the mass transfer coefficient, $(J_v)_{H_2O}$ is the permeate flux emanating from salt-free water, $(J_v)_{salt}$ is the permeate flux emanating from the saline solution, π_b is osmotic pressure at the solution bulk concentration, bar π_p is the osmotic pressure on the permeate and ΔP is the applied pressure.

Initially, this experiment was carried out at a crossflow velocity of 34.6 cm/s by determining the pure-water flux, followed by the addition of the salt into the feed solution to prepare 2 g/L (concentration of salt) and measurement of the permeate water flux and permeate salt concentration. This step was measured at 10 and 16 bar of applied pressure.

To evaluate the influence of the solution pH on the denial of salt, the solution pH was elevated to 10 by adding the desired quantity of 1 M potassium hydroxide (KOH) and then incrementally decreasing the pH by slowly adding 1M HCl.

The conductivity and pH of each solution were determined using a Thermo Scientific conductivity meter (Orion 4-Star, Singapore) as presented in Figure 2.7. Conductivities of different solutions containing various salt concentrations (NaCl, $MgSO_4$, $MgCl_2$ and $Na2SO_4$) were measured, and relationships were established by determining the concentrations of salts and the corresponding conductivities. Thus, a standard curve was obtained based on the data

received from conductivity and salt concentration for each solution. A linear relationship could be observed for concentrations of different salts in the feed and permeation solutions.

2.4.11 Zeta Potential (ZP)

ZPs of the surfaces of all membranes were estimated using a SurPASS electrokinetic analyser (Anton-Paar GmbH, Graz, Austria) (Fig. 2.9). Actually, ZPs for all membranes were measured from the calculated streaming potential using the Fairbrother-Mastin approach. The streaming potential measurements of all membranes were conducted in 1-mM KCl of background electrolyte solution. HCl and KOH were employed to adjust the pH by means of automatic titration. For each measurement, the cell was cleaned thoroughly before the test and the pH adjustment. In addition, the measurements of the streaming potential were taken at room temperature (approximately 21°C), which was determined using the system's temperature probe.

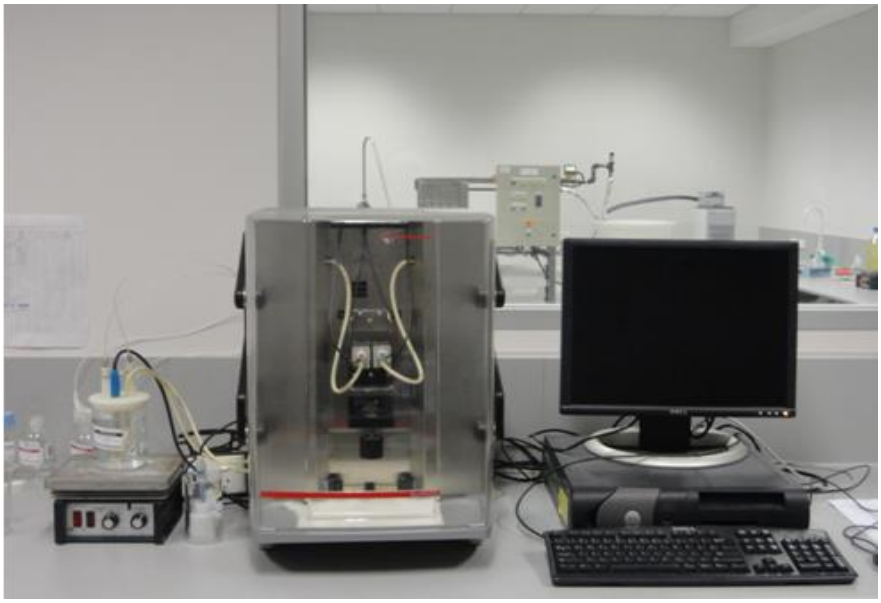

Figure 2.9. Photograph of the SurPASS electrokinetic analyser.

RESULTS AND DISCUSSION

Results and Discussion

Introduction

In this section, the results of various properties analyses, including optimum sonication time, conductivity, the hydrophobicity, mechanical characteristics, solubility, swelling ratio, the permeability and salt-rejection capability, of different BP membranes fabricated under various combinations with both unfunctionalised and functionalised CNTs in the presence of different surfactants and dispersants are presented and discussed in detail. To facilitate this discussion, the entire work is divided into the following sub-sections.

1. Characterisation of various properties, including water permeability of MWNT BP membranes (Chapter 3).
2. Evaluation of commercial membranes (nylon) coated by thin layers of MWNT for salt-rejection capability (Chapter 4).
3. Evaluation of MWNT/chitosan membranes for rejection of mono- and divalent ions (Chapter 5).
4. Evaluation of MWNT/chitosan and MWNT/chitosan-crosslinked membranes for salt-rejection capability (Chapter 6).
5. Evaluation of unfunctionalised MWNT/chitosan and functionalised MWNT/chitosan membranes for salt-rejection capability (Chapter 7).

Chapter 3: Characterisation of Various Properties of MWNT BP Membranes

MWNT BP membranes prepared from MWNT-Trix dispersion solutions by vacuum-filtration technique were subjected to two types of additional treatments: 1) annealing at 500°C under argon gas and 2) annealing at 500°C under argon gas followed by soaking in a chitosan polymer solution. The effect of annealing and polymer soakage on the electrical, mechanical and morphological properties, water permeability and the suitability of these BP membranes under different pressures were investigated.

3. 1 Optimum sonication time

Dispersion of CNTs in a solution is commonly carried out by sonolysis using an ultrasonic horn; however, excessive sonication can damage the nanotubes, adversely affecting its physical properties [239, 240]. A strong correlation between UV-vis absorbance intensity and the dispersed amount of MWNTs was observed in the previous study [241]. The complete dispersion could be ascertained by monitoring the plateauing of the UV-vis absorbance intensity against the disappearance of visible aggregates under light microscopy. In addition, the UV-vis-NIR method was also employed to explore materials incorporating CNTs and the optimisation of the sonication time for producing stable dispersions. Figure 3.1A presents a typical UV-vis absorption spectra of a dispersion solution containing MWNTs (0.1% w/v) and Trix (1% w/v) during sonolysis.

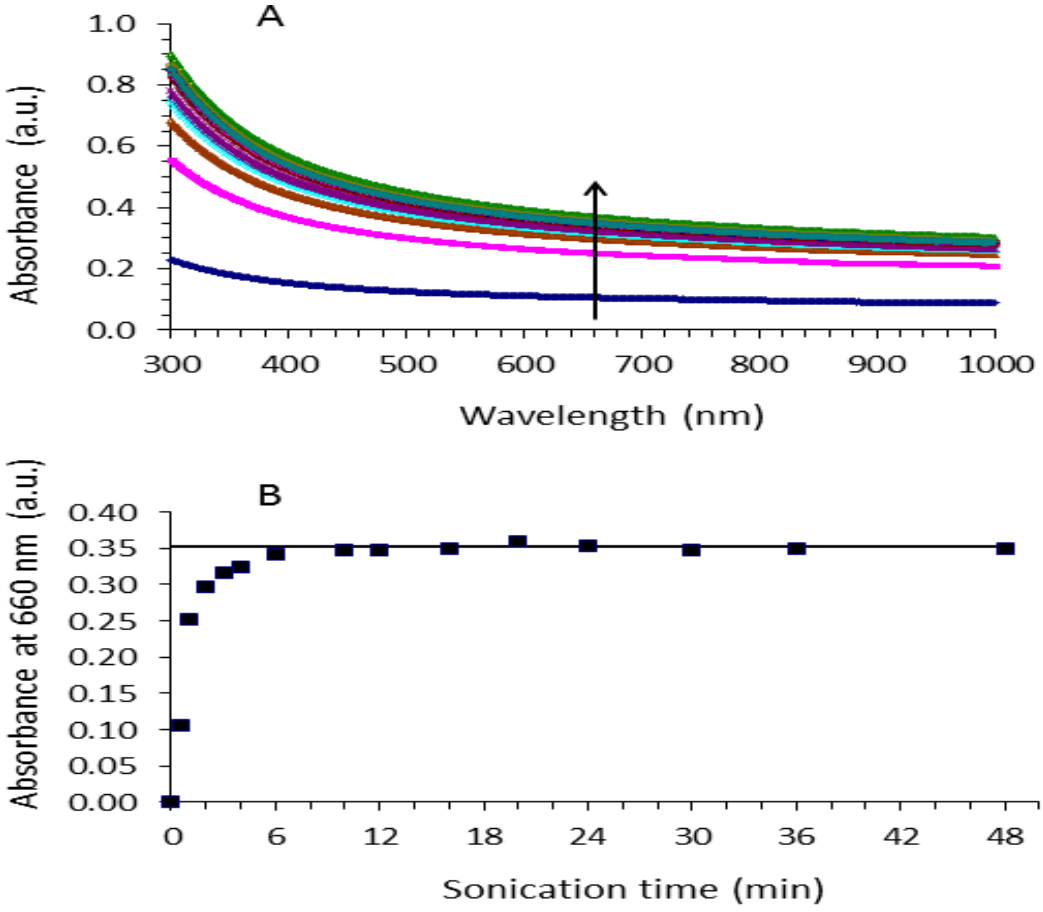

Figure 3. 1. A) UV-vis spectra of a typical MWNT-Trix dispersion (diluted 1/150); the arrow indicates the direction of increasing sonication time; B) effect of increasing the sonication time on the absorbance at 660 nm of the MWNT-Trix dispersion solution; straight line indicates the well-dispersed state of the MWNTs.

It is clear that absorbance intensity increases with increasing sonication time. A gradual increase in absorbance at all wavelengths with increased sonication time may be attributed to further dispersing of MWNTs into solution [242]. Figure 3.2.1B demonstrates that the absorbance intensity (at 660 nm) reaches a plateau value after approximately 10 min of sonication. In addition, an optical microscopy study revealed that the dispersions sonicated for a minimum of 20 min did not contain any visible aggregates, as shown Figure 3.2.2.

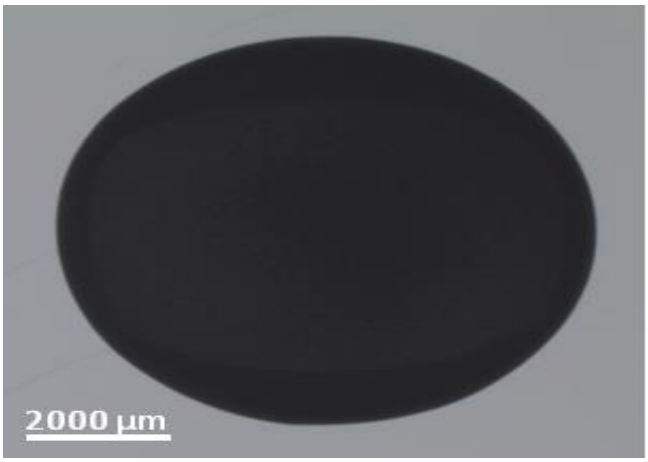

Figure 3. 2. Optical microscope images of a MWNT-Trix dispersion solution sonicated for 20 minutes; image taken immediately following sonication using a 10× objective lens.

Furthermore, increasing the sonication time can lead to increase the energy, which increases the degradation of the MWNTs, causing a concomitant reduction in the physical properties of the resulting dispersion [243]. Thus, it is assumed that MWNT has been completely dispersed after 20 min of sonication. This is equivalent to an energy input of 24 kJ/mg of dispersed MWNT. The sonication time is shorter than that required (30 min) to disperse a similar amount of SWNT (0.1% w/v) using a similar concentration of Trix (1% w/v) [181]. These observations are consistent with our previous work and the commonly accepted view that MWNT is easier to disperse than SWNT.

3. 2 Physical properties

Different physical properties of BP membranes fabricated under different conditions were determined by various instrumentation techniques. These are presented and discussed hereunder.

3.2.1 Electric conductivity

Electrically conducting membranes may facilitate enhanced separation ability in the presence of electric potential [244, 245]. Therefore, it was decided to measure the conductivity of the fabricated BP membranes using the two-point probe technique (see experimental section). Figure 3.3 presents a current–voltage (I–V) plot of a BP membrane obtained from a MWNT-Trix 1% (w/v) dispersion solution.

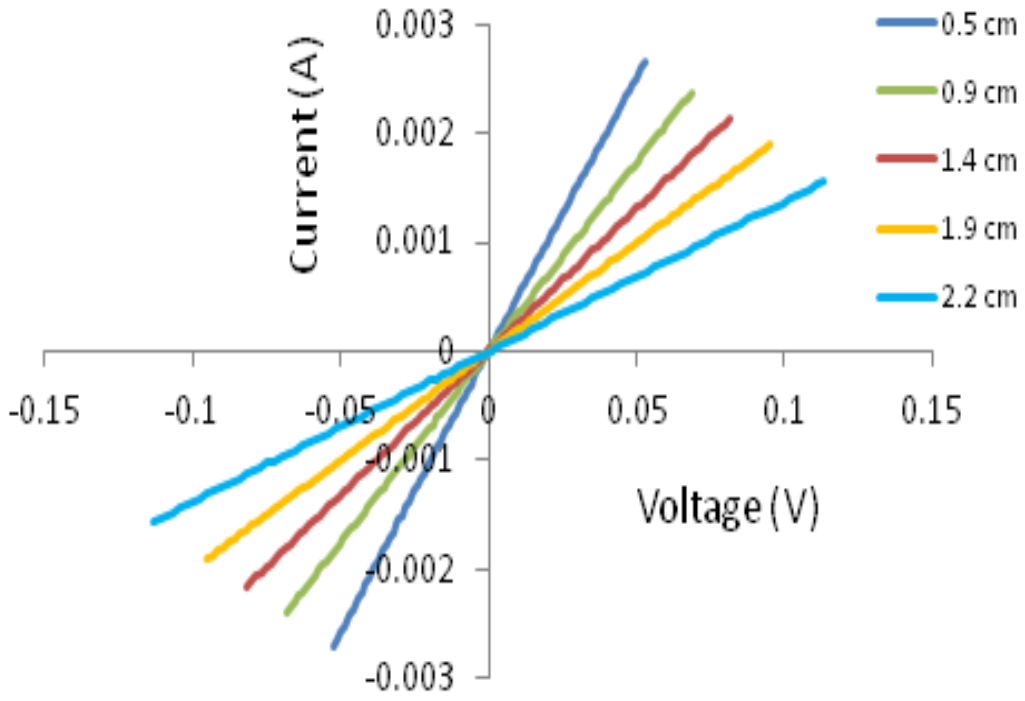

Figure 3.3. I–V plot obtained at five different lengths of a strip of the BP membrane fabricated from the MWNT (0.1% w/v) and Trix (1% w/v) dispersion solution.

The linear I–V relationship in Figure 3.3 illustrates the Ohmic behaviour of the BP membrane, with the inverse of the slope of each plot related to the resistance. The resulting resistances are plotted against the BP-membrane length and are shown in Figure 3. 4.

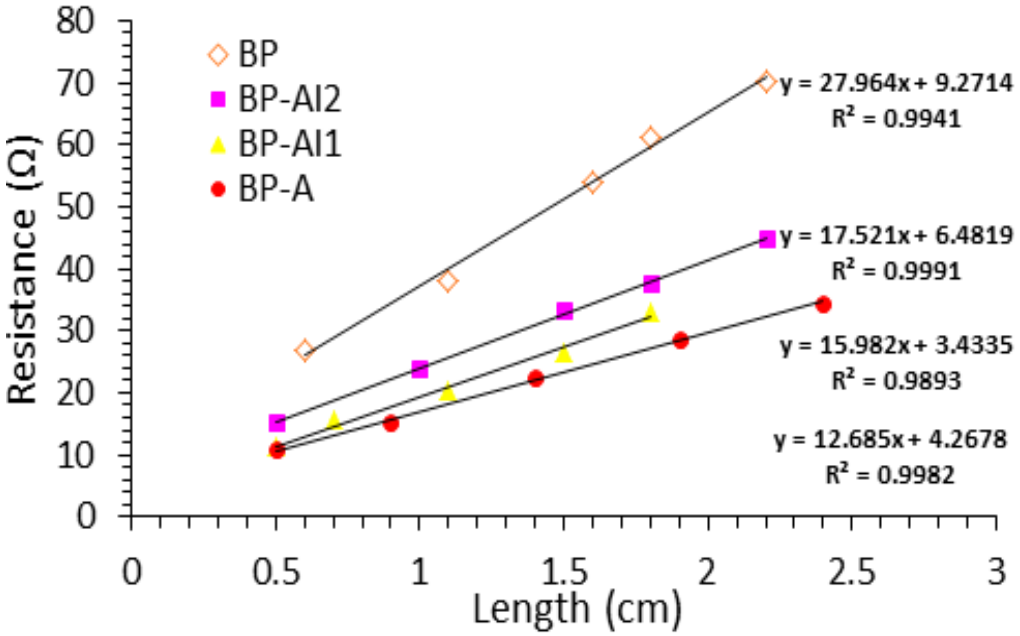

Figure 3.4. Effect of length on the resistance of different BP membranes: MWNT BP-Trix (1% w/v), (BP-A) MWNT BP after annealing at 500°C for 2 h, (BP-AI1) MWNT BP after annealing and soaking in chitosan low Mw 0.1% (w/v) for 24 h, and (BP-AI2) MWNT after annealing and soaking in chitosan low Mw 0.1% (w/v) for 96 h.

The data from Figure 3. 3 can be fitted to the following equation [180, 181, 246]:

$$R_T = \frac{1}{\sigma A} l + R_c \,, \qquad (10)$$

where R_T is the total resistance, A is the cross-section area, σ is the bulk conductivity of the BP membrane, l is the length of the strip and R_c is the contact resistance. The conductivity of the buckypaper membranes was calculated using the above equation. The average conductivity was calculated based on five independent measurements.

Various results are summarised in Table 5, where it is shown that conductivity increased from 19 ± 2 S/cm to 42 ± 2 S/cm after annealing of the BP membrane. This significant increase could suggest that the removal of surfactant from BP membranes by heating lowers the resistance of the CNT junctions in the CNT network. In contrast, intercalation decreased conductivity, therefore electrical conductivity decreased with increasing soakage time. This suggests that intercalating leads chitosan to impede connectivity between the MWNTs, which promotes increased junction resistance, thereby lowering conductivity.

Table 5. Summary of results of properties of various BP membranes and effects of changing the preparation environments of the properties of a range of membranes: (BP) MWNT-Trix BP and (BP-A) MWNT BP after annealing at 500°C for 2 h; (BP-AI1) MWNT BP after annealing and soaking in chitosan low Mw 0.1% (w/v) for 24 h; and (BP-AI2) MWNT after annealing and soaking in chitosan low Mw 0.1% (w/v) for 96 h.

BP membrane	Contact angle (°)	Tensile strength (MPa)	Young's modulus (MPa)	Strain at break (%)	Conductivity (S/cm)	Thickness (µm)
BP	31 ± 4	2.2 ± 0.2	122 ± 26	2.7 ± 0.6	19 ± 2	50 ± 2
BP-A	71 ± 4	1.4 ± 0.1	85 ± 4	0.63 ± 0.02	42 ± 2	48 ± 3
BP-AI1	43 ± 2	2.7 ± 2.7	296 ± 57	0.93 ± 0.3	23 ± 3	58 ± 2
BP-AI2	36 ± 4	4.2 ± 0.7	443 ± 20	2.3 ± 0.9	19 ± 3	63 ± 3

3.2.2 Hydrophobicity of BP

Further, the hydrophobicity of materials can be assessed by the contact angle. A contact angle <90° demonstrates that the materials have an affinity for water and total wetting can occur at 0°, whereas contact angles >90° indicate hydrophobic materials. Therefore, the contact angle is an important characteristic, as it reveals whether the membrane interacts easily with solution [247, 248]. The contact angle of formed BP membranes was determined using the 2-µL aliquots of Milli-Q water, as described in the experimental section (Chapter 2) and as demonstrated in Table 5. As expected, the BP membranes exhibited hydrophilic interactions with water and ranged 31 ± 4°–71 ± 4°. The contact-angle values were significantly lower than those expected for a CNT surface and were a great deal lower than those previously reported for MWNT BPs [249]. One possible reason for these low measures is that water is able to cross the porous BP membranes and therefore does not make true surface contact with them. Significant increases in permeate flux water rates through BP membranes can be achieved by vacuum pressure [250]. Alternatively, the lowered contact angle may suggest that MWNTs created by the CVD method are of high polarity. The low contact angles might also be attributed to the ability of chitosan polymer solution to coat the outside of the MWNTs more effectively (Table 5). The contact angles of BPs soaking in chitosan polymer solution were lower than the angles of BP-A (annealing BP membrane at 500°C). This may be due to high surface roughness corresponding to large pore density, as

surface roughness can lead to a reduced contact angle of water [251]. The contact angles for both BPs soaking in chitosan polymer solutions (BP-AI1 and BP-AI2) decreased with increased soaking time, which may be attributed to the increased hydrophilicity caused by the hydrophilic groups ($–NH_2$ and –OH) on the surfaces of chitosan [252]. This indicates that polar groups on dispersant molecules are able to interact favourably with the dispersed MWNTs in solution. The contact-angle analysis results suggest MWNT-Trix (BP) and MWNT-Trix soaking in chitosan solution (BP-AI1 and BP-AI2) are of significantly higher polarity than would be expected for an allotrope of pure carbon.

3. 3 Mechanical properties

Mechanical strength is crucial for membrane sustenance at high-pressure, high working temperatures and varying flow rates for prolonged periods. This is because the membrane must be able to continue the application of an extensive range of pressures, high temperatures and flow rates for long periods [180, 242]. In this study, the BPs were subjected to tensile testing. The resulting stress–strain curves (Fig. 3.5) were used to calculate the mechanical parameters of tensile strength, ductility and Young's modulus (Table 5).

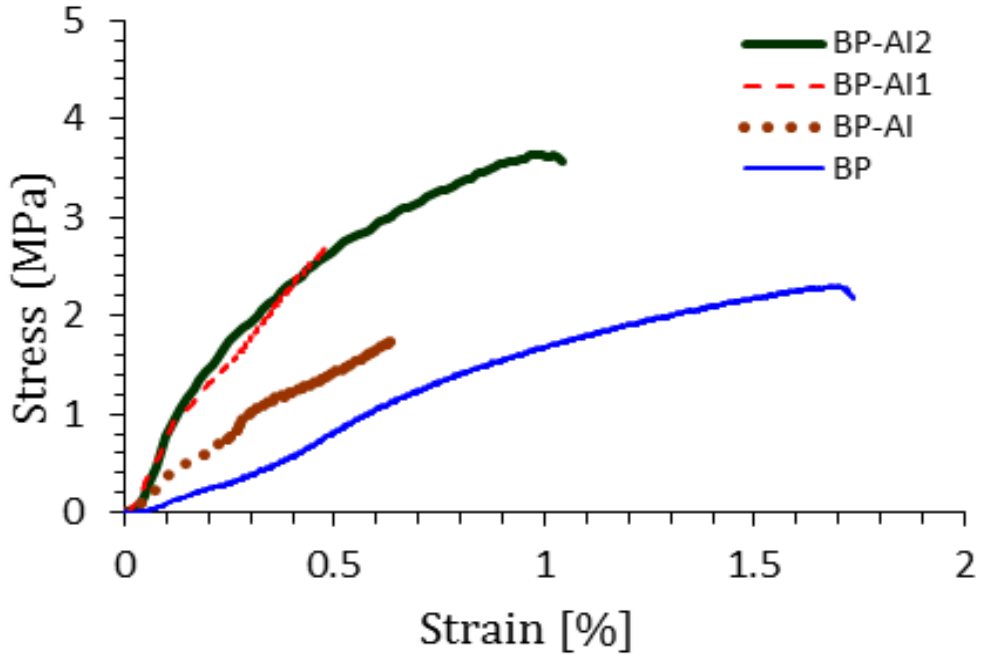

Figure 3.5. Stress–strain curve for different BPs: (BP) MWNT-Trix BP and (BP-A) MWNT BP after annealing at 500°C for 2 h; (BP-AI1) MWNT BP after annealing and soaking in chitosan low Mw 0.1% (w/v) for 24 h; and (BP-AI2) MWNT after annealing and soaking in chitosan low Mw 0.1% (w/v) for 96 h.

The tensile strength and Young's modulus values are affected by both annealing and intercalation, the linear relationship at higher strains; suggesting a highly brittle failure mechanism. For example, tensile strength and Young's modulus of BP-A (BP annealing) were the lowest observed, at 1.4 ± 0.1 MPa and 85 ± 4 MPa, whereas the values obtained for BP-AI2 (BP soaking at 96 h) at 4.2 ± 0.7 and 443 ± 20 MPa, were the highest observed. Moreover, the low mechanical property values of membranes may be attributed to the sonication times. The previous study reported that changing the sonication times could affect the mechanical properties of BP membranes [242]. A series of BPs were fabricated from dispersions made using different sonication times from 15–60 min, and were then subjected to mechanical properties tests. These experiments showed that the range of sonication times used to fabricate the initial dispersion had little effect on the mechanical properties of the final mechanical properties.

The addition of chitosan and increased soaking time brought considerable improvement in tensile strength and Young's modulus. The tensile strength and Young's modulus values increased by 3.5 times and 2 times respectively when the annealed BP was immersed in 0.1% (w/v) and soaked for 24 h. Similarly, these parameter values for BP-AI2 were 5 and 3 times greater, respectively. Coleman et al. reported similar results for a different polymer (polyvinyl alcohol [PVA] and PVP), where Young's modulus and tensile strength increased by factors of 3 and 9, respectively [253]. This was explained by the significantly improved load transmission when the biopolymer intercalated with the membrane [253]. In the present study, increases were found, but in the case of chitosan, the increase in Young's modulus was greater than the increase in tensile strength.

3. 4 Thermal stability of membranes

For many separation applications, it is essential that the membrane or adsorbent employed possesses thermal stability. Therefore, TGA was used to determine the effect of temperature (25–1000°C) on MWNT BP membranes. Figure 3.6 presents the comparison of obtained thermograms of all the BP membranes. A small loss of mass was seen in the temperature range of 100–200°C that may have occurred due to leftover water trapped inside the BP membranes.

In the case of the MWNT-Trix (BP), the mass loss in the range 200°–500°C may correlate with the decomposition of dispersant molecules (Trix, 1% w/v) [181]. However, the mass loss in the range 200°–500°C for both BPs soaking in chitosan (BP-AI1 and BP-AI2)

may relate to the decomposition of the molecules of chitosan 0.1% (w/v), which was absorbed by the surface of BPs during the soaking process for 24 and 96 h respectively. Therefore, it can be deduced that the degree of thermal stability is decreased by increasing the soaking time of BP MWNT membranes in chitosan solution. Conversely, the TGA curve (Fig. 3.6) demonstrates no decrease in mass in the range 200°–500°C for BP-A (BP annealing at 500°C for 2 h), indicating that the surfactant (Trix, 1% w/v) was completely removed from the BP after annealing at 500°C for 2 h.

Further, no other considerable decreases in mass for any of the BP samples in the range 500–800°C were observed, whereas minute losses of mass were recorded for all BPs at the temperature range 860–900°C. This indicates that the increase in temperature resulted in a catalysed loss of carbon. This loss was probably caused by the carbon shells (metallic iron catalyst particles), which were used to create the CNTs and were not separated during purification [254].

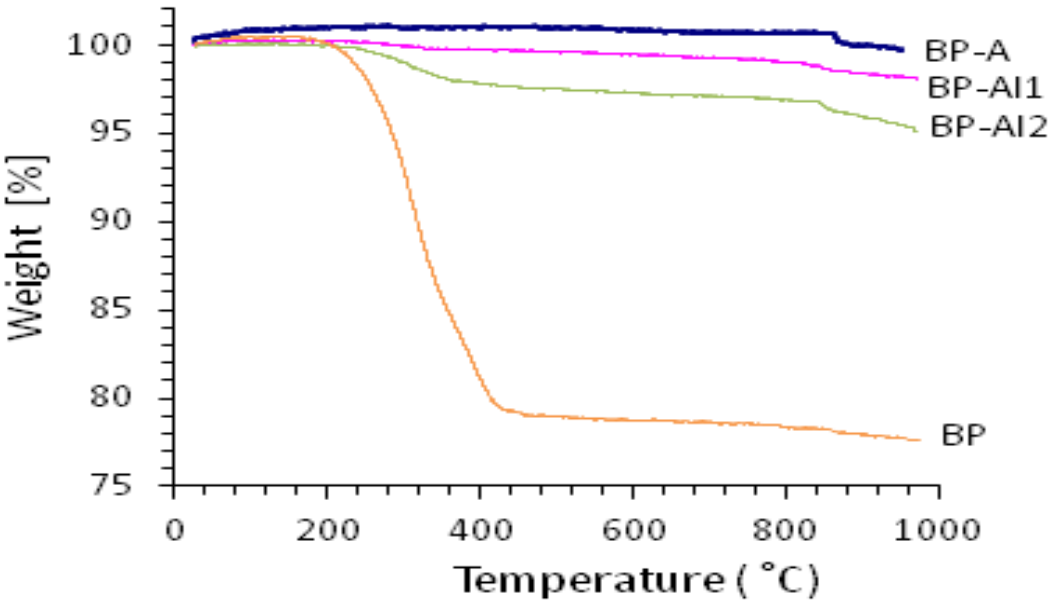

Figure 3.6. Effect of changing the preparation environment on thermal stability for a range of membranes: (BP) MWNT BP-Trix 1% (w/v), (BP-A) MWNT BP annealing, (BP-AI1) MWNT BP after annealing and soaking in chitosan low Mw 0.1% (w/v) for 24 h and (BP-AI2) MWNT after annealing and soaking in chitosan low Mw 0.1% (w/v) for 96 h.

3. 5 Surface morphology and area

The surface morphologies of the BP samples were investigated using SEM. In each buckypaper membrane, a randomly criss-crossed mat of MWNTs was extracted, with the diameter of the pores and other surface features highly dependent on the fabrication conditions (especially, the identity of the employed dispersant). Figure 3.7B presents an SEM image of a BP strip after soaking in chitosan solution for 24 h. A comparative analysis with annealed BP (Fig. 3.7A) reveals the presence of a polymer coating in Figure 3.7b and that only a fraction of the pores intercalated with polymer. The cross-sectional analysis (Fig. 3.7C) showed that the polymer intercalated beyond the surface layer. The image suggests that only a fraction of the internal space of the BP was filled with biopolymer. This demonstrates agreement with previous reports [253, 255], which demonstrated that the surface of the BP membrane was coated by polymer. In the image, this coating is relatively thin, and the pores between the nanotubes can be seen on the surface of the BP membranes. In addition, in the cross-sectional SEM image (Fig. 3.7C), the tubes consist of relatively round, small and homogeneously sized (in the outer shell), randomly entangled tubules. The investigation of the SEM image of a BP prepared from MWNT and Trix (Fig. 3.7A) exposed a highly porous surface structure and overall morphology similar to that reported for BP membranes prepared using the same materials [256, 257].

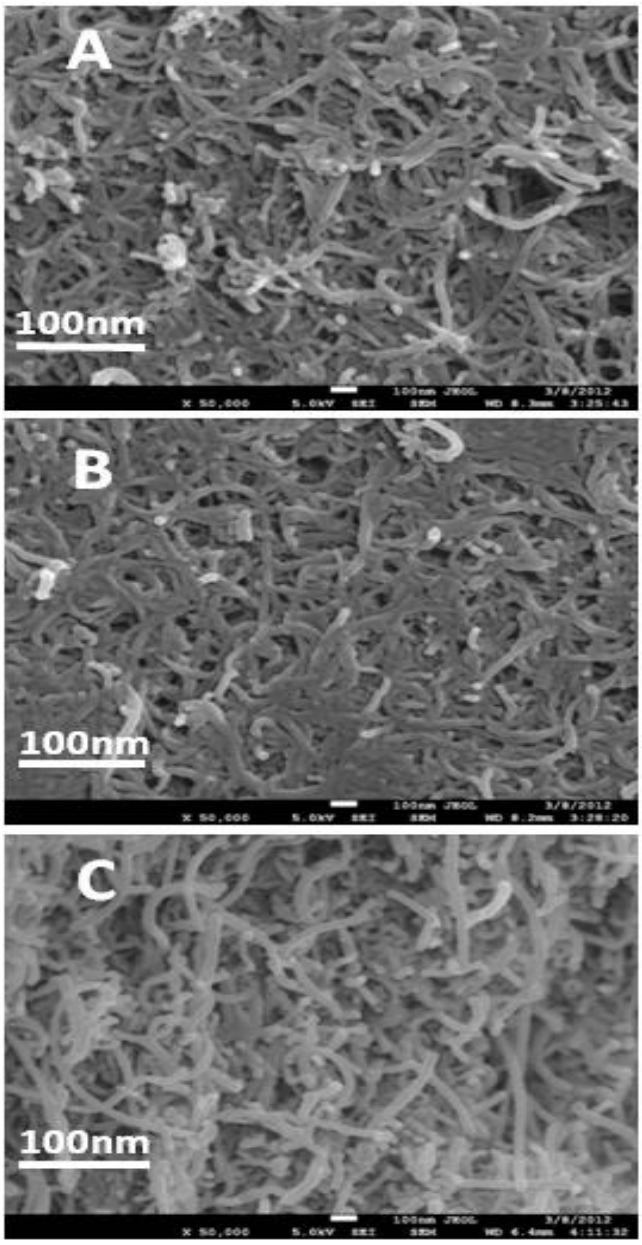

Figure 3.7. SEM images of MWNT BP membrane fabricated using the filtration method: A) after annealing at 500°C for 2 h; B) after soaking in chitosan low Mw 0.1% (w/v) for 24 h; and C) cross-section of MWNT BP membrane after annealing and soaking for 24 h in low-Mw chitosan 0.1%.

Nitrogen adsorption/desorption isotherms were obtained to gain a greater understanding of the surface area and pore structure of the BP membranes. The BP samples were cut into small pieces and de-gassed under vacuum at 200°C to remove any adsorbed gas, water and surfactant molecules before measuring. The TGA analysis (Fig. 3.6) indicated the stability of all BP samples at this temperature. Some of the isotherms typically obtained are illustrated in Figure 3.8. MWNT BPs exhibit an isotherm of general type IV [198, 242] with

hysteresis occurring at high P/P_o. The difference between the filling rate and removal rate of the adsorbent, caused by the mechanism of capillary condensation, results in hysteresis in porous material [242]. Nitrogen adsorption/desorption below P/P_o = 0.1 can be related the presence of micropores with diameters lower than 2 nm. These may attributed to the interstitial pores located between individual nanotubes within carbon nanotubes bundles [258, 259].

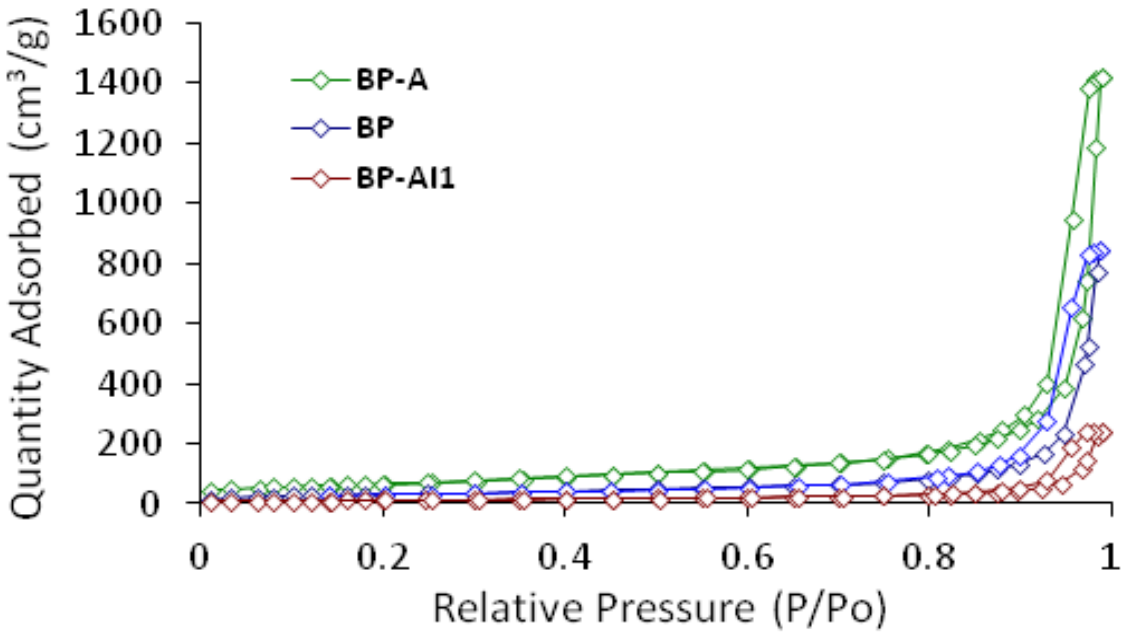

Figure 3.8. Comparison of the adsorption/desorption isotherms of MWNT-Trix 1% w/v BP membrane (BP): MWNT BP membrane after annealing at 500°C for 2 h (BP-A) and MWNT BP membrane soaking in chitosan low Mw 0.1% (w/v) for 24 h (BP-AI1).

Considerable improvement in the adsorptive capacity was attained after the annealing step. When the ratio of P and P_o reached a value of ~1, the adsorbed volume increased from 850 cm^3/g for buckypaper membrane before annealing (BP) to a value of 1,400 cm^3/g for buckypaper annealing at 500°C (BP-A). The total BET surface area (Table 6) for BP-A membrane (after annealing) was 232 ± 4 m^2/g, which agrees well with the value reported in previous study (229.3 m^2/g for MWNT heat-treated) [260]. However, the surface-area value of BP membrane (before annealing) was approximately 2 times lower than those measured for either BP membrane reported in previous studies [256, 257], indicating that the types of CNTs and surfactants are important contributing factors to the lower water permeability of BP membranes.

Table 6. Membrane water permeability (*f*), water-transport initiation volume, surface area and pore characteristics of BP membranes: (BP) MWNT/Trix 0.6% (w/v), (BP-A) MWNT/Trix after annealing, (BP-AI1) MWNT/Trix after annealing and soaking in chitosan low Mw 0.1% (w/v) for 24 h and (BP-AI2) MWNT/Trix after annealing and soaking in chitosan low Mw 0.1% (w/v) for 96 h.

BP membrane	Membrane water permeability (L/m^2 h bar)	Surface area (m/g)	D_{bun} (nm)	Average pore width (nm)	Interbundle pore volume (%)	Intertube pore volume (%)
BP	58 ± 7	114 ± 2	23 ± 2	18 ± 2	92 ± 2	8 ± 1
BP-A	108 ± 16	232 ± 4	11 ± 4	25 ± 4	98 ± 4	2 ± 0.4
BP-AI1	59 ± 6	40 ± 1	67 ± 1	16 ± 2	87 ± 2	13 ± 2
BP-AI2	44 ± 6	–	–	–	–	–

Adsorptive capacity after soaking decreased from 1,400 cm^3/g for the BP-A membrane (after annealing) to ~300 cm^3/g for BP-AI1 membrane (soaking in chitosan solution) as shown in Figure 3.8; however, the total surface-area value for soaking in chitosan solution (BP-AI1) was 40 ± 1 m^2/g. This is approximately 3 times lower than the values obtained for BP membrane (114 ± 2 m^2/g), as demonstrated in Table 6. In addition, the total surface-area values for BP membrane were also considerably (approximately 3 times) lower than those values found for BP-A (232 ± 4 m^2/g). This suggests that chitosan molecules effectively fill (intercalate) the pores of the buckypaper membranes, thereby making narrow pores at CNT junctions and decreasing porosity.

Pore-distribution data (pore-structure characteristics) calculated using N_2 adsorption/ desorption isotherms are presented in Figure 3.8 and summarised in Table 6. The MWNT BP-A membrane contained a considerable number of pores, with the highest average pore width approximately 25 ± 4 nm. Its pore width was greater than former values observed on different MWNT BP membranes [260]. An MWMT/Trix soaking in chitosan solution had fewer pores, with the lowest average pore width approximately 16 ± 2 nm.

Further, the surface area fundamentally depends on the outer surfaces of the nanotube bundles, which were calculated using [194]

$$A_{BET} = \frac{4}{p_{CNT}\, D_{bun}}\ , \qquad (11)$$

where A_{BET} is the BET surface area, D_{bun} is the CNT-bundle diameter and ρ_{CNT} is the nanotube-bundle density (determined as 1500 kg/m^3 [194] respectively). The average pore and bundle diameters of all BP membranes measured are presented in Table 6. The results demonstrate significant differences between BP membranes. The bundle diameters *(D_{bun})* appear to be inversely related to the surface area (i.e. the higher the nanotube-bundle diameters the lower the surface area of the BP membrane). In addition, the nanotube-bundle diameters increased from 23 ± 2 to 67 ± 1 nm upon soaking in chitosan solution 0.1% w/v for 24 h.

In further analyses of this hypothesis, the isotherm data collected from three BP membranes (Fig. 3.8) were used to calculate effective pore-size distribution and the total porosity of BP membranes using the BJH and HK methods [235, 236]. The HK method is employed to determine the distribution of small pores (<2 nm), and the BJH method is used to estimate large pores (>2 nm). Therefore, a combination of the BJH and HK methods can be used to determine the pore-size distribution for each BP membrane (Figs. 3.9A–C and Table 6).

The large peak from 0.5–1 nm is related to the pores between individual MWNTs (intertube pore volume), whereas the wide distribution of peaks from 2–100 nm are linked to the interbundle pore volume. The large pores are also visible in the SEM images (Figs. 3.7A–B)[194] and are in agreement with the average pore diameter estimated as listed in Table 6. In addition, the results in Table 6 show that the interbundle pore volume is largest for BP-A and smallest for BP-AI1, which is consistent with the treatment of the present study. It demonstrates that biopolymer (chitosan 0.1% w/v) intercalation results in a reduction of the surface area and porosity (interbundle pore volume).

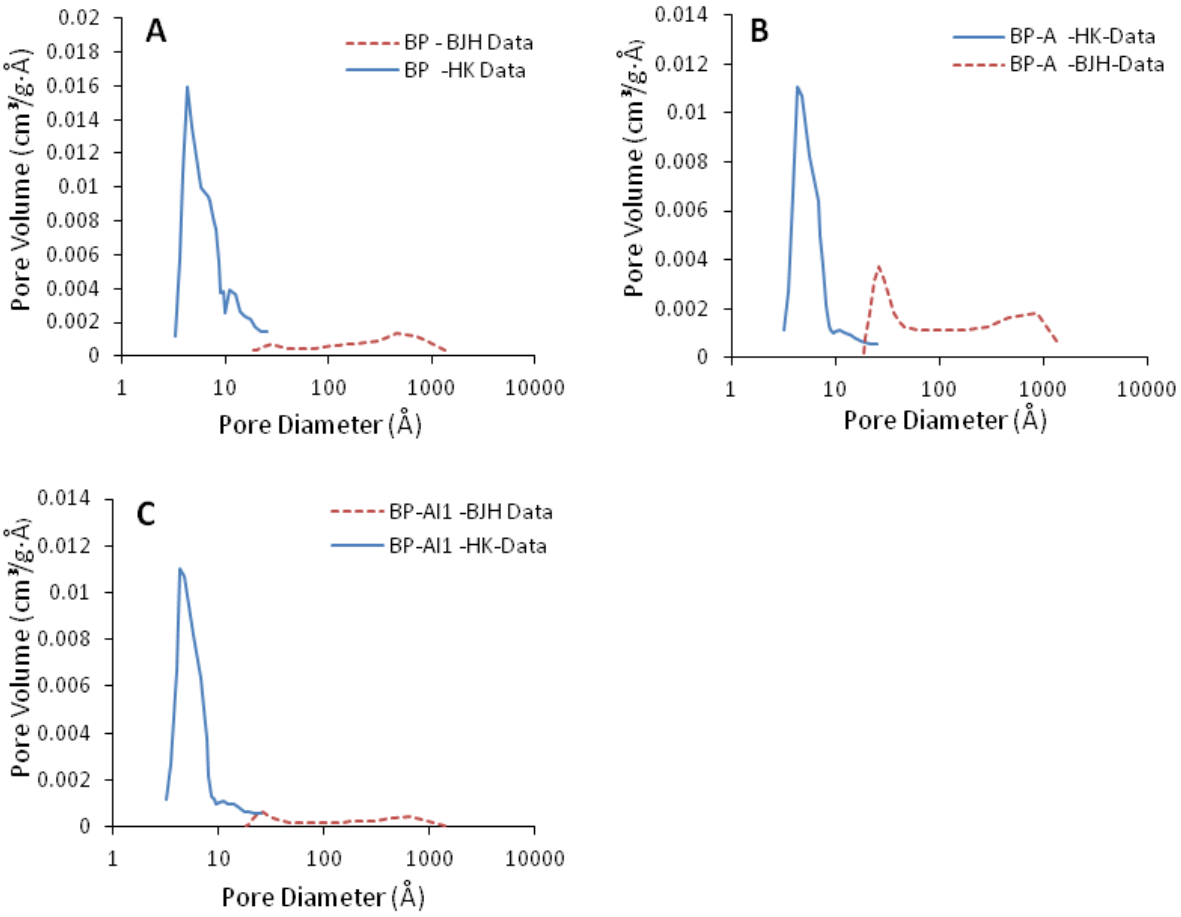

Figure 3.9. Total pore volume: a function of pore diameter for A) MWNT-Trix 1% w/v BP membrane (BP), B) MWNT BP membrane after annealing at 500°C for 2 h (BP-A) and C) MWNT BP membrane soaking in chitosan low Mw 0.1% (w/v) for 24 h (BP-AI1).

3. 6 Permeability studies

The discussions in the previous sections illustrate the possibility of incorporating various macro-cyclic ligands into MWNT BPs to develop mechanically strong, high porosity and hydrophilic membranes. These characteristics are essential if membranes are to be used in NF and microfiltration processes.

The next step in investigating the BPs' suitability for filtration applications was to test their water permeability using a customised dead-end filtration mechanism. The results of these tests are tabulated in Table 6 and show that all the BP membranes demonstrated water permeability at pressures <1.3 bar. Water-permeability graphs for MWNT BP annealed and soaked in biopolymer chitosan are illustrated in Figure 3.10. All the filtration trails indicated a linear increase in the accumulative permeate with time (Fig 3.10A). The slope for different applied pressures gives the stable permeate flux *J*, which increased with the pressure applied,

until the BP membrane were cracked by pressure for all buckypaper membranes. The required pressure for transporting water across the different BP membranes ranged 0.01–1.3 bar (Fig. 3.10B). The plot of the permeate flux against the applied pressures indicates a linear relationship for all buckypaper membranes, as illustrated in Figure 3.10B. Equation (12) was used to estimate the membrane flux:

$$f = \frac{J}{A.\Delta P}, \qquad (12)$$

where J represents the slopes of the graphs illustrated in Figure 3.10A, A is the effective area of the membrane exposed to water and ΔP is the sampling pressure [181]. All BP membranes were tested under different pressures to induce transport of water across them at 21°C.

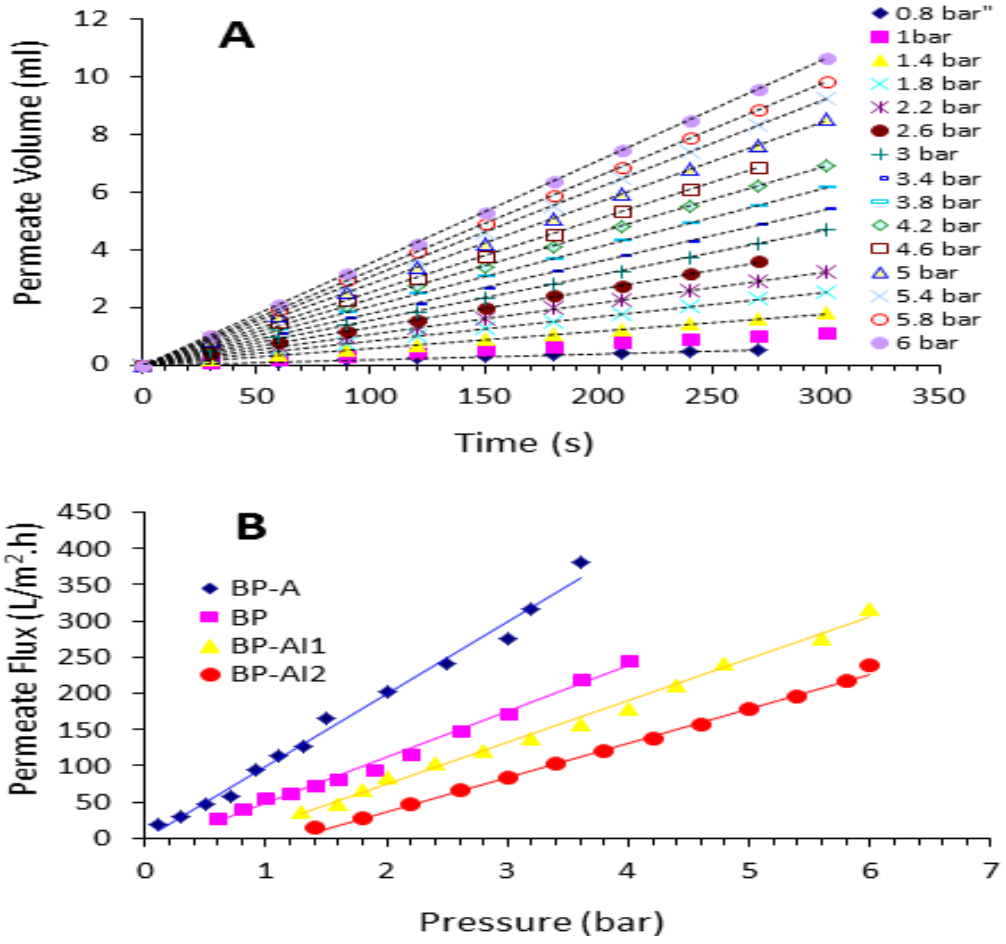

Figure 3.10. A) Plots of water-infiltration volume as a function of time under different pressures on BP membranes; and B) comparison of the permeation flux of (BP) MWNT-Trix 0.6% (w/v) BP, (BP-A) MWNT BP after annealing at 500°C for 2 h; (BP-AI1) MWNT BP soaking in chitosan low Mw 0.1% (w/v) for 24 h; and (BP-AI2) MWNT BP soaking in chitosan low Mw 0.1% (w/v) for 24 h.

A significant increase in water permeability was observed when the dispersant was evaporated or removed by annealing at 500°C in the MWNT/Trix BP. The maximum permeability increase occurred in the MWMT/Trix BP-A membrane with an average membrane flux at 108 ± 16 L/m^2 h bar, which was nearly 2 times greater than that obtained for the MWNT/Trix BP membrane before annealing (58 ± 7 L/m^2 h bar). The observed membrane flux of MWNT/Trix soaking for 24 h was similar to that of the MWNT/Trix BP membrane before annealing (59 ± 6 L/m^2 h bar), whereas the observed membrane flux of MWNT/Trix soaking for 96 h was lower than that of other BP membranes (44 ± 6 L/m^2 h bar). As expected, the MWNT/Trix BP-A membrane had the highest permeability, at 108 ± 16 L/m^2 h bar. The BP-A membrane was most permeable, consistent with its greater pore-width range (25 ± 4 nm) and surface area (232 ± 4 m^2/g), as shown in Table 6. Further, chitosan (adsorbed or intercalated) greatly affected the permeability characteristics of MWNT/Trix soaking for 24 and 96 h. The movement of water molecules through these buckypaper membranes immersed in chitosan (BP-AI1and BP-AI2) was 2 times less than the MWNT/Trix BP membrane (BP-A) after annealing. The performance of the other buckypaper membrane (MWNT-Trix) was comparable to that achieved by Sweetman et al. [181] for SWNT/Trix membranes prepared under the same conditions. The water permeability for the SWNT/Trix BP membrane (85 ± 5 L/m^2 h bar) appears to be greater than that of the MWNT/Trix buckypaper membrane (BP) before annealing produced in this study (58 ± 7 L/m^2 h bar) [181]. This may be because the SWNT/Trix BP has a high surface area (790 ± 4 m^2/g), whereas the MWNT-Trix had a lower surface area (114 ± 2 m^2/g). However, the value of water permeability for SWNT/Trix was less than the BP-A membrane (108 ± 16 L/m^2 h bar). A possible explanation is that the BP (MWNT-annealing) was deformed under the different pressure and annealed at the high temperature (500°C). The deformation or damage may have caused large empty spaces between the NT, which allowed water to cross the BP-A membranes at higher rates of flux. Therefore, larger internal pores in the BP (MWNT-annealing) play a significant role in faster transportation of water molecules. As reported in the experiments, the average pore width (Table 6) of all BP membranes is greater than 15 nm, which is larger than the kinetic diameter of a water molecule (0.30 nm) [261]. Consequently, the water molecules can flow through the BP membranes, enhancing the flux of the blend membranes.

3. 7 Conclusions

In this chapter, the researcher investigated the preparation, characterisation and water permeability of four different porous BP membranes produced by adopting different methods, such as annealing at 500°C and soaking in biopolymer chitosan. These treatments resulted in significant changes. For example, the conductivity increased from 19 ± 2 S/cm to 42 ± 2 S/cm after annealing. This suggests that removing the dispersant Trix from the BP membrane can lead to a reduction in the resistance of the CNT junctions in the CNTs network. In contrast, soaking the membrane in chitosan 0.1% (w/v) resulted in a decrease in electrical conductivity. Soaking in chitosan resulted in an enhancement in the Young's modulus and tensile-strength values. SEM images demonstrated that the intercalated chitosan coated the entire external surface of the BP. However, the pores were still clearly visible and not completely filled. The BET and permeability towards water measurements demonstrated similar trends (i.e. reduction in magnitude through soaking and increased by annealing). The results obtained by the BET, BJH and HK methods demonstrated that soaking the membrane in concentration 0.1% (w/v) of chitosan produced smaller surface areas and pore sizes than MWNT-Trix and annealing MWNT BP membranes. These results are consistent with the observation that the water permeability of MWNT BP soaking in chitosan was lower than that of membranes prepared from MWNT-Trix and annealing MWNT BPs.

Chapter 4: Salt Rejection of Commercial Membranes Coated with Thin Layer Masses of MWNTs

This chapter discusses the fabrication and characterisation of commercial membranes (nylon) coated with different masses of MWNT. These results provide the basis for subsequent work exploring the fabrication, properties and applications of coating membranes using MWNT. All coated membranes were prepared by vacuum filtration of MWNT dispersion through a commercial membrane filter. They were characterised by contact angle, electrical conductivity, mechanical properties, optical and SEM, surface area, pore distribution and salt-rejection behaviours.

4. 1 Electrical properties of coated membranes

In general, CNTs are hydrophobic materials; however, CNTs can be dispersed to make aqueous solutions suitable for a wider variety of applications, such as for producing thin membranes and coating membranes [180, 262, 263]. However, some difficulties may affect the quality of membranes formed from these solutions. These difficulties can be divided into several factors, including the CNT types, purity, sonication time, method and type of membrane used for the filtration procedure. In this chapter, all coated membranes were fabricated using the same CNT type (MWNTs), purity >95%, sonication time (30 min) and commercial filter membrane (nylon). The only variable factor was the amount of MWNTs added to the solution for making the coated membranes.

Assessing the electrical properties of membranes is of interest, as they can broaden the range of potential applications. For example, Madaeni et al. [264] reported that UF membranes coated by a conducting polymer (polypyrrole) rejected higher amounts of BSA than the corresponding non-conducting membranes. This indicated that the conducting polymers could affect selective ion transport in the electrical field. Moreover, the nanostructures of some materials have demonstrated a tuneable wettability in response to an applied electrical potential [265]. Therefore, the conductivity of the coated membranes in the present study was evaluated using the two-point probe method (Chapter 2). Hydrophilic commercial membranes (nylon) were coated using different amounts of MWNTs to assess the performance of membranes for the rejection of salts.

The I–V characteristics of the different coated membranes were examined at 21°C. The linear I–V characteristics for coated membranes (coated with 30 mg of MWNTs combined with 1% w/v Trix) demonstrated Ohmic behaviour, with the inverse of the slope plot relating to the resistance of the sample, as presented in Figure 4.2, whereas the resistance obtained from Figure 4.1 was plotted against the coated membrane length, as presented in Figure 4.2.

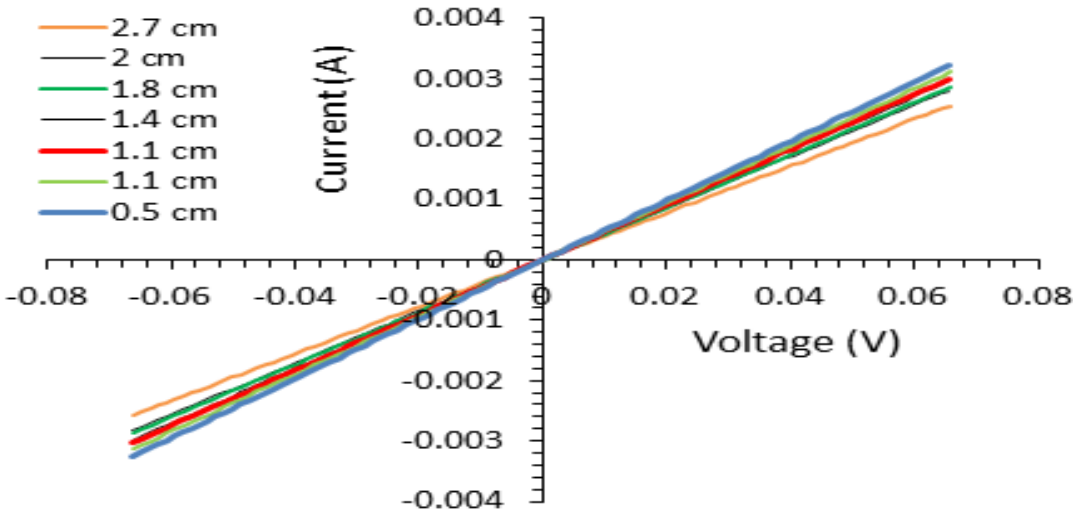

Figure 4.1. I–V characteristics of different lengths of commercial membrane (nylon) strips coated with 30 mg of MWNTs combined with Trix (1% w/v).

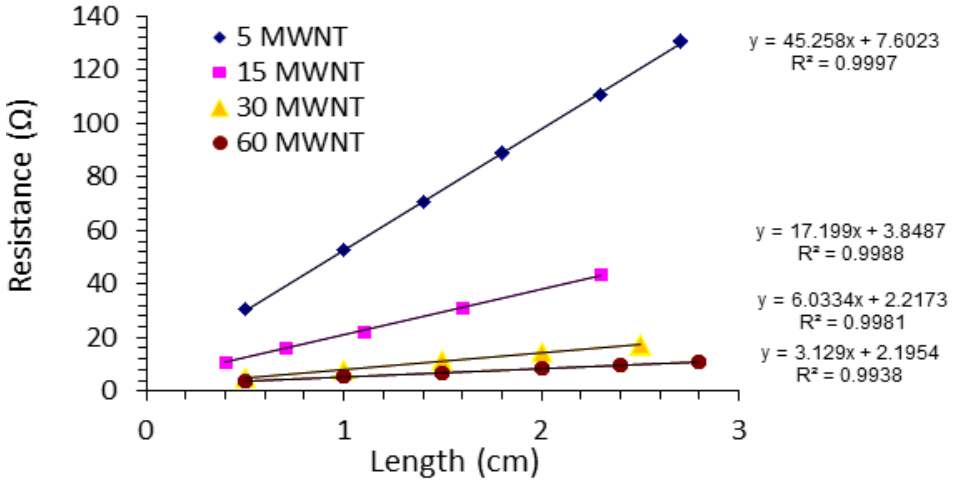

Figure 4.2. Effect of length on the resistance of the commercial membranes (nylon) coated with different amounts of MWNTs (5, 15, 30 and 60 mg) incorporated with Trix (1% w/v); all coated membranes were prepared using a filtration method.

Table 7. Physical properties of coated membranes with and without MWNTs; all values repeated are the means of at least five samples, with ± 1 standard deviation.

Membrane	Contact angle (°)	Elongation (%)	Tensile strength (MPa)	Young's modulus (MPa)	Conductivity (S/cm)	Thickness (µm)
Filter paper (nylon)	17 ± 3	18 ± 2	2.52 ± 0.1	63 ± 1	–	150 ± 1
5 MWNT	25 ± 3	11 ± 1	3.4 ± 0.2	101 ± 6	3.8 ± 0.1	167 ± 1
15 MWNT	31 ± 4	6 ± 1	2.98 ± 0.33	118 ± 4	8.4 ± 0.7	188 ± 2
30 MWNT	46 ± 2	3.4 ± 0.9	2.55 ± 0.24	137 ± 4	19 ± 1	216 ± 1
60 MWNT	63 ± 3	2.7 ± 0.7	2.52 ± 0.38	154 ± 1	28 ± 2	292 ± 1

The linear I-V relationships represented in Figure 4.2 indicate that the coated membranes showed ohmic behaviour, with the inverse of the slope of each plot corresponding to the coated membranes. These resistances were plotted against the coated membranes' lengths presented in Figure 4.2. The resistance at zero length related to the contact resistance, which occurred at the electrode-coated membrane interface. The use of silver paint and a constant force, as explained in the experimental section (Chapter 2), helped to ensure that this value remained constant between individual measurements. The straight lines in Figure 4.2 can be obtained using equation 10 (Chapter 3), as summarised in Table 7.

The results (Table 7) demonstrate that increasing the amount of MWNT coating increased the conductivity of the coated membranes. The increase may be due to the presence of the CNTs-coated membrane interface, as the nylon membrane is insulating [182, 266]. The electrical conductivity increased with MWNT content; that is, 3.8 ± 0.1 S/cm (5 mg MWNT), 8.4 ± 0.7 S/cm (15 mg MWNT), 19 ± 1 S/cm (30 mg MWNT) and 28 ± 2 S/cm (60 mg MWNT). Broza et al. [266] reported that increasing the mass of the MWNT leads to a significant enhancement of the conductivity of the nanocomposites. They also found the greatest values of electrical conductivity at higher levels of MWNT content. This suggests that a small mass of MWNT content (5 mg MWNT) cannot effectively coat the entire surface

of commercial membranes. This can create many cracks at the surface and MWNT junctions in the CNT network. These cracks may lead to increases in the resistance and reductions in the conductivity at the membranes' surfaces. Moreover, the results of earlier examinations of BPs membranes indicated that the conductivity of BP membranes (24 ± 16 S/cm) prepared using MWNT-Trix were higher than that of corresponding coated membranes (19 ± 1 S/cm) fabricated using the same mass of MWNTs (30 mg) and dispersant molecules [256, 257]. In contrast, the conductivity of a coated membrane (30 mg MWNT) was reported at 19 ± 1 S/cm, which is similar to that reported here (Chapter 3) for a MWNT/Trix BP membrane.

4. 2 Wettability of coated membranes

A membrane's surface wettability is an important characteristic, as it provides details about the nature of the surface. Coated membranes, in particular, should have hydrophilic (wettable) surfaces if they are to be used as filtration membranes for natural water systems. A hydrophilic surface can enhance water permeation through the membranes. Recently, direct methods have been adapted for contact-angle measurements using goniometers or contact-angle analysers [267]. Figure 4.3 and Table 7 demonstrate that the contact angles of all the coated membranes increased with increasing MWNT content, ranging 25° ± 3° to 63° ± 16°. This indicates that the surfaces of coated membranes are hydrophilic, most likely owing to the presence of the dispersant molecules (Trix) on the surface of the nanotubes. The contact angles for some of these coated membranes by MWNT-Trix are significantly lower than those reported previously for SWNT-Trix BP membranes (73 ± 4°) [180]. In the case of the commercial membranes (nylon) coated with 30 mg of MWNT-Trix, the contact-angle values were slightly lower than those obtained from the SWNT and MWNT-Trix BP membranes, which were 54 ± 4° and 55 ± 10° respectively [181]. This indicates that water can be moved more easily through the pores of these coated membranes than SWNT and MWNT BP membranes, and lower pressures may be required to achieve transport via these coated membranes.

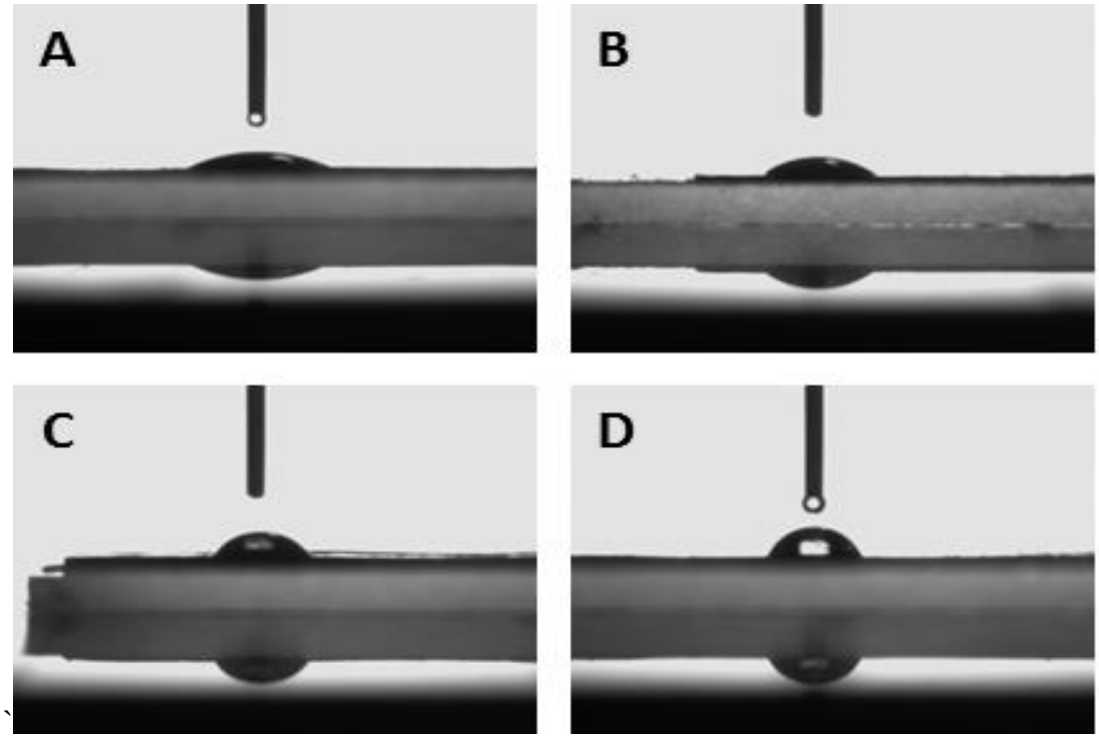

Figure 4.3. Contact angle of the commercial membranes (nylon) were coated with different amounts of MWNT: A) 5 mg; B) 15 mg; C) 30 mg; and D) 60 mg and mixing with Trix (1% w/v) as dispersion; all the CNTs with Trix (1% w/v) were sonicated for 30 min and then deposited on the surfaces of commercial membranes using a filtration method.

4. 3 Mechanical properties of coated membranes

The membrane's mechanical strength is of primary importance in seawater separation mechanisms. This is because the membrane must be able to withstand various pressure loads, flow rates and high temperatures for extended periods [242]. Therefore, a study on the mechanical features of BPs was conducted using the tensile testing methodology. The results are plotted in Figure 4.4, initially indicating a linear stress-versus-strain relationship, which implies elastic deformation. Still, at higher strain levels, small deviances from the linear relationship could be seen, which suggests that the materials have a high brittle failure mechanism. Low strain fracture was seen in 3–13% of the coated membranes. The stress-versus-strain plots were used to determine mechanical properties, such as Young's modulus, breaking extension and tensile strength. Table 7 summarises the values found for different BPs.

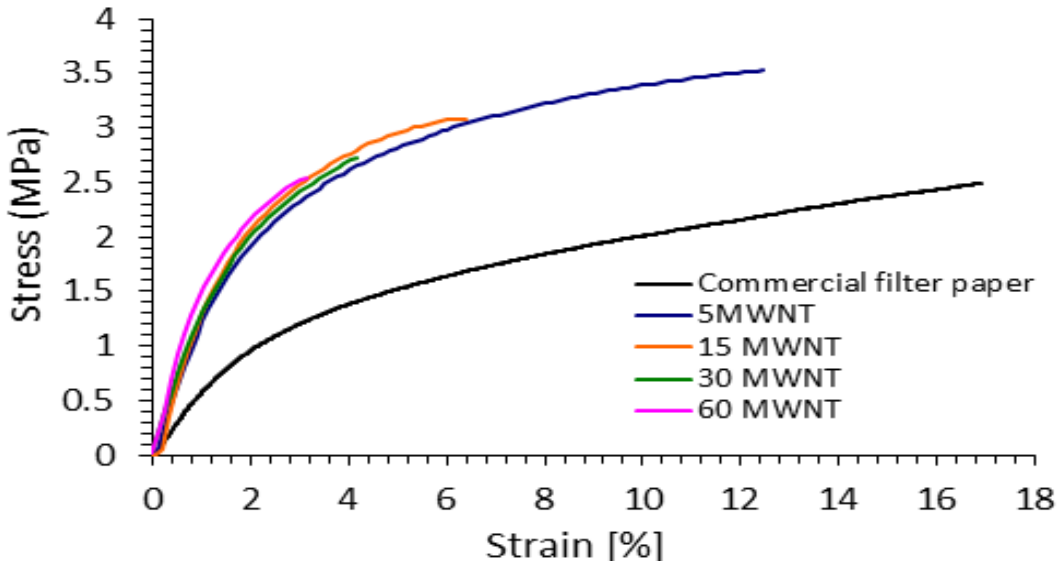

Figure 4.4. Stress–strain curves of typical coated MWNT-coated membranes; commercial filter paper is presented as a comparison.

The results for the three mechanical properties (tensile strength, Young's modulus and elongation) for coated membranes are within a narrow range and similar to those previously obtained for CNT membranes [180, 242, 256, 257]. The coated membranes resulting from dispersions in MWNT and surfactants showed Young's moduli in the range 63–154 MPa, elongation in the range 2.7–18% and tensile strength in the range 2.5–3.4 MPa. The mechanical characteristics of the coated membranes were low because the dispersants in the membrane were similarly sized. Recent research supports this hypothesis, showing that, only when high molecular mass dispersants, such as polysaccharides and proteins, were included in the membrane, was there a significant increase in the strength of BPs made from SWNT and MWNT [180, 242, 256]. Moreover, the results demonstrate an increase in Young's modulus with an increasing amount of MWNTs. For example, coating the surface of the commercial membranes with 60 mg MWNT resulted in a 2.4 times value increase in Young's modulus compared to the commercial membranes (nylon). Further, the tensile strength was highest when 5 mg of MWNTs was deposited onto the surface of the commercial membranes. Increases in the MWNT coating decreased tensile-strength values. The values of tensile strength increased with increased MWNTs, even up to high CNT content (e.g. 30 mg). Moreover, the elongation of the commercial membrane (nylon) reduced with increasing amounts of MWNTs, as demonstrated in Figure 4.4 and Table 7. This is consistent with the stiffening effect of the CNTs. Wang et al. [224] observed similar behaviour; the increase in

the MWNT content affected the elongation properties, whereas the Young's modulus increased and tensile strength remained stable at higher concentrations of MWNT. In contrast, the mechanical properties reported here for the commercial membranes coated with 30 and 60 mg of MWNTs are lower than those obtained previously for CNT membranes prepared using different types of CNTs and surfactants [180, 181, 257]. In addition, the mechanical properties of coated membrane (coated by 30 mg of MWNT/Trix) are similar to those BP membranes prepared using identical conditions in Chapter 3. This suggests that changing the substrate type or the amount of CNTs and dispersants may affect the mechanical properties of coated membranes.

4. 4 Surface morphology of coated membranes

In order to further increase our understanding of the major changes on the surface morphology of the commercial membranes (nylon) coated by MWNT using SEM. For instance, Figure 4.5A–K shows the SEM micro-graph of the four coated membranes, which reveals surface morphology having large nanotube bundles with diameters in excess of 100 nm and pore sizes significantly smaller than those of SWNT/Trix and MWNT/Trix CNT membranes [180, 242, 256, 257].

Figures 4.5A–K also show that the morphologies of all coated membranes share many similarities. Figures 4.5A–B show the surface morphologies of coated membranes covered with 5 mg of MWNT using dispersions (Triton X-100, 0.6% w/v) with minor differences from other coated membranes (images 4.5C–K). Moreover, the SEM images demonstrate that pore sizes changed with increased MWNTs. Tang et al. [252] reported that the pore size and porosity of a membrane can be decreased by increasing the MWNT content. There were only relatively minor differences in the surface morphology of coated membranes due to the different masses of MWNTs used. For example, Figures 4.5A–B show that the surface of the commercial membrane containing 5 mg of MWNT had more surface pores than the other three coated membranes (Figs. 4.5C–K). Therefore, the SEM images reveal little observable difference between the surface morphologies of these coated membranes prepared using different amounts of MWNT mixed with Trix 0.6% (w/v) as dispersants. In addition, SEM images of the coated membranes in Figures 4.5A–K are less clear than the SEM images of the BPs prepared from SWNT and MWNT-Trix [180, 181, 257]. This could be related to a layer of nylon (support layer), as shown in Figure 4.6, which may reduce the conductivity at the surface, thereby lowering the SEM quality. From Figures 4.5A–K, it becomes clear that

coating by CNTs may lead to a change in the effective pore size of the commercial membrane (nylon). This pore-size control is useful for separation processes, such as desalination.

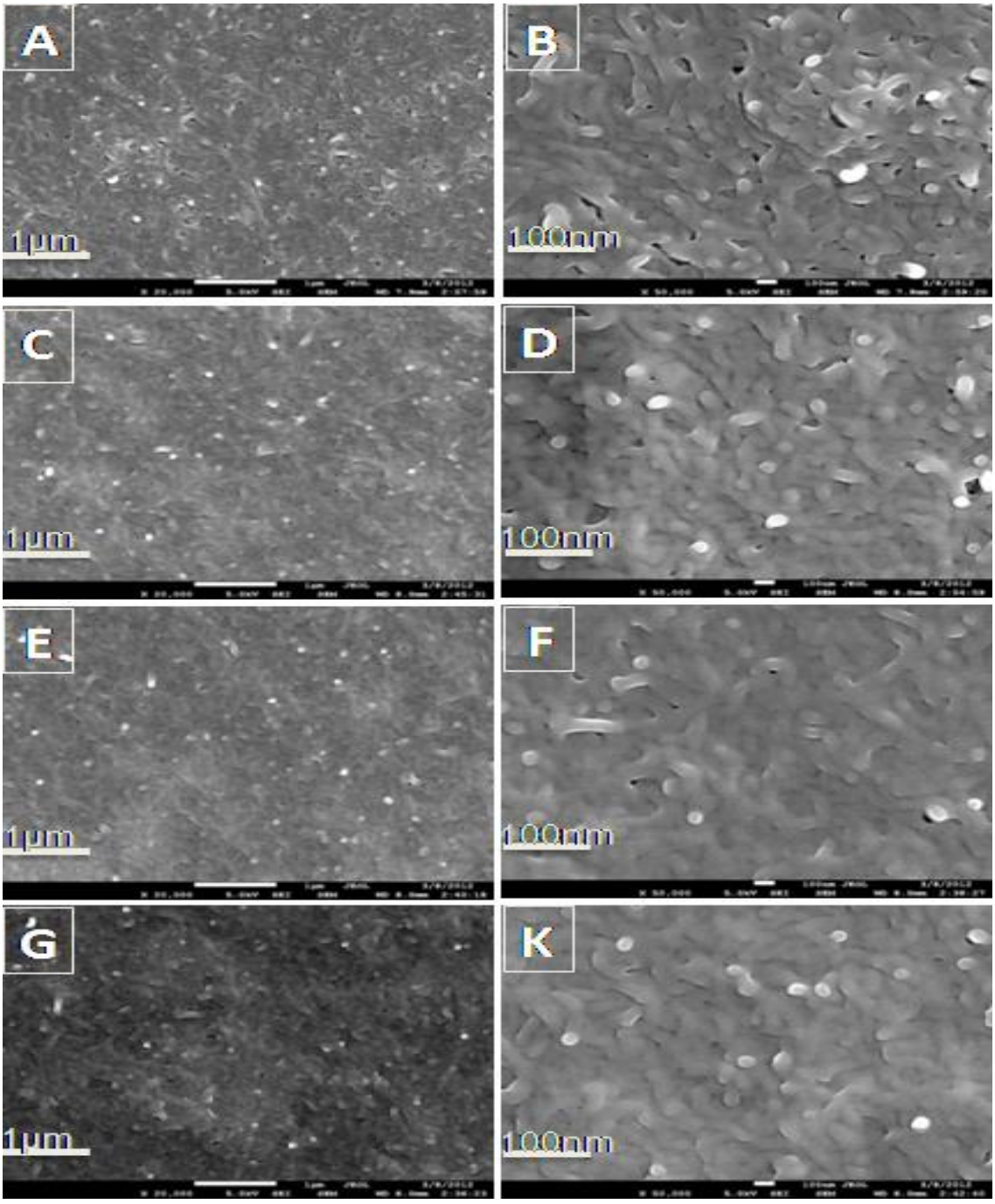

Figure 4.5. A–B) SEM images for the commercial membranes coated by MWNT—content 5 mg; C–D) MWNT—content 15 mg; E–F) MWNT—content 30 mg; and G–K) MWNT—content 60 mg.

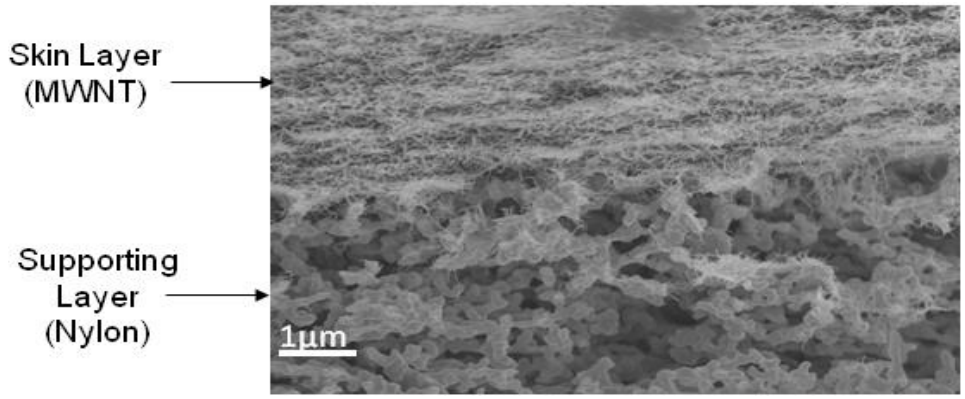

Figure 4.6. SEM cross-section image for the commercial membrane coated by MWNT, content 60 mg.

Further, the thicknesses of the coated membranes were determined using optical microscopy. Measurements were made at 10 points for each membrane and the results used to calculate the mean thickness as presented in Table 7. Figures 4.7A–D indicate that increasing the amount of MWNTs on the commercial membrane led to an increase in the thickness from 150 ± 1 to 292 ± 1 µm as a result of the coating. This suggests that water will more easily flow into the pores of the coated membrane with the lowest thickness, and that less pressure will be required to achieve transport by this coated membrane.

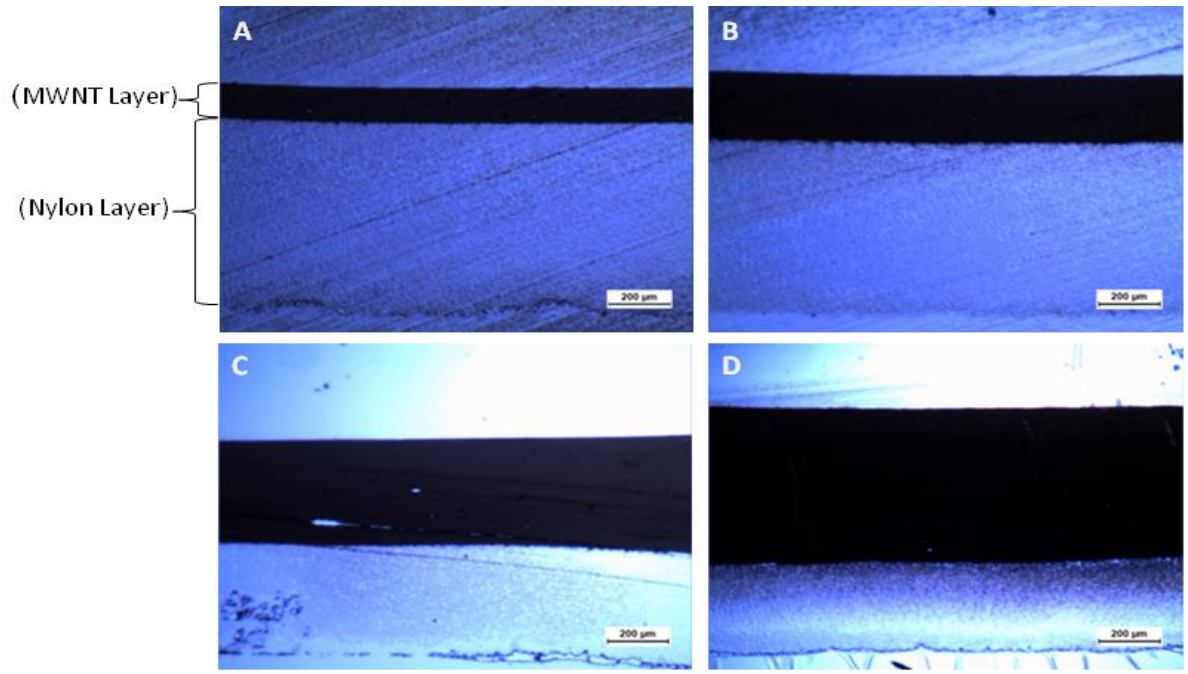

Figure 4.7. Optical images of the cross-section of the commercial membrane coated with: A) 5 mg of MWNT; B) 15 mg of MWNT; C) 30 mg of MWNT; and D) 60 mg of MWNT.

4. 5 Surface areas and pore structures of coated membranes

The surface areas and pore structures of all commercial membranes coated with MWNT were investigated in detail using the BET analysis of isotherms obtained from N_2 adsorption/desorption measurements at 77 K [234]. Figure 4.8 demonstrates the typical isotherms obtained. The commercial membranes (nylon) coated by MWNTs demonstrated a general type IV isotherm with hysteresis at higher P/P_o [181]. It has been suggested that hysteresis can occur due to multi-layer adsorption in materials or in porous materials by the differences in the rates of filling and removal of the adsorbent through a capillary condensation mechanism [181, 268].

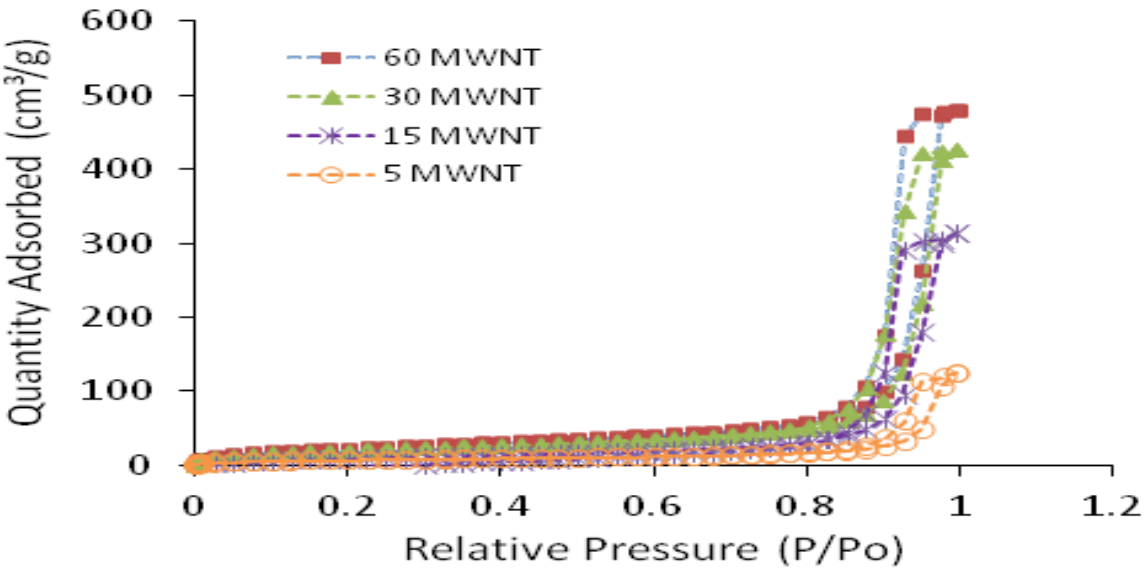

Figure 4.8. Adsorption isotherm demonstrates a comparative plot of the P/P_o and adsorption of all commercial membranes (nylon) coated with different amounts of MWNTs.

BET analysis of the adsorption isotherms revealed specific surface areas of the coated membranes ranging 22–81 m^2/g (Table 8). The surface area of the coating membrane coated with 5-mg MWNT was significantly lower than the other coating membranes, whereas the surface area for other coating membranes was gradually increased by increasing the MWNT mass. The coated membranes exhibited surface-area values lower than the MWNT BPs (161–229 m^2/g) [260].

Table 8. The surface areas (A_{BET}), average pore diameters (d_{BET}), average bundle diameters (D_{bun}) and water permeability of commercial membranes (nylon) coated by different amounts of MWNT using filtration system.

Coating membrane	A_{BET}(m^2/g)	Pore diameter (nm)	Bundle diameter (nm)	Interbundle pore volume (%)	Water permeability (L/m^2 h bar)
Filter paper (nylon)	–	–	–	–	2864 ± 172
5 MWNT	22 ± 2	2.1 ± 0.1	121 ± 2	82 ± 2	313 ± 54
15 MWNT	39 ± 2	17 ± 2	68 ± 1	95 ± 2	96 ± 13
30 MWNT	70 ± 1	17 ± 2	38 ± 1	84 ± 1	40 ± 5
60 MWNT	81 ± 1	17 ± 1	33 ± 1	95 ± 1	26 ± 6

The outer surfaces of the nanotube bundles can be estimated using equation 11 [194]. The average pore diameter and bundle diameter of all coating membranes determined are presented in Table 8. The results (Table 8) demonstrate significant differences between coating membranes. The bundle diameters demonstrated an inverse relationship with the surface area (i.e. the higher the nanotube-bundle diameters the lower the surface area). In addition, the nanotube-bundle diameters decreased from 121 ± 2 to 33 ± 1 nm by increasing the MWNT content.

The pore-size distribution within the coated membranes was estimated using two methods. The HK method was employed to measure small-diameter pore sizes (<2 nm), and the BJH method was used to measure larger pore sizes (>2 nm) [181, 194]. The pore-size distribution results are presented in Figure 4.9.

The distribution of pore sizes demonstrates a large peak (left, 0.5–1 nm) that may correspond to intrabundle pores. A broad distribution of peaks (right) is present in all coated membranes from 2–100 nm. These can be attributed to the larger pores visible in the SEM images (Fig. 4.5) [194]. Numerical integration of the curves seen in Figure 4.9 reveal that these larger interbundle pores (right peaks) are responsible for 82–95% of the total free volume of the commercial membranes coated by different amounts of MWNT. These values agree well with those reported in a previous study using CNT (SWNT and MWNT) BPs fabricated with different dispersants [257].

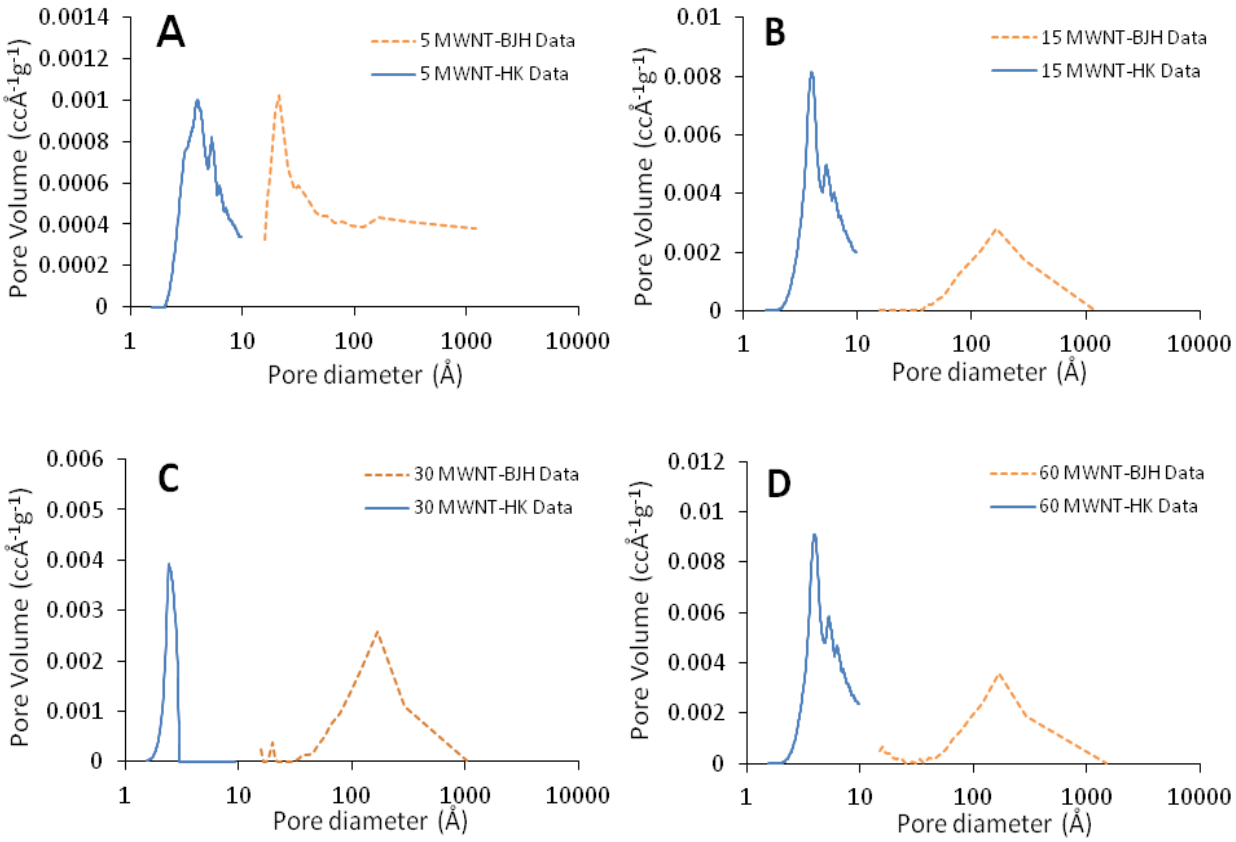

Figure 4.9. Pore-size distributions for coated commercial membranes (nylon) by MWNTs were determined using HK (blue line) and BJH (orange dotted line) methods: A) 5-mg MWNT; B) 15-mg MWNT; C) 30-mg MWNT; and D) 60-mg MWNT.

4. 6 Permeability and salt rejection of coated membranes

A key consideration when evaluating a potential filtration membrane is its permeability, particularly towards water. To investigate the permeability of the coated commercial membrane (nylon), water was selected as the infiltration liquid using a custom-made dead-end filtration-cell setup (Fig. 2.6, Chapter 2). Water also provides a suitable viscosity for the permeability tests to estimate the volume and penetration times across the commercial membranes coated by different amounts of MWNT [260] without fouling problems. The water-permeability experiments were conducted on all membranes (commercial and coated). Figure 4.10A demonstrates that pressure increases applied to a coated membrane (containing 60 mg of MWNT and Trix 1% w/v as surfactant) resulted in an increase in the permeate volume *(J)*.

The resulting permeability of the non-coated and coated membranes is calculated from the permeation flux (Fig. 4.10B) using equation 12 [181] and is summarised in Table 8. All

coated membranes became permeable to water at pressure of approximately 0.4 bar. The water-transport behaviour of the coated membranes decreased with increasing MWNT content. The water permeability of the nylon membrane (commercial membrane) was significantly reduced when coated by MWNT (Fig. 4.10B). For example, the water permeability of nylon reduced from 2864 ± 172 L/m^2 to 313 ± 54 L/m^2 h bar after coating with 5-mg MWNT. This may be attributed to the differences in pore sizes and free volume between the supporting (nylon) and skin (MWNT) layers, as presented in Figure 3.3.6.

To further investigate water permeability by varying the MWNT of the coated membranes, the membrane flux was measured for 5MWNT/Trix, 15MWNT/Trix, 30MWNT/Trix and 60MWNT/Trix (Table 8). The results were 313 ± 172 L/m^2 h bar, 96 ± 13 L/m^2 h bar, 40 ± 5 L/m^2 h bar and 26 ± 6 L/m^2 h bar, respectively. Compared to 5MWNT/Trix, the lowest permeability was a factor of 12, as observed in the 60MWNT/Trix, whereas the 30MWNT/Trix exhibited nearly 8 times less permeability. The 15MWNT permeability was also 3 times lower. No apparent correlation was observed in the average internal pore diameter determined using BET and SEM analyses for the above coated membranes. However, the membrane flux with maximum permeability (5MWNT/Trix) had an average thickness of 197 ± 1 µm. Additionally, the highest thickness of the coated membranes was 292 ± 1 µm, the highest surface area was 81 ± 1 m^2/g and the highest mass of MWNT (containing 60 mg of MWNT and Trix 1% w/v as surfactant) exhibited the lowest permeation flux rate (26 ± 6 L/m^2 h bar). From the above coated membranes (5MWNT/Trix and 60MWNT/Trix), it was found that the water permeability decreased with increasing MWNT content, which may have been caused by the decreased hydrophilicity of coated membranes due to increasing MWNT content (Fig. 4.3 and Table 7). Moreover, the results obtained for the coated membranes are contradictory to those obtained for the membranes made by Kim et al.[269], who reported that the permeability of the membranes increased by increasing the weight fraction of the CNTs. This is because the researchers used functionalised CNTs to fabricate their membranes, and functionalised CNT can increase hydrophilicity caused by the hydrophilic groups (–COOH and –OH) on the membrane surfaces. This may then increase the water permeability of the membranes. Therefore, the nature and concentration of MWNT determines the effective water permeability, which thus determines the mass transfer through the coated membranes.

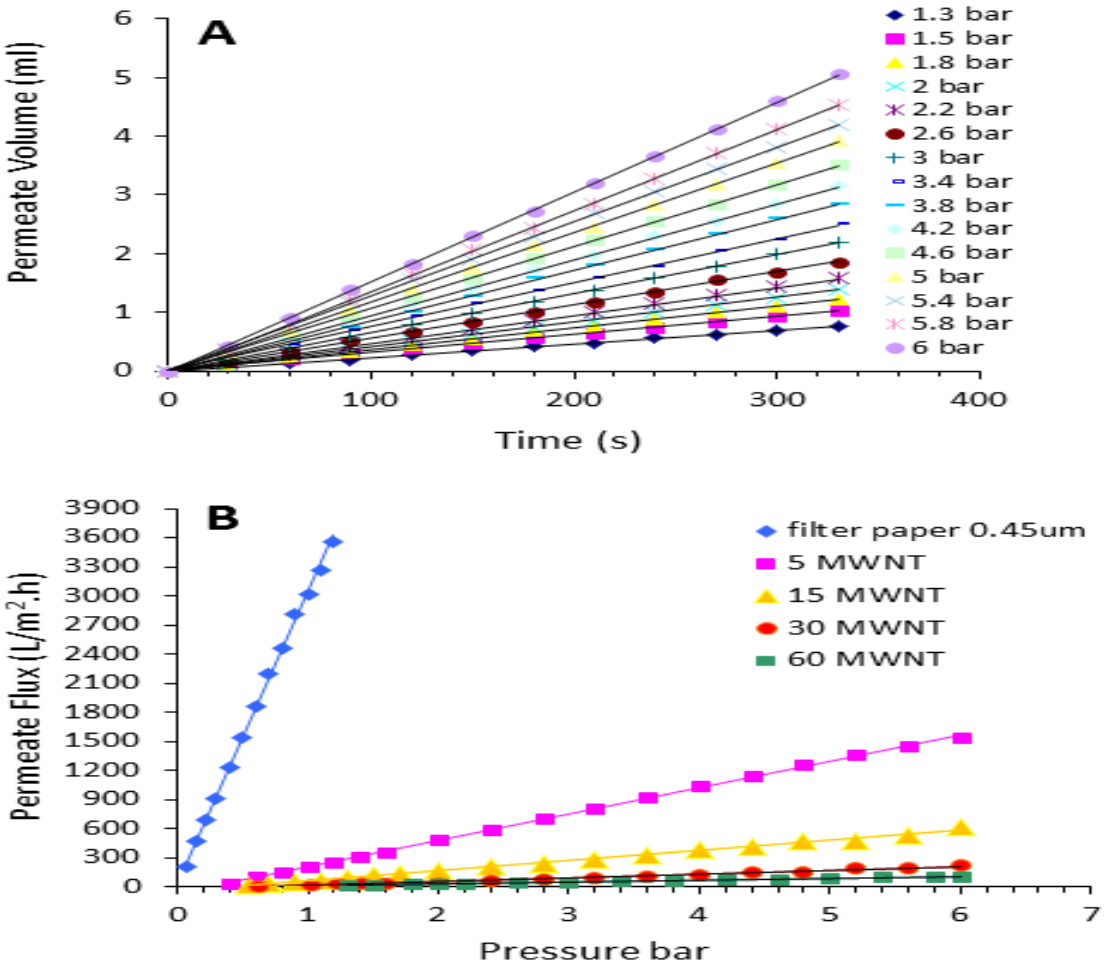

Figure 4.10. A) Permeate (water infiltration) volume as a function of time under different applied air pressures for commercial membranes coated with 60 mg of MWNTs; B) permeate flux rate of water versus applied pressure for the non-coated and four coated membranes.

The MWNT-coated membrane ability to reject single salts (NaCl or $MgSO_4$) was investigated by performing transport experiments using a salt solution (2 g/L) as the feed. The membranes were placed between two layers of a custom-built dead-end filtration-cell unit (Fig. 2.6, Chapter 2), and pressure was applied to force the solution through the coated membranes. The permeate solution (NaCl or $MgSO_4$), which passed across the coated membranes, was collected (150 mL) at constant permeate flux for 3 h (Fig. 4.11A). It was then analysed using a conductivity meter (Fig. 2.7, Chapter 2 and Appendix Figure 1). The rejection ability was calculated using equation 7 (Chapter 2).

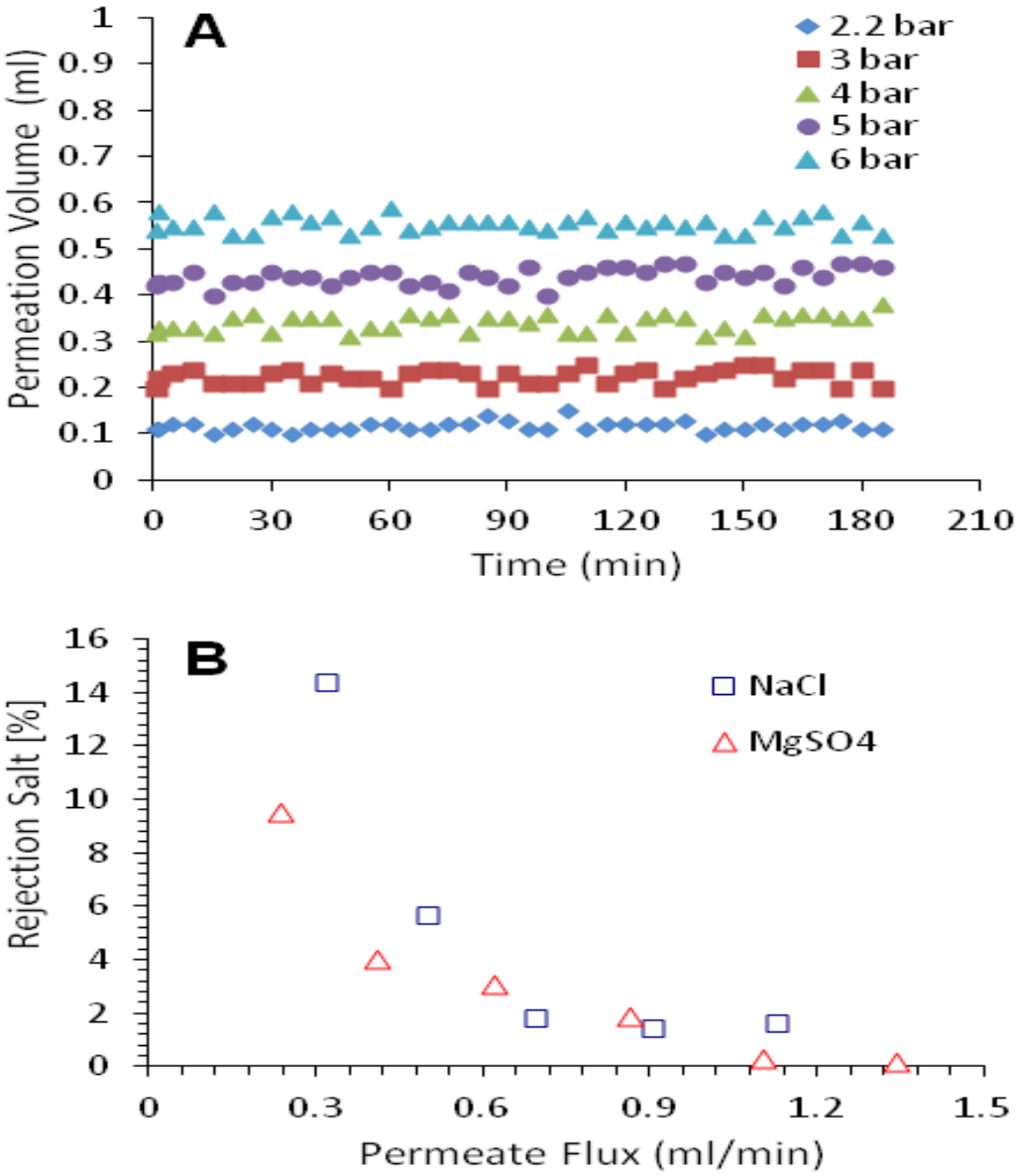

Figure 4.11. A) Permeation volumes as functions of time at applied pressures and B) effect of increasing the permeate flux on the salt rejection of the commercial membranes coated with 60 mg of MWNT.

The salt rejections obtained from equation 7 are demonstrated in Figure 4.11B. Commercial membranes coated with 60 mg of MWNT showed low rejection of both NaCl and $MgSO_4$, and the rejection of these salts was decreased by increasing the permeate flux. These findings are consistent with a previous study by Padaki et al. [270], who reported membrane performance for salt (NaCl) rejection at different fluxes (L/m^2 h) and pressures (1–8 bar). The rejection was significantly decreased with increased flux. This may suggest that the membrane broke at low pressure, leading to the reduced salt (NaCl) rejection by

increasing the permeate flux. In addition, the low salt rejection indicated that the interbundle pores of the MWNT-coated membranes might be larger than the salt size. Thus, the NaCl and $MgSO_4$ molecules could be passed through the interbundle pores of the MWNT-coated membranes. Moreover, a previous study showed that salt can be adsorbed by CNT membranes [262]. Adsorption and convection control the passage of salt across the membranes when the pore sizes are greater than the salt molecules. Salt passage is retarded across the membrane layer; therefore, salt retention is governed by the adsorption mechanism until the material is saturated. A membrane can reject or separate the components of a mixture using one or more mechanisms, such as adsorption, electrostatic interactions and size exclusion [78]. Size exclusion is the primary rejection mechanism for molecule removal by way of an analyte's physical size. Clearly, the changed structure and increase in the MWNT interbundle pores can be expected to improve the permeation flux by decreasing the rejection salts. For example, the commercial membrane coated by 60 mg of MWNT as a skin layer had a poor ability to reject the salts (NaCl and $MgSO_4$). The results illustrate that salt rejection decreased dramatically from ~14% for NaCl and ~10% at permeate flux for $MgSO_4$ (0.3 mL/min), to 1.6% at a permeate flux of ~1.1 mL/min for NaCl and 0.2% at a permeate flux of ~1.3 mL/min for $MgSO_4$. Since the percentage of rejection reduced as the permeate flux increased, the major removal mechanism may have been adsorption. Initially, there were more sites available on the MWNT bundles coating the membranes, which allowed greater adsorption and a higher initial level of salt rejection. Over time, the MWNT bundles coating the membranes became saturated with salts. This saturated state reduced the membrane's ability to reject salts. Thus, the low overall salt-rejection capacity of the coated membranes can be attributed to adsorption occurring mainly at the surface and large interbundle pores between the MWNTs.

4. 7 Conclusions

The surfaces of the hydrophilic commercial membranes (nylon) were successfully coated by homogenous solutions containing MWNTs and Trix as surfactant. The electrical conductivity and some mechanical properties, such as the Young's modulus, increased by increasing the mass of the MWNTs. However, other mechanical properties (tensile strength and elongation) and the hydrophilicity of the coated membranes decreased by increasing the MWNT content. Moreover, the water permeability of the coated membranes was significantly reduced by increasing the mass of the MWNTs. The permeability was several orders of

magnitude lower than the non-coated membranes (commercial nylon membrane). The single salts (NaCl or $MgSO_4$) were only rejected by coated membranes with the highest MWNT content (commercial nylon membranes coated with 60 mg of MWNT). However, the results of the salt-rejection experiments indicated that MWNT-coated membranes have limited use at high pressures. Salt rejection is governed by the adsorption mechanism until the material is saturated. The potential use of these materials for the rejection of salts from aqueous solutions requires further investigation. This should include an investigation using MWNTs with other materials, such as polymers or biopolymers, to improve the ability of the coated membranes to reject salts from aqueous solutions.

Chapter 5: Rejection of Mono- and Divalent Ions by Composite BP MWNT/chitosan Membranes

BP membranes were prepared with MWNT (150 mg) and biopolymer surfactant chitosan (0.1–0.4% w/v) as a dispersion material according to the method described in the experimental section. Various properties of these BP membranes were investigated. Based on these results, their suitability for the rejection of mono- and divalent ions from aqueous solution is presented hereunder.

5. 1 Electrical properties

Electrical properties, such as conductivity and the BP membranes' resistances to different MWNT/chitosan byckypaper membranes, were determined using the methods presented in the experimental section. The length-resistant characteristics of BP membranes were obtained under controlled ambient conditions (21°C and 45% RH). Results are shown in Figure 5.1 and Table 9. All BP the membranes demonstrated linear length-resistant characteristics (Fig. 5.1).

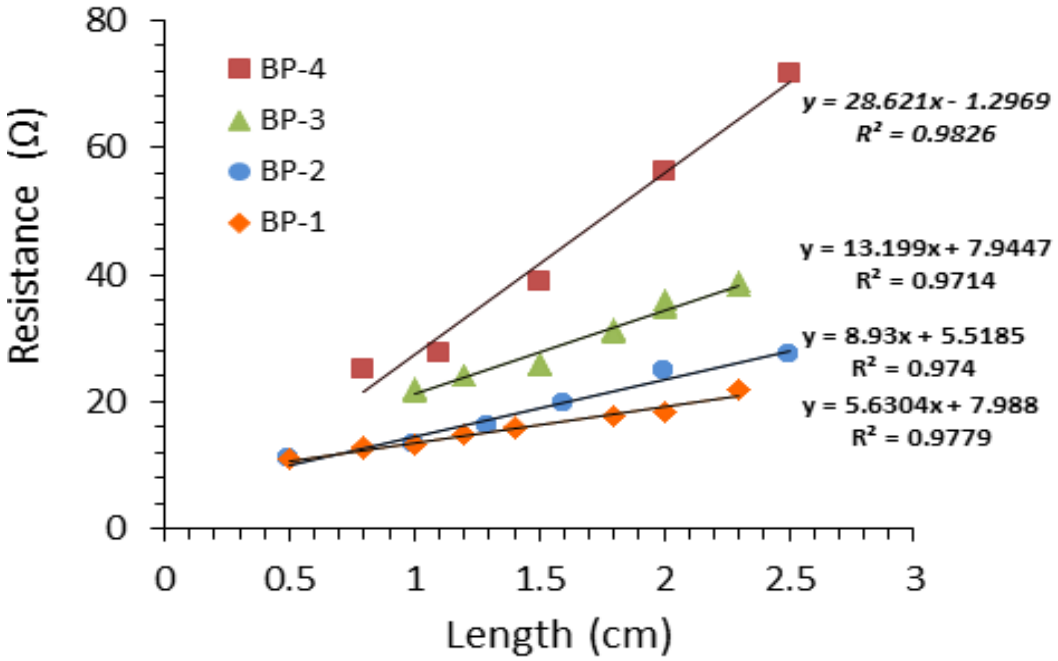

Figure 5.1. Electrical resistance as a function of length of the strip for different BP membranes: BP-1 (MWNT/chitosan 0.1% w/v); BP-2 (MWNT/chitosan 0.2% w/v); BP-3 (MWNT/chitosan 0.3% w/v); and BP-4 (MWNT/chitosan 0.4% w/v); all MWNT/chitosan were fabricated using a filtration method.

Table 9 shows that the conductivity values of MWNT/chitosan BP membranes decreased with increased concentrations of chitosan. For example, the BP membrane (MWNT/chitosan-1) with the lowest concentration of chitosan (0.1% w/v) produced the highest conductivity (83 ± 3 S/cm), and the BP membrane (MWNT/chitosan-4) with the highest concentration (0.4% w/v) exhibited the lowest conductivity (17 ± 1 S/cm). This indicates that the biopolymer chitosan was likely wrapped around the nanotubes (MWNTs), resulting in greater resistance on the surface of the membranes, thereby reducing conductivity. Several previous studies [180, 246] reported similar observations; that is, increasing the biopolymer concentrations can play an important role in the reduction of the conductivity of BP membranes. Therefore, it is suggested that the conductivity of BP membranes is affected by increasing the concentration of these biopolymers. Moreover, conductivity of the BP membrane (MWNT/chitosan-1) is 83 ± 3 S/cm, which is significantly higher than those values obtained for BP membranes prepared with the same CNTs (MWNT) but mixed with Trix, ciprofloxacin hydrogen chloride (cipro) and gellan gum as dispersants [246, 257]. The conductivity values obtained for all BP membranes are also comparable to those obtained for other BP membranes prepared from SWNTs and dispersants, such as Trix and cipro [180, 181].

Table 9. Effect of increasing the concentration of chitosan on the different properties of MWNT/chitosan: MWNT/chitosan-1 (0.1% w/v); MWNT/chitosan-2 (0.2% w/v); MWNT/chitosan-3 (0.3% w/v); MWNT/chitosan-4 (0.4% w/v); all MWNT/chitosan were prepared using a filtration method.

BP membrane	Contact angle (°)	Thickness (µm)	Conductivity (S/cm)	Permeability ($Lm^{-2} h^{-1} bar$)
MWNT/chitosan-1	124 ± 3	34 ± 1	83 ± 3	5.73 ± 0.3
MWNT/chitosan-2	106 ± 2	43 ± 1	54 ± 3	1.65 ± 0.04
MWNT/chitosan-3	96 ± 5	51 ± 1	20 ± 2	1.06 ± 0.07
MWNT/chitosan-4	91 ± 4	60 ± 2	17 ± 1	0.59 ± 0.04

5. 2 Contact angle

CNT is hydrophobic and chitosan surfactant is hydrophilic and able to wrap around CNTs, thereby increasing the adsorption capacity for CNT [210, 269]. The contact angles of

four different MWNT/chitosan membranes were measured as previously. Images of the contact angles are shown in Figure 5.2 and the obtained results from these photos are listed in Table 9. The contact angle decreased from 124° for MWNT/chitosan-1 to 91° for MWNT/chitosan-4, with the lowest (0.1%w/v) and highest (0.4%w/v) chitosan respectively. The hydrophilicity of the BP membranes was gradually enhanced by increasing the concentration of chitosan. Improvement in the hydrophilicity of the MWNT/chitosan BP membranes may have been due to the presence of three functional groups (amino, primary and secondary hydroxyl) in the glucosamine unit of chitosan [220]. This suggests that the hydrophilicity of the MWNT/chitosan BP membranes could be improved by increasing the chitosan concentrations. Consequently, all the examined BP membranes can be expected to interact with aqueous solutions positively, which is an essential prerequisite for their use in filtration mechanisms.

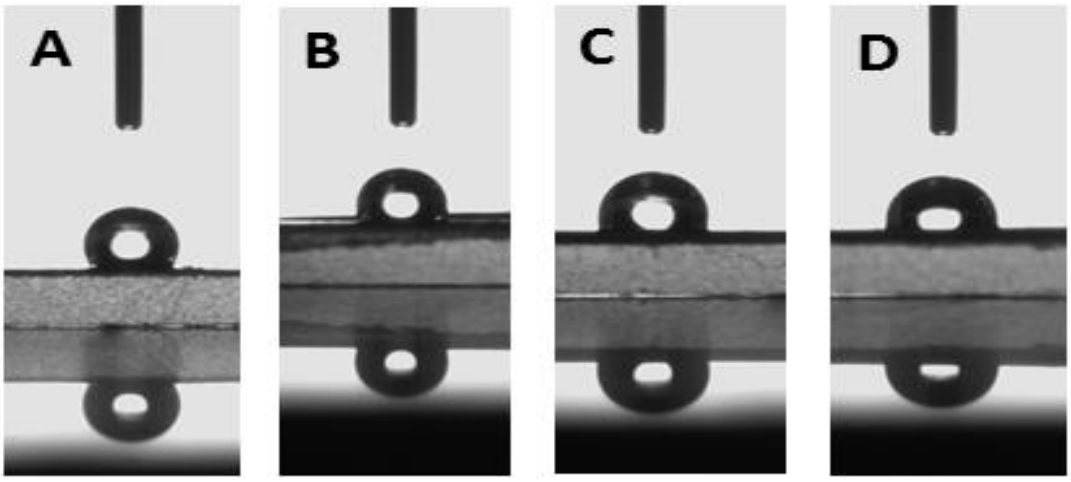

Figure 5.2. Contact angle for BP membranes: A) MWNT/chitosan-1 (0.1% w/v); B) MWNT/chitosan-2 (0.2% w/v); C) MWNT/chitosan-3 (0.3% w/v); and C) MWNT/chitosan-4 (0.4% w/v).

5. 3 Mechanical properties

Various mechanical properties, such as elongation, tensile strength, Young's modulus and toughness, of four different MWNT/chitosan BP membranes prepared with different concentrations of chitosan, 0.1–0.4% (w/v) and MWNTs are presented in Figure 5.3 and summarised in Table 10.

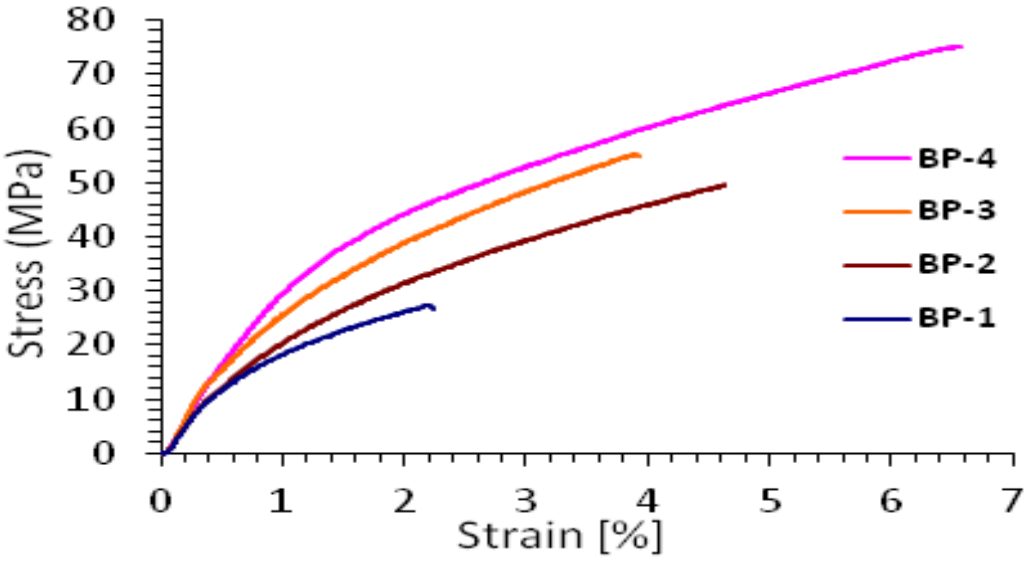

Figure 5.3. Stress–strain curves for different BP membranes: BP-1 (MWNT/chitosan 0.1% w/v); BP-2 (MWNT/chitosan 0.2% w/v); BP-3 (MWNT/chitosan 0.3% w/v); and BP-4 (MWNT/chitosan 0.4% w/v).

Table 10. Effect of increasing the concentrations of low-Mw chitosan on the mechanical properties of MWNT/chitosan: BP-1 (MWNT/chitosan 0.1% w/v); BP-2 (MWNT/chitosan 0.2% w/v); BP-3 (MWNT/chitosan 0.3% w/v); and BP-4 (MWNT/chitosan 0.4% w/v); all MWNT/chitosan were made using a filtration method.

BP membrane	Elongation (%)	Tensile strength (MPa)	Young's modulus (GPa)	Toughness (J/g)
BP-1	2.3 ± 0.6	35 ± 2	2.48 ± 0.07	1.03 ± 0.07
BP-2	5.2 ± 0.5	52 ± 3	2.83 ± 0.11	2.1 ± 0.2
BP-3	4.2 ± 0.4	60 ± 3	3.37 ± 0.05	2.5 ± 0.4
BP-4	7 ± 1	75 ± 3	3.73 ± 0.08	4.3 ± 0.7

The results of the MWNT/chitosan BP membranes show that the tensile strength, Young's modulus, elongation and toughness gradually increased with increased chitosan content. Coleman et al. [253] reported that these measures were significantly improved in BP membranes by polymer incorporation. This indicated that the polymer placed between nanotubes fills the voids or the free volume and reinforces the MWNT network in the BP membranes [173]. The tensile strength and Young's modulus of MWNT/chitosan-4 (0.4% w/v) were 75 ± 3 MPa and 3.717 ± 0.07 GPa respectively, and those properties of

MWNT/chitosan-1 (0.1% w/v) were 35 ± 2 MPa and 2.483 ± 0.071 GPa respectively. This means that the lower amount of chitosan 0.1% (w/v) does not adequately fill the spaces in the CNTs matrix. The results of the present study for MWNT-chitosan BP membranes fabricated using biopolymer as dispersants agree well with the values of Wang et al. [224] who prepared MWNT/chitosan composites at different concentrations of MWNT using the solution-evaporation method. The results demonstrated significant improvement of the MWNT/ chitosan composite membranes' mechanical properties. The tensile strength values reported for MWNT/chitosan membrane containing 0.2 % w/v and 0.4 % w/v are similar to those values obtained in the present study for MWNT/chitosan-2 (0.2% w/v) and MWNT/chitosan-4 (0.2% w/v) BP membranes. In addition, the mechanical properties of the MWNT/chitosan BP membranes were significantly higher than those recently reported for BPs fabricated from MWNTs and SWNTs with different dispersants [242, 256, 257] and from the BPs produced by a similar method in this study (Chapter 3 and 4). This indicates that the MWNT/chitosan BP membranes' mechanical properties are adequate for their use in membrane desalination.

5. 4 Surface morphology

To understand the surface morphologies and pore-structure differences between the MWNTs of the BP membranes further, we obtained and analysed SEM images. These images of different MWNT/chitosan BP membranes were prepared as before and are presented in Figures 5.4 A–D. These figures demonstrate that there are differences among the images obtained at different concentrations (range 0.1–0.4% w/v) of chitosan. Figures 5.4A and 5.4B show that CNTs in MWNT/chitosan-1 and MWNT/chitosan-2 aligned randomly, and the pores (or free spaces) were spread along the surfaces of the BP membranes and MWNT/chitosan-3 and MWNT/chitosan-4 containing higher amounts of chitosan (0.3% and 0.4% w/v) (Figs. 5.4C and 5.4D); the pores were also filled/covered with chitosan. The pores in the nanotubes for the MWNT/chitosan-1 and MWNT/chitosan-2 BPs were considerably larger than those in the MWNT/chitosan-3 and MWNT/chitosan-4. This suggests that the porosity of MWNT/chitosan BP membranes decreased as the dispersant molecular mass increased (Figs. 5.4A–D).

Figures 5.5 A–B show two layers: the top layer consists of MWNT bundles aligned randomly on one another, creating small pores (active layer), whereas the bottom layer is hydrophobic filter paper with larger pores of 0.22-µm PVDF, which were used as a supporting layer for preparing the BP membranes. In addition, the thicknesses of all the BP

membranes were also estimated by SEM (Fig. 5.4A, Table 9). The results indicate that the thicknesses of the membranes increased with greater polymer (chitosan) concentrations. The thickness of the membrane with the highest mass of chitosan MWNT/chitosan-4 (0.4% w/v) was 57%, which was higher than the thicknesses of the BP membranes with the lowest mass of MWNT/chitosan-1 (i.e. MWNT/chitosan 0.1% w/v). This suggests that the water permeability and salt rejection can be affected by increasing the concentration of chitosan.

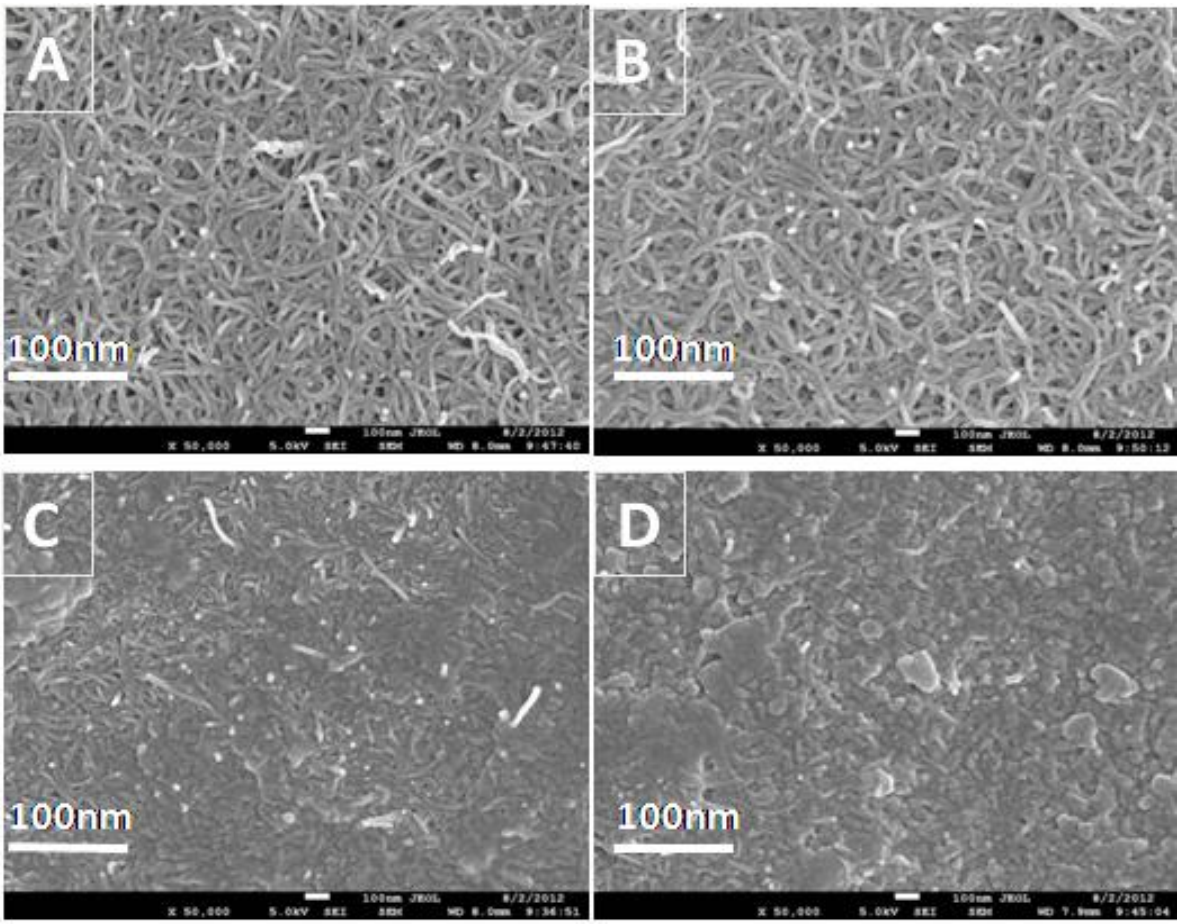

Figure 5.4. SEM images of BP membranes prepared with A) BP-1 (MWNT/chitosan 0.1% w/v); B) BP-2 (MWNT/chitosan 0.2% w/v); C) BP-3 (MWNT/chitosan 0.3% w/v); and D) BP-4 (MWNT/chitosan 0.4% w/v); all of the above BPs were prepared from 250-mL dispersions that were sonicated for 30 min and filtered through 0.22-µm PVDF filter membranes.

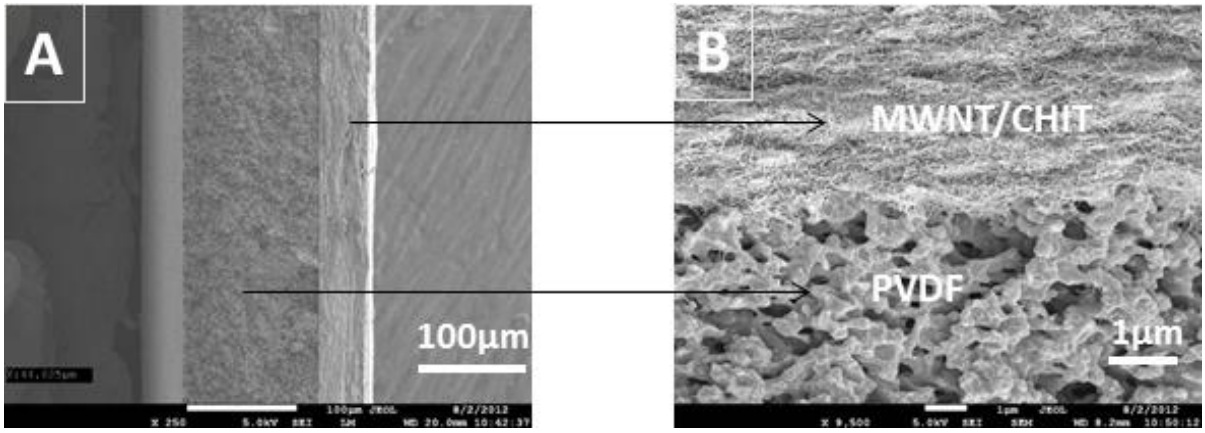

Figure 5.5. SEM cross-section images for the BP membrane BP-2 (MWNT/chitosan) prepared from 0.1% w/v of MWNT dispersed in water (250 mL) for 30 min using 0.2% w/v of chitosan as surfactant with the final solution filtered through 0.22-µm PVDF filter membranes.

5. 5 Surface areas and pore structures

Nitrogen adsorption/desorption isotherms of the four MWNT-chitosan membranes (MWNT/chitosan-1, -2, -3 and -4) were conducted at 77 K to obtain more details about the surface area and average internal pore distribution. Adsorption/desorption for MWNT/chitosan-1 and -2 are shown in Figure 5.6. Both membranes' isotherms are classified as common type IV isotherms displaying hysteresis at higher $P/P_{o,}$ which are lower than to those reported previously for BP membranes fabricated using MWNTs combined with Trix and cipro as surfactants [257]. This indicates that the internal morphologies of MWNT BP membranes can be affected by changing the type of dispersant. For example, it was difficult to calculate the adsorption of gas molecules on a solid surface of BPs using the BET method for MWNT/chitosan-3 and -4. This was confirmed by the free volume (interbundle pore volume) on the surfaces of these BP membranes, which were supposed to be completely blocked by the amounts of chitosan seen in Figures 5.4 C–D. This indicts that the water permeability can be affected by increasing the chitosan mass.

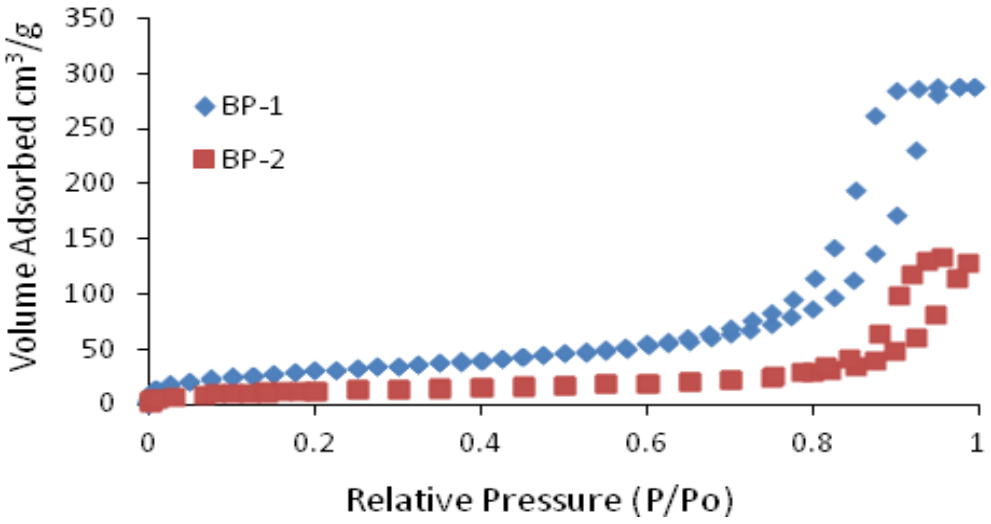

Figure 5.6. Adsorption isotherm demonstrates a comparative plot of the P/P_o and adsorption of BP-1 (MWNT/chitosan 0.1% w/v) and BP-2 (MWNT/chitosan 0.2% w/v) BP membranes fabricated using a filtration method.

The BET analysis of the adsorption isotherms assisted with the estimation of the specific surface area of MWNT/chitosan-1 and -2 membranes with a range 45–89 m^2/g (Table 11). These results indicate that the specific surface area of MWNT/chitosan-2 was about half the value of BP-1. The specific surface areas of these BPs membranes (MWNT/chitosan-1 and -2) was significantly lower than that measured in previous studies on BP membranes prepared from MWNTs and other dispersants (Trix and cipro) [257, 260]. This suggests that the surface area of the BP membrane is significantly influenced by changing the dispersant type and concentration.

Table 11. The surface area (A_{BET}), average pore diameter (d_{BET}), average bundle diameter (Dbun), interbundle pore volume and intertube pores of BP membranes prepared by filtration method.

BP membrane	A_{BET} (m^2/g)	Average pore diameter (nm)	D_{bun} (nm)	Interbundle pore volume (%)	Intertube pores (%)
BP-1	89 ± 6	10 ± 1	30 ± 2	90 ± 4	10 ± 1
BP-2	45 ± 5	19 ± 2	59 ± 4	82 ± 5	18 ± 2

The HK and BJH methods were used to determine the pore volume of BP membranes [235, 236]. Plots of pore volume as a function of pore diameter for MWNT/chitosan-1 and

MWNT/chitosan-2 are presented in Figure 5.7. The large peak between 0.5 and 1 nm is correlated to the intertube pores and the small peak from 2–50 nm, corresponding to the interbundle pores. These pores are also visible in the SEM images in Figures 5.4A–B. Results of the interbundle pore volume (Table 11) demonstrate reasonable similarity (82–90%) for both BP membranes. These results are slightly lower than those reported for the MWNT-Trix BP membranes [257]. Therefore, the intertube pore (<2 nm) is approximately 10% of the total free volume of the MWNT/chitosan-1 and 18% of the MWNT/chitosan-2. This suggests that increasing the concentration of chitosan can increase the percentage of intertube pores (<2 nm).

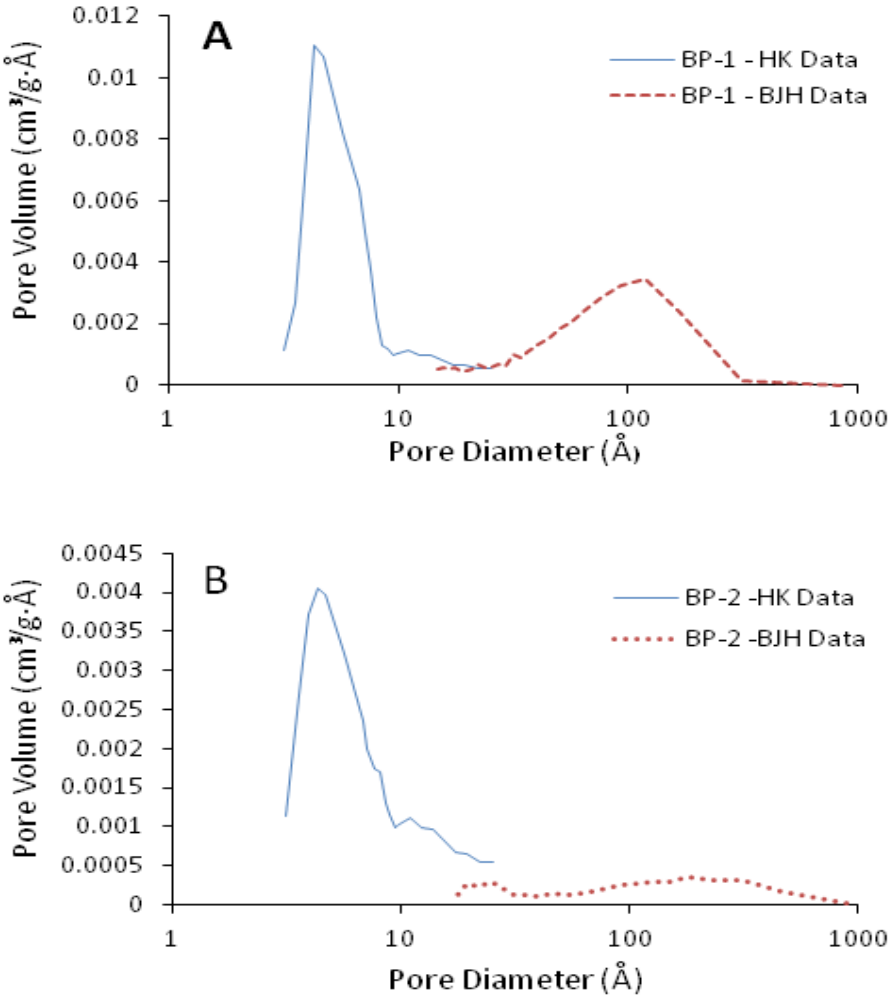

Figure 5.7. Pore-size distributions for BP membranes determined using the HK (blue line) and BJH methods (red dotted line) obtained from nitrogen adsorption/desorption isotherms: A) MWNT-chitosan 0.1% w/v (BP-1); and D) MWNT-chitosan 0.2% w/v (BP-2).

Surface area was used to determine nanotube-bundle diameter (D_{bun}) by applying equation 10; results are given in Table 11 [194]. The nanotube-bundle diameters increased from 30 ± 2 to 59 ± 4 nm by increasing the concentration of chitosan from 0.1–0.2% w/v. The results of D_{bun} for MWNT/chitosan-1 and -2 are greater than the results obtained for different BP membranes previously [181, 257].

5. 6 Water permeability

Water permeability of the MWNT/chitosan membrane was studied using a crossflow RO/NF method, as described in the experimental section, at pressure ranges 3–18 bar for 8 h; results are shown in Figure 5.8 as a function of pressure versus water permeation flux.

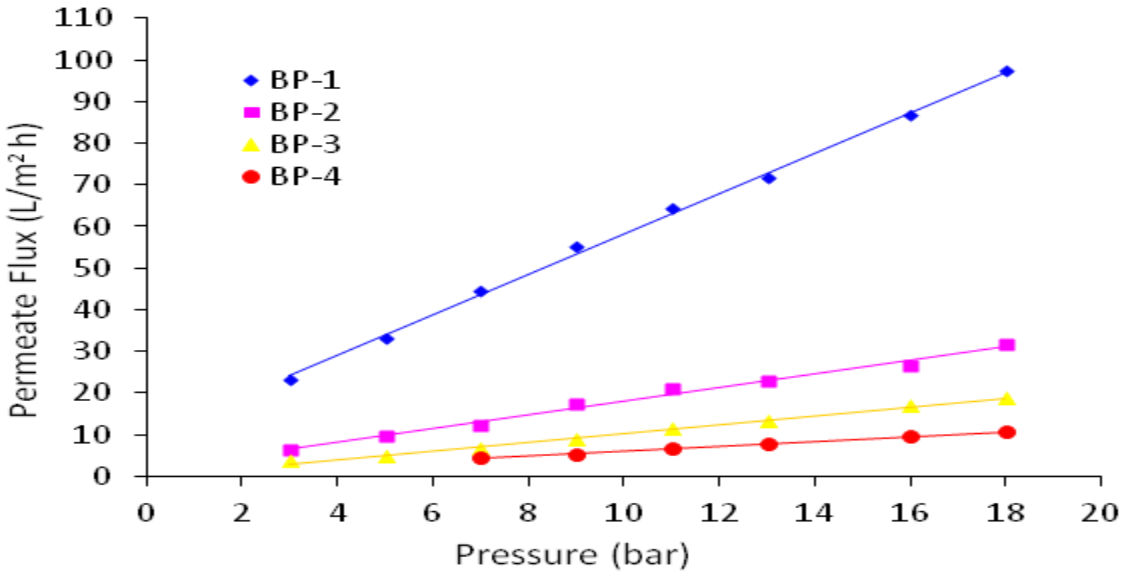

Figure 5. 8. Permeate flux as a function of pressure of different membranes of MWNT-chitosan low Mw: BP-1 (MWNT: low-Mw chitosan 0.1% w\v); BP-2 (MWNT: low-Mw chitosan 0.2% w\v); BP-3 (MWNT: low-Mw chitosan 0.3% w\v); BP-4 (MWNT: low-Mw chitosan 0.4% w\v)

Increasing the pressure increased the water permeation flux linearly; however, the water-permeability coefficient of the BP membranes (MWNT/chitosan-1 to -4) was calculated using equation 12; results are summarised in Table 9. Water permeability of MWNT/chitosan-1 is 5.73 ± 0.3 L/m^2 h bar and decreases with increased chitosan content. For example, water permeability obtained from Figure 3.4.8 was reduced from 5.73 ± 0.3 L/m^2 h bar (MWNT/chitosan-1) to 0.59 ± 0.04 L/m^2 h bar (MWNT/chitosan-4) by increasing the amount of chitosan. This indicates that water will flow more slowly into the pores of MWNT/chitosan-4 BP membranes than -1 BP membranes, and high pressures will be needed

to achieve transport through -4 BP membranes. This is in agreement with results obtained by SEM images of MWNT/chitosan-1 in Figure 5.4 showing that MWNT/chitosan-1 is highly permeable. It is noteworthy that the MWNT/chitosan BP membranes were less permeable to water than the BP membranes produced through the study described earlier in chapter 3. The water permeability of MWNT/chitosan is also comparable to that of SWNT and MWNT membranes produced with other dispersants, such as Trix and cipro [181, 256, 257]. These values are slightly higher than those of the MWNT/chitosan BP membranes in the present chapter. This is because MWNT/chitosan BP membranes have low surface areas (Table 11) and pore sizes (see SEM images in Figure 5.4). Consequently, the thickness of the top selective layer of buckypaper membranes rises with the increase of the solution concentration of the active layer, which results in lower flux.

5. 7 Salt-rejection capability

We know that the rejection and separation of ions require nano-sized pore structure and a charged surface in the membrane [271]. For industry reasons, nano-filter membranes carrying a negative charge receive more consideration than those carrying a positive charge. This is because the majority of NF processes focus on retaining multivalent anions and molecules of low molecular weight. Some of the negatively charged membranes commercially available include Filmtec, DK series, NF series, Denko, Nitto and NTR series. Still, a positively charged NF membrane is required for processes involving salt rejection and mono- and divalent ion retention. Therefore, to create a positively charged membrane, a series of composite MWNT/chitosan BP membranes were prepared as described in Chapter 2, with concentrations of chitosan at 0.1, 0.2, 0.3 and 0.4% w/v, respectively, and were accordingly coded as MWNT/chitosan-1 (BP-1), MWNT/chitosan-2 (BP-2), MWNT/chitosan-3 (BP-3) and MWNT/chitosan-4 (BP-4). Filmtec provided the four BP hydrophilic membranes used for this study, each with a surface area of 4×10 cm^2.

Membranes with pore radii of about 1 nm will reject ions with molecular weights 200–20,000 due to electrostatic interactions [272]. Increased concentrations typically result in decreased rejection of NaCl by nano-filter membranes. Common uses of nano-filtration include water softening, drinking water treatment, de-sulphatation and humic substance removal; frequent industrial applications include salt and organic fractionation [272].

Ion size and valency influence the rejection rate of nano-filtrate membranes to inorganic electrolytes [70]. Electrolyte rejection and transport mechanisms of amphoteric

nano-filtrate membranes could be due to convection (C), diffusion (D) or/and electro-migration (EM) [273]. The most important criteria for low-concentration inorganic electrolyte Nano-filtrate is the electrolyte ion charge [274]. The rejection levels increase with greater membrane charge density irrespective of electrolyte type and permeate volume, as lesser co-ions enter the membrane pores [70, 274].

Salt retention is a characteristic frequently used by NF and RO membrane manufacturers to explain membrane performance. Therefore, the salt-rejection behaviours of four MWNT/chitosan membranes were examined using crossflow system experiments with two inorganic electrolyte solutions ($MgSO_4$ and NaCl), a 2,000-mg/L salt concentration, applied pressure ranging 3–18, flux ranging 0–30 µm/s bar and a temperature of 20°C for 8 h (Fig 2.8, Chapter 2). The corresponding results are displayed in Figures 5.9A and C. The observed rejection (R_{obs}) (as described by equation 7 of the experimental section) order follows that R(NaCl) > R($MgSO_4$). This experiment illustrates the expected Donnan feature of salt rejection of MWNT/chitosan BP membranes, which are positively charged. The result of the experiment is contradictory to the observed behaviour of the order of rejection R(MgSO4) > R(NaCl), as seen in previous works [70, 275]. This is because of the Donnan features of salt rejection of nano-filtrate membranes, which are negatively charged. The orders of the Mg^{2+} and the Na^{+} influence the rejection rate to an electrolyte containing anions, such as Cl^{-}. Similarly, the orders of Cl^{-} and SO_4^{2-} influence the rejection rate of an electrolyte containing a cation, such as Na^{+}; Both are attributed to the Donnan exclusion effect. The influence of ion-valence on electrolyte retention is in agreement with the qualitative characteristics of the Donnan exclusion mechanism [276].

Furthermore, the active layer of the MWNT/chitosan BP membrane contains amino groups; therefore, it has strong adsorption of Cl^{-} and SO_4^{2-}. As a result, the Cl^{-} was rejected and a positive surface charge was acquired by the active layer of the membrane because of the adsorption of anions from the electrolyte solution. This charge distribution was the main driver of membrane performance. The results for the MWNT/chitosan BP are contradictory to those obtained for the NF membrane made using sulphated chitosan (SCS), which contains sulphate groups, and so displayed a stronger repulsion to SO_4^{2-} than to Cl^{-} ions [273]. This is because the active layer of membrane has a negatively charged surface distribution. Therefore, the membrane adsorbs the Cl^{-} anions by interacting with the amino groups on the chitosan, which carry a positive charge. However, these results could vary when sea or

brackish water is used, as the Cl^- could get pushed forward by high pressure or other ions, such as F^-, in a process similar to the anion-selective mechanism. But with Mg^{2+}, it is easier to combine anions on the surface of the membrane [273, 275], decreasing the effective charge of the membrane surface and resulting in lower rejection performance. Na^+ is more easily hydrated by water and has a smaller radius than Mg^{2+} (the hydrated ionic radius for Na^+ is 0.36 nm, whereas Mg^{2+} is 0.43nm [271, 277]). Therefore, over time, the rejection rate NaCl will decrease.

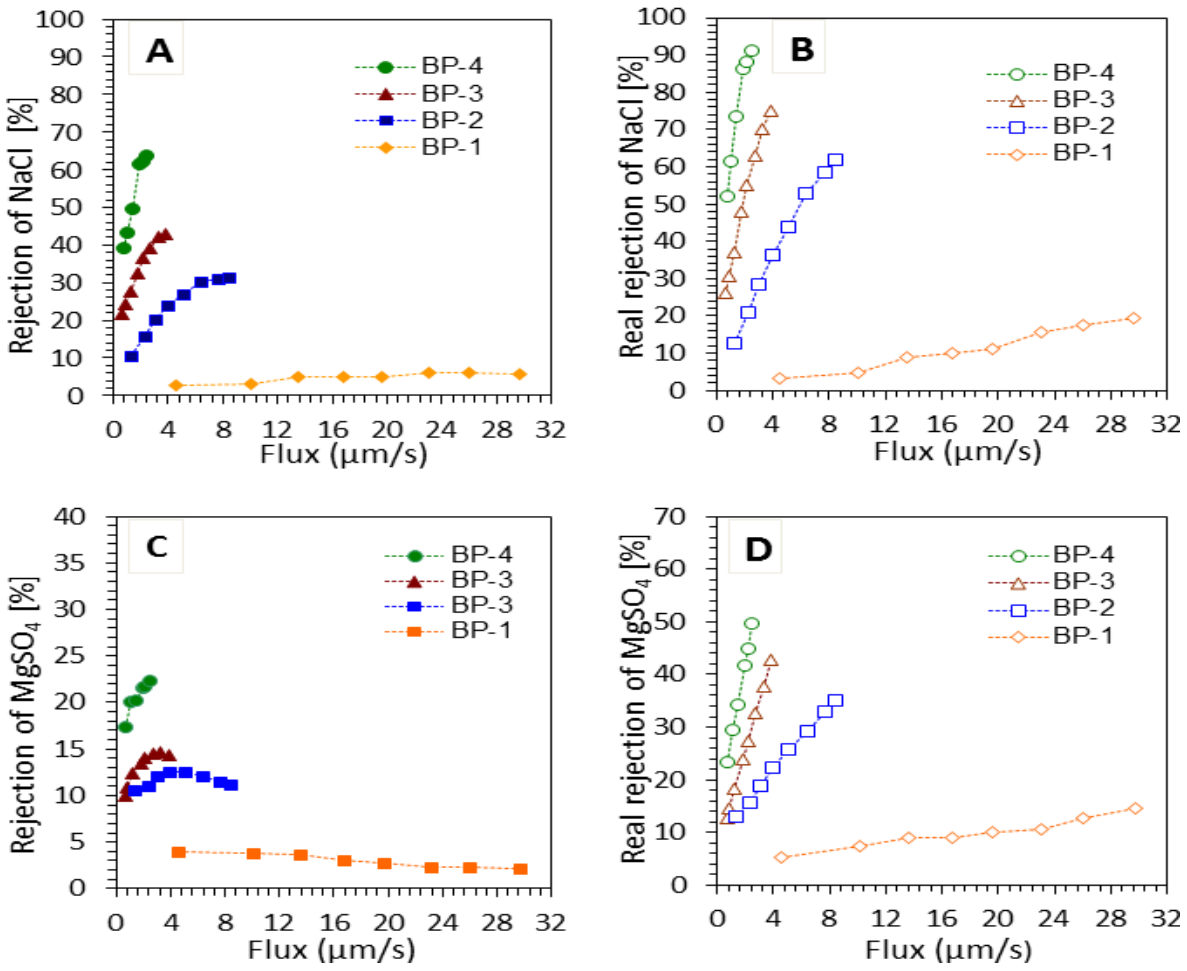

Figure 5.9. Comparison of the performance of membranes for rejection salts: A) NaCl rejection (%); B) real rejection of NaCl; C) $MgSO_4$ rejection (%); and D) real rejection of $MgSO_4$ using different MWNT/chitosan BP membranes, such as BP-1 (MWNT/chitosan 0.1% w/v); BP-2 (MWNT/chitosan 0.2% w/v); BP-3 (MWNT/chitosan 0.3% w/v); and BP-4 (MWNT/chitosan 0.4% w/v); all MWNT/chitosan membranes were fabricated using a filtration method.

The study also investigated the effect of chitosan solution concentrations of 0.1, 0.2, 0.3 and 0.4 % w/v on the rejection performance of the MWNT/chitosan BP membranes (Figs.

5.9A–D). The decrease in the permeate flux and rejection rate of 2,000 mg/L NaCl and $MgSO_4$ solutions increased with the chitosan concentration until it reached 0.4 wt%. This was caused by increases in the thickness of the selective layer as the solution concentration of the active layer increased, resulting in a higher rate of rejection to the inorganic electrolyte solution and lower flux. This is in agreement with the previous study [273].

Further, the irreversible thermodynamic model provided greater clarification of the rejection behaviours of $MgSO_4$ and NaCl salts by BP membranes. It was used to explain the solute rejection of NF/RO membranes and their rejection mechanisms [237]. The real rejection R_{real} (Fig. 5.9B and D) for various permeate fluxes could be calculated using equation 7, with the observed rejection R_{obs} data (Figs. 5.9A and C) determined by equation 6, and the coefficient of mass transfer k, which is dependent on the cell crossflow given by equation 8. The real rejection values of the four BP membranes (Figs. 5.9D & D) were much higher than the experimental rejection for the two salts. A more unexpected observation is that the rejections attained for all BP membranes were higher for NaCl than $MgSO_4$, even in BP-1, wherein NaCl rejection was not significantly high. As previously discussed, this consistently high rejection could be explained by the adsorption rate of NaCl to the BP membranes (Appendix Figure 2).

Understanding the basic mechanisms of this separation behaviour is a key factor for the future development of industrial membrane applications. NF membranes have a slightly charged surface. As the dimensions of the pores are <1 order of magnitude below the size of the largest ions, charge interaction plays a dominant role. For the MWNT/chitosan BP membranes, which are positively charged, a higher level of retention is expected for NaCl than $MgSO_4$, and this cannot be fully explained by effect of charges alone. It is clarified that due to positive charge on the top layer, the buckypaper membranes behaves much higher rejection for mono-valent cations (e.g. Na^+) than for multi-valent cations (e.g. Mg^{2+}) if the electrolytes have the same mono-valent counterion (e.g. Cl^-). Therefore, by properly balancing chitosan amino groups conditions, a desired positively charged buckypaper membranes could be obtained for removal of mono-valent cations from solution, all play vital parts in the rejection of NaCl (more so than in the rejection of $MgSO_4$).

In addition, detailed comprehension of the effect of pH on separation for different types of electrolytes would be immensely significant in deciding strategies for research to attain optimum operating conditions for various processes [278]. The membrane

characteristics and, therefore, the retentive characteristics, are influenced by the pH value of the feed solution. Consequently, the rejection of NaCl (2,000 mg/L) through the MWNT/chitosan-2 (BP-2) BP membrane was studied at a permeate flux of 0.58 mL/min (Fig. 5.10A) in feed solutions with pH levels ranging 3–10 (Fig. 5.10B), crossflow velocity of 34.7 cm/s (100 L/h) and 20°C ± 2°C using a crossflow RO/NF system (Fig. 2.8, Chapter 2). The rejection of NaCl was sensitive to the feed solution pH (Fig. 5.10B), as the BP-2 membrane's rejection of it increased gradually as the feed solution pH decreased from 10 to 3.

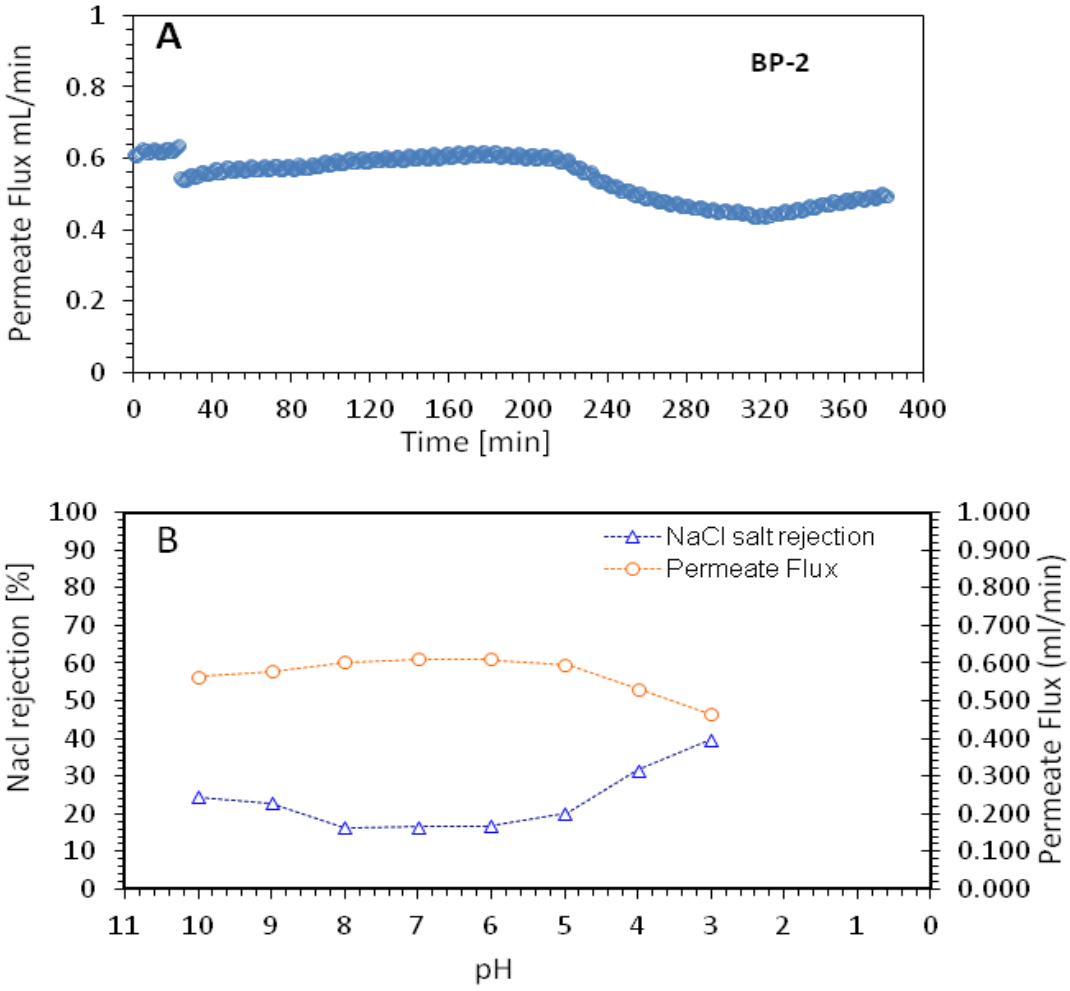

Figure 5.10. Effect of changing pH on A) permeation flux and B) salt rejection using MWNT-chitosan 0.2% (w/v) BP membranes prepared using a filtration method.

The BP membrane's active skin layer contained chitosan, which has amine functional groups. Changes in the solution pH can lead to speciation of this functional group, thus causing changes in the conformation of the BP-membrane matrix. Therefore, the chitosan membrane pore size can become smaller as the solution pH decreases (Fig. 5.10A) due to

changes in the conformation of the BP-membrane matrix. It has been reported that this sensitivity is mainly caused by chitosan amino groups, which constitute a weak base with an intrinsic *pKa* of approximately 6.5 [254, 279].

Composite membranes can be characterised by their resultant rejection of the mono- and divalent ions. From SEM images, they can be characterised as NF (sieve and softening) membranes, but because of the $–NH_2$ functional groups (which enhance the $Cl^–$ rejection by chemisorption at low pH), the membrane may also be categorised as RO. These results may change when brackish or seawater is used because greater pressure by other ions, such as $F^–$, in a mechanism similar to the anion-selective membrane, may push the attracted $Cl^–$ forward. Moreover, the trends were clarified from this section by the suitable of physical properties, water flux and increasing salt rejection (NaCl) at low pH as a result of MWNT/chitosan 02% (w/v) buckypaper membrane. For the practical preparation, a balance choice MWNT and chitosan 0.2% (w/v) can be produced a series of positively charged NF membranes to meet different industrial demands. For further research, we can optimize the parameters and obtain a membrane for electrolyte separation with suitable pure water flux and high rejection at low pH if amines of chitosan at the top layer of buckypaper membranes are cross-linked or modified by materials such as polyethylene glycol diglycidyl ether (PEDGE), glycerine, MWNT-COOH and MWNT-NH_2. Therefore, by properly chitosan and cross-linking chitosan 0.2% (w/v) incorporating unfunctionalised and functionalised MWNTs conditions, a desired positively charged buckypaper membranes could be increased for removal of salts from water or for separation of mon-ovalent and multi-valent ions or mono-valent cations (e.g. Na^+) and multi-valent cations (e.g. Mg^{2+}).

5. 8 ZP of the MWNT/chitosan BP membrane

The most important of the characteristics addressed is the surface potential of the membrane, which is generally measured as the ZP. The ZPs of several MWNT/chitosan BP membranes were determined using the electrolyte typically employed for ZP analysis (1-mM KCl). The ZPs of the surfaces of a few MWNT/chitosan BP membranes are shown in Figure 5.11. Generally, the membrane's ZP varies between positive and negative values, as the pH varies. Consequently, the varying pH also varies the electrostatic interaction between the membrane surface and the ionic compounds. The part played by the electrostatic potential, which exists at the adsorption surface near the membrane/feed interface, is significant in evaluating the effect of pH on the adsorption charge of the hydrophobic groups [280].

The ZPs of the surfaces of MWNT/chitosan BP membranes can vary as a function of the solution chemistry (e.g. pH and ionic strength). The ZP values of the surfaces of the MWNT/chitosan BP membranes as a function of the feed solution pH are shown in Figure 5.11.

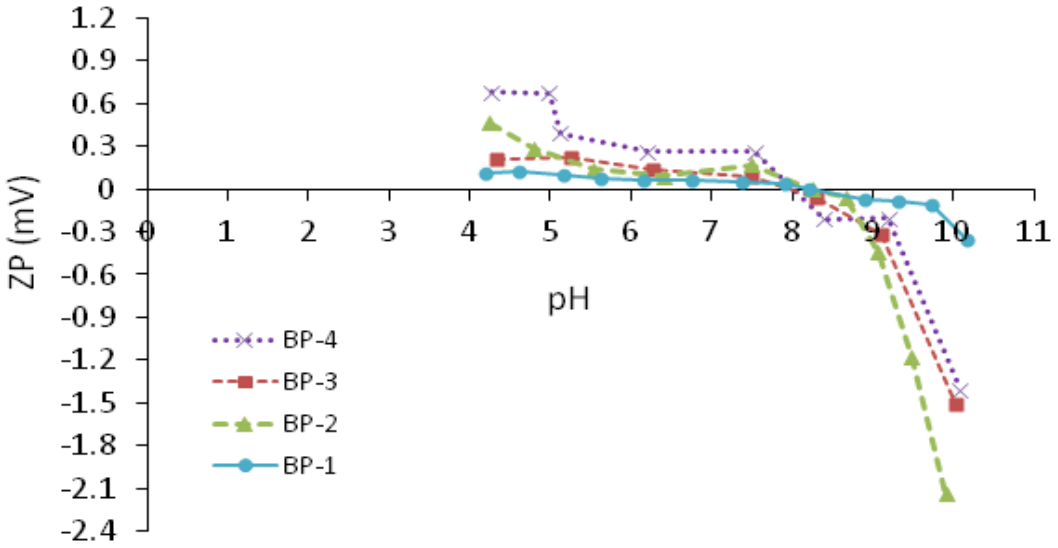

Figure 5.11. ZP of MWNT-chitosan BP membranes: (BP-1) MWNT-chitosan 0.1% (w/v); (BP-2) MWNT-chitosan 0.2% (w/v); (BP-3) MWNT-chitosan 0.3% (w/v); and (BP-4) MWNT-chitosan 0.4% (w/v).

Several studies [281, 282] reported that the ZP of a more negatively charged membrane can lead to a greater salt rejection due to increased electrostatic interactions between the negatively charged membrane surface and negatively charged solutes. However, all the MWNT/chitosan BP membranes had positive charges (pH 4–8) due to the positively charged chitosan. The surface charges of all MWNT/chitosan BP membranes > pH 8 were negative. In addition, the pH values at the zero charge point for most of the MWNT/chitosan BP membranes were pH 7–8. Other studies [283] reported that the ZP values of CNT/chitosan were more negative, and a zero charge point was observed at pH 5.30. The positive surface charge below the isoelectric point would result from the protonation of the amine functional groups ($–NH_2$ to $–NH_3^+$), and the negative charge above the isoelectric point would result from de-protonation of the hydroxyl groups (–OH to $–O^-$) [284, 285].

5. 9 Conclusions

MWNT/chitosan BP membranes were successfully fabricated from MWNT/chitosan dispersions. The selective uptake of inorganic salt indicates that these BP-membrane systems

are an encouraging subject for selective membrane research. The electrical conductivity and permeability to water were reduced with increasing concentrations of chitosan. In contrast, the hydrophobicity of the surface, the mechanical properties and salt rejection of the BP membranes were enhanced by increasing the amount of chitosan. The enhancement of these properties may improve the usability of MWNT/chitosan BP membranes in RO applications. Moreover, the performance of the MWNT/chitosan BP membranes in terms of water flux, reverse-salt flux, and the rejection of salts under various experimental conditions was investigated using a crossflow RO/NF mode. The MWNT/chitosan-1 BP membrane (which contains the lowest amount of chitosan) performed better than the BP-4 membrane (which contains the highest) in terms of water flux, though the rejection of salt by BP-4 was largely improved. This is because the thickness of the top selective layer of buckypaper membranes rising with the increase of the solution concentration of the active layer, which results in lower flux and higher rejection to an inorganic electrolyte solution.

Experiments on the amphoteric MWNT/chitosan BP membranes indicate that a positively charged surface as the anion valence predominately influences the salt rejection; that is, mono-valent anions, such as Cl^-, experience strong repulsion by the BP membranes, and divalent anions, such as SO_4^{2-}, experience low repulsion. Moreover, due to positive charge on the top layer, the buckypaper membranes behaves much higher rejection for mono-valent cations (e.g. Na^+) than for multi-valent cations (e.g. Mg^{2+}) if the electrolytes have the same mono-valent counterion (e.g. Cl^-). In addition, the cation shield effect on the positively charged membrane groups becomes stronger, thereby decreasing the salt-rejection level. Therefore, the rejection of salt with lower molecular weight (NaCl) was higher than that of the salt with higher molecular weight (MgSO4). More research is required to discover the reasons for this unexpected behaviour.

Chapter 6: Properties of MWNT/chitosan and MWNT/chitosan-Crosslinked Membranes

Three BP membranes were prepared using the vacuum-filtration method, as described in the experimental section, from solutions of chitosan, chitosan-PEDGE and chitosan-glycerin in the presence of MWNT. Chitosan (0.2% w/v) was mixed with PEDGE or glycerin at ratio of 5:1 containing MWNT (0.1% w/v) and are respectively referred to as MWNT/chitosan, MWNT/chitosan-PEDGE and MWNT/chitosan-glycerin. The resulting BP membranes were characterised by their physiochemical properties, water permeability and ability to reject single salts from aqueous solutions. Chitosan contains chemically reactive groups (–OH and –NH2) and is insoluble in alkaline mediums and organic solvents. In contrast, it is soluble in a dilute acid (low-pH environment). Chitosan was chosen as the material for membrane applications because a soluble water polymer with *pKa* <6.5 [222] should be treated with crosslinking agents. McCloskey et al. [286] reported that chitosan has considerably more complex structures when mixed with PEDGE because the crosslinking agent may react with amino groups of chitosan, whereas the reaction between chitosan and glycerin can occur through hydroxyl groups [112].

6. 1 Optimisation of sonication time

This study represents the first time a crosslinked chitosan (containing 20% glycerin or PEDGE by weight relative to chitosan) has been used as a dispersant for preparing CNT dispersions. UV-vis-NIR spectroscopy was used to compare non-crosslinked and crosslinked chitosan for dispersing MWNTs (Fig. 6.1A). The absorbance of MWNT/chitosan dispersion was measured at wavelengths of 300–1,000 nm. This absorbance was amplified by increasing the sonication time, which agreed well with studies described earlier [180, 242, 257]. These data are shown in Figure 6.1B, where the absorbance of the dispersions at 660 nm was plotted as a function of sonication time. This wavelength (660 nm) was chosen to avoid absorbance attributable to surfactant (chitosan or crosslinked chitosan) and the solvent (Milli-Q water). The results obtained from the UV-vis-NIR spectra suggest that a 10-min sonication was sufficient for good dispersion of the MWNT in the solution containing chitosan and/or chitosan-glycerin, whereas 20-min sonications should be used to disperse MWNT in the solution containing chitosan-PEDGE. The results in Figure 6.1B suggest that 20 min is a

suitable amount of time to disperse the MWNT in both solutions (chitosan and crosslinked chitosan). Accordingly, sonication times of 20 min were chosen to ensure significant dispersion of the MWNTs.

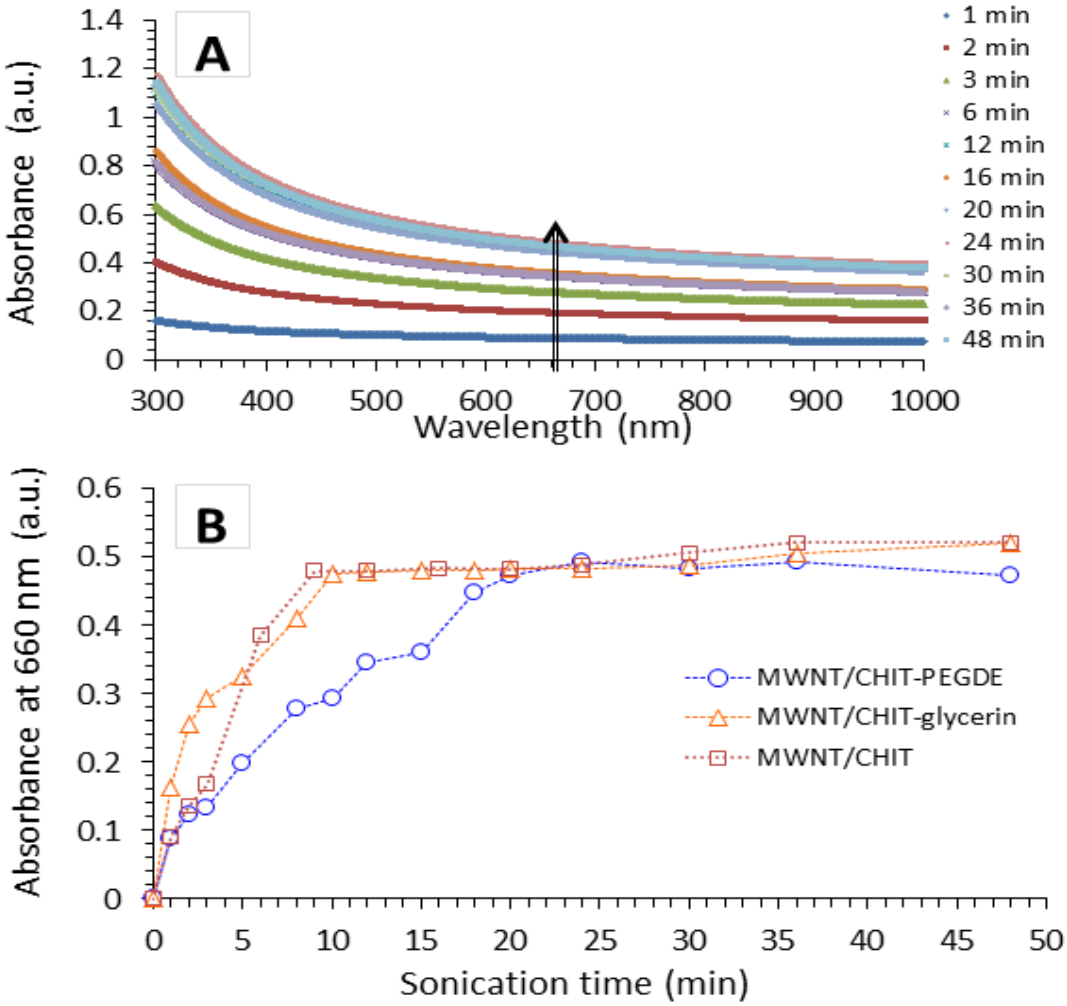

Figure 6.1. A) UV-vis spectra of MWNT/chitosan dispersion as a function of sonication time and B) comparison of the effect of increasing sonication time on the absorbance at 660 nm of MWNT/chitosan, MWNT/chitosan-glycerin and MWNT/chitosan-PEDGE dispersions.

6. 2 Electrical properties of BP membranes

The I-V characteristics of MWNT/chitosan, MWNT/chitosan-glycerin and MWNT/ chitosan-PEDGE dispersions membranes were determined using the two-point probe method under ambient conditions of 21°C and 45% relative humidity. All BP membranes showed linear I–V characteristics, indicating ohmic behaviour. Figure 6.2 shows resistance (R_T) as a function of length of the BP membranes.

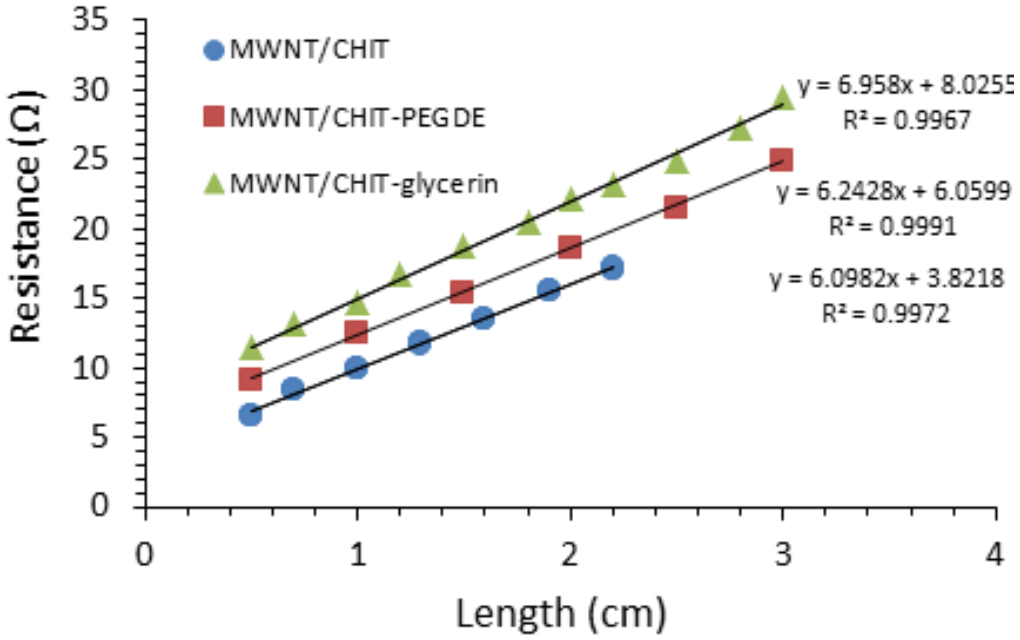

Figure 6.2. Resistance as a function of sample length for three different BP membranes.

The electrical conductivity of MWNT/chitosan and MWNT/chitosan-crosslinked (chitosan-glycerin and chitosan-PEDGE) was determined from the results in Figure 6.2 using equation 10 (summarised in Table 12). The conductivity value (70 ± 1 S/cm) of MWNT/chitosan was slightly higher than that of the MWNT/chitosan-crosslinked (MWNT/chitosan-glycerin or MWNT/chitosan-PEDGE) membranes. Their conductivity values were 66 ± 1 or 60 ± 1 S/cm respectively. The chitosan-crosslinked as a dispersant did not have a significant effect on the electrical conductivity of the MWNTs. In contrast, the conductivity values of MWNT/chitosan and MWNT/chitosan-crosslinked BP membranes investigated here were higher than the reported conductivity values for the BP membranes of MWNT dispersed with Trix or cipro. For example, the conductivity values of the MWNT-Trix and MWNT-cipro BPs were 55 ± 10 and 41 ± 5 S/cm respectively [257] (lower than those of the three membranes). Therefore, it is suggested that the conductivity of BP membranes (MWNT/chitosan and MWNT/chitosan-crosslinked) is not affected by the concentration of these biopolymers (chitosan and chitosan-crosslinked).

Table 12. Physical properties of MWNT-chitosan and MWNT-chitosan-crosslinked BP membranes: values obtained are the average of at least five samples, with the errors estimated from the standard deviation of all measurements.

BP membrane	Contact angle (°)	Conductivity S/cm	Thickness (µm)	Elongation (%)	Tensile strength (MPa)	Young's modulus (GPa)	Toughness J/g
MWNT/chitosan	102 ± 3	70 ± 1	52 ± 3	5.7 ± 0.5	56 ± 3	2.9 ± 0.11	2.1 ± 0.3
MWNT/chitosan - glycerin	80 ± 2	66 ± 1	52 ± 6	6.4 ± 2	49 ± 4	2.8 ± 0.19	2.2 ± 0.8
MWNT/chitosan - PEDGE	76 ± 3	60 ± 1	58 ± 4	8.1 ± 2	59 ± 3	2.7 ± 0.19	2.3 ± 0.2

6. 3 Wettability of BP membranes

Hydrophobicity provides information about the nature of the membrane surface, and contact angle determines the hydrophobicity; that is, if the contact angle is high, the material is hydrophobic. The contact angles of the surfaces of the three BP membranes were determined as described in the experimental section; results are shown in Figures 6.3A–C and Table 12. For example, the contact angle of the MWNT/chitosan (un-crosslinked chitosan) BP membrane was 102° ± 3°, indicating a hydrophobic surface (i.e. it will not adsorb or be wetted by water). However, the contact-angle values for the MWNT/chitosan-glycerin and MWNT/chitosan-PEDGE (crosslinked chitosan) BP membranes were 80° ± 2° and 76° ± 3° respectively, showing hydrophilicity. The high contact-angle value of the MWNT/chitosan BP suggests that most of the membrane's surface consisted of MWNT. It is likely that some of the chitosan was lost during the filtration process. The contact angles of the three BP membranes are also consistent with their respective conductivity results (Table 12); MWNT/chitosan exhibited the highest conductivity. This could also indicate that there was a greater proportion of MWNT on its surface than on the other membranes. Moreover, the contact-angle values determined from Figure 6.3 were significantly higher than those of other studies. For example, the contact-angle values of the MWNT/chitosan composite membranes decreased from 86–56.5° [283]. In addition, the MWNT dispersed with different surfactants (cipro and Trix) had contact angles of 41° ± 5° and 55° ± 10° respectively [257].

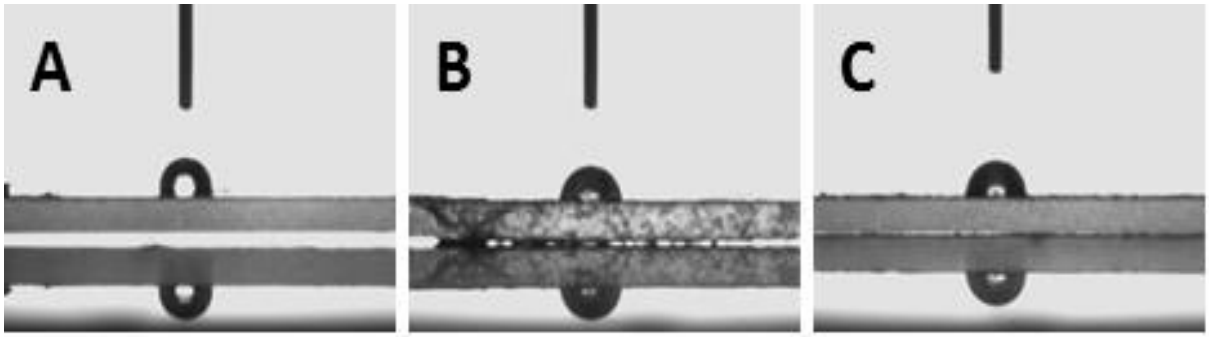

Figure 6.3. Contact-angle photos for BP membranes: A) MWNT/-chitosan 0.2 (w/v); B) MWNT/chitosan-glycerin 0.2% (w/v); and C) MWNT/chitosan-PEDGE 0.2% (w/v).

6. 4 Morphology of BP membranes

SEM images of the three BP membranes (MWNT/chitosan, MWNT/chitosan-glycerin and MWNT/chitosan-PEDGE) are shown in Figures 6.4A–C. MWNT (0.1% w/v), chitosan (0.2% w/v) and glycerin or PEDGE (20% by weight relative to chitosan) were used. For further details, refer to the experimental section. In the case of MWNT/chitosan-crosslinked BP membranes (Figs. 6.4B and C), nanopore formation occurs during the crosslinking method; that is, these BP membranes fabricated with dispersions containing MWNT/chitosan-glycerin or MWNT/chitosan-PEDGE exhibit pore formation. This pore formation is related to phase separation through the crosslinking method, which generally occurs when chitosan is crosslinked in the presence of glycerin or PEDGE [286, 287]. Once the crosslinking method is complete and the MWNT/chitosan-crosslinked BP membranes are washed, glycerin and PEDGE that are not bound to the chitosan network are removed, and the porous, crosslinked chitosan phase begins. Thus, pore formation is seen in the SEM images of MWNT/chitosan-PEDGE (Fig. 6.4B). Similarly, pores are not seen in the images of MWNT/chitosan-glycerin (Fig. 6.4C). This indicates that the pores on the surfaces of BP membranes are highly dependent on the identity of the surfactants used. In contrast, the MWNT/chitosan (Fig. 6.4A) revealed a randomly entangled mat/network of MWNTs with small-sized pores between bundles of nanotubes. Figure 6.4A shows that these pores had similar overall morphologies to the pores of BP-2 (Fig. 6.4B). Moreover, the SEM images of the three BP membranes show that the MWNTs are well dispersed through the chitosan and crosslinked chitosan solutions (i.e. there are not many aggregates). However, it is clear from the SEM images (Figs. 6.4A–C) that the BP membranes had much larger agglomerates of nanotubes with small numbers of irregularly sized pores compared to those of the BP membranes formed from MWNT/Trix

[256, 257]. Whitten et al. had similar results for SWNTs, showing that biopolymers (chitosan) can suspend much larger agglomerates of nanotubes than low-molecular-weight (Trix) surfactants because of their greater molecular weights [288].

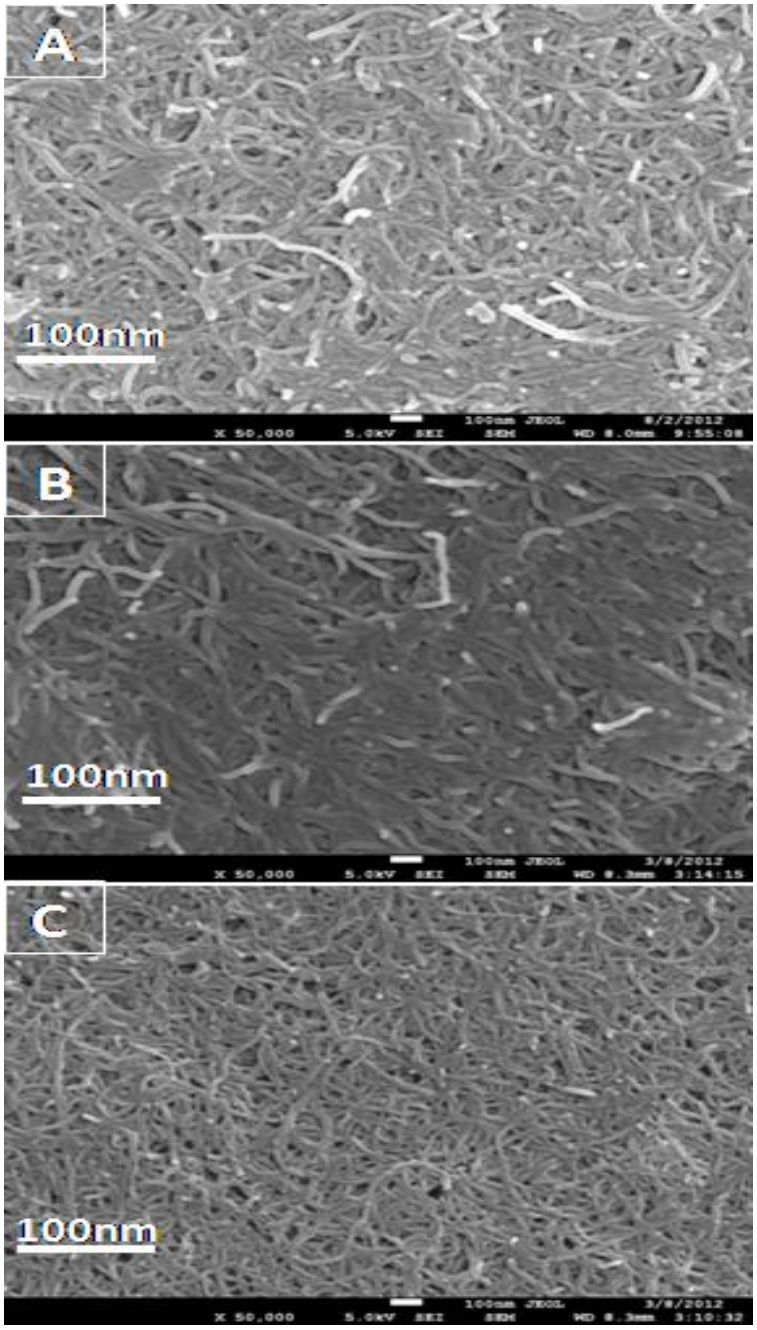

Figure 6.4. SEM images of the surface morphology of three BP membranes: A) MWNT/chitosan BP; B) MWNT/chitosan-glycerin BP; and C) MWNT/chitosan-PEDGE BP obtained at 50 KV magnification; BPs were fabricated from dispersions made by sonicating samples containing 0.1% (w/v) MWNTs and different dispersants (chitosan, chitosan-glycerin and chitosan-PEDGE) for 30 min.

6. 5 Mechanical characteristics

Mechanical properties are a critical factor in determining the usability of BP membranes for filtration. Typically, straightforward strategies are used to detect high-performance engineering polymers for membrane materials, to improve crosslinked polymers or to produce polymer composite membranes [289, 290]. In this work, tensile stress–strain curves of the MWNT/chitosan and MWNT/chitosan-crosslinked membrane samples were developed as discussed earlier and are shown in Figure 6.5.

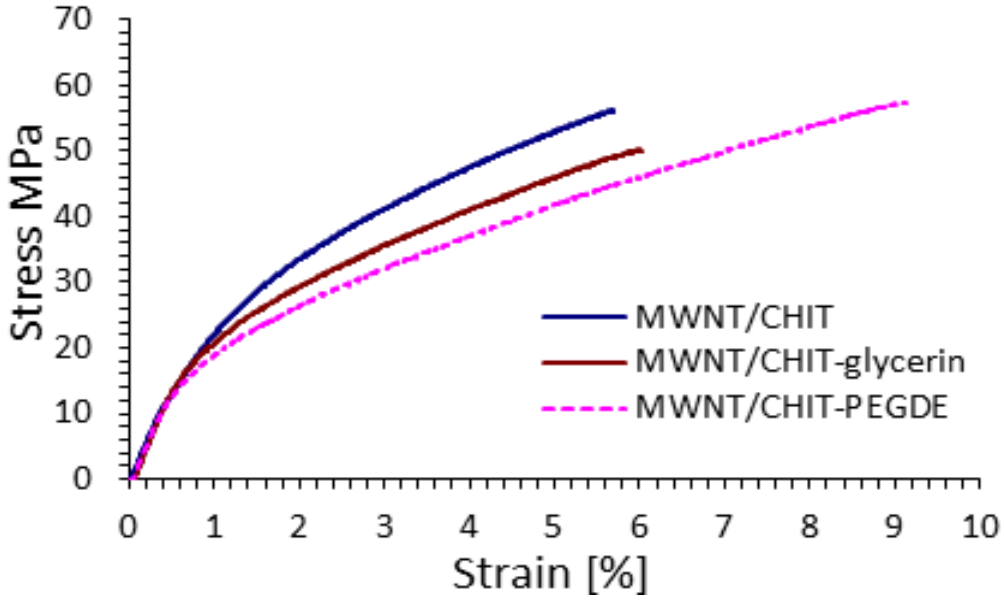

Figure 6.5. Stress–strain curves of MWNT/chitosan (MWNT/CHIT) and MWNT/chitosan-crosslinked (MWNT/CHIT-glycerin and MWNT/CHIT-PEDGE) BP membranes.

The values of the tensile properties (i.e. elongation, tensile strength, Young's modulus and toughness) are summarised in Table 12. These properties for the three BP membranes fell within a relatively small range of values. For example, the tensile strength of MWNT/chitosan-PEDGE (59 ± 3 MPa) was slightly higher than for MWNT/chitosan (56 ± 3 MPa) and MWNT/chitosan-glycerin (49 ± 4 MPa). Moreover, MWNT/chitosan-PEDGE BP had the lowest value of Young's modulus, at 2.67 ± 0.19 GPa. The values for MWNT-chitosan were 2.91 ± 0.11 GPa, and were 2.82 ± 0.19 GPa for MWNT/chitosan-glycerin. In contrast, the elongation-to-break value for the MWNT/chitosan BP membranes was 5.7 ± 0.5%, which is lower than the values obtained for both of the crosslinked membranes (i.e. 8.1 ± 2% and 6.4 ± 2% for the MWNT/chitosan-PEDGE and the MWNT/chitosan-glycerin membranes respectively). The toughness value of the MWNT/chitosan-PEDGE BP

membrane was highest (3.8 ± 0.8 J/g). These enhanced mechanical properties can be attributed to the addition of PEDGE (crosslinking agent), which may be bonded with amino groups of chitosan [112].

All the mechanical properties (Table 12) of the three BP membranes also fell in a narrower range of values, similar to those reported in Table 5.4 (Ch. 3) for MWNT/chitosan BP membranes (BP-2) prepared from the same batch of MWNTs and 0.2% (w/v) of chitosan as dispersant. In contrast, the mechanical properties reported here were much higher than the mechanical properties of BPs prepared by the vacuum-filtration method using MWNTs and various dispersions, such as Trix, cipro and τ-carrageenan [182, 257]. A recent investigation supports this hypothesis, showing that only when high molecular mass dispersants, such as polysaccharides and proteins, were included in the membrane, was there a significant increase in the strength of BPs made from SWNT [180].

6. 6 Solubility testing

Chitosan is easily soluble in dilute acids or at a pH <6.5 due to a primary amine group in its structure with the capacity for pronation and formation of a water-soluble substance. Therefore, crosslinking treatment is required to reinforce the chemical stability of chitosan membranes in low-pH or acidic solutions. Ngah et al. [110] reported that the crosslinked chitosan was insoluble. The solubility behaviours of MWNT-chitosan and MWNT-chitosan-crosslinked membranes were determined and are summarised in Table 13.

The solubility results presented in Table 13 show that the MWNT combined with pure chitosan (not crosslinked MWNT/chitosan) was soluble in acidic solution but insoluble in Milli-Q water and NaOH. This is because chitosan has a primary amine group ($–NH_2$) that makes it easily soluble in dilute acid solutions [110]. However, after crosslinking, MWNT-chitosan-glycerin and MWNT/chitosan-PEDGE membranes were insoluble in Milli-Q water and acidic and alkaline solutions (Table 13).

McCloskey et al. [286] reported that the composite membranes prepared from chitosan-PEDGE insoluble in a 3 wt% acetic-acid solution due to the crosslinking reaction were indeed effective. In addition, the results reported in this chapter for the solubility of MWNT/chitosan and MWNT/chitosan-PEDGE are consistent with results obtained in a previous study on chitosan and crosslinked chitosan (chitosan-PEDGE) [110]. It is well known that chitosan can be chemically crosslinked with a variety of crosslinking agents, such

as PEDGE [110, 112]. The results (Table 13) suggest that the crosslinked MWNT/chitosan BP membranes with glycerin or PEDGE are insoluble in both acidic and basic solutions.

Table 13. Solubility effect of MWNT-chitosan and MWNT-chitosan-crosslinked BP membranes tested on their solubility in 1–5% (v/v) each of acetic acid, Milli-Q water and 3-M sodium hydroxide by adding three small pieces (1 × 1 cm^2) of BP membrane to each solution for 24 h at 21°C with stirring.

	Solubility				
BP membrane	**Milli-Q water**	**Acetic acid 1% (v/v)**	**Acetic acid 3% (v/v)**	**Acetic acid 5% (v/v)**	**NaOH 3 M**
MWNT/chitosan	insoluble	soluble	soluble	soluble	insoluble
MWNT/chitosan-glycerin	insoluble	insoluble	insoluble	insoluble	insoluble
MWNT/chitosan-PEDGE	insoluble	insoluble	insoluble	insoluble	insoluble

6. 7 Swelling ratio

The swelling behaviours of the MWNT/chitosan and MWNT/chitosan-crosslinked membranes were calculated using equation 3; results are listed in Table 14.These results reveal that the MWNT/chitosan BP membrane had a greater degree of swelling than the MWNT/chitosan-glycerin and MWNT/chitosan-PEDGE BP membranes in Milli-Q water (~7 pH) due to the higher numbers of hydroxyl groups attached to uncrossed chitosan. On the other hand, the swelling results at pH ~7 agree well with those reported for chitosan hydrogels crosslinked at the surface with other crosslinkers, such as glutaraldehyde [291]. At low pH (acetic-acid solutions), the MWNT-chitosan BP membranes dissolved, making it impossible to estimate the swelling behaviours due to their physical instability [292]. However, bonding glycerin or PEDGE onto the MWNT/chitosan BP membranes improved the swelling resistance in water, acetic acid and sodium hydroxide. Therefore, the MWNT/chitosan-glycerin and MWNT/chitosan-PEDGE BP membranes are stable in acidic and basic solutions and did not swell to the same extent as the MWNT/chitosan BP membrane in aqueous solution. The swelling of chitosan is caused by the electrostatic repulsion between chitosan chains [293]. Tanabe et al. [294] reported that the swelling of chitosan composite membranes can be decreased by preventing the movement of chitosan chains, suggesting that the

observed decrease in swelling could be attributed to the hydrogen bonding between glycerin and chitosan that limits chitosan chain movement.

Table 14. Comparison of the swelling behaviour, porosity and thickness of MWNT-chitosan-crosslinked BP membranes: the swelling behaviours of the three BP membranes were measured in 1–5% (v/v) each of acetic acid, Milli-Q water and 3-M sodium hydroxide by adding three small pieces (1 × 1 cm^2) of BP membrane to each solution for 24 h at 21°C.

BP membrane	Swelling[a]					Thickness (µm)	Porosity[b] (%)
	Milli-Q water (mg)	Acetic acid 1% (v/v)	Acetic acid 3% (v/v)	Acetic acid 5% (v/v)	NaOH 3 M		
MWNT/chitosan	331 ± 15	–	–	–	196 ± 11	52 ± 3	76 ± 2
MWNT/chitosan-glycerin	34 ± 5	45 ± 6	83 ± 10	88 ± 8	54 ± 2	52 ± 6	34 ± 3
MWNT/chitosan-PEDGE	52 ± 3	82 ± 9	104 ± 10	105 ± 10	52 ± 6	58 ± 4	25 ± 2

a Calculated by equation 3 (Ch. 2)

b Calculated by equation 4 (Ch. 2)

These results reveal that the MWNT/chitosan BP membrane had a greater degree of swelling than the MWNT/chitosan-glycerin and MWNT/chitosan-PEDGE BP membranes in Milli-Q water (~7 pH) due to the higher numbers of hydroxyl groups attached to uncrossed chitosan. On the other hand, the swelling results at pH ~7 agree well with those reported for chitosan hydrogels crosslinked at the surface with other crosslinkers, such as glutaraldehyde [291]. At low pH (acetic-acid solutions), the MWNT-chitosan BP membranes dissolved, making it impossible to estimate the swelling behaviours due to their physical instability [292]. However, bonding glycerin or PEDGE onto the MWNT/chitosan BP membranes improved the swelling resistance in water, acetic acid and sodium hydroxide. Therefore, the MWNT/chitosan-glycerin and MWNT/chitosan-PEDGE BP membranes are stable in acidic and basic solutions and did not swell to the same extent as the MWNT/chitosan BP membrane

in aqueous solution. The swelling of chitosan is caused by the electrostatic repulsion between chitosan chains [293]. Tanabe et al. [294] reported that the swelling of chitosan composite membranes can be decreased by preventing the movement of chitosan chains, suggesting that the observed decrease in swelling could be attributed to the hydrogen bonding between glycerin and chitosan that limits chitosan chain movement.

6. 8 Surface areas and pore structures of membranes

Nitrogen adsorption/desorption isotherms were obtained at 77 K to further investigate the interbundle and intrabundle pore structures and surfaces of the three BP membranes. This allowed the evaluation of the specific surface areas of the BPs, as well as the average pore diameter. Typical isotherms obtained from these membranes are shown in Figure 6.6, and various data derived from the isotherms are presented in Table 15.

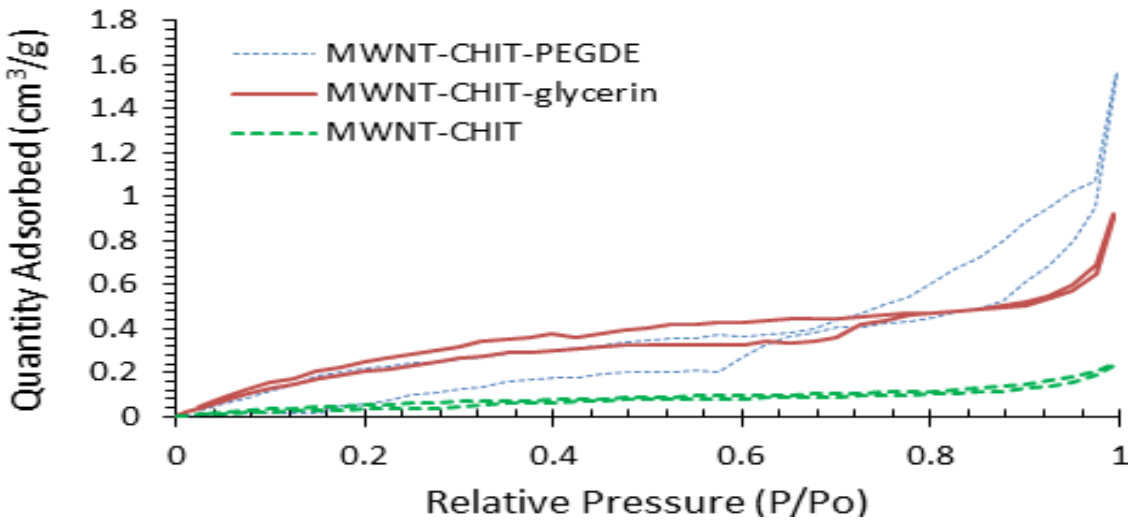

Figure 6.6. Adsorption isotherm demonstrates a comparative plot of the P/P_o and adsorption of all BP membranes fabricated using a filtration method.

Table 15 shows that the specific surface areas of all BPs were significantly lower than those determined in previous studies of BP membranes prepared using MWNTs with other dispersants, such as Trix and cipro, as well as with MWNT and chitosan [256, 257, 260]. The variations in nitrogen adsorption/desorption at P/P_o <0.1 are likely related to the presence of pores with diameters <2 nm.

Table 15. The surface areas (A_{BET}), average pore diameters (d_{BET}), average bundle diameters (D_{bun}) and water permeability of commercial MWNT/chitosan, MWNT/chitosan-glycerine and MWNT/chitosan-PEDGE BP membranes.

Membrane	A_{BET} (m^2/g)	Pore diameter (nm)	Interbundle pore volume (%)	Water permeability (L m^{-2} h^{-1} bar)
MWNT/chitosan	11 ± 2	2.1 ± 0.1	67 ± 4	12 ± 1
MWNT/chitosan-glycerin	1 ± 0.2	3.7 ± 0.1	13 ± 1	9 ± 0.3
MWNT/chitosan-PEDGE	0.07 ± 0.01	2.5 ± 0.1	*	3 ± 0.1

*Unable to estimate

Each isotherm in Figure 6.6 was used to calculate pore-size distribution using the BJH and HK methods [235, 236]. The HK method provides information relative to the distribution of small pores (i.e. <2 nm), whereas the BJH method can assess the distribution of the large pores of all BP membranes. Results were obtained for pore-size distribution of each BP membrane (Fig. 6.7) by combining the data from these two methods. The large peak from 0.5–1 nm is related to the pores between MWNT (intrabundle). However, variation >1 nm appeared in the distributions of the large pores. These interbundle pores are shown in the SEM images (Figs. 6.4A–C) [194]. The small peaks (dot peaks) at 2.1 nm for the MWNT-chitosan BP membrane (Fig. 6.7A), at 3.7 nm for the MWNT/chitosan-glycerin BP membrane (Fig. 6.7B) and at 2.5 nm for the MWNT/chitosan-PEDGE BP membrane (Fig. 6.7C) are related to the interbundle pores. Numerical integration of the curves of Figure 6.7A–C reveal that these larger interbundle pores are responsible for 67% of the total free volume of MWNT/chitosan and only 13% of MWNT/chitosan-glycerin. The interbundle pore volume percentages for the three BP membranes are very small compared to the values of the results for the MWNT-Trix, MWNT-cipro, MWNT-C6S, MWNT-PTS and MWNT-TSP, BP membranes [256, 257]. In addition, the MWNT buck-ypapers investigated in this chapter have much lower internal pores separating aggregates of MWNT with a small average diameter. This accounts for why the interbundle pore volumes determined for the MWNT buckypaper membranes (range 13–67%) are, on average, much lower than what was measured previously for the resultant buckypaper membranes composed of SWNTs (range

76-93%) [242]. Data of the pore structure information resulted through analysis of nitrogen adsorption/desorption isotherms therefore exposed that there are generally some significant differences for buckypaper membranes fabricated using the different classes of CNTs and surfactants. Therefore, the results in this chapter indicate that it may be possible to control the porosity of buckypaper membranes by using MWNT with chitosan and chitosan-crosslinked to be useful for desalination area.

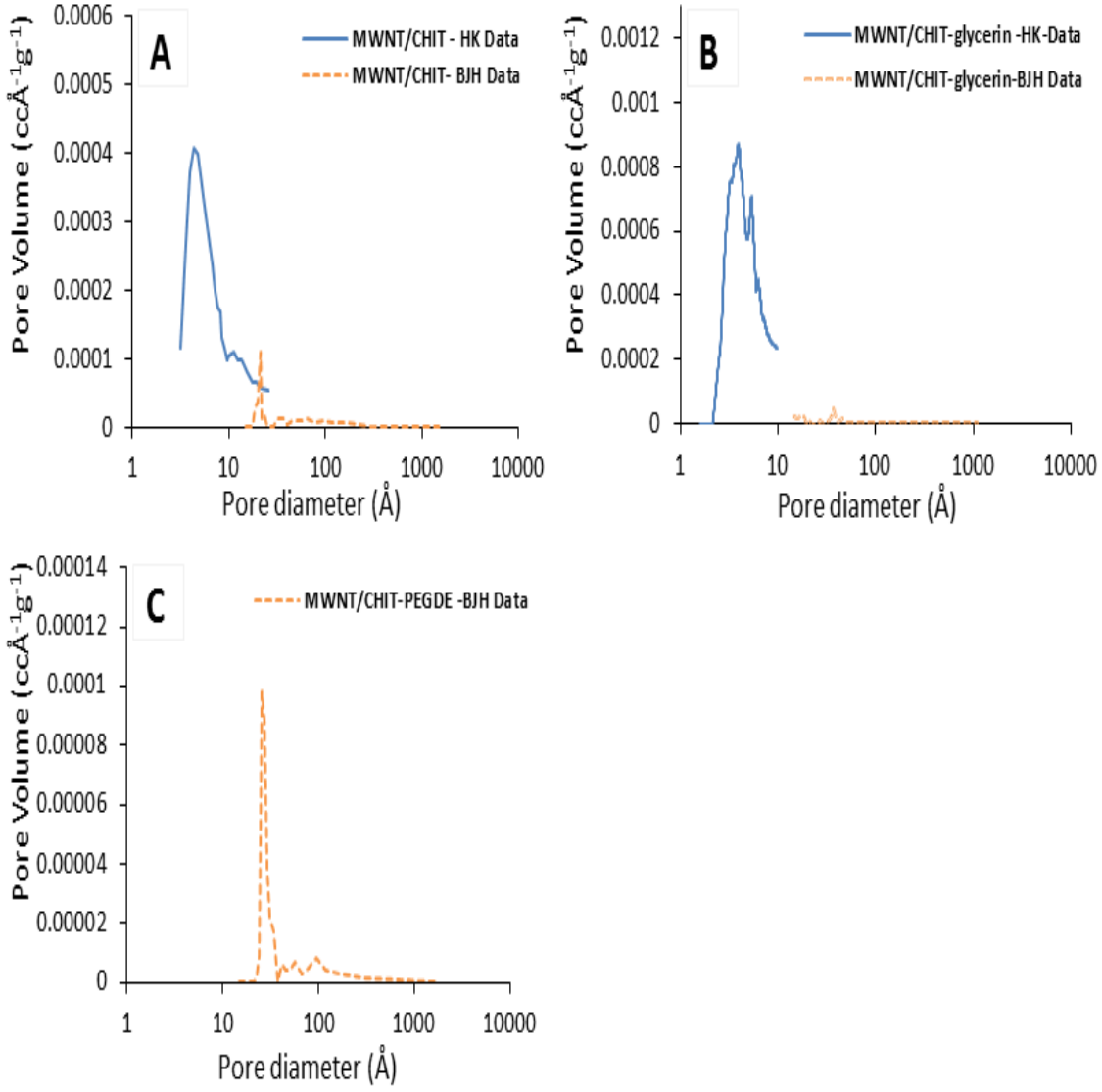

Figure 6.7. Pore-size distributions for BP membranes were determined using the HK (blue peak) and BJH methods (orange dotted peak), which were obtained from nitrogen adsorption/desorption isotherms: A) MWNT/chitosan; B) MWNT/chitosan-glycerin; and C) MWNT/chitosan-PEDGE; all BP membranes were prepared using a filtration method.

6. 9 Water permeability

Water permeability was determined for the large BP membranes (10 × 4 cm^2) using the procedure outlined in the experimental section, wherein the permeate flux was plotted against applied pressure to force the liquid through the membrane. Results are plotted in Figure 6.8, and water permeability was calculated from the slopes of the curves in Figure 6.8 using equation 12.

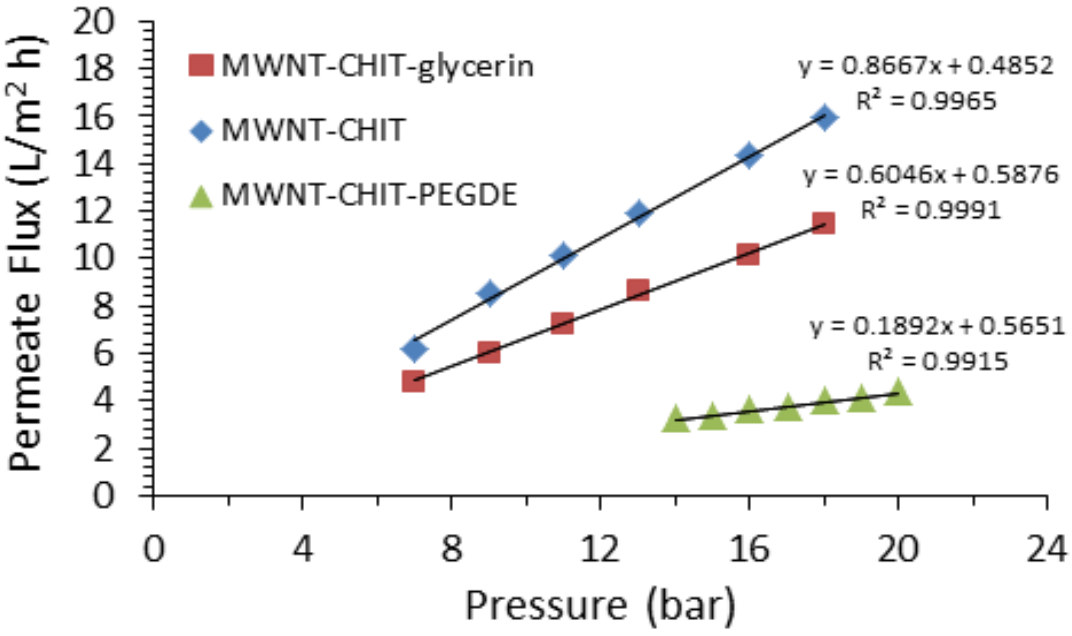

Figure 6.8. Permeate flux as a function of applied pressure of three BP membranes; the resulting straight lines represent a linear fit to the experimental data obtained.

The permeate fluxes of all BP membranes (i.e. MWNT/chitosan and MWNT/chitosan-crosslinked) increased with greater applied pressure [181]; results are presented in Table 15. After 8 h of operation for each BP membrane, the MWNT/chitosan BP membrane exhibited an average water-permeability rate of approximately 12 ± 1 L/m^2 h bar. This was 1.3 times higher than the average water-permeability rate (9 ± 0.3 L/m^2 h bar) of the MWNT/chitosan-glycerin, and 4.4 times greater than the average water-permeability rate (3 ± 0.1 L/m^2 h bar) of the MWNT/chitosan-PEDGE. In particular, the water permeability obtained with the MWNT/chitosan-PEDGE BP membrane was significantly lower (approximately a 78% decrease in flux during an 8-h filtration experiment) than that obtained with the MWNT/chitosan membrane. In addition, there was good agreement between the membrane permeability to water obtained for the three BPs (Table 15) and their porosities (Table 14). Many studies have reported that the crosslinking (crosslinking agent) of chitosan membranes

caused reductions in pore size and water permeability [273, 295, 296]. This shows that the MWNT/chitosan-crosslinked (MWNT/chitosan-PEDGE) can cause a reduction in membrane efficiency when filtering water. Therefore, the change in water permeability was due to changes in the surface area, porosity and pore structure of these BP membranes.

6. 10 Salt-rejection capability

We conducted permeation experiments for the three BP membranes (MWNT/chitosan, MWNT/chitosan-glycerin and MWNT/chitosan-PEDGE) using a crossflow RO/NF system with four inorganic electrolytic solutions (NaCl, $MgCl_2$, $MgSO_4$ and Na_2SO_4) having salt concentrations of 2,000 mg/L and applied pressures ranging 3–18 bar, at a temperature of 20°C for 8 h (Fig 2.8, Chapter 2).

The rejections (R_{obs}) of the four electrolytic solutions by MWNT/chitosan, MWNT/chitosan-Glycerin and MWNT/chitosan-PEDGE (as described by equation 7 in the experimental section) were also plotted against permeate flux (Fig. 6.9) as indicated above (Fig. 2.8, Chapter 2). Figures 6.9A–F and Table 16 reveal that, first, R_{obs} increases as the permeate flux is increased, approaching the maximum value. This value is known as the 'reflection coefficient', as mentioned in the Spiegler-Kedem analysis [297]. Second, the R_{obs} for the three BP membranes show good agreement for $MgCl_2$ but show distinctly different values for other electrolyte types, such as NaCl, $MgSO_4$ and Na_2SO_4. These two observations imply some interaction between the ions and the membrane, such that the 'steric hindrance' effect and the 'special sorption of ions' of the membrane must also be considered.

The most significant aspect of these experiments is the dependence of salt rejection on anion valence and concentration. Salt rejection follows the order of $R(MgCl_2) > R(NaCl) > R(MgSO_4) > R(Na_2SO_4)$ for a specific set of given operating conditions. This result contradicts the observed behaviours in previous studies showing the order of rejection as $R(MgCl_2) < R(NaCl) < R(MgSO_4) < R(Na_2SO_4)$, which may be because due to negative charge on the top layer, the membrane behaves much higher rejection for multi-valent ions (e.g. SO_4^{2-}) than for mono-valent ions (e.g. Cl^-).[273, 298]. Additionally, previous study show that the rejection of various inorganic electrolytes follows the order of $R(MgCl_2) > R(NaCl) > R(MgSO_4)$, illustrating the static electrification feature of a positively charged membrane [271]. The functional active layer of the composite membrane displays stronger sorption to Cl^- rather than SO_4^{2-} ions. It is also easier for Mg^{2+} ions to combine with anions on the surface

of the membrane, resulting in a decreased effective surface charge and leading to $R(Na_2SO_4) < R(MgSO_4) < R(NaCl) < R(MgCl_2)$.

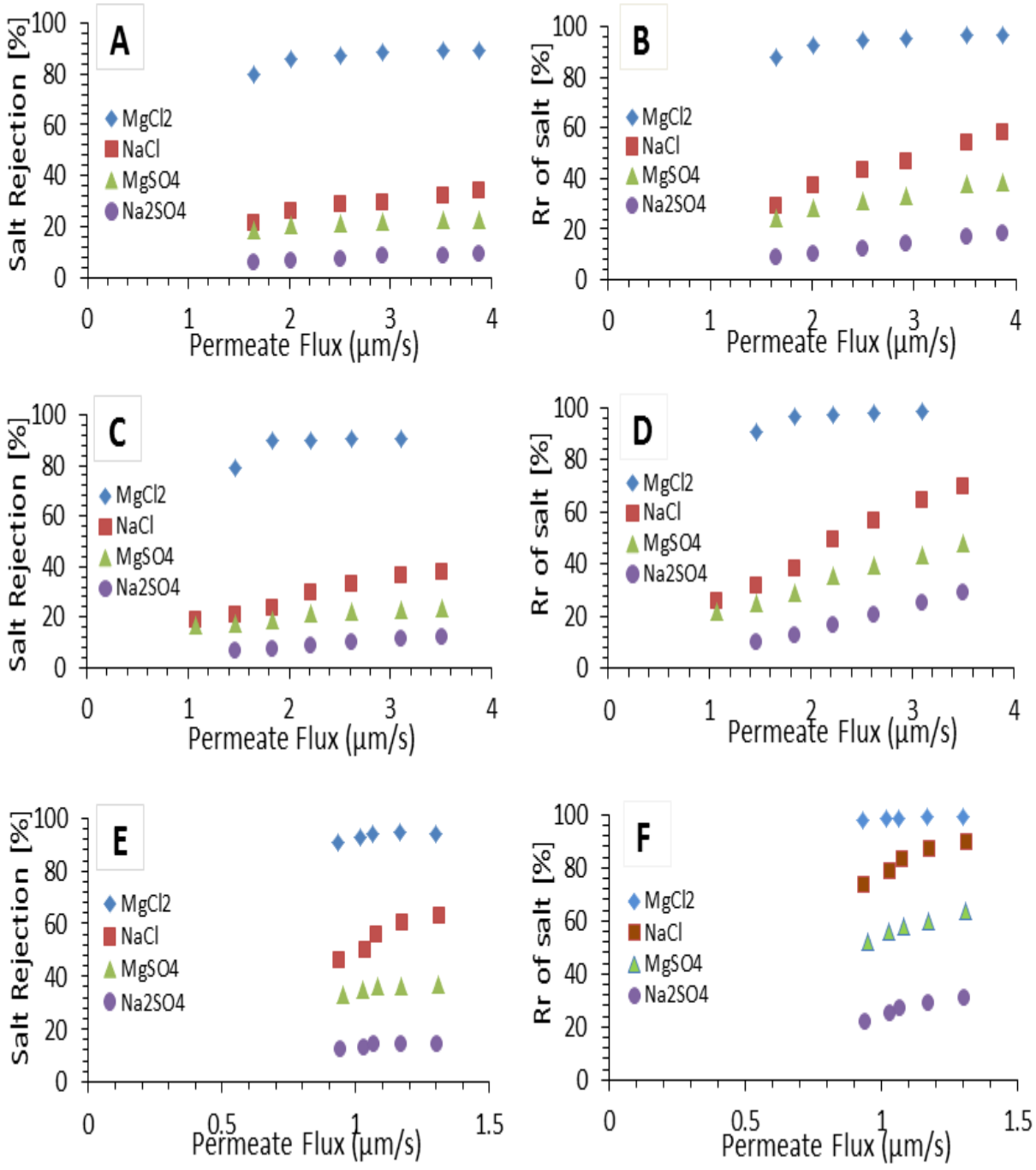

Figure 6.9. Comparison of (left) the observed and (right) real rejections (R_r) of salts as a function of permeate flux for the three BP membranes: A) and B) MWNT/chitosan; C) and D) MWNT/chitosan-glycerin; and E) and F) MWNT/chitosan-PEDGE.

Table 16. Rejection (%) and flux of different salts by BP membranes.

Feed solution (2g/l)	BP-membrane Type					
	MWNT/chitosan		MWNT/chitosan-glycerin		MWNT/chitosan-PEDGE	
	(L/m^2 h)	Flux R (%)	(L/m^2 h)	Flux R (%)	(L/m^2 h)	Flux R (%)
NaCl	6–14	21–3	4–13	19 –38	3–5	46–63
$MgCl_2$	5–11	80–89	4–12	79–91	3–5	91–95
$MgSO_4$	6–18	18–23	6–13	17–23	3–5	33–37
Na_2SO_4	8–18	6–9	4–11	7–12	3–5	12–14

The variation in surface charge density can be used to explain the rejection of electrolytes. Separation of the electrolyte valence type is dependent on the membrane charge [277, 278, 299, 300]. An increased surface charge results in greater rejection of co-ions (Mg^{2+} and Na^+ in this case) because of electrostatic repulsion (called the Donnan effect). Rejection increases for both electrolytes; however, in NaCl, the Na^+ carries a lower positive charge than Mg^{2+}, therefore the rejection ratio of NaCl is significantly lower than $MgCl_2$.

The separation of $MgCl_2$ could be larger than that of Na_2SO_4 and NaCl, as was also found by Rios et al. [299] in their study of a positively charged membrane. Therefore, the membrane charge determines the dependence of the separation on the electrolyte valence type, on the rejection of salt by the three charged BP membranes, which occurs predominantly through surface interaction between the membrane and ions.

A study by Maria et al. [298] reported that the rejection order $R(MgSO_4) > R(MgCl_2)$ agrees with the decreasing order of the anion charge density, with the repulsive force of the anions gradually weakening. Because the solute rejection is primarily determined by anion repulsion, the NF membrane surface must have developed a negative charge distribution. Still, the results of our experiments show the rejection order as $R(MgCl_2) > R(MgSO_4)$ because of the positively charged membrane. Thus, the Cl^- underwent rejection and a decreased cation charge density level, resulting in a gradually weakening in the force of attraction on the cation. In addition, lower rejection to inorganic electrolytes such as $MgSO_4$ by three buckypaper membranes generally resulted from low repulsion between the

membrane active layer and anions (SO_4^{2-}) due to the active layer of the buckypaper membranes not contain sulfate groups.

Maria et al. [298] also reported that the rejection order $R(Na_2SO_4) > R(MgSO_4)$ matches the increased level of density of cation charges, with the forces of attraction on the cations becoming stronger. Our research shows that the rejection order $R(MgSO_4) > R(Na_2SO_4)$ could be explained by the active layer of the membrane acquiring a positive surface charge distribution by the adsorption of anions from the electrolyte solution, and that the membrane performance is determined by this charge distribution.

As the concentration of the electrolyte increases the salt rejection decreases because the cation shield affects the membrane's repulsive force on the anions [298]. This effect is more obvious for Cl^- ions than sulphate ions. As the sulphate ion gains a higher charge density, the rejection rate becomes stronger on the positively charged membrane. Our investigation showed that the rejection of the Cl^- ion > SO_4^{2-} can also be explained by the active layer of the membrane acquiring a positive surface charge distribution by the adsorption of anions, such as the Cl^-, from the electrolyte solution.

Further, the adsorption of atoms, ions or molecules by membrane materials can be a significant component in the membrane's salt removal or rejection. Adsorption is a key factor in the transport mechanism of water and some solutes across the membrane [83]. Several studies have detected significant adsorption of some compounds, such as trace organics, into the membrane polymer [83, 301, 302]; therefore, a charged particle or ion (e.g. Cl^-) can be adsorbed by the amino ($–NH_2$) present in chitosan, which comprises coordination sites and has demonstrated high rejection of NaCl and $MgCl_2$ salts. This is because the chitosan membranes are positively charged, which means they can adsorb negatively charged ions [222]. In addition, most polymeric membranes, such as NF/RO membranes, are usually comprised of a functional group, such as hydroxyl (–OH), carboxyl (–COOH) and amine ($–NH_2$). These functional groups permit the production of fixed-charge groups inside the membrane as it is soaked in an aqueous solution. In response to the solution pH, the function groups can be deprotonated ($–COOH \rightarrow –COO^-$) or protonated ($–NH2 \rightarrow –NH_3^+$) to provide the membrane surface with a positive or negative charge respectively [303]. This charge can be affected by the dispersion of ions from the BP membrane and solution interface by an electrical charge. The ions adsorb at the membrane surface because they are linked to it by

electrical forces. The electrical potential at the surface of BP membranes can be measured experimentally and is known as the ZP of the membrane surface [304].

In addition, the three membranes' real rejections (R_r) of single salts, such as $MgCl_2$, NaCl, MgSO4 and Na_2SO_4 (Figs. 6.9B, D and F), were evaluated using the irreversible thermodynamic model to clarify the membranes' rejection behaviours towards the salts. The R_r was determined from the observed rejection (Figs. 6.9A, C and E), which was calculated by equation 7 (Chapter 2), and by the mass transfer coefficient (k_f), which was calculated by equation 9 (Chapter 2) using equation 8 (Chapter 2). The percentages of real rejection of all salts by the three BPs increased rapidly with greater permeate flux and were slightly higher than the observed rejections (R_{obs}) obtained by equation 7 (Chapter 2).

The correlation curves plotted for various salts $R(MgCl_2) > R(NaCl) > R(MgSO_4) > R(Na_2SO_4)$ imply that influences other than electrostatic repulsion, such as charge density, affect the cation shield and surface charge of the membrane, which also influence the process of separation. If all the factors of the mechanistic model are identified and defined, it will be easier to comprehend and calculate the salt retention rates; however, this is easier said than done, as the identification of all factors will be complicated, and should be the subject of future research.

The rejection of NaCl by MWNT/chitosan and MWNT/chitosan-crosslinked BP membranes was studied at 20°C at a range of pH levels (3–10), and the permeation flux remained constant (Fig. 6.10A). The rejection results are presented in Figure 6.10B. All the membranes (MWNT/chitosan and MWNT/chitosan-crosslinked) had increased salt (NaCl) rejection when the feed solution pH became acidic. The increase in the rejection of NaCl by all three BP membranes when subjected to lower pH may be attributed to the protonation of free amino groups in chitosan. Previous studies have described that $–NH_2$ on chitosan can be protonated at low pH. As a result, the NH_3^+ group on the chitosan can play an important role because the group is chiefly responsible for interactions with anions and negatively charged surfaces [305, 306]. Figure 6.10B demonstrates that charge repulsion can result in higher rejection based on steric interactions. It is likely that the evidence would be much clearer if smaller ions were selected. Complete rejection efficiency can be reached by positively charging all three BP membranes as revealed by ZP (Fig. 6.11).

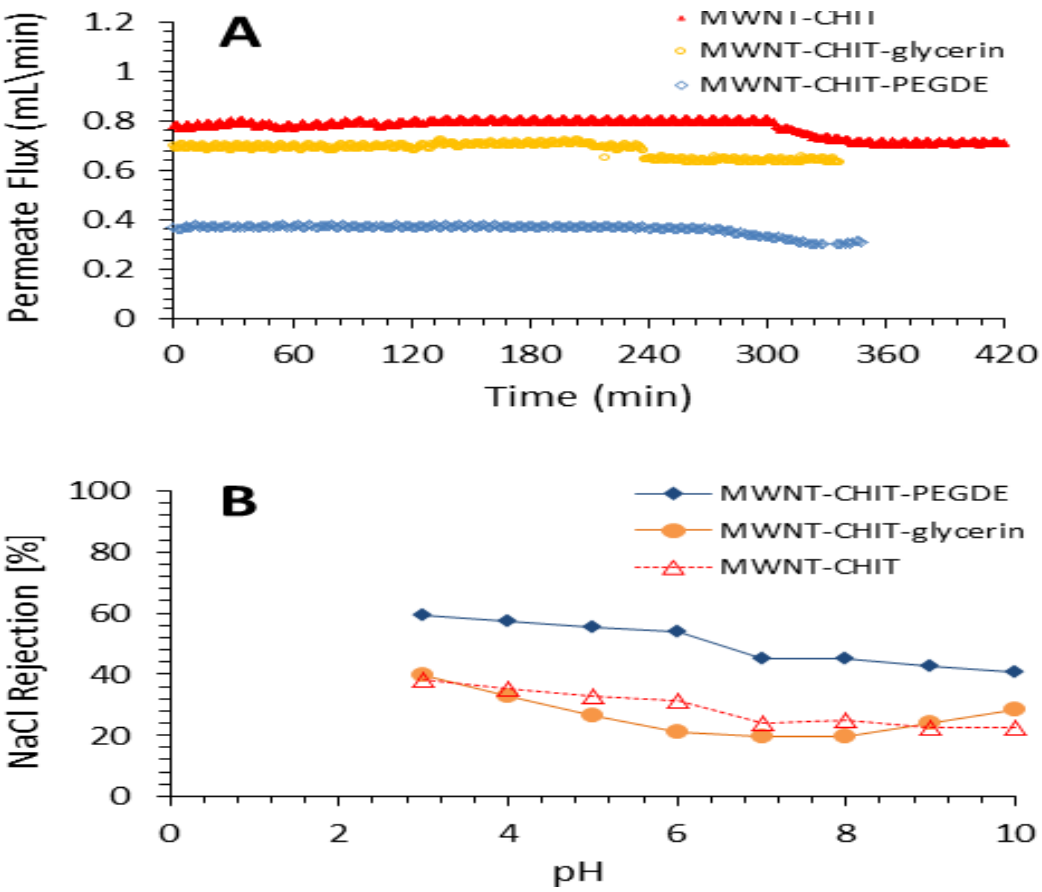

Figure 6.10. A) Permeate flux as a function of time for the filtration of an NaCl-water emulsion (2,000 ppm NaCl) at 20°C; B) comparison of NaCl rejection as a function of pH for the three BP membranes.

6. 11 Zeta potential (ZP)

Membrane-surface charge density can be determined by measuring the ZP of the membrane. Techniques to estimate the ZP have been explained in detail by Childress and Elimelech [284]. The ZPs of the three BP membranes (MWNT/chitosan, MWNT/chitosan-glycerin and MWNT/chitosan-PEDGE) were determined by the method described in the experimental section. The results are plotted as a function of pH in Figure 6.11.

These BP membranes are negatively charged at high pH, positively charged at low pH and become more positive as the solution pH decreases. The isoelectric point of BP-membrane surfaces are in the range of 6–8 pH. The MWNT/chitosan-PEDGE BP membrane is more negative at high pH than are the MWNT/chitosan and MWNT/chitosan-glycerin BP membranes. Moreover, the difference in pH values can correlate with the dissociation of the membrane functional groups (i.e. amide functional groups). This is dependent on the pH of

the feed solution and can carry a fixed positive or negative charge [284, 303]. To some extent, the membrane pore size can be modified by a charge interaction between groups [303]. However, NaCl rejection by the three BP membranes was lower when the pH was close to the membrane isoelectric point. Thus, the membrane-surface charge is an important factor in the rejection mechanism through charge repulsion.

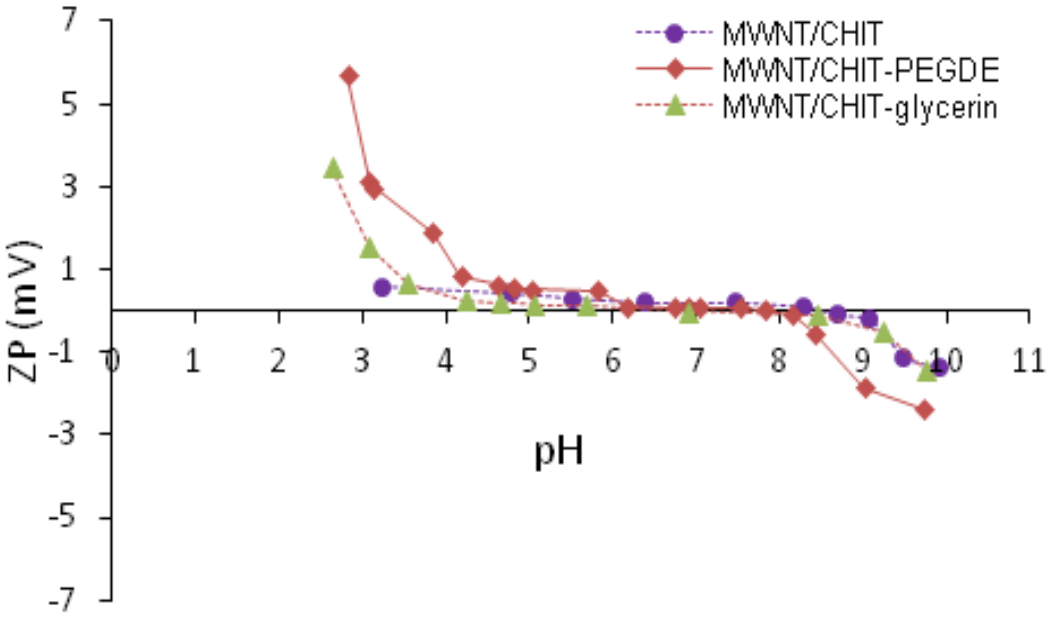

Figure 6.11. ZPs of the three BP membranes as a function of pH.

6. 12 Conclusions

Three BP membranes were developed based on a crosslinked chitosan; that is, chitosan-glycerin and chitosan-PEDGE combined with MWNT for water filtration. The chitosan, chitosan-glycerin and chitosan-PEDGE offered a pathway for enhancing the dispersal of MWNTs in water. They also provided an excellent conductivity range (60–70 S/cm) and an extremely high tensile strength compared to the BPs prepared by the vacuum-filtration method using MWNTs and various dispersants, such as Trix, cipro and τ-carrageenan [182, 257].

The interconnected porous structure with a small specific surface area suggested that the incorporation of MWNT could be achieved by packing hydrophilic chains (chitosan and crosslinked chitosan) in the interface. This would create a suitable surface (due to groups –

NH2 and –OH on the surface of BP membranes) for water permeation and salt rejection. Further, the permeate flux sequence of BP membranes is MWNT/chitosan > MWNT/chitosan-glycerin > MWNT/chitosan-PEDGE. The MWNT/chitosan BP membrane provides more accessible free volume for water transport than the MWNT/chitosan-PEDGE and MWNT/chitosan -glycerin content.

The rejection sequence of BP membranes is MWNT/chitosan-PEDGE > MWNT/ chitosan-glycerin > MWNT/chitosan. In addition, the rejection of both Na_2SO_4 and $MgSO_4$ by the three BP membranes was significantly lower than the rejection of $MgCl_2$ and NaCl. This may due to the low charge densities at each membrane's surface and that the three membranes' active layers did not contain sulphate groups. This can increase the rejection of Na_2SO_4 and $MgSO_4$ through the repulsion between the active layer of the BP membranes and the anion SO_4^{2-}.

Chapter 7: Properties of Unfunctionalised and Functionalised MWNT/Chitosan Membranes

BP membranes were fabricated by combining chitosan with MWNT, MWNT-COOH or MWNT-NH_2 in a dispersing aqueous solution using a vacuum-filtration method, as described in the experimental section. Complete solution dispersion was ensured by sonication. MWNT, MWNT-COOH or MWNT-NH_2 (15 mg each) was dispersed in 15 mL of water containing 0.2% (w/v) of chitosan. UV-vis-NIR spectrophotometry was used to assess the effects of increasing sonication time on the absorption spectra of these dispersions. The resulting BP membranes were compared by evaluating their properties and water permeability with their abilities to reject the salts from aqueous solutions.

7. 1 Optimisation of sonication time

To prepare the BP membranes, it was necessary to produce a homogeneous MWNT dispersion. However, CNTs are non-polar, strongly hydrophobic [263] and have low solubility in polar solvents, such as water. To avoid the attaching or modification of hydrophilic functional groups (e.g. –COOH) into the surface of the MWNTs, they were treated with strong acid (e.g. H_2SO_4 and HNO_3). Carboxyl groups are known to attach to the surfaces of MWNTs by the acid-treated method, producing better dispersion in polar solution (water) [307-309].

UV-vis-NIR absorption spectra of the MWNT-COOH dispersed in chitosan solution were taken. Figure 7.1A indicates that absorbance seemed stabilised from around 660 nm. Thus, absorbance at 660 nm was taken for each of the dispersion solutions containing MWNT/chitosan, MWNT-COOH/chitosan or MWNT-NH_2/chitosan and is plotted as a function of sonication time (Fig. 7.1B).

Absorbance increases significantly with sonication time up to about 10 min, followed by a plateau. This result agrees with behaviours previously observed with SWNT and MWNT dispersions, where absorbance was significantly increased by increasing sonication time [180-182, 257]. The results obtained from the UV-vis-NIR spectra reveal that 12-min sonications were sufficient for the three dispersion solutions (i.e. MWNT, MWNT-COOH and MWNT-NH_2) to be well dispersed in chitosan solution. After 12 min, there were no significant changes in the absorbance of the three dispersions at 660 nm. Similar results to these were

produced when absorption spectra were investigated for a 0.1% (w/v) MWNTs and 1.0% (w/v) ciprofloxacin solution, although as expected the spectra lacked features due to the van Hove singularities [257]. However, 20 min was chosen as the optimal sonication time for preparing all three MWNT dispersions because it allowed enough time for MWNT and modified MWNT to have a strong interaction with chitosan and miscibility with water. At 660 nm, the MWNT-COOH had the highest absorbance compared to MWNT and MWNT-NH_2. This may be attributed to the polar functional groups, such as carboxylic acid, attached to the surfaces of the MWNTs [309].

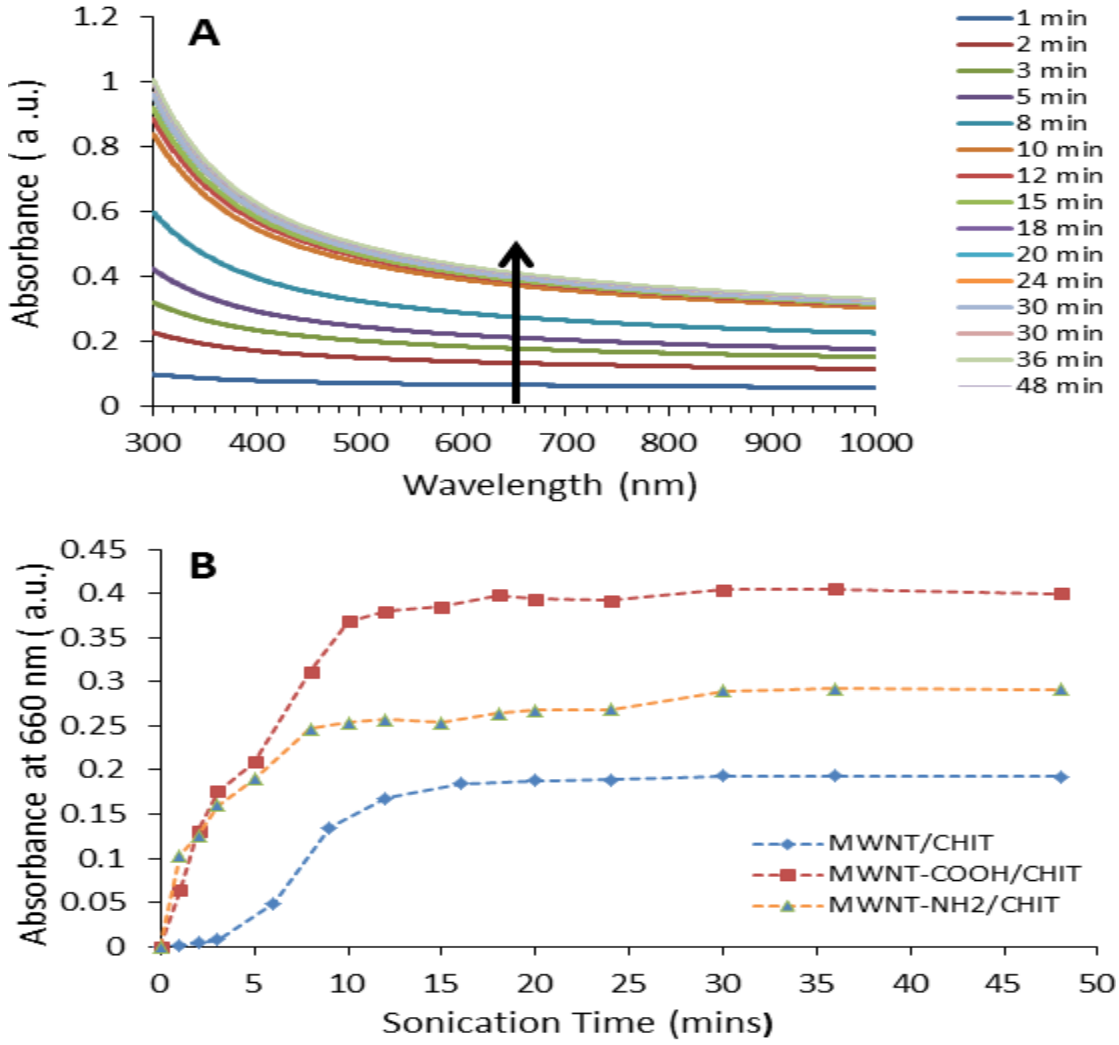

Figure 7.1. A) UV-vis spectra of MWNT-COOH/chitosan dispersion as a function of sonication time; B) comparison of the effects of increasing sonication time on absorbance at 660 nm of MWNT/chitosan, MWNT-COOH/chitosan and MWNT-NH_2/chitosan dispersions.

7. 2 Conductivity of BP membranes

Conductivity is a significant factor the BP membrane's usability as a filter in separation applications. The electrical characteristics (i.e. resistance and conductivity) were thus determined using equation 10 (see experimental section) and a two-point probe method under ambient conditions (21°C and 45% RH). Current variations were linear to variations in voltage for all three membranes, showing that they followed ohmic behaviour. The linear relationships observed in Figure 7.2 were obtained by equation 10, and the conductivity values for the three BPs are presented in Table 17. These results reveal that the conductivity of MWNT/chitosan is 70 ± 1, which is much higher than that of the two BP membranes with MWNT-COOH/chitosan and MWNT-NH_2/chitosan.

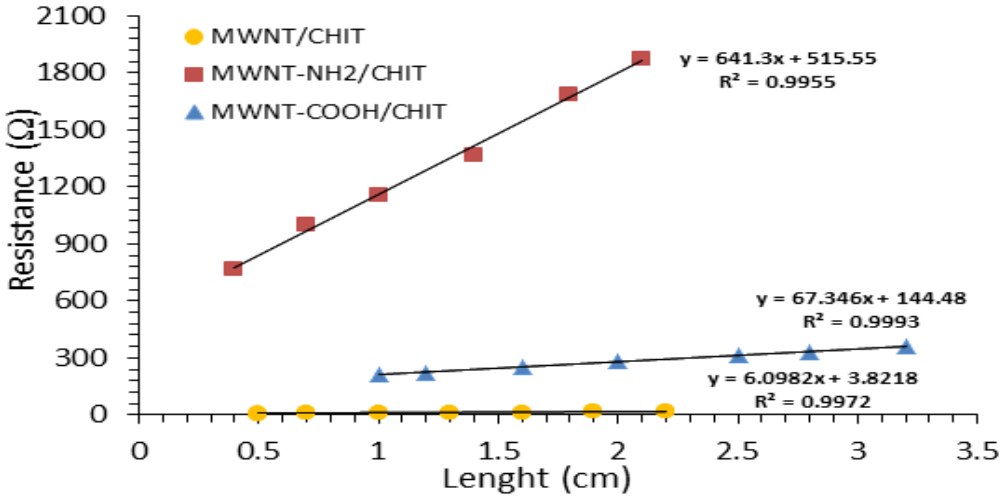

Figure 7.2. Effect of changed length on the resistance of BP membranes produced from different dispersions containing 0.2% (w/v) chitosan (CHIT) combined with 0.1% (w/w) MWNT, MWNT-COOH and MWNT-NH_2; all BP membranes were fabricated by filtering 0.25 L of dispersion through 0.22-µm PVDF.

Table 17. Conductivities, contact angles and mechanical properties of BPs prepared using different types of CNTs/chitosan; the errors are represented with standard deviations; values for all BP membranes represent an average of the conductivities of two BPs.

BP membrane	Contact angle (°)	Conductivity (S/cm)	Elongation (%)	Tensile strength (MPa)	Young modulus (GPa)	Toughness (J/g)
MWNT/chitosan	105 ± 2	70 ± 1	4.7 ± 0.7	57 ± 3	2.8 ± 0.1	2.1 ± 0.2
MWNT-COOH/ chitosan	36 ± 3	7 ± 1	5.7 ± 0.1	60 ± 2	3.3 ± 0.1	2.2 ± 0.3
MWNT-NH_2/ chitosan	92 ± 4	1.0 ± 0.3	3.5 ± 0.9	17 ± 2	2.2 ± 0.06	0.5 ± 0.1

This conductivity value 70 ± 1S/cm of MWNT/chitosan is about 10 times higher than that of MWNT-COOH/chitosan and 70 times higher than that of MWNT-NH_2/chitosan. These significant changes in conductivity can be attributed to the functionalisation process (i.e. attaching –COOH and –NH_2 groups to the surface of MWNTs). Sahoo et al. [179] reported that the properties of CNT, such as electrical and transport behaviour, are influenced by covalent functionalisation due to a change in sp^2 to sp^3 carbon atoms. This suggests that the surface of the MWNT-COOH/chitosan and MWNT-NH_2/chitosan BP membranes may not allow the electrons to move easily on the surface due to the interaction between the carboxyl groups –COOH and –NH_2 groups on the surfaces of MWNTs with high chemical reactivity of a large number of functional groups (-NH_2 and -OH) on the backbone of chitosan. It is worth noting that the incorporation of MWNT-COOH and MWNT-NH_2 with chitosan resulted in a BP membrane of significantly lower conductivity than was obtained when MWNT was used with Trix and chitosan as dispersants. This implies that the BP membranes prepared from MWNT-COOH and MWNT-NH_2 dispersions containing shorter MWNTs would have a larger number of CNT-CNT junctions, thereby increasing resistance and decreasing conductivity. Coupled with this, the functionalisation of MWNT with COOH and NH_2 also reduces contact and leads to higher junction resistance. This suggested that the conductive for the MWNT-COOH/chitosan and MWNT-NH_2/chitosan BP is more difficult than those of the MWNT/chitosan BP due to the hydrogen bond interaction between the COOH and –NH_2 groups on the surface of the MWNT and –NH_2 and OH groups of chitosan. This interaction limits the movement of MWNT-COOH/chitosan and MWNT- NH_2/chitosan BP membranes to form conductive networks on their surfaces.

7. 3 Mechanical properties

Typical stress–strain curves for the three BP membranes are presented in Figure 6.3, and the resulting properties are summarised in Table 17. All the membranes were tested at room temperature (21°C). The values of tensile strength, Young's modulus, elongation and toughness for MWNT-COOH-chitosan and MWNT/chitosan membranes were very similar, whereas the MWNT-NH_2/chitosan membrane was significantly weaker. For example, the MWNT-NH_2-chitosan BP membrane gave an elongation value of 3.5 ± 0.9%, which was lower than those of the MWNT-COOH/chitosan (5.7 ± 0.1%) and MWNT/chitosan (4.7 ± 0.7%) membranes. This suggests that the MWNT-NH_2/chitosan BP membranes are easier to break than membranes composed of MWNT-COOH/chitosan. In contrast, the tensile strength

of the MWNT-COOH/chitosan BP membrane (60 ± 2 MPa) and its Young's modulus (3.3 ± 0.097 GPa) were both greater than the tensile strength and Young's modulus values obtained for the MWNT/chitosan (57 ± 3 MPa and 3.8 ± 0.114 GPa respectively) and for the MWNT-NH_2-chitosan BP (17 ± 2 MPa and 2.2 ± 0.064 GPa respectively). The tensile strengths of the MWNT-COOH/chitosan and MWNT/chitosan membranes were approximately 3 times higher than that of the MWNT-NH_2/chitosan BP membrane. However, the tensile strength and elongation of the MWNT-COOH/chitosan BP were both slightly higher than the values obtained for the MWNT/chitosan BP membrane. This may have been the result of strong interactions between chitosan and MWNT-COOH. The functionalised MWNTs formed by acid treatment contain –COOH groups, which facilitate enhanced interaction with –NH_2 groups in the chitosan chain.

Further, the toughness value (2.2 ± 0.3J/g) of the MWNT-COOH/chitosan BP was similar to that of an MWNT/hitosan membrane, whereas the toughness value of the MWNT-NH_2/chitosan was 0.5 ± 0.1 J/g. This indicates that the mechanical characteristics of the BP membranes were improved by –COOH groups attached to the surface of the MWNT. However, the mechanical properties of MWNT-NH_2/chitosan were poorer that those of the MWNT-COOH/chitosan. Thus, the mechanical properties of BP membranes are highly dependent on the CNT-CNT junctions [310]. The junction strength is determined by adsorbed surfactant molecules, as it is suggested that no chemical bonding between MWNT-NH_2 and chitosan occurred. This may increase the number of CNT-CNT junctions, which can lead to significant reductions in the mechanical properties of the membranes. In contrast, the mechanical properties reported previously for BPs using different types of CNTs (SWNT and MWNT) and dispersions (Trix and cipro) are lower than those obtained here for the three BP membranes [181, 256, 257]. The values for the mechanical properties obtained from BP membranes prepared using MWNT-COOH and chitosan (in the present section) were also significantly greater than those obtained using MWNT and Trix (see previous sections). The results of a recent study agree well with a previous investigation showing that the mechanical properties of BP membranes were significantly enhanced only when high molecular mass dispersants, such as chitosan, were incorporated into the CNTs [180].

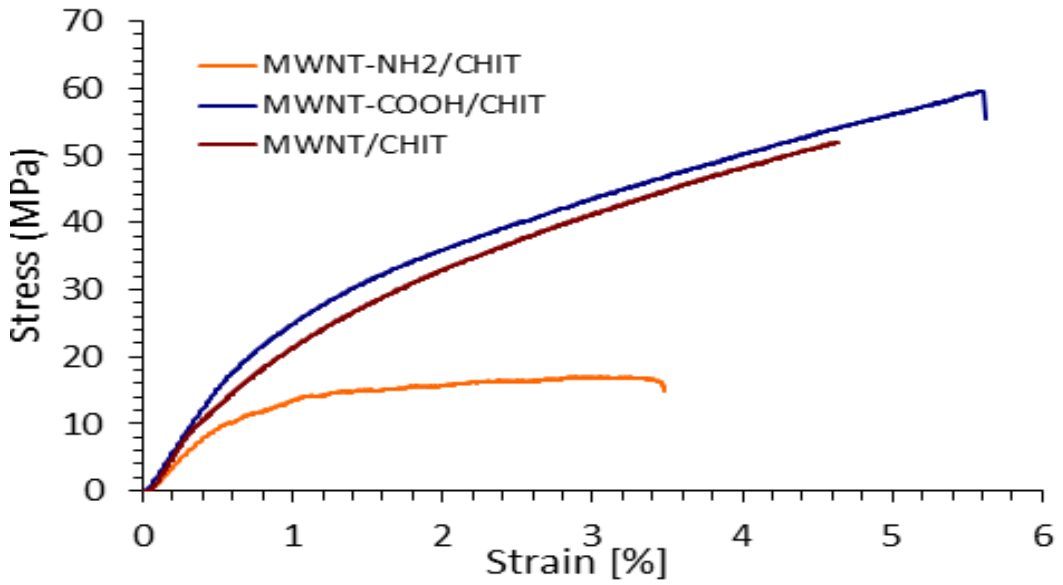

Figure 7.3.Study of the effects of MWNT surface modifications and combining chitosan 0.2% (w/v) on the mechanical properties of BP membranes; all BP membranes were fabricated by filtering 0.25 L of dispersion through 0.22-µm PVDF.

7. 4 Morphology of BP membranes

The surface morphologies and cross-sections of the BP membranes were investigated using SEM images to confirm the visible pore sizes on the surfaces and the quality of the dispersion of MWNTs in the solution. Several previous studies reported that the surface morphology of the BP membrane was highly dependent on the dispersants used [180, 181, 257]. SEM images in Figures 7.4A, C and E show that the three BP membranes were well dispersed in the aqueous solution containing 0.2% w/v of chitosan and possessed a large number of irregularly sized pores aggregated on the surface (dark region). The SEM images also confirmed that the pores of the MWNT-COOH/chitosan BP membrane were slightly larger than those present in the MWNT/chitosan and the MWNT-NH_2/chitosan BP membranes.

These SEM images suggest that MWNTs modified with functional groups (–COOH) and combined with a hydrophilic biopolymer, such as chitosan, can produce BP membranes with high porous structures and large pore sizes. However, there was generally little observable difference between the surface morphologies of the other two BP membranes (MWNT/chitosan and MWNT-NH_2/chitosan). The images of these BP membranes (Figs. 7.4A and F) are not as clear as the image of the MWNT-COOH/chitosan BP membrane (Fig.

7.4C), with very few surface pores and large aggregates of MWNTs. In addition, the cross-section of SEM images presented in Figures 7.4B and D show that there are few variations in the cross-sections of MWNT/chitosan and MWNT-COOH/chitosan BP membranes. However, the cross-sections of SEM images of the MWNT-NH_2/chitosan (Fig. 7.4F) have aggregates of MWNTs, but MWNT-NH_2 was not as clear as the other BP membranes due to the low conductivity of the MWNT-NH_2/chitosan membrane's surface (Table 17).

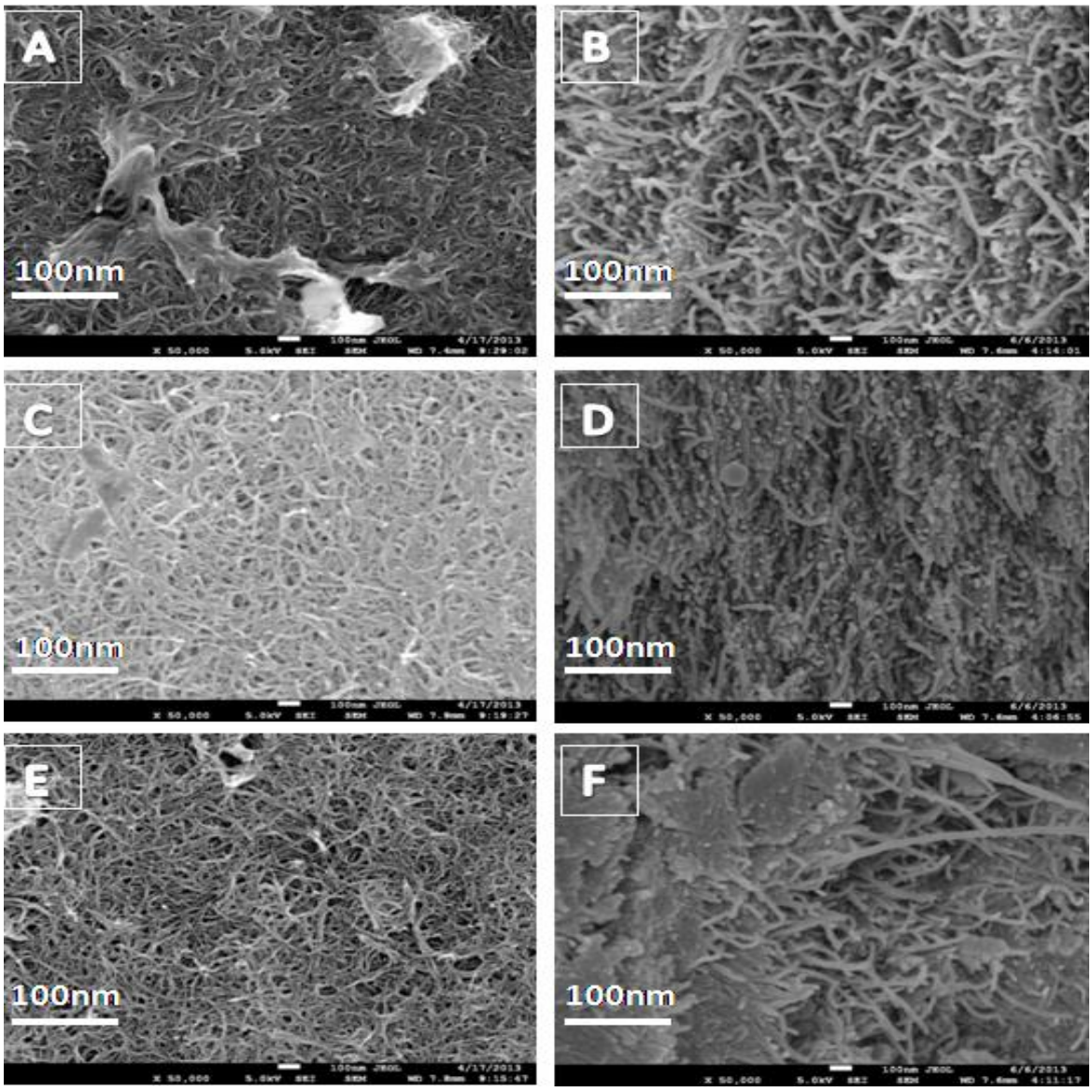

Figure 7.4. SEM images of the surfaces (A, C and E) and cross-sections (B, D and F) of BP membranes formed from (A and B) MWNT/chitosan, (C and D) MWNT-COOH/chitosan and (E and F) MWNT-NH_2/chitosan; all BP membranes were fabricated by filtering 0.25 L of dispersion through 0.22-µm PVDF.

7. 5 Surface areas and pore structures of BP membranes

Further investigations of the surface areas and pore structures of BP membranes were conducted in detail using BET [234] analysis of isotherms obtained by nitrogen adsorption/desorption measurements according to the method described in the experimental section. The results revealed that the three BP membranes had a common type IV isotherm with hysteresis at higher pressures (Fig. 7.5). In addition, the hysteresis occurs because of variations among the ratios of the adsorbent removal and filling that takes place during a capillary condensation mechanism [311]. The contributions of the surface area, interbundle and intra-tube are generally dependent on the outer surfaces of the BPs. The CNT-bundle diameter was calculated by equation 11 [194]. The specific surface area, average pore diameter, pore volume and average bundle diameter for each of the three BP membranes are summarised in Table 18.

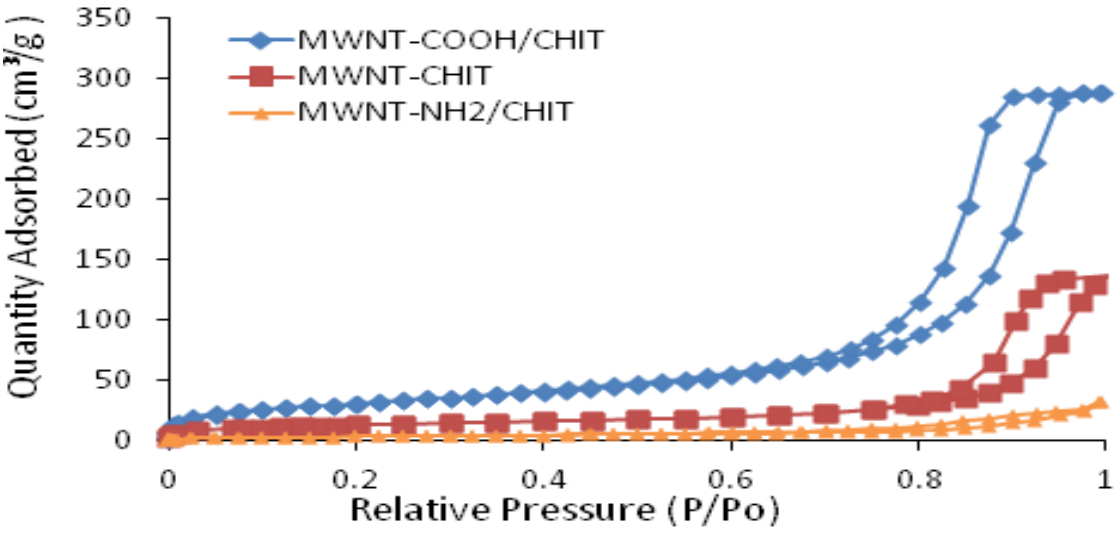

Figure 7. 5. Nitrogen adsorption/desorption isotherms for different BP membranes; all BP membranes were prepared using a filtration method.

The diameters of the nanotube bundles exhibited an inverse of the values of the surface areas of BP membranes. For example, the MWNT-COOH/chitosan BP with the most surface area exhibited the smallest nanotube-bundle diameters (24 ± 3 nm). But MWNT-NH_2/chitosan, having the lowest surface area, showed the largest nanotube-bundle diameters (222 ± 12 nm). The MWNT-COOH/chitosan BP membranes fabricated in the current study had greater surface areas (112 ± 4 m^2/g) than the other two BP membranes (i.e. 45 ± 2 m^2/g for MWNT-chitosan and 12 ± 2 m^2/g for MWNT-NH_2/chitosan). This probably occurred due

to the presence of the carboxyl functional groups, which improve interaction with chitosan while amine groups decrease it. Abdel Salam et al. [312] reported that the surface area of the MWNT/chitosan nano-composite membrane was increased through modified CNTs due to the better dispersion of MWNTs within the chitosan solution, which may cause decreased tangling, folding of the CNTs and improvement of their accessibility for nitrogen adsorption. These changes may have a substantial effect on the permeability behaviour of water for these BP membranes. Measurement of the surface area using a nitrogen adsorption/desorption method for BP membranes of MWNT-Trix gave values of 114 ± 2 m^2/g (Chapter 3), which are significantly larger than those obtained in the present study. In addition, the surface-area values reported previously for MWNT-Trix and MWNT-cipro BP membranes were 300 ± 1 and 250 ± 1 m^2/g respectively, which are also greater than the surface area values determined here and also the average pore diameters of the MWNT-Trix and MWNT BP membranes (24–26 nm) were larger than that of the pore diameter measured here [257].

Table 18. Surface area (A_{BET}), average pore-size diameter (d_{BET}), average bundle diameter (D_{bun}), interbundle pores, intrabundle pores and water permeability of BP membranes prepared by a filtration method.

BP membrane	Surface area (m^2/g)	Average pore size (nm)	Average bundle diameter (nm)	Interbundle pore volume (%)	Intrabundle pore volume (%)	Water permeability (L/h.m^2.bar)
MWNT/chitosan	45 ± 2	21 ± 2	59 ± 5	82 ± 2	18 ± 2	1.6 ± 0.1
MWNT-COOH/chitosan	112 ± 4	10 ± 1	24 ± 3	90 ± 4	10 ± 1	6.6 ± 0.2
MWNT-NH_2/chitosan	12 ± 2	10 ± 1	222 ± 12	85 ± 2	15 ± 1	0.5 ± 0.1

Data obtained from nitrogen adsorption/desorption (Fig. 7.5) were used to determine the pore-size distribution within the BP membranes by the HK and BJH methods [235, 236]. The HK method estimates pore sizes <2 nm, and the BJH method calculates pore sizes >2 nm [194]. The two data sets obtained from these methods are combined to give a final pore-size distribution, which is presented in Figures 7.6A–C for all three BP membranes.

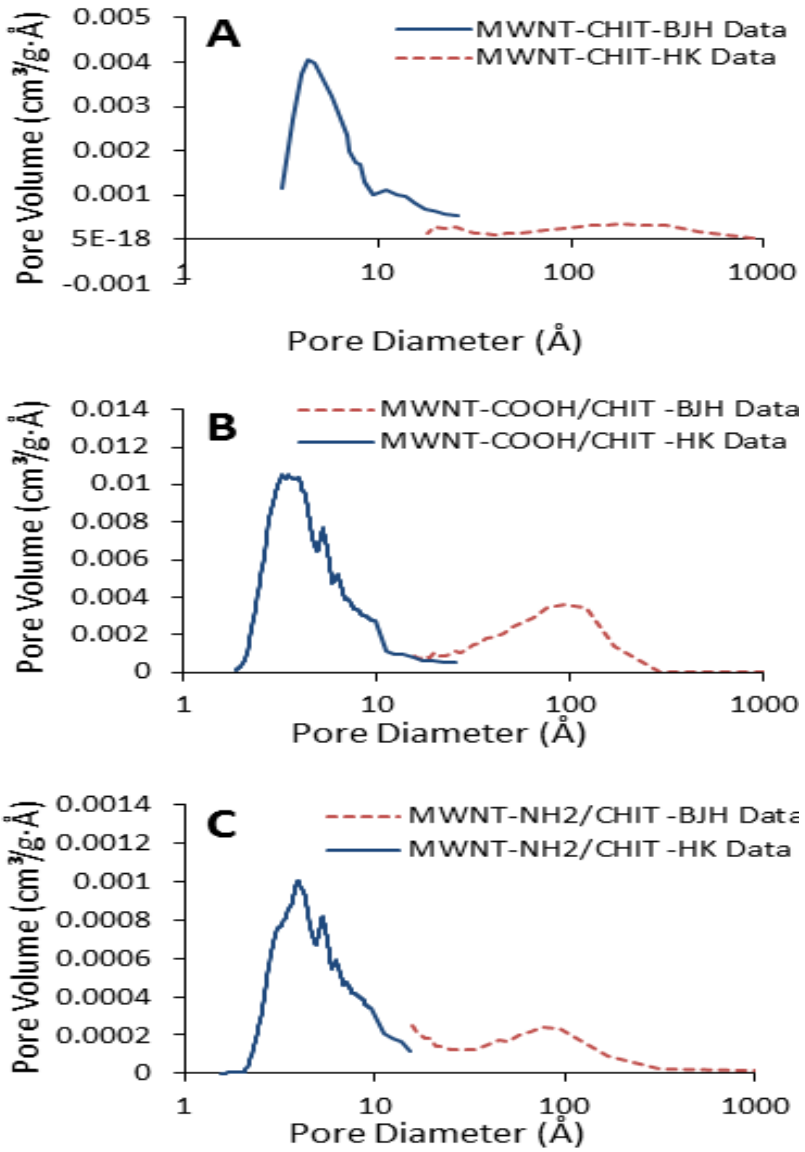

Figure 7.6. Total pore volume as a function of pore diameter for different BP membranes: HK (blue line peak) and BJH methods (orange dotted peak) data obtained from nitrogen adsorption/desorption isotherms for the following: a) MWNT/chitosan; b) MWNT-COOH/chitosan; and c) MWNT-NT_2/chitosan; all BP membranes were prepared using a filtration method.

The large peaks (blue lines) in Figure 7.6 for each BP membrane from 0.5–2 nm provide information about the intrabundle pores, whereas the small peaks (dotted lines) from 2–10 nm relate to the interbundle pores. Table 18 illustrates that the three BPs are different in the distributions of their interbundle and intertube pore volumes. For example, the interbundle pore volume of 90 ± 4% appears to make a larger contribution to porosity in the MWNT-COOH/chitosan BP. This value is very near those of MWNT/chitosan and MWNT-

NH_2/chitosan (82 ± 2% and 85 ± 2% respectively). Consequently, the intrabundle pore volume of the MWNT-chitosan (18 ± 2%) was higher than the values obtained for the MWNT-COOH/chitosan (10 ± 1%) and MWNT-NH_2/chitosan (15 ± 1%) BP membranes. The results (surface area, pore diameter, nanotube-bundle diameters and pore-size distribution volume) indicate that functionalisation of the CNT surface has a significant effect on the pore-size distribution of BP membranes.

7. 6 Water permeability

The water permeability of the three BP membranes prepared from the different types of MWNTs was determined using the crossflow NF/RO method outlined in the experimental section; results are presented in Table 18 and Figure 7.7.

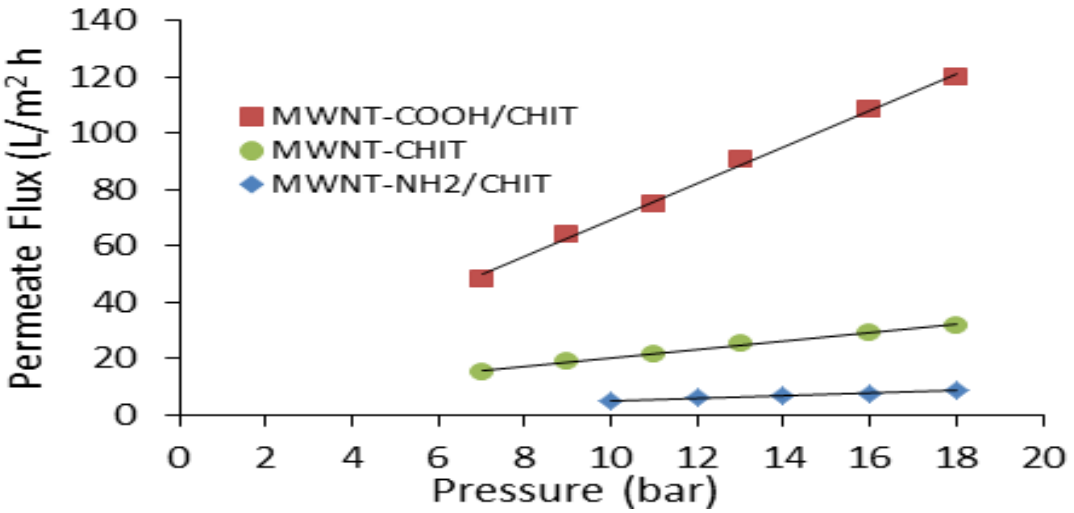

Figure 7.7. Effects of different applied pressures on permeation flux of the three BP membranes.

Water permeability through the MWNT-COOH/chitosan BP membrane was 6.6 ± 0.2 L/m^2 h bar, which is greater than that of MWNT-NH_2/chitosan (0.5 ± 0.1 L/m^2 h bar) and MWNT/chitosan (1.6 ± 0.1 L/m^2 h bar). This indicates that the addition of polar groups, particularly the –COOH group, to MWNTs enhances the water flux rate through the BP membrane, thereby showing that the higher flux of MWNT-COOH/chitosan has improved surface hydrophilicity, and the surface area introduces a more water-permeable structure into the membranes. As a result, the order of the water permeability according to the BP membranes was MWNT-COOH/chitosan > MWNT/chitosan > MWNT-NH_2/chitosan (Table 18). The results obtained for water permeability were consistent with the surface areas of the

BP membranes (Table 17), which increased significantly with attachment of the carboxyl groups (–COOH) on the surfaces of the MWNTs. This suggests that a BP membrane comprised of chitosan and MWNT-carboxylate forms a hydrophilic membrane (contact angle 36° ± 3°, Table 17) with suitable surface area (112 ± 4 m^2/g). In contrast, the MWNT-NH_2/chitosan exhibited lower water permeability than the other two BP membranes (MWNT-COOH/chitosan and MWNT/chitosan) because the MWNT-NH_2/chitosan had less surface area (12 ± 2 m^2/g) with low hydrophilicity (contact angle 92° ± 4°, Table 17), leading to a reduction in the permeate flux in this case. Therefore, the presence of the –COOH groups significantly increases internal pores in the MWNT-COOH/chitosan BP membranes and should facilitate faster transport of water molecules through the membrane of MWNT-COOH. It also indicates that the permeating water molecules need more energy to transfer through the MWNT/chitosan and MWNNH_2/chitosan BP membranes due to their crystalline nature; whereas, with MWNT-COOH/chitosan BP membranes, water molecules require less energy. This may due to the molecular sieving action, which was attributed to the greater number of pores between CNTs in the surfaces of the BP membranes (Fig. 7.4). Therefore, the water permeation values were greater for MWNT-COOH/chitosan membranes, signifying that water transport is minimal due to the membranes' greater selective nature. The values of water permeability for the three BP membranes were also considerably lower than those reported for the MWNT BP membranes prepared using Trix in Chapter 3 and a previous study [256]. This is because all BP membranes have lower surface areas (Table 18) and smaller pore sizes (see SEM images in Figure 7.7) than BP membranes prepared using Trix (Chapter 3).

7. 7 Salt-rejection capability

To investigate the effects of unfunctionalised and functionalised MWNTs on rejection of a single salt ($MgSO_4$ and NaCl), the same methodology used in the experimental study section was employed; that is, MWNT-unfunctionalised and MWNT-functionalised with carboxyl (COOH) and amine (-NH_2) groups mixed with 0.2 % w/v chitosan (CHIT) aqueous solution. Thus, we prepared complex BP membranes consisting of series of MWNT-unfunctionalised and MWNT-functionalised in combination with chitosan. These membranes were code named MWNT/chitosan, MWNT-COOH/chitosan and MWNT-NH_2/chitosan.

A free solution comprising a single salt ($MgSO_4$ and NaCl at 200 mg/l) at varying initial permeate fluxes ranging 3–38 μm/s was used for the conduction of the three MWNT/chitosan, MWNT-COOH/chitosan and MWNT-NH_2/chitosan BPs. The required

chemical and physical operating conditions, including pH, crossflow velocity and temperature (at 20°C), were constant during the experiment. Figures 7.8A–D illustrate the salt-rejection patterns and permeate flux behaviours of the three BP membranes. In the absence of a colloidal foulant, increases in permeate flux resulted in greater salt rejection. The results also seem to suggest that salt rejection in an RO/NF system is not affected by increases in permeate flux along the member module of a pressure vessel. Figures 7.8A–D also reveal that gradually increasing the initial permeate (3–38 μm/s) progressively increases salt-rejection levels due to the 'dilution effect' [313-315].

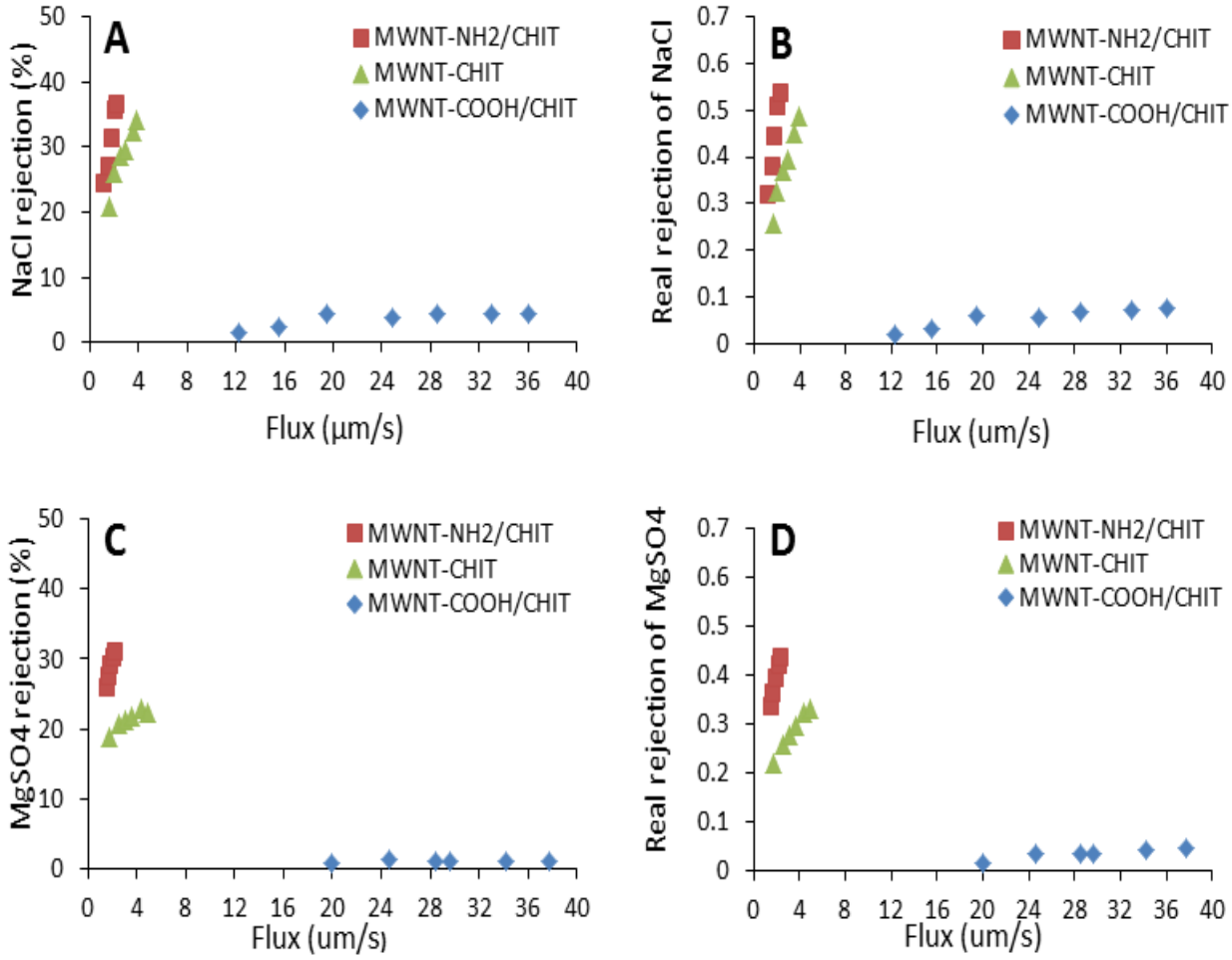

Figure 7.8. Comparison of the BP membranes' salt-rejection performances: A) observed rejection (%) of NaCl; B) real rejection of NaCl; C) observed rejection (%) of $MgSO_4$; and D) real rejection of $MgSO_4$ using three different BP membranes of MWNT/chitosan, MWNT-COOH/chitosan and MWNT-NH_2/chitosan; all BP membranes were fabricated using a filtration method.

Figures 7.8A–D show that the MWNT-COOH/chitosan BP can be compared to a UF membrane, as it has lower rejection levels for both of the single salts, exhibiting greater pure-water flux than the other two BP membranes. It appears that the base composite BP membrane (MWNT-COOH/chitosan) situ amine crosslinked with MWNT-COOH affects the characteristics of the top layer. This behaviour can be attributed to the varied surface charge densities of the membrane.

We also used various BP membranes of MWNT/chitosan and MWNT-NH_2/chitosan material of similar thicknesses as the top layers of the composite BP membranes to amine crosslink with the same medium. When MWNT/chitosan and MWNT-NH_2/chitosan were mixed with 0.2 wt% chitosan for use as a top layer (the denseness is controlled by the solution and the filtration method), there was a great decrease in pure-water flux (Fig. 7.7) and an increase in rejection levels for both single salts, as shown in Figures 7.8A–D. The composite BP membranes (MWNT/chitosan and MWNT-NH_2/chitosan BP membranes) were also able to reject NaCl and $MgSO_4$ electrolytes. However, the principle of charge influence alone does not explain the greater rejection of NaCl than $MgSO_4$.

Some studies [298, 316-318] have presented the effective charge density of the membrane as dependent on the concentration of the feed, with this density lower than the fixed membrane charge for low electrolytic concentrations. This has been explained in these studies by the adsorption of counter-ions on the membrane surface and partial electrolytic dissociation of the functional groups of the membrane. Decreasing electrolytic concentrations also resulted in decreases in the charge densities on the RO membranes [319]. Variation of the effective charge density based on electrolytic concentration was also observed with NF membranes [320].

Furthermore, when ion groups are attached to the membrane by either physical adsorption or chemical bonding, there is a profound influence on the transportation of ions of different valencies. This phenomenon can be quantified using the fixed-charge theory, which combines two popular physiochemical principles: the Nernst-Planck Flux equation and the Donnan ion-distribution principle. The Nernst-Planck equation is a linear superposition of Faraday's ion-conduction flux and Fickian diffusion flux, and is often used to describe the transportation of ions in charged membranes. Because of the Donnan exclusion effect, if the matrix of the charged membrane has more counter-ions, there should be fewer co-ions in the polymer than in the solution concentration to balance the charges in the solution. A term for

bulk flow can be included in the Nernst-Planck equation to represent the effect of friction due to the flux of the water driven by pressure on the flux of the counter-ions and co-ions [304, 321].

The observed single salt-rejection order (equation 7, experimental section), as seen in Figures 7.8A and C, is $R(MgSO_4) < R(NaCl)$, illustrating that the salt-rejection pattern of MWNT/chitosan BP membranes is positively charged in accordance with the Donnan principle. However, these results contradict some previous research indicating that $R(NaCl) < R(MgSO_4)$ [70, 275], which can be attributed to the Donnan feature of salt rejection on negatively charged NF membranes. The rejection level also depends on the valency of the electrolytes, and several studies have found that the rejection rate of salts with the same cation (Na^+) is greater for divalent anions SO_4^{-2} than monovalent ions (Cl^-), and that electrolytes with monovalent counter-ions (Na^+) have a greater rejection rate than electrolytes with divalent counter-ions (Mg^{2+}) [271]. Sun et al. [275] showed that an increase in the concentration of the feed increased the Na^+ concentration, thereby increasing the permeation rate of Na^+, such that electro neutrality on either side of the membrane was broken. To return the membrane to electro neutrality, more Cl^- and SO_4^{-2} ions must undergo permeation from up-stream to down-stream, thus decreasing rejections. Since the permeate velocity of Cl^- is faster than that of SO_4^{2-} ions, the rejection of sodium chloride solution decreases. Our research shows that the rejection level of NaCl is much greater than $MgSO_4$ in both BP membranes (MWNT-NH_2/chitosan and MWNT/chitosan), as illustrated in Figures 7.8A–D. This could be because the permeate velocity of Cl^- ions is lesser than that of the SO_4^{2-} ions, thereby increasing the rejection level of NaCl solution, while the rejection level of the $MgSO_4^{2-}$ solution decreases. Moreover, the order of separation of $MgSO_4 <$ NaCl, as illustrated in Figures 7.8A–D, was dependent on the electrolytes with monovalent counter-ions (Na^+) exhibiting greater rejection than the divalent counter-ions and monovalent anions (Cl^-), as we used positively charged BP membranes. Subsequently, salt-rejection dependency can be estimated if the BP-membrane charge is known, due to interactions between the BP membrane and ions on the surface. Additionally, the lower rejection level of $MgSO_4$ can be explained by the decrease in the effective surface charge of the membrane, due to the combining of anions of SO_4^{2-} and Mg^{2+}, which leads to decreased rejection performance [273].

Additionally, salt retention is strongly influenced by the adsorption property of the polymeric membrane. The adsorption process is recognised as the primary step in the water transportation process, and in some cases, the transportation of solutes through the membrane in the well-recognised model of sorption-diffusion [83, 322]. Surface diffusion is considerably quicker than diffusion by sorption; therefore, the process of salt transportation through the membrane can be improved if the membrane pores are larger than the salt, as shown in the MWNT-COOH/chitosan BP membrane. The significance of the effect on solute retention depends on the pore distribution and size of the membrane. Adsorption and exclusion by size contribute to the retention of the solute according to the pore size [323].

We also researched some models based on the orthodox irreversible thermodynamics (IT) theory to explain the transportation of single salts ($MgSO_4$ and NaCl) across the membrane. IT models have been successfully applied in the prediction of transportation patterns across NF membranes for single and binary solute systems [324, 325]— quite lately for studying multiple systems [326, 327] and industrial feed [328-330]. Due to the phenomenon of concentration polarisation, accumulation of the solute occurs on the surface of the membrane, with the concentration stronger on the surface than in the feed solution. Therefore, real rejection (R_{real}) can be estimated from the rejection observed (equation 7, experimental section), consideration of the effect of concentration polarisation (equation 8) and the coefficient of mass transfer (equation 9). The R_{real} values of the three BP membranes are much greater than the experimental rejection of the two single salts ($MgSO_4$ and NaCl), as illustrated in Figures 7.8B and D. Unexpectedly, the rejection levels for all BP membranes are much higher for NaCl than $MgSO_4$. The assumption of electro neutrality of the membrane and feed permeate solutions is supported by the presence of a low-density charge on the surface membrane, which allows application of the Donnan equilibrium at either solution-membrane interface.

Considering that the hydration of the membrane's ions is similar to the hydration in an aqueous solution, the cations of smaller radii have a strong influence on the ionic mobility ratio in the membrane. It is noteworthy that ion hydration reduces the interactions between the fixed anionic charges and cations. Studying the results, we can conclude that the level of monovalent cation uptake, combined with the requirement to sustain electro neutrality in the bulk polymer network of the membrane, controls the mobile divalent cation adsorption. These results are surprising, as the monovalent cations with low surface charge density are

influenced by the repulsive forces of hydration. In addition, the Donnan exclusion theory is not useful for quantitative predictions of ion rejection. Therefore, this could require a more complex theoretical description. Mindful of the results of the BP-membrane experiments, which definitely indicated the presence of a positive charge distribution on the membrane surface, the following points were considered in building the mass transfer model.

- Concentration polarisation of the feed solution is adjacent to the membrane.
- ENP equations are used to describe the convection, diffusion and electro-migration across the active layer of the membrane.
- The membrane-solution active layer interface is described using Donnan equilibrium.
- Sorption-diffusion is used to describe the transportation of solutes through the membrane.

Many polymeric membranes consist of ionisable surface functions, such as the amine ($R\text{-}NH_3^+$), carboxylic ($R\text{-}COO^-$) and sulfonic ($R\text{-}SO_3^-$) surface groups. If protolysis of these functional groups results in surface charges [280, 331], the following reactions of dissociation could occur.

$$R - NH_3^+ \rightarrow R - NH_2 + H^+ \quad (1)$$

$$R - COOH \rightarrow R - COO^- + H^+ \quad (2)$$

$$R - SO_3H \rightarrow R - SO_3^- + H^+ \quad (3)$$

The surface charge depends on the ionisation level and, thus, the pH of the aqueous solution. From the equations above, we can infer that the surface of the membrane with amine functional groups could have a positive charge when pH is low, and the surface of the membrane with carboxyl functional groups could have a negative charge when pH ranges from moderate to high.

We examined three BP membranes (MWNT/chitosan, MWNT-COOH/chitosan and MWNT-NH_2/chitosan) for the rejection levels of NaCl (concentration 2,000 mg/l) at various pH values (ranging 10–3), at a constant temperature of 20°C; the results are illustrated in Figure 7.9. When the solution pH indicated acidity (i.e. low pH), two membranes (MWNT/chitosan and MWNT-NH_2/chitosan) exhibited increased NaCl rejection, with MWNT-NH_2/chitosan exhibiting the maximum increase greater than MWNT/chitosan. This could be explained by the protonation of the free amino functional groups in chitosan, with the chitosan molecules becoming uncoiled and elongated and assuming rodlike shapes.

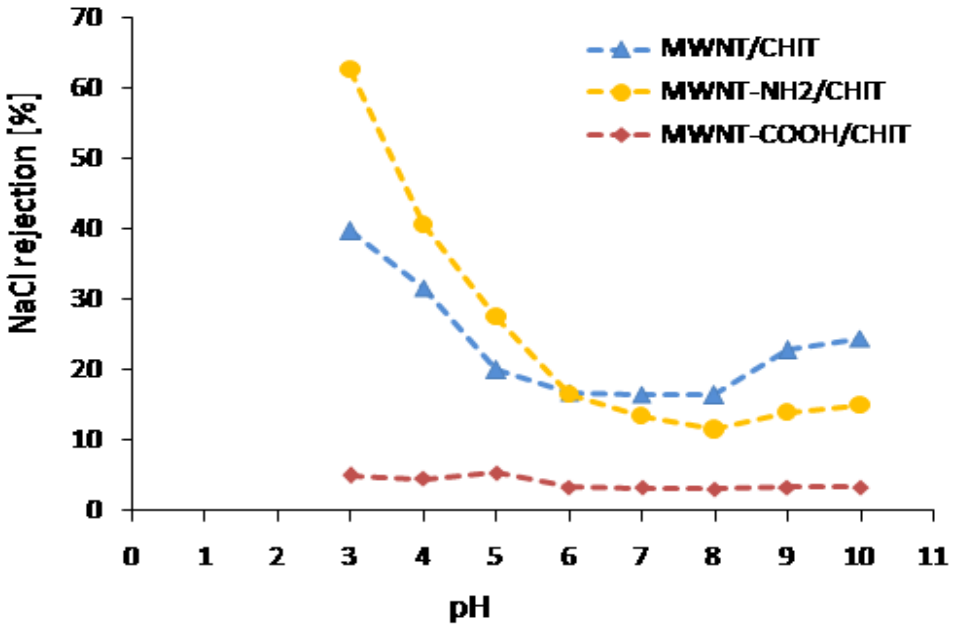

Figure 7.9. Comparison of rejection of NaCl through three BP membranes as a function of pH values of the feed solution: RO experimental conditions were initial concentration of NaCl in the feed = 2 g/L; crossflow rate = 100 L/min; and crossflow velocity = 34.6 cm/s; temperature = 20 ± 2°C.

This drives the equilibrium ($-NH_2 + H^+ \leftrightarrow NH_3^+$) to the right, increasing the mutual repulsiveness of the charged groups and the internal osmotic pressure, which supplies the force for uncoiling [332, 333]. The salt absorption capability of the membrane then increases, resulting in greater NaCl rejection. On the contrary, compared to the MWNT/chitosan and MWNT-NH_2/chitosan BP membranes, the MWNT-COOH/chitosan membrane's NaCl rejection is least affected by the pH, resulting in blockage of the free amino functional groups of chitosan during the crosslinking process [333].

7. 8 Zeta potential (ZP)

The ZPs of the three BP membranes' surfaces were determined and plotted as a function of the feed solution pH (Fig, 7.10). The ZP values do not seem to be sensitive to pH, but a previous study [283] showed that increases in pH and decreases in ZP, as well as the values of CNT/chitosan, are more negative than are those of the present BP membranes. This may be attributed to differences in the concentrations of dispersant (chitosan) used.

The active layers of the MWNT/chitosan and MWNT-NH_2/chitosan membranes exhibited similar ZP data as a function of pH, and there was a notable difference in the ZP data of the active layers of the MWNT-COOH/chitosan membrane. These results are

consistent with the structural differences of the BP membranes described previously. Both the MWNT/chitosan and MWNT-NH_2/chitosan membranes were more positively charged than the MWNT-COOH/chitosan membrane, particularly at low pH. Results reported here indicate that the active layers of the MWNT/chitosan and MWNT-NH_2/chitosan membranes contain significantly more ionisable functional groups than the active layers of the MWNT-COOH-chitosan membrane.

Previous studies [281, 282] reported that a more negative membrane exhibits a greater salt rejection due to an increasing electrostatic interaction between the negatively charged membrane surface and charged solutes. However, a positive surface charge below the isoelectric point emerges as a result of protonation of the amine functional groups (–NH_2 to –NH_3^+), and a negative charge above the isoelectric point forms as a result of protonation of the hydroxyl groups (–OH to –O^-) [284, 285]. Figure 7.10 reveals that the MWNT/chitosan and MWNT-NH_2-chitosan BP membranes were positive at pH 4–8. This can be attributed to protonation of the amine functional groups on the MWNT surface and on the backbone of chitosan, suggesting that the adsorption of NaCl can be increased by decreasing the pH.

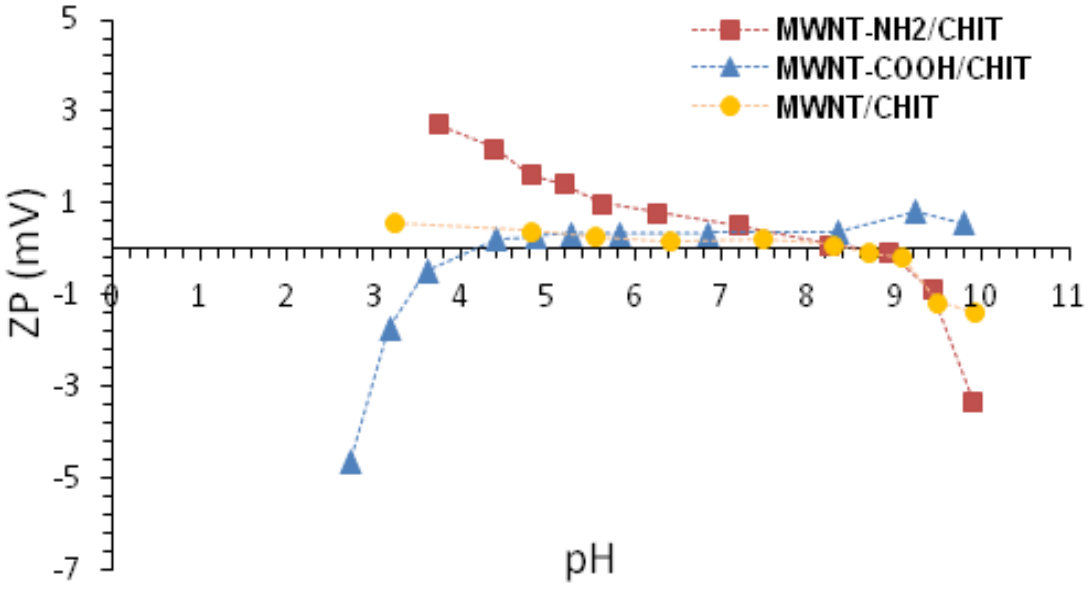

Figure 7.10. ZPs of the membranes as a function of pH.

7. 9 Conclusions

Three types of BP membranes (MWNT-chitosan, MWNT-COOH/chitosan and MWNT-NH_2/chitosan) were prepared using a filtration method. The MWNT/chitosan BP membranes had the highest electrical conductivity, whereas the BP membranes modified by

functional groups (MWNT-COOH/chitosan and MWNT-NH_2/chitosan) had significantly lower electrical conductivity values. In contrast, the combination of MWNT-COOH and chitosan dispersant slightly enhanced the mechanical properties of the BP membranes through the interaction of MWNT-COOH and chitosan at low pH.

The water permeability increased significantly with the use of the MWNT-COOH/chitosan BP membrane (6.6 ± 0.2 L/m^2 h bar), whose permeability is 4.1 times higher than that of MWNT/chitosan (1.6 ± 0.1 L/m^2 h bar) and 13.2 times higher than that of MWNT-NH_2/chitosan (0.5 L/m^2 h bar). This is because the oxidized MWNT can be enhanced for water adsorption due the superior wettability and larger internal pores in the MWNT-COOH/chitosan BP, which plays a significant role in speeding the transportation of water molecules. On the other hand, the results show that the single salt-rejection capacities (NaCl and $MgSO_4$) improved significantly when both MWNT/chitosan and MWNT-NH_2/chitosan BP membranes were used. This may due to presence of –NH_2 groups in the chitosan structure and the attachment to MWNT, which can be an effective adsorbent for salts from solution due to its positive charge. However, the rejection capacity of single salts by MWNT-COOH/ chitosan BP was significantly decreased. This may be due to the formation of amide linkages by the reactive primary amine groups of chitosan and because the attachment of the -COOH groups to MWNT resulted in low surface charge density and larger internal pores. In addition, we found that the interaction between anionic and cation charges is decreased via ion hydration. This result is unexpected, since the rejection of NaCl with low molecular weight and small surface charge density is affected by repulsive hydration forces.

Chapter 8: Conclusions and Future Work

8. 1 Conclusions

Various BP membranes were developed with MWNT-Trix, MWNT-coated commercial nylon, MWNT/chitosan, MWNT/chitosan-glycerin, MWNT/chitosan-PEDGE, MWNT-COOH/chitosan and MWNT-NH_2/chitosan in the presence of aqueous surfactant solutions (specific objective 1). The solutions were dispersed by sonication for 20–30 min and then filtered by vacuum-filtration. The membranes were then characterised and analysed in detail to evaluate different physical-mechanical properties, such as electrical resistance, conductivity, tensile strength, elongation, Young's modulus, toughness, morphology by SEM, pore size, pore structure by nitrogen adsorption/desorption, average CNT-bundle diameter, CNT interbundle volume, CNT intrabundle volume, water permeability, swelling ratio and ZP, to ascertain the suitability of the membranes for effective salt-rejection applications/processes for seawater desalination (specific objectives 2-4). This work generated the following conclusions.

MWNT-Trix

Four different porous BP membranes were produced with MWNT-Trix by annealing at 500°C and then soaking in biopolymer chitosan. Annealing and soaking resulted in significant changes in the BP membranes. Conductivity increased from 19 ± 2 S/cm to 42 ± 2 S/cm after annealing, meaning that annealing removed the dispersant Trix from the BP membrane and thereby reduced the resistance of the CNT junctions in the CNTs network. In contrast, soaking the membrane in chitosan 0.1% (w/v) decreased electrical conductivity but increased Young's modulus and tensile strength.

SEM images revealed that the intercalated chitosan coated the entire external surface of the BP (MWNT), though pores were still clearly visible and not completely filled.

The BET experiment showed that water permeability decreased with soaking and increased with annealing. The results obtained by the BET, BJH and HK methods showed that soaking in chitosan 0.1% (w/v) produced smaller surface areas and pore sizes in the MWNT membrane than in the MWNT-Trix and annealed MWNT BPs. These results are consistent with the observation that the water permeability of MWNT BP soaked in chitosan was less than that of membranes prepared from MWNT-Trix and annealed MWNT BPs.

MWNT-coated commercial nylon membranes

The surfaces of hydrophilic commercial membranes (nylon) were successfully coated with MWNT in homogenous solutions containing MWNTs and Trix (as surfactants).

Electrical conductivity and Young's modulus intensified with increased MWNT mass; but tensile strength, elongation, hydrophilicity and water permeability of the coated membranes decreased with increased MWNT mass. The permeability was several orders of magnitude lower than that of non-coated membranes (i.e. commercial nylon).

The single salts (NaCl and $MgSO_4$) were rejected by MWNT-coated nylon membranes containing 60 mg of MWNT, indicating that MWNT-coated membranes had limited salt-rejection abilities at high pressures. Further evaluation is needed with aqueous solutions containing large-sized BP membranes of MWNTs and chitosan. This could improve the ability of the BP membranes to reject salts from aqueous solutions.

MWNT/chitosan

MWNT/chitosan BP membranes were successfully fabricated from MWNT/chitosan dispersions. The selective uptake of inorganic salts indicated that these BP-membrane systems are an intriguing subject for selective membrane research.

Electrical conductivity and water permeability were reduced, but the surface hydrophobicity, mechanical properties and salt-rejection abilities of the BP membranes were enhanced, by increasing the amount of chitosan. The enhancement of these properties may improve the usefulness of MWNT/chitosan BP membranes in RO applications.

In the experiment using a crossflow RO/NF mode, the MWNT/chitosan-1 (BP-1) membrane containing the least amount chitosan (i.e. 0.1% w/v) performed better in terms of water flux than the MWNT/chitosan-1 (BP-4) membrane, which contained the greatest amount of chitosan (i.e. 0.4% w/v); however, the salt-rejection ability of MWNT/chitosan-4 (BP-4) was largely improved. The salt rejection was also affected by pore size, solution pH changes and membrane-surface charges. The rejection of low-molecular-weight salt (NaCl) was higher than that of high-molecular-weight salt ($MgSO_4$). More research is required to discover the reasons for this unexpected behaviour. In addition, due to positive charge on the top layer of buckypaper membranes, the membrane behaves much higher rejection for mono-valent cations (e.g. Na^+) than for multi-valent cations (e.g. Mg^{2+}) if the electrolytes have the same monovalent counterion (e.g. Cl^-). Therefore, by properly balancing MWNT and

chitosan amine conditions, a desired positively charged membrane can be used for removal of salt (NaCl) from water or for separation of monovalent ions and monovalent cations.

MWNT/chitosan, MWNT/chitosan-glycerin and MWNT/chitosan-PEDGE

Three BP membranes were developed based on a crosslinked chitosan (i.e. chitosan-glycerin and chitosan-PEDGE combined with MWNT) for water filtration. The chitosan, chitosan-glycerin and chitosan-PEDGE offered a pathway for enhancing the dispersal of MWNTs in water, presenting a promising system for selective membrane research.

These three BP membranes produced an excellent conductivity range (60–70 S/cm) and an extremely high tensile strength compared to BP membranes prepared with MWNTs and various dispersants, such as Trix, cipro and τ-carrageenan [182, 257].

The interconnected porous structure with a small specific surface area suggests that the incorporation of MWNT could be achieved by packing hydrophilic chains (chitosan and crosslinked chitosan) in the interface, thereby creating a suitable surface for water permeation and salt rejection. The rejection sequence of BP membranes is MWNT/chitosan-PEDGE > MWNT/chitosan-glycerin > MWNT /chitosan, and the permeate flux sequence of BP membrane is MWNT/chitosan > MWNT/chitosan-glycerin > MWNT/chitosan-PEDGE.

The BP membranes' water permeability decreased, and filtration-rejection efficiency for salts increased, with MWNT/chitosan-PEDGE and MWNT/chitosan-glycerin. MWNT/chitosan BP membranes produce more accessible free volume for water transport than MWNT-chitosan-PEDGE and MWNT-CHIT-glycerin.

The BP membranes' rejection of Na_2SO_4 and $MgSO_4$ was significantly lower than the rejection of $MgCl_2$ and NaCl. This may due to low charge density at the membrane surface and because the active layers of three BP membranes did not contain sulphate groups. This can increase the rejection of Na_2SO_4 and $MgSO_4$ through repulsion between the active layer and anion SO_4^{2-}.

MWNT/chitosan, MWNT-COOH/chitosan and MWNT-NH_2/chitosan

Three different BP membranes (MWNT/chitosan, MWNT-COOH/ chitosan and MWNT-NH_2/chitosan) were prepared using a filtration method. The MWNT/chitosan BP membrane had the highest electrical conductivity and the MWNT-COOH/chitosan and MWNT-NH_2/chitosan membranes had the lowest.

In contrast, MWNT-COOH/chitosan slightly enhanced the mechanical properties of the BP membranes through the interaction of MWNT-COOH and chitosan at low pH. The

water permeability of the MWNT-COOH/chitosan BP membranes was 6.6 ± 0.2 L/m^2 h bar, which is 4.1 times higher than that of the MWNT-chitosan (1.6 ± 0.1 L/m^2 h bar) and 13.2 times higher than that of the MWNT-NH_2/chitosan (0.5 L/m^2 h bar). This indicates that MWNT-COOH is a good modifier for the preparation of functional nanoporous BP membranes because it increased the hydrophilicity of the BP-membrane surface, enhancing the water permeability through pore size and porosity adjustments.

Salt rejection of NaCl and $MgSO_4$ presented the order of rejection as MWNT-NH_2/ chitosan > MWNT/chitosan > MWNT-COOH/chitosan. These results suggest that the salt can be adsorbed to the BP-membrane surface, primarily due to interactions between -NH_2 groups and salts. The presence of the –NH_2 groups can have dramatic effects on rejection and surface charge density. In addition, the rejection of NaCl can be increased by decreasing the pH of the feed solution.

In conclusion, we developed improved BP membranes with nano-material CNT using MWNT, modified MWNT, chitosan, chitosan-glycerin and chitosan-PEDGE and Trix as surfactants and dispersing agents in aqueous solutions with vacuum-filtration. These BP membranes produced an extremely high mechanical properties and salt rejection compared to membranes prepared in previous studies [242, 256, 257, 270] . Some of these membranes (i.e. MWNT/chitosan, MWNT/chitosan-glycerin, MWNT/chitosan-PEDGE and MWNT-NH_2/chitosan) have excellent mechanical properties and salt rejection to be suitable for future desalination-process applications, which may ultimately solve the worldwide water shortage problem.

8. 2 Future Research

The results of this thesis are critical and provide a new scope for further fundamental and applied research. BP membranes possess the ability to reject salts from aqueous solutions; however, the potential use of these membranes for seawater desalination may require for the practical preparation, a balance choice between the preparation conditions in MWNT and chitosan cross-linked processes can be produced and a series of positively charged nanofiltration membranes be made to meet different industrial demands. Moreover, investigations of the BP membrane's rejection of a range of trace organic molecules should be done. Future work should also explore the effects of biological/protein fouling and chlorine on the removal efficiency of BP membranes.

THESIS-RELATED POSTER PRESENTATIONS

1. Alshahrani, Ahmed, Long Nghiem, and Marc in het Panhuis, Characteristics of SWNT-chitosan-glycerin membranes formed by evaporative casting method. Poster presentation at the Twelfth International Conference on the Science and Application of Nanotubes, Brisbane Convention and Exhibition Centre, Australia, 24–29 June 2012.

2. Alshahrani, Ahmed, Long Nghiem, and Marc in het Panhuis, Characteristics of MWNT/chitosan and MWNT/chitosan-polyethylene glycol-diglycidyl ether membranes formed by filtration method. Poster presentation at the 2nd Saudi International Nanotechnology Conference (2SINC) in King Abdulaziz City for Science and Technology (KACST), Saudi Arabia, 11–13 November 2012.

APPENDIX A

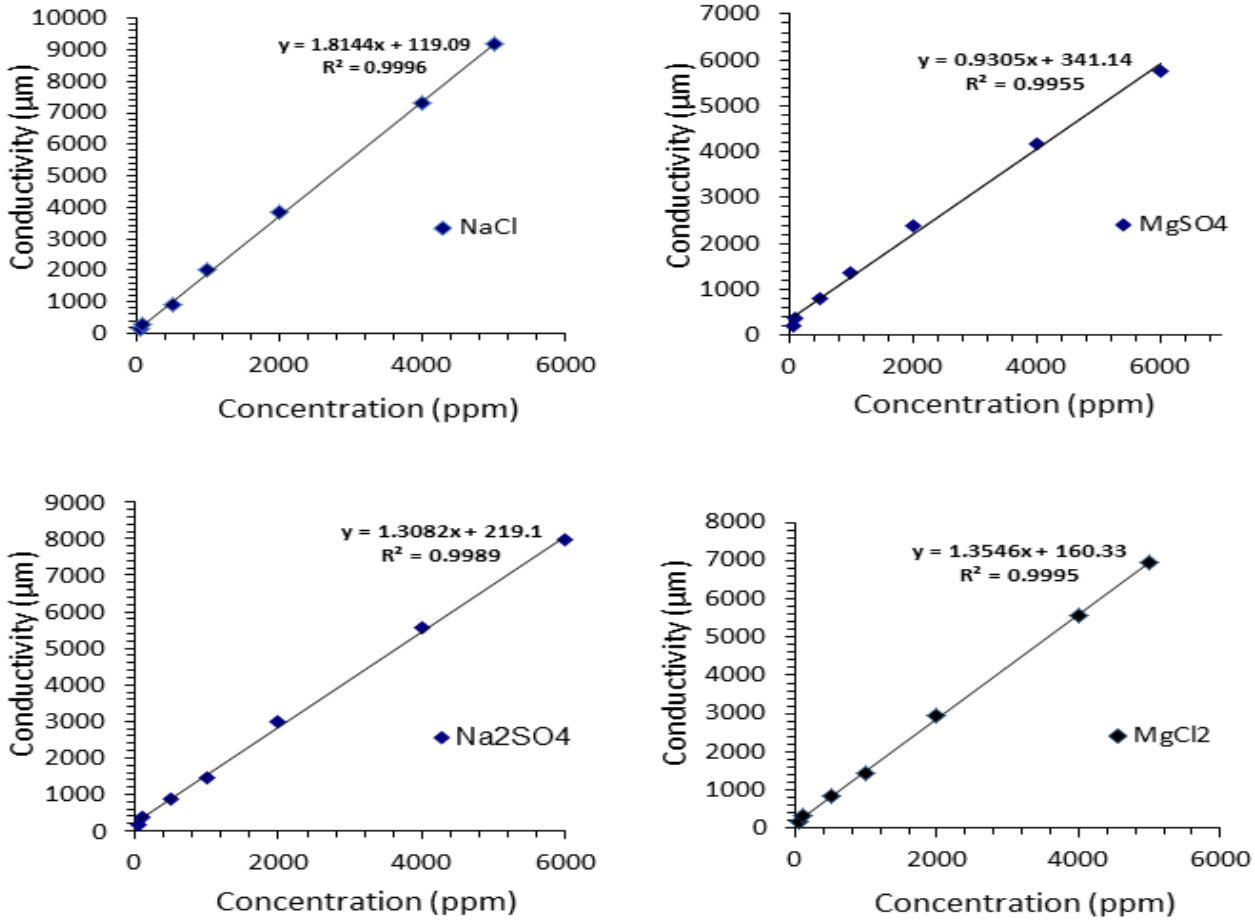

Appendix Figure 1. The standard calibrations of different salts using Orion 4 Star™ conductivity meter (Thermo Scientific, Singapore).

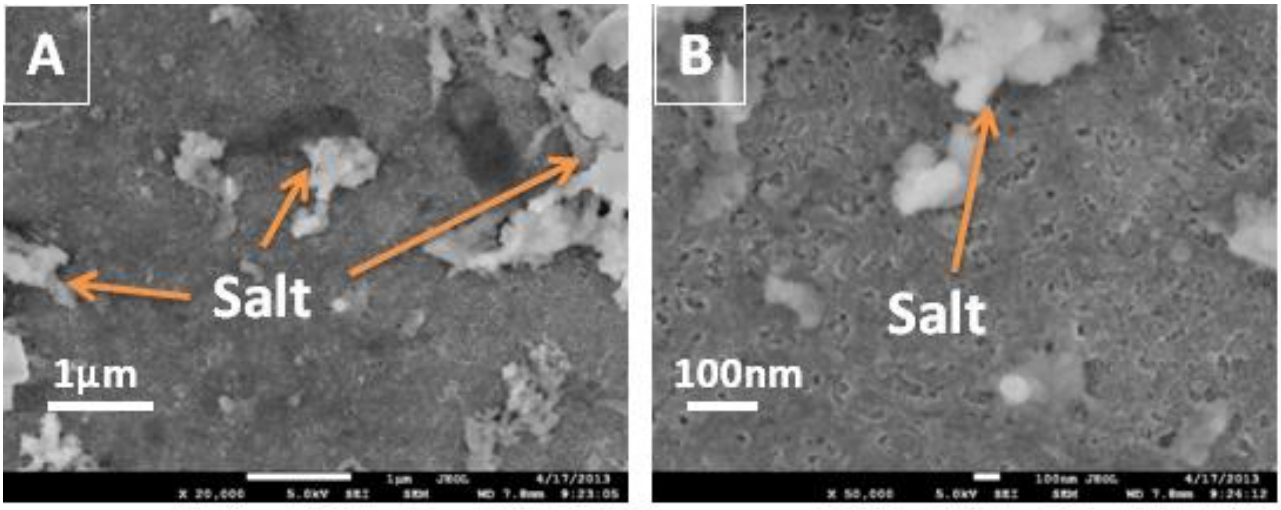

Appendix Figure 2. A and B SEM images show the mass of salt (NaCl) removed from solution by MWNT/chitosan 0.2% (w/v) buckypaper membranes.

REFERENCES

1. Jury, W.A. and J.H. Vaux, *The role of science in solving the world's emerging water problems.* Proceedings of the National Academy of Sciences of the United States of America, 2005. **102**(44): p. 15715-15720.
2. Service, R.F., *Desalination Freshens Up,* in *Science*. 2006: United States. p. 1088-1090.
3. Shatat, M. and S.B. Riffat, *Water desalination technologies utilizing conventional and renewable energy sources.* International Journal of Low-Carbon Technologies, 2012(Journal Article).
4. Khawaji, A.D., I.K. Kutubkhanah, and J.-M. Wie, *Advances in seawater desalination technologies.* Desalination, 2008. **221**(1): p. 47-69.
5. Postel, S.L., G.C. Daily, and P.R. Ehrlich, *Human Appropriation of Renewable Fresh Water*. Science, 1996. **271**(5250): p. 785-788.
6. Darrel Jenerette, G. and L. Larsen, *A global perspective on changing sustainable urban water supplies.* Global and Planetary Change, 2006. **50**(3): p. 202-211.
7. Kim, I.-C. and K.-H. Lee, *Dyeing process wastewater treatment using fouling resistant nanofiltration and reverse osmosis membranes.* Desalination, 2006. **192**(1): p. 246-251.
8. Ju, H., et al., *Crosslinked poly(ethylene oxide) fouling resistant coating materials for oil/water separation.* Journal of Membrane Science, 2008. **307**(2): p. 260-267.
9. Howe, E.D., *Fundamentals of water desalination*. 1974, New York: Marcel Dekker.
10. Porteous, A., *Desalination technology : developments and practice / edited by Andrew Porteous*, ed. A. Porteous. 1983, London: Applied Science.
11. Van der Bruggen, B., *Desalination by distillation and by reverse osmosis — trends towards the future.* Membrane Technology, 2003. **2003**(2): p. 6-9.
12. Rautenbach, R., *Progress in distillation.* Desalination, 1993. **93**(1-3): p. 1-13.
13. Inventory, I.D., *No. 15.* International Desalination Association, Topsfield, MA, USA.
14. Buros, O., *The Desalting ABCs*. 1990, International Desalination Association: International Desalination Association.
15. Jambi, F. and J. Wie. *The Royal Commission Gas Turbine/HRSG/Desalination Cogeneration Plant, 1989 ASME COGEN-TURBO*. in *3rd International Symposium on Turbomachinery, Combined-Cycle and Cogeneration, American Society of Mechanical Engineers, New York*. 1989.
16. Kamaluddin, B.A., S. Khan, and B.M. Ahmed, *Selection of optimally matched cogeneration plants.* Desalination, 1993. **93**(1): p. 311-321.
17. El-Nashar, A.M., *Cogeneration for power and desalination—state of the art review.* Desalination, 2001. **134**(1): p. 7-28.
18. Al Ghamdi, M., C. Hughes, and S. Kotake, *The Makkah-Taif MSF desalination plant.* Desalination, 1987. **66**: p. 3-10.
19. Sommariva, C., *The 72 MIGD multi-stage flash distillation plant at Al Taweelah, Abu Dhabi, UAE, Desal.* Water Reuse, 1996. **6**(1): p. 30-36.
20. Khawaji, A., J. Wie, and T. Khan. *Operating experience of the Royal Commission acid-dosed MSF seawater desalination plant*. in *Proceedings of IDA World Congress on Desalination and Water Reuse*. 1997.
21. Hasson, D. and R. Semiat, *Scale control in saline and wastewater desalination.* Israel journal of chemistry, 2006. **46**(1): p. 97-104.
22. SpA-Rome-Italy, N.I., *The application of a high temperature scale control additive in a Middle East MSF plant.* Desalination, 1983. **47**: p. 19-24.

23. Harris, A., *Sea water chemistry and scale control.* Desalination technology development and practice. London: Applied Science Publishers, 1983: p. 31-56.
24. Khawaji, A.D. and J.-M. Wie, *Potabilization of desalinated water at Madinat Yanbu Al-Sinaiyah.* Desalination, 1994. **98**(1): p. 135-146.
25. Gabbrielli, E., *A tailored process for remineralization and potabilization of desalinated water.* Desalination, 1981. **39**: p. 503-520.
26. Yamauchi, V., et al., *Remineralization of desalinated water by limestone dissolution filter.* Desalination, 1987. **66**: p. 365-383.
27. Nada, N., A. Zahrani, and B. Ericsson, *Experience on pre-and post-treatment from sea water desalination plants in Saudi Arabia.* Desalination, 1987. **66**: p. 303-318.
28. Al-Rqobah, H. and A.H. Al-Munayyis, *A recarbonation process for treatment of distilled water produced by MSF plants in Kuwait.* Desalination, 1989. **73**: p. 295-312.
29. Al-Radif, A., et al., *Review of design & specifications of the world largest MSF units 4×(10− 12.8 MIGD).* Desalination, 1991. **84**(1): p. 45-84.
30. Yearbook, I.D., *Yearbook 2006–2007.* Water Desalination Report, Global Water Intelligence and International Desalination Association, Topsfield, MA, USA, 2007.
31. Al-Shammiri, M. and M. Safar, *Multi-effect distillation plants: state of the art.* Desalination, 1999. **126**(1): p. 45-59.
32. Ophir, A. and F. Lokiec, *Advanced MED process for most economical sea water desalination.* Desalination, 2005. **182**(1): p. 187-198.
33. Michels, T., *Recent achievements of low temperature multiple effect desalination in the western areas of Abu Dhabi. UAE.* Desalination, 1993. **93**(1): p. 111-118.
34. Darwish, M. *Desalination Process: A technical comparison*. in *Proceedings of IDA World Congress on Desalination and Water Sciences, Abu Dhabi, United Arab Emirates*. 1995.
35. Awerbuch, L. *Vision for Desalination–Challenges and Opportunities*. in *Proceedings of the IDA World Congress and Water Reuse, Manama, Bahrain*. 2002.
36. Lee, K.P., T.C. Arnot, and D. Mattia, *A review of reverse osmosis membrane materials for desalination—development to date and future potential.* Journal of Membrane Science, 2011. **370**(1): p. 1-22.
37. Al-Badawi, A., et al. *Operation and analysis of Jeddah 1-Phase II plant*. in *Proceedings of the IDA and World Congress on Desalination and Water Sciences, Abu Dhabi, United Arab Emirates*. 1995.
38. Nada, N., et al. *Design features of the largest SWRO plant in the world—33.8 MGD in Madina and Yanbu*. in *Proceedings of the IDA and World Congress on Desalination and Water Sciences, Abu Dhabi, United Arab Emirates*. 1995.
39. Baig, M.B., A. Kutbi, and A. Aziz, *Design features of a 20 migd SWRO desalination plant, Al Jubail, Saudi Arabia.* Desalination, 1998. **118**(1): p. 5-12.
40. *Shaping the Future of New York*. 2014 [cited 2014 29-09]; Available from: http://macaulay.cuny.edu/eportfolios/tomkiewiczs10/?page_id=552.
41. Bou-Hamdashad, S., *Performdashance evaluation of three different pretreatmdashent systemdashs for seawater reverse osmdashosis technique.* Desalination, 1997. **110**(1): p. 85-91.
42. Al-Sheikh, A.H.H., *Seawater reverse osmosis pretreatment with an emphasis on the Jeddah Plant operation experience.* Desalination, 1997. **110**(1): p. 183-192.
43. Durham, B. and A. Walton, *Membrane pretreatment of reverse osmosis: long-term experience on difficult waters.* Desalination, 1999. **122**(2): p. 157-170.
44. Ebrahim, S.H., M.M. Abdel-Jawad, and M. Safar, *Conventional pretreatment system for the Doha Reverse Osmosis Plant: Technical and economic assessment.* Desalination, 1995. **102**(1): p. 179-187.

45. Rautenbach, R., T. Linn, and D. Al-Gobaisi, *Present and future pretreatment concepts—strategies for reliable and low-maintenance reverse osmosis seawater desalination.* Desalination, 1997. **110**(1): p. 97-106.
46. Amjad, Z., *RO systems: current fouling problems and solutions.* INTERNATIONAL DESALINATION AND WATER REUSE QUARTERLY, 1997. **6**: p. 55-59.
47. Moch Jr, I., *Hollow fiber permeators & reverse osmosis, Desal.* Water Reuse, 1993. **3**(2): p. 30-37.
48. Shaban, H., *Reverse osmosis membranes for seawater desalination state-of-the-art.* Separation and Purification Methods, 1990. **19**(2): p. 121-131.
49. Bou-Hamad, S., et al., *Comparative performance analysis of two seawater reverse osmosis plants: twin hollow fine fiber and spiral wound membranes.* Desalination, 1998. **120**(1): p. 95-106.
50. Johnson, W., *The story of freeze desalting, Desal.* Water Reuse, 1993. **3**(4): p. 20-27.
51. Greenlee, L.F., et al., *Reverse osmosis desalination: Water sources, technology, and today's challenges.* Water Research, 2009. **43**(9): p. 2317-2348.
52. Macedonio, F., et al., *Efficient technologies for worldwide clean water supply.* Chemical Engineering and Processing 2012. **51**: p. 2-17.
53. Reid, C.E. and E.J. Breton, *Water and ion flow across cellulosic membranes.* Journal of Applied Polymer Science, 1959. **1**(2): p. 133-143.
54. Singh, R., *Hybrid membrane systems for water purification: technology, systems design and operations*, ed. . 2006: Elsevier Science & Technology Books.
55. Loeb S and Sourirajan S, *High flow porous membrane for separation water from saline solutions*. 1960: US, Patent 3133132.
56. Loeb, S., *In synthetic membranes.* American Chemical Society: Washington, D. C, 1981: p. 1-9.
57. Cadotte, J.E., *Materials science of synthetic membranes, Edited by Lloyd, D. R.* . American Chemical Society: Washington D.C., 1985: p. 273-294.
58. Geise, G.M., et al., *Water purification by membranes: the role of polymer science.* Journal of Polymer Science Part B: Polymer Physics, 2010. **48**(15): p. 1685-1718.
59. Geise, G.M., et al., *Water permeability and water/salt selectivity tradeoff in polymers for desalination.* Journal of Membrane Science, 2011. **369**(1): p. 130-138.
60. Xie, W., et al., *Fundamental salt and water transport properties in directly copolymerized disulfonated poly (arylene ether sulfone) random copolymers.* Polymer, 2011. **52**(9): p. 2032-2043.
61. Jorgen Wagner, B., Sc, Chem. Eng, Membrane Filtration Handbook Practical Tips and Hint, Second Edition, Revision 2. November 2001, *Membrane Filtration Handbook Practical Tips and Hint, ,* ed. R.N. Second Edition. 2001: Osmonics, Inc.
62. van Reis, R. and A. Zydney, *Bioprocess membrane technology.* Journal of Membrane Science, 2007. **297**(1): p. 16-50.
63. Ho, W.S. and K.K. Sirkar, *Membrane Handbook;* . 1992, USA: Kluwer Academic.
64. Gutman, R.G., *Membrane filtration: the technology of pressure-driven crossflow processes*. 1987, Bristol, England: A. Hilger.
65. Rautenbach, R. and R. Albrecht, *Membrane processes*. 1989, Chichester: Wiley.
66. Cheryan, M., *Ultrafiltration and microfiltration handbook*. 1998, Boca Raton: CRC Press.
67. Lightfoot, E.N., *Membrane separations technology: Principles and applications.* Chemical Engineering Science, 1996. **51**(2): p. 325-326.
68. Lonsdale, H.K., U. Merten, and R.L. Riley, *Transport properties of cellulose acetate osmotic membranes.* Journal of Applied Polymer Science, 1965. **9**(4): p. 1341-1362.

69. Nilsson, J.L., *Protein fouling of uf membranes: Causes and consequences.* Journal of Membrane Science, 1990. **52**(2): p. 121-142.
70. Petersen, R.J., *Composite reverse osmosis and nanofiltration membranes.* Journal of Membrane Science, 1993. **83**(1): p. 81-150.
71. Yoon, Y. and R.M. Lueptow, *Removal of organic contaminants by RO and NF membranes.* Journal of Membrane Science, 2005. **261**(1): p. 76-86.
72. Van der Bruggen, B. and C. Vandecasteele, *Removal of pollutants from surface water and groundwater by nanofiltration: overview of possible applications in the drinking water industry.* Environmental Pollution, 2003. **122**(3): p. 435-445.
73. Mänttäri, M., J. Nuortila-Jokinen, and M. Nyström, *Evaluation of nanofiltration membranes for filtration of paper mill total effluent.* Filtration and Separation, 1997. **34**(3): p. 275-280.
74. Hassan, A., et al., *A demonstration plant based on the new NF-SWRO process1.* Desalination, 2000. **131**(1-3): p. 157-171.
75. Atra, R., et al., *Investigation of ultra- and nanofiltration for utilization of whey protein and lactose.* Journal of Food Engineering, 2005. **67**(3): p. 325-332.
76. Bowen, W.R. and J.S. Welfoot, *Modelling the performance of membrane nanofiltration-critical assessment and model development.* Chemical Engineering Science, 2002. **57**(7): p. 1121-1137.
77. Bowen, W.R. and J.S. Welfoot, *Modelling of membrane nanofiltration-pore size distribution effects.* Chemical Engineering Science, 2002. **57**(8): p. 1393-1407.
78. Bellona, C., et al., *Factors affecting the rejection of organic solutes during NF/RO treatment—a literature review.* Water research, 2004. **38**(12): p. 2795-2809.
79. Bolong, N., et al., *A review of the effects of emerging contaminants in wastewater and options for their removal.* Desalination, 2009. **239**(1): p. 229-246.
80. Van der Bruggen, B. and C. Vandecasteele, *Modelling of the retention of uncharged molecules with nanofiltration.* Water research, 2002. **36**(5): p. 1360-1368.
81. NAKAO, S.-I. and S. KIMURA, *Models of membrane transport phenomena and their applications for ultrafiltration data.* Journal of Chemical Engineering of Japan, 1982. **15**(3): p. 200-205.
82. Nghiem, L. and A. Schäfer, *Adsorption and transport of trace contaminant estrone in NF/RO membranes.* Environmental engineering science, 2002. **19**(6): p. 441-451.
83. Williams, M.E., et al., *Separation of organic pollutants by reverse osmosis and nanofiltration membranes: Mathematical models and experimental verification.* Industrial & Engineering Chemistry Research 1999. **38**(10): p. 3683-3695.
84. Nghiem, L.D., A.I. SchÃ¤fer, and M. Elimelech, *Removal of natural hormones by nanofiltration membranes: measurement, modeling, and mechanisms*, in *Environmental science & technology*. 2004: United States. p. 1888-1896.
85. Nghiem, L.D., A.I. Schäfer, and M. Elimelech, *Role of electrostatic interactions in the retention of pharmaceutically active contaminants by a loose nanofiltration membrane.* Journal of Membrane Science, 2006. **286**(1): p. 52-59.
86. Kimura, K., et al., *Rejection of organic micropollutants (disinfection by-products, endocrine disrupting compounds, and pharmaceutically active compounds) by NF/RO membranes.* Journal of Membrane Science, 2003. **227**(1): p. 113-121.
87. Mohan, D. and C.U. Pittman Jr, *Activated carbons and low cost adsorbents for remediation of tri-and hexavalent chromium from water.* Journal of hazardous materials, 2006. **137**(2): p. 762-811.
88. Pollard, S., et al., *Low-cost adsorbents for waste and wastewater treatment: a review.* Science of the Total Environment, 1992. **116**(1): p. 31-52.

89. Babel, S. and T.A. Kurniawan, *Low-cost adsorbents for heavy metals uptake from contaminated water: a review.* Journal of hazardous materials, 2003. **97**(1): p. 219-243.
90. Davis, M.E., *Ordered porous materials for emerging applications.* Nature, 2002. **417**(6891): p. 813-821.
91. Oki, T. and S. Kanae, *Global hydrological cycles and world water resources.* Science (New York, N.Y.), 2006. **313**(5790): p. 1068-1072.
92. Lonsdale, H.K., *The growth of membrane technology.* Journal of Membrane Science, 1982. **10**(2-3): p. 81-181.
93. Avlonitis S, Hanbury W, and Hodgkiess T, *Chlorine Degradation of Aromatic Polyamides.* Desalination, 1992. **85**: p. 321-334
94. Kang, G.-D., et al., *Study on hypochlorite degradation of aromatic polyamide reverse osmosis membrane.* Journal of Membrane Science, 2007. **300**(1-2): p. 165-171.
95. Baker, J.S. and L.Y. Dudley, *Biofouling in membrane systems A review.* Desalination, 1998. **118**(1-3): p. 81-89.
96. Al-Ahmad, M., et al., *Biofuoling in RO membrane systems Part 1: Fundamentals and control.* Desalination, 2000. **132**(1): p. 173-179.
97. Aimar, P., M. Meireles, and V. Sanchez, *A contribution to the translation of retention curves into pore-size distribution for sieving membranes* Journal of Membrane Science, 1990. **54**(3): p. 321-338.
98. Brady-Estvez, A.S., S. Kang, and M. Elimelech, *A single-walled-carbon-nanotube filter for removal of viral and bacterial pathogens.* Small 2008. **4**(4): p. 481.
99. Zydney, A.L., *Protein Separations Using Membrane Filtration: New Opportunities for Whey Fractionation.* International Dairy Journal, 1998. **8**(3): p. 243-250.
100. Chen, M.Y., D.J. Lee, and J. Tay, *Extracellular Polymeric Substances in Fouling Layer.* Separation Science and Technology, 2006. **41**(7): p. 1467-1474.
101. Sagle, A.C., et al., *PEG-coated reverse osmosis membranes: Desalination properties and fouling resistance.* Journal of Membrane Science, 2009. **340**(1): p. 92-108.
102. *Crystalline ropes of metallic carbon nanotubes.* Science, 1996. **273**(5274): p. 483-487.
103. Marshall, A.D., P.A. Munro, and G. Tragardh, *THE Effect of Protein Fouling in Micofiltration and Ul trafiltration on Permeate Flux, Protein Retention and Selectivity - A Literature-Review* Desalination, 1993. **91**(1): p. 65-108.
104. Chan, R. and V. Chen, *Characterization of protein fouling on membranes: opportunities and challenges.* Journal of Membrane Science, 2004. **242**(1): p. 169-188.
105. Latour, J.R.A. and C.J. Rini, *Theoretical analysis of adsorption thermodynamics for hydrophobic peptide residues on SAM surfaces of varying functionality.* Journal of biomedical materials research, 2002. **60**(4): p. 564-577.
106. Nabe, A., E. Staude, and G. Belfort, *Surface modification of polysulfone ultrafiltration membranes and fouling by BSA solutions.* Journal of Membrane Science, 1997. **133**(1): p. 57-72.
107. Zhao, Y.-H., et al., *Improving hydrophilicity and protein resistance of poly(vinylidene fluoride) membranes by blending with amphiphilic hyperbranched-star polymer.* Langmuir : the ACS journal of surfaces and colloids, 2007. **23**(10): p. 5779-5786.
108. Ostuni, E., et al., *A Survey of Structure−Property Relationships of Surfaces that Resist the Adsorption of Protein.* Langmuir, 2001. **17**(18): p. 5605-5620.
109. Razatos, A., et al., *Force Measurements between Bacteria and Poly(ethylene glycol)-Coated Surfaces.* Langmuir, 2000. **16**(24): p. 9155-9158.

110. Wan Ngah, W.S., C.S. Endud, and R. Mayanar, *Removal of copper(II) ions from aqueous solution onto chitosan and cross-linked chitosan beads.* Reactive and Functional Polymers, 2002. **50**(2): p. 181-190.
111. Kurbus, T., et al., *The use of experimental design for the evaluation of the influence of variables on the H< sub> 2</sub> O< sub> 2</sub>/UV treatment of model textile waste water.* Dyes and Pigments, 2003. **58**(2): p. 171-178.
112. Grgorio, C., *Recent developments in polysaccharide-based materials used as adsorbents in wastewater treatment.* Progress in Polymer Science, 2005. **30**(1): p. 38-70.
113. Chung, H.-J., K.-S. Woo, and S.-T. Lim, *Glass transition and enthalpy relaxation of cross-linked corn starches.* Carbohydrate Polymers, 2004. **55**(1): p. 9-15.
114. Fleischer, R.L., et al., *Particle Track Etching.* Science, 1972. **178**(4058): p. 255-263.
115. Lee, S.B. and C.R. Martin, *Controlling the Transport Properties of Gold Nanotubule Membranes Using Chemisorbed Thiols.* Chemistry of Materials, 2001. **13**(10): p. 3236-3244.
116. Shao P, Ji G, and Chen P, *Gold nanotube membranes: Preparation, characterization and application for enantioseparation.* Journal of Membrane Science, 2005. **255**(1): p. 1-11.
117. Martin, C.R., et al., *Investigations of the Transport Properties of Gold Nanotubule Membranes.* The Journal of Physical Chemistry B, 2001. **105**(10): p. 1925-1934.
118. Beginn, U., G. Zipp, and M. Mller, *Functional Membranes Containing Ion-Selective Matrix-Fixed Supramolecular Channels.* Advanced Materials, 2000. **12**(7): p. 510-513.
119. Kato, T., et al., *Self-assembly of functional columnar liquid crystals.* Chemical communications (Cambridge, England), 2009(7): p. 729.
120. Czaplewski, K.F., J.T. Hupp, and R.Q. Snurr, *Molecular Squares as Molecular Sieves: Size-Selective Transport Through Porous-Membrane-Supported Thin-Film Materials.* Advanced Materials, 2001. **13**(24): p. 1895.
121. Hillmyer, M.A., *Nanoporous materials from block copolymer precursors*. 2005, Springer-Verlag Berlin: Berlin p. 137-181.
122. Hamley, I.W., *Ordering in thin films of block copolymers: Fundamentals to potential applications.* Progress in Polymer Science, 2009. **34**(11): p. 1161-1210.
123. Konagaya, S., et al., *New chlorine-resistant polyamide reverse osmosis membrane with hollow fiber configuration.* Journal of Applied Polymer Science, 2001. **79**(3): p. 517-527.
124. Murphy, P.E., *Chapter 5 - Governance*, in *The Business of Resort Management*. 2008, Butterworth-Heinemann: Oxford. p. 113-138.
125. Taniguchi, M., J.E. Kilduff, and G. Belfort, *Low fouling synthetic membranes by UV-assisted graft polymerization: monomer selection to mitigate fouling by natural organic matter.* Journal of Membrane Science, 2003. **222**(1): p. 59-70.
126. Akbari, A., et al., *Treatment of textile dye effluents using a new photografted nanofiltration membrane.* Desalination, 2002. **149**(1): p. 101-107.
127. Hegazy, E.-S.A., A.M. Dessouki, and H.A. El-Boohy, *Radiation-induced graft polymerization of acrylamide I. Preparation conditions and gel determination for polyethylene-grafted films.* Journal of Polymer Science Part A: Polymer Chemistry, 1986. **24**(8): p. 1933-1942.
128. Dessouki, A.M., *Post radiation grafting of vinyl acetate onto low-density polyethylene film preparation and properties of membrane.* 1987. **29**(5): p. 359-364.
129. Lazzari, M. and M.A. Lpez-Quintela, *Block Copolymers as a Tool for Nanomaterial Fabrication.* Advanced Materials, 2003. **15**(19): p. 1583-1594.

130. Adam J. Meuler, M.A.H., Frank S. Bates, , *Ordered Network Mesostructures in Block Polymer Materials.* Macromolecules, 2009. **42** (19): p. 7221–7250.
131. Yang SY, et al., *Nanoporous Membranes with Ultrahigh Selectivity and Flux for the Filtration of Viruses.* Advanced Materials, 2006. **18**(6): p. 709-712.
132. Li, Y. and T. Ito, *Size-exclusion properties of nanoporous films derived from polystyrene-poly(methylmethacrylate) diblock copolymers assessed using direct electrochemistry of ferritin.* Analytical chemistry, 2009. **81**(2): p. 851-855.
133. Yang, S.Y., et al., *Virus filtration membranes prepared from nanoporous block copolymers with good dimensional stability under high pressures and excellent solvent resistance.* Advanced Functional Materials 2008. **18**(9): p. 1371-1377.
134. Zalusky, A.S., et al., *Ordered nanoporous polymers from polystyrene-polylactide block copolymers.* Journal of the American Chemical Society, 2002. **124**(43): p. 12761-12773.
135. Sidorenko, A., et al., *Ordered reactive nanomembranes/nanotemplates from thin films of block copolymer supramolecular assembly.* Journal of the American Chemical Society, 2003. **125**(40): p. 12211-12216.
136. Strathmann, H., ed. *"Synthetic Membranes and Their Preparation" in Handbook of Industrial Membrane Technology*. 1990, Noyes Publications: Park Ridge, NJ 1-60.
137. Cadotte, J.E., et al., *Interfacial Synthesis in the Preparation of Reverse Osmosis Membranes.* Journal of Macromolecular Science: Part A - Chemistry, 1981. **15**(5): p. 727-755.
138. Morgan, G.R., *Population dynamics and management of the western rock lobster fishery.* Marine Policy, 1980. **4**(1): p. 52-60.
139. Tavolaro, A. and E. Drioli, *Zeolite Membranes.* Advanced Materials, 1999. **11**(12): p. 975-996.
140. Liu, N., et al., *Removal of organics from produced water by reverse osmosis using MFI-type zeolite membranes.* Journal of Membrane Science, 2008. **325**(1): p. 357-361.
141. Lia, L., et al., *Reverse osmosis of ionic aqueous solutions on aMFI zeolite membrane.* Desalination, 2004. **170**(3): p. 309-316.
142. Thomson, K.T., *Handbook of Zeolite Science and Technology Edited by Scott M. Auerbach.* Journal of the American Chemical Society, 2004. **126**(28): p. 8858-8859.
143. Lin, J. and S. Murad, *A computer simulation study of the separation of aqueous solutions using thin zeolite membranes.* Molecular Physics, 2001. **99**(14): p. 1175-1181.
144. Li, L., et al., *Desalination by reverse osmosis using MFI zeolite membranes.* Journal of Membrane Science, 2004. **243**(1): p. 401-404.
145. Li, L., J. Dong, and T.M. Nenoff, *Transport of water and alkali metal ions through MFI zeolite membranes during reverse osmosis.* Separation and Purification Technology, 2007. **53**(1): p. 42-48.
146. Hasegawa, Y., et al., *Influence of acid on the permeation properties of NaA-type zeolite membranes.* Journal of Membrane Science. **349**(1): p. 189-194.
147. Gin, D.L., et al., *Polymerized lyotropic liquid crystal assemblies for materials applications.* Accounts of chemical research, 2001. **34**(12): p. 973-980.
148. Gin, D.L., et al., *Recent Advances in the Design of Polymerizable Lyotropic Liquid-Crystal Assemblies for Heterogeneous Catalysis and Selective Separations.* Advanced Functional Materials, 2006. **16**(7): p. 865-878.
149. O'Brien, D.F., et al., *Polymerization of Preformed Self-Organized Assemblies.* Accounts of chemical research, 1998. **31**(12): p. 861-868.
150. Mueller, A. and D.F. O'Brien, *Supramolecular materials via polymerization of mesophases of hydrated amphiphiles.* Chemical Reviews, 2002. **102**(3): p. 727-758.

151. Tiddy, G.J.T., *Surfactant-water liquid crystal phases.* Physics Reports, 1980. **57**(1): p. 1-46.
152. Gin, D.L., et al., *Polymerized lyotropic liquid crystal assemblies for membrane applications.* Macromolecular Rapid Communications 2008. **29**(5): p. 367-389.
153. Iijima, S., *Helical Microtubules of Graphitic Carbon.* Nature, 1991. **354**(6348): p. 56-58.
154. Baughman, R.H., A.A. Zakhidov, and W.A. de Heer, *Carbon Nanotubes: The Route toward Applications.* Science, 2002. **297**(5582): p. 787-792.
155. Noy, A., et al., *Nanofluidics in carbon nanotubes.* Nano Today, 2007. **2**(6): p. 22-29.
156. Selbmann, D., et al., *A parametric study of the synthesis and purification of single-walled carbon nanotubes using the high-pressure carbon monoxide process.* Applied Physics A, 2008. **90**(4): p. 637-643.
157. Terranova, M.L., V. Sessa, and M. Rossi, *The World of Carbon Nanotubes: An Overview of CVD Growth Methodologies.* Chemical Vapor Deposition, 2006. **12**(6): p. 315-325.
158. Pichler, T., *Carbon ahead.* Nature Materials, 2007. **6**(5): p. 332-333.
159. Hamada, N., S. Sawada, and A. Oshiyama, *New One-Dimensional Conductors - Graphitic Microtubles* Physical Review Letters, 1992. **68**(10): p. 1579-1581.
160. Moniruzzaman, M. and K.I. Winey, *Polymer Nanocomposites Containing Carbon Nanotubes.* Macromolecules, 2006. **39**(16): p. 5194-5205.
161. Franklin, N.R., et al., *Integration of suspended carbon nanotube arrays into electronic devices and electromechanical systems.* Applied Physics Letters, 2002. **81**(5): p. 913.
162. Kociak, M., et al., *Superconductivity in ropes of single-walled carbon nanotubes.* Physical Review Letters, 2001. **86**(11): p. 2416-2419.
163. Tang, Z.K., et al., *Superconductivity in 4 Angstrom Single-Walled Carbon Nanotubes.* Science, 2001. **292**(5526): p. 2462-2465.
164. Berber, S., Y.-K. Kwon, and D. Tomanek, *Unusually High Thermal Conductivity of Carbon Nanotubes.* Physical Review Letters, 2000. **84**(20): p. 4613-4616.
165. Peigney, A., et al., *Specific surface area of carbon nanotubes and bundles of carbon nanotubes.* Carbon, 2001. **39**(4): p. 507-514.
166. Frackowiak, E., et al., *Enhanced capacitance of carbon nanotubes through chemical activation.* Chemical Physics Letters, 2002. **361**(1): p. 35-41.
167. Bhushan, B., *Springer handbook of nanotechnology*. 2004, New York: Springer-Verlag.
168. Popov, V.N., *Carbon nanotubes: properties and application.* Materials Science & Engineering R, 2004. **43**(3): p. 61-102.
169. Kong, J., et al., *Nanotube Molecular Wires as Chemical Sensors.* Science, 2000. **287**(5453): p. 622-625.
170. Philip, G.C., et al., *Extreme Oxygen Sensitivity of Electronic Properties of Carbon Nanotubes.* Science, 2000. **287**(5459): p. 1801-1804.
171. Paul, C., *A recipe for strength*, in *Nature*. 1999: London. p. 210.
172. Planeix, J.M., et al., *Application of Carbon Nanotubes as Supports in Heterogeneous Catalysis.* Journal of the American Chemical Society, 1994. **116**(17): p. 7935-7936.
173. Hinds, B.J., et al., *Aligned multiwalled carbon nanotube membranes.* Science (New York, N.Y.), 2004. **303**(5654): p. 62-65.
174. Holt, J.K., et al., *Fast Mass Transport through Sub-2-Nanometer Carbon Nanotubes.* Science, 2006. **312**(5776): p. 1034-1037.
175. Qin, L.C., et al., *The smallest carbon nanotube.* Nature, 2000. **408**(6808): p. 50.
176. Wang, N., G.D. Li, and J.S. Chen, *Materials science Single-walled 4 Å carbon nanotube arrays.* Nature, 2000. **408**(6808): p. 50-51.

177. Ackerman, D.M., et al., *Diffusivities of Ar and Ne in Carbon Nanotubes.* Molecular Simulation, 2003. **29**(10-11): p. 677-684.
178. Skoulidas, A.I., et al., *Rapid transport of gases in carbon nanotubes.* Physical Review Letters, 2002. **89**(18): p. 185901.
179. Sahoo, N.G., et al., *Polymer nanocomposites based on functionalized carbon nanotubes.* Progress in Polymer Science, 2010. **35**(7): p. 837-867.
180. Boge Jenny, et al., *The effect of preparation conditions and biopolymer dispersants on the properties of SWNT buckypapers.* J. Mater. Chem, 2009. **19,** : p. 9131–9140
181. Sweetman, L.J., et al., *Synthesis, properties and water permeability of SWNT buckypapers.* J. Mater. Chem., 2012. **22**(27): p. 138-1381.
182. Aldalbahi, A. and M. in het Panhuis, *Electrical and mechanical characteristics of buckypapers and evaporative cast films prepared using single and multi-walled carbon nanotubes and the biopolymer carrageenan.* Carbon, 2012. **50**(3): p. 1197-1208.
183. Islam, M.S., *Perspectives of the coastal and marine fisheries of the Bay of Bengal, Bangladesh.* Ocean & Coastal Management, 2003. **46**(8): p. 763-796.
184. Bandyopadhyaya, R., et al., *Stabilization of Individual Carbon Nanotubes in Aqueous Solutions.* Nano letters, 2002. **2**(1): p. 25-28.
185. Yang, H., et al., *Diameter-selective dispersion of single-walled carbon nanotubes using a water-soluble, biocompatible polymer.* Chemical communications (Cambridge, England), 2006(13): p. 1425.
186. Peng, F.B., et al., *Novel nanocomposite pervaporation membranes composed of poly(vinyl alcohol) and chitosan-wrapped carbon nanotube.* Journal of Membrane Science, 2007. **300**(1-2): p. 13-19.
187. Kim, S.W., et al., *Surface modifications for the effective dispersion of carbon nanotubes in solvents and polymers.* Carbon, 2012. **50**(1): p. 3-33.
188. Gao C , V.C., Jin YZ, Li W , and . Armes SP,, *Multihydroxy Polymer-Functionalized Carbon Nanotubes: Synthesis, Derivatization, and Metal Loading.* Macromolecules, 2005. **38** p. 8634-8648.
189. Liu, J., et al., *Fullerene Pipes.* Science, 1998. **280**(5367): p. 1253-1256.
190. Akos, K., et al., *Controlling the pore diameter distribution of multi-wall carbon nanotube buckypapers.* Carbon, 2007. **45**(8): p. 1696-1698.
191. Sears, K., et al., *Recent Developments in Carbon Nanotube Membranes for Water Purification and Gas Separation.* Materials 2010. **3**(1): p. 127-149.
192. Brady-Estévez, A.S., S. Kang, and M. Elimelech, *A single-walled-carbon-nanotube filter for removal of viral and bacterial pathogens.* Small 2008. **4**(4): p. 481-484.
193. Gou, J., *Single-walled nanotube bucky paper and nanocomposite.* Polymer International, 2006. **55**(11): p. 1283-1288.
194. Frizzell, C.J., et al., *Reinforcement of macroscopic carbon nanotube structures by polymer intercalation: The role of polymer molecular weight and chain conformation.* Physical Review B 2005. **72**(24): p. 245420.
195. Cooper, S.M., et al., *Gas permeability of a buckypaper membrane.* Nano Letters 2003. **3**(2): p. 189-192.
196. Smajda, R., et al., *Structure and gas permeability of multi-wall carbon nanotube buckypapers.* Carbon, 2007. **45**(6): p. 1176-1184.
197. Viswanathan, G., D.B. Kane, and P.J. Lipowicz, *High efficiency fine particulate filtration using carbon nanotube coatings.* Advanced Materials 2004. **16**(22): p. 2045-2045.
198. Cinke, M., et al., *Pore structure of raw and purified HiPco single-walled carbon nanotubes.* Chemical Physics Letters, 2002. **365**(1): p. 69-74.

199. Rozenberg, B.A. and R. Tenne, *Polymer-assisted fabrication of nanoparticles and nanocomposites.* Progress in Polymer Science, 2008. **33**(1): p. 40-112.
200. Dumée L , F., et al., *Characterization and evaluation of carbon nanotube Bucky-Paper membranes for direct contact membrane distillation.* Journal of Membrane Science, 2010. **351**(1): p. 36-43.
201. Coleman, J.N., et al., *Improving the mechanical properties of single-walled carbon nanotube sheets by intercalation of polymeric adhesives.* Applied Physics Letters, 2003. **82**(11): p. 1682.
202. Ren, Z.F., et al., *Synthesis of Large Arrays of Well-Aligned Carbon Nanotubes on Glass.* Science, 1998. **282**(5391): p. 1105-1107.
203. Huang, Z.P., et al., *Growth of highly oriented carbon nanotubes by plasma-enhanced hot filament chemical vapor deposition.* Applied Physics Letters, 1998. **73**(26): p. 3845.
204. Murakami, Y., et al., *Growth of vertically aligned single-walled carbon nanotube films on quartz substrates and their optical anisotropy.* Chemical Physics Letters, 2004. **385**(3): p. 298-303.
205. Ge, L., et al., *Carbon Nanotube-Based Synthetic Gecko Tapes.* Proceedings of the National Academy of Sciences of the United States of America, 2007. **104**(26): p. 10792-10795.
206. Dresselhaus, M.S., G. Dresselhaus, and P. Avouris, *Carbon nanotubes: synthesis, structure, properties, and applications*. Vol. 80. 2001, Berlin: Springer.
207. Srivastava, A., S. Talapatra, and R. Vajtai, *Carbon nanotube filters.* Nature Materials, 2004. **3**(9): p. 610-614.
208. Fornasiero, F., et al., *Ion Exclusion by sub-2-nm Carbon Nanotube Pores.* Proceedings of the National Academy of Sciences of the United States of America, 2008. **105**(45): p. 17250-17255.
209. Hummer, G., J.C. Rasaiah, and J.P. Noworyta, *Water conduction through the hydrophobic channel of a carbon nanotube.* Nature, 2001. **414**(6860): p. 188-190.
210. Majumder, M., et al., *Nanoscale hydrodynamics: enhanced flow in carbon nanotubes.* Nature, 2005. **438**(7064): p. 44-44.
211. Kalra, A., S. Garde, and G. Hummer, *Osmotic water transport through carbon nanotube membranes.* Proceedings of the National Academy of Sciences of the United States of America, 2003. **100**(18): p. 10175-10180.
212. Whitby, M. and N. Quirke, *Fluid flow in carbon nanotubes and nanopipes.* Nature Nanotechnology, 2007. **2**(2): p. 87-94.
213. Gordillo, M.C. and J. MarÌ, *Hydrogen bond structure of liquid water confined in nanotubes.* Chemical Physics Letters, 2000. **329**(5): p. 341-345.
214. Walther, J.H., et al., *Carbon Nanotubes in Water: Structural Characteristics and Energetics.* The Journal of Physical Chemistry B, 2001. **105**(41): p. 9980-9987.
215. Mashl, R.J., et al., *Anomalously Immobilized Water: A New Water Phase Induced by Confinement in Nanotubes.* Nano letters, 2003. **3**(5): p. 589-592.
216. Zhu, F. and K. Schulten, *Water and Proton Conduction through Carbon Nanotubes as Models for Biological Channels.* Biophysical Journal, 2003. **85**(1): p. 236-244.
217. Kolesnikov, A.I., et al., *Anomalously soft dynamics of water in a nanotube: a revelation of nanoscale confinement.* Physical Review Letters, 2004. **93**(3): p. 035503.
218. Zhikang Xu, X.H., Lingshu Wan, *Surface Engineering of Polymer Membranes*. 2009 New York: Berlin Heidelberg.
219. Pauliukaite, R., et al., *Comparative study of different cross-linking agents for the immobilization of functionalized carbon nanotubes within a chitosan film supported on a graphite-epoxy composite electrode.* Analytical chemistry, 2009. **81**(13): p. 5364.

220. Venkatesan, J. and S.-K. Kim, *Chitosan composites for bone tissue engineering--an overview.* Marine drugs, 2010. **8**(8): p. 2252-2266.
221. Rinaudo, M., G. Pavlov, and J. Desbrières, *Influence of acetic acid concentration on the solubilization of chitosan.* Polymer, 1999. **40**(25): p. 7029-7032.
222. Zeng, X. and E. Ruckenstein, *Cross-linked macroporous chitosan anion-exchange membranes for protein separations.* Journal of Membrane Science, 1998. **148**(2): p. 195-205.
223. Carson, T.R., *The Crab Nebula: By Simon Mitton. .* Endeavour, 1980. **4**(3): p. 125-126.
224. Wang, S.-F., et al., *Preparation and mechanical properties of chitosan/carbon nanotubes composites.* Biomacromolecules, 2005. **6**(6): p. 3067-3072.
225. Berger, J., et al., *Structure and interactions in chitosan hydrogels formed by complexation or aggregation for biomedical applications.* European journal of pharmaceutics and biopharmaceutics 2004. **57**(1): p. 35-52.
226. Uragami, T., et al., *Transport of nucleic acid bases against their concentration gradients through quaternized chitosan membrane.* Carbohydrate Polymers, 1993. **21**(4): p. 289-293.
227. Yao, K.D., et al., *Investigation of pH-sensitive drug delivery system of chitosan/gelatin hybrid polymer network.* Polymer International, 1995. **38**(1): p. 77-82.
228. Dumitriu, S. and E. Chornet, *Inclusion and release of proteins from polysaccharide-based polyion complexes.* Advanced Drug Delivery Reviews, 1998. **31**(3): p. 223-246.
229. Moridiz V, Mottaghital A B, and Haghi AK, *A detailed review of recent progress in carbon nanotube-chitosan nanocomposites* Cellulose Chem. Technol, 2011. **45**(9-10): p. 549-563.
230. Du, D., et al., *Amperometric detection of triazophos pesticide using acetylcholinesterase biosensor based on multiwall carbon nanotube-chitosan matrix.* Sensors & Actuators: B. Chemical, 2007. **127**(2): p. 531-535.
231. Ferrisa CJ and Marc in het Panhuis, *Gel-carbon nanotube composites: the effect of carbon nanotubes on gelation and conductivity behaviour.* Soft Matter, 2009. **5** p. 1466-1473.
232. Zeng, X. and E. Ruckenstein, *Control of Pore Sizes in Macroporous Chitosan and Chitin Membranes.* Industrial & Engineering Chemistry Research, 1996. **35**(11): p. 4169-4175.
233. Callister, W., *Materials science and engineering: an introduction* 2003: Chichester: Wiley.
234. Brunauer, S., P.H. Emmett, and E. Teller, *Adsorption of Gases in Multimolecular Layers.* Journal of the American Chemical Society, 1938. **60**(2): p. 309-319.
235. Barrett E P, Joyner L G, and Halenda P P, *The determination of pore volume and area distribution in porous substancea.* Journal of the American Chemical Society, 1951. **73**(1): p. 373-380.
236. Horvath G and Kawazoe K, *Method for the calculation of effective pore size distribution in molecular sieve carbon.* Journal of Chemical Engineering of Japan, 1983. **16**(6): p. 470–475.
237. Xie, M., et al., *Comparison of the removal of hydrophobic trace organic contaminants by forward osmosis and reverse osmosis.* Water research, 2012. **46**(8): p. 2683-2692.
238. Sutzkover, I., D. Hasson, and R. Semiat, *Simple technique for measuring the concentration polarization level in a reverse osmosis system.* Desalination, 2000. **131**(1): p. 117-127.

239. Lu, K.L., et al., *Mechanical damage of carbon nanotubes by ultrasound.* Carbon, 1996. **34**(6): p. 814-816.
240. Hilding, J., et al., *Dispersion of Carbon Nanotubes in Liquids.* Journal of Dispersion Science and Technology, 2003. **24**(1): p. 1-41.
241. Yu, J., et al., *Controlling the dispersion of multi-wall carbon nanotubes in aqueous surfactant solution.* Carbon, 2007. **45**(3): p. 618-623.
242. Sweetman, L.J., *Synthesis, characterisation and applications of carbon nanotube membranes containing macrocycles and antibiotics*. 2012, Dissertation/Thesis,School of Chemistry, Wollongong University.
243. Pasquali, M., et al., *Kinetics of nanotube and microfiber scission under sonication.* Journal of Physical Chemistry C, 2009. **113**(48): p. 20599-20605.
244. Park, J.G., et al., *Effects of surfactants and alignment on the physical properties of single-walled carbon nanotube buckypaper.* Journal of Applied Physics, 2009. **106**(10): p. 104310.
245. Vecitis, C.D., et al., *Electrochemical multiwalled carbon nanotube filter for viral and bacterial removal and inactivation.* Environmental science & technology. **45**(8): p. 3672.
246. Songmee, N., P. Singjai, and M. in het Panhuis, *Gel-carbon nanotube materials: the relationship between nanotube network connectivity and conductivity.* Nanoscale, 2010. **2**(9): p. 174-1745.
247. Hausman, R., et al., *Functionalization of polybenzimidizole membranes to impart negative charge and hydrophilicity.* Journal of Membrane Science, 2010. **363**(1): p. 195-203.
248. Dumée, L.F., et al., *Characterization and evaluation of carbon nanotube Bucky-Paper membranes for direct contact membrane distillation.* Journal of Membrane Science, 2010. **351**(1): p. 36-43.
249. Musso, S., et al., *Physical and mechanical properties of thick self-standing layers of multiwall carbon nanotubes.* Diamond & Related Materials, 2007. **16**(4): p. 1174-1178.
250. Wang, B., et al., *Processing and property investigation of single-walled carbon nanotube (SWNT) buckypaper/epoxy resin matrix nanocomposites.* Composites Part A, 2004. **35**(10): p. 1225-1232.
251. Fan, Z., et al., *Performance improvement of polysulfone ultrafiltration membrane by blending with polyaniline nanofibers.* Journal of Membrane Science, 2008. **320**(1): p. 363-371.
252. Tang, C., et al., *Water transport behavior of chitosan porous membranes containing multi-walled carbon nanotubes (MWNTs).* Journal of Membrane Science, 2009. **337**(1): p. 240-247.
253. Coleman, J.N., et al., *Improving the mechanical properties of single-walled carbon nanotube sheets by intercalation of polymeric adhesives.* Applied Physics Letters, 2003. **82**(11): p. 1682-1684.
254. Spinks, G.M., et al., *Mechanical properties of chitosan/CNT microfibers obtained with improved dispersion.* Sensors & Actuators: B. Chemical, 2006. **115**(2): p. 678-684.
255. Frizzell, C.J., et al., *Reinforcement of macroscopic carbon nanotube structures by polymer intercalation: The role of polymer molecular weight and chain conformation.* Physical Review B, 2005. **72**(24).
256. Rashid, M.H.O., et al., *Synthesis, properties, water and solute permeability of MWNT buckypapers.* JOURNAL OF MEMBRANE SCIENCE, 2014. **456**: p. 175-184.
257. Sweetman L J, et al., *Bacterial Filtration Using Carbon Nanotube/Antibiotic Buckypaper Membranes.* Journal of Nanomaterials, 2013. **1**: p. 1-11.

258. Smajda, R., et al., *Structure and gas permeability of multi-wall carbon nanotube buckypapers.* Carbon, 2007. **45**(6): p. 1176-1184.
259. Muramatsu, H., et al., *Pore structure and oxidation stability of double-walled carbon nanotube-derived bucky paper.* Chemical Physics Letters, 2005. **414**(4): p. 444-448.
260. Wang, S., et al., *Nanoscale infiltration behaviour and through-thickness permeability of carbon nanotube buckypapers.* Nanotechnology 2013. **24**(1): p. 015704.
261. Qiu, S., et al., *Preparation and Pervaporation Property of Chitosan Membrane with Functionalized Multiwalled Carbon Nanotubes.* Industrial & Engineering Chemistry Research 2010. **49**(22): p. 11667-11675.
262. Yang, H.Y., et al., *Carbon nanotube membranes with ultrahigh specific adsorption capacity for water desalination and purification.* Nature communications, 2013. **4**(Journal Article): p. 2220.
263. Hu, L., D.S. Hecht, and G. Grüner, *Carbon nanotube thin films: fabrication, properties, and applications.* Chemical reviews, 2010. **110**(10): p. 5790-5844.
264. Madaeni, S.S. and S. Molaeipour, *Investigation of filtration capability of conductive composite membrane in separation of protein from water.* Ionics. **16**(1): p. 75-80.
265. Krupenkin, T.N., et al., *From rolling ball to complete wetting: the dynamic tuning of liquids on nanostructured surfaces.* Langmuir : the ACS journal of surfaces and colloids, 2004. **20**(10): p. 3824-3827.
266. Broza, G., et al., *Nanocomposites of poly(vinyl chloride) with carbon nanotubes (CNT).* Composites Science and Technology, 2007. **67**(5): p. 890-894.
267. Zielecka, M., *Methods of contact angle measurement as a tool for characterization of wettability of polymers.* Polimery 2004. **49**(5): p. 327-332.
268. Nepal, A., et al., *One-step synthesis of graphene via catalyst-free gas-phase hydrocarbon detonation.* Nanotechnology. , 2013. **24**: p. 245602.
269. Kim, S., et al., *Polysulfone and functionalized carbon nanotube mixed matrix membranes for gas separation: Theory and experiment.* Journal of Membrane Science, 2007. **294**(1): p. 147-158.
270. Padaki, M., et al., *New polypropylene supported chitosan NF-membrane for desalination application.* Desalination, 2011. **280**(1): p. 419-423.
271. Tongwen, X. and Y. Weihua, *A novel positively charged composite membranes for nanofiltration prepared from poly (2, 6-dimethyl-1, 4-phenylene oxide) by in situ amines crosslinking.* Journal of membrane science, 2003. **215**(1): p. 25-32.
272. Hagmeyer, G. and R. Gimbel, *Modelling the rejection of nanofiltration membranes using zeta potential measurements.* Separation and purification technology, 1999. **15**(1): p. 19-30.
273. Miao, J., G.-h. Chen, and C.-j. Gao, *A novel kind of amphoteric composite nanofiltration membrane prepared from sulfated chitosan (SCS).* Desalination, 2005. **181**(1): p. 173-183.
274. Wang, X.-L., W.-N. Wang, and D.-X. Wang, *Experimental investigation on separation performance of nanofiltration membranes for inorganic electrolyte solutions.* Desalination, 2002. **145**(1): p. 115-122.
275. Sun, H., et al., *A novel composite nanofiltration (NF) membrane prepared from glycolchitin/poly (acrylonitrile)(PAN) by epichlorohydrin cross-linking.* Journal of membrane science, 2007. **297**(1): p. 51-58.
276. Fievet, P., et al., *Electrolyte transport through amphoteric nanofiltration membranes.* Chemical engineering science, 2002. **57**(15): p. 2921-2931.
277. Schaep, J., et al., *Influence of ion size and charge in nanofiltration.* Separation and Purification Technology, 1998. **14**(1): p. 155-162.

278. Xu, Y. and R.E. Lebrun, *Investigation of the solute separation by charged nanofiltration membrane: effect of pH, ionic strength and solute type.* Journal of membrane science, 1999. **158**(1): p. 93-104.
279. Park, S.-B., et al., *A novel pH-sensitive membrane from chitosan — TEOS IPN; preparation and its drug permeation characteristics.* Biomaterials, 2001. **22**(4): p. 323-330.
280. Clasen, C., T. Wilhelms, and W.-M. Kulicke, *Formation and characterization of chitosan membranes.* Biomacromolecules, 2006. **7**(11): p. 3210-3222.
281. Schäfer, A.I., et al., *Natural organic matter removal by nanofiltration: effects of solution chemistry on retention of low molar mass acids versus bulk organic matter.* Journal of Membrane Science, 2004. **242**(1): p. 73-85.
282. Tu, K.L., A.R. Chivas, and L.D. Nghiem, *Effects of membrane fouling and scaling on boron rejection by nanofiltration and reverse osmosis membranes.* Desalination, 2011. **279**(1): p. 269-277.
283. Zhan, Y., et al., *Carbon nanotube–chitosan composite electrodes for electrochemical removal of Cu(II) ions.* Journal of Alloys and Compounds, 2011. **509**(18): p. 5667-5671.
284. Childress, A.E. and M. Elimelech, *Effect of solution chemistry on the surface charge of polymeric reverse osmosis and nanofiltration membranes.* Journal of Membrane Science, 1996. **119**(2): p. 253-268.
285. Timmer, J.M.K., *Properties of nanofiltration membranes; model development and industrial application*. PhD Dissertation 2001, Technische Universiteit Eindhoven.
286. McCloskey B D, Ju H, and Freeman B D, *Composite Membranes Based on a Selective Chitosan-Poly(ethylene glycol) Hybrid Layer: Synthesis, Characterization, and Performance in Oil-Water Purification,.* Ind. Eng. Chem. Res. , 2010. **49** p. 366–373.
287. Dusek, K., *Phase separation during the formation of three-dimensional polymers.* 1967. **16**(3): p. 1289-1299.
288. Whitten, P.G., et al., *Free standing carbon nanotube composite bio-electrodes.* Journal of Biomedical Materials Research. Part B, Applied Biomaterials, 2007. **82**(1): p. 37-43.
289. Ulbricht, M., *Advanced functional polymer membranes.* Polymer, 2006. **47**(7): p. 2217-2262.
290. Wijmans, J.G. and R.W. Baker, *The solution-diffusion model: a review.* Journal of Membrane Science, 1995. **107**(1–2): p. 1-21.
291. Goycoolea, F.M., et al., *PH- and temperature-sensitive chitosan hydrogels: Swelling and MRI studies.* Macromolecular Chemistry and Physics, 2011. **212**(9): p. 887-895.
292. Ganji, F. and M.J. Abdekhodaie, *Chitosan-g-PLGA copolymer as a thermosensitive membrane.* Carbohydrate Polymers. **80**(3): p. 740-746.
293. Qu, X., et al., *Novel pH-sensitive chitosan hydrogels: swelling behavior and states of water.* Polymer, 2000. **41**(12): p. 4589-4598.
294. Tanabe, T., et al., *Preparation and characterization of keratin–chitosan composite film.* Biomaterials, 2002. **23**(3): p. 817-825.
295. Krajewska, B. and A. Olech, *Pore structure of gel chitosan membranes. I. Solute diffusion measurements.* Polymer Gels and Networks, 1996. **4**(1): p. 33-43.
296. Musale, D.A. and A. Kumar, *Effects of surface crosslinking on sieving characteristics of chitosan/poly(acrylonitrile) composite nanofiltration membranes.* Separation and Purification Technology, 2000. **21**(1): p. 27-37.
297. Spiegler, K. and O. Kedem, *Thermodynamics of hyperfiltration (reverse osmosis): criteria for efficient membranes.* Desalination, 1966. **1**(4): p. 311-326.

298. Afonso, M.D. and M.N. de Pinho, *Transport of MgSO< sub> 4</sub>, MgCl< sub> 2</sub>, and Na< sub> 2</sub> SO< sub> 4</sub> across an amphoteric nanofiltration membrane.* Journal of Membrane Science, 2000. **179**(1): p. 137-154.
299. Rios, G., et al., *Investigation of ion separation by microporous nanofiltration membranes.* AIChE journal, 1996. **42**(9): p. 2521-2528.
300. Pontalier, P.-Y., A. Ismail, and M. Ghoul, *Mechanisms for the selective rejection of solutes in nanofiltration membranes.* Separation and purification technology, 1997. **12**(2): p. 175-181.
301. Chian, E.S.K., W.N. Bruce, and H.H.P. Fang, *Removal of pesticides by reverse osmosis.* Environmental science & technology, 1975. **9**(1): p. 52-59.
302. Kiso, Y., et al., *Effects of hydrophobicity and molecular size on rejection of aromatic pesticides with nanofiltration membranes.* Journal of Membrane Science, 2001. **192**(1): p. 1-10.
303. Childress, A.E. and M. Elimelech, *Relating nanofiltration membrane performance to membrane charge (electrokinetic) characteristics.* Environmental science & technology, 2000. **34**(17): p. 3710-3716.
304. Mulder, M., *Basic principles of membrane technology*. 2003, Boston: Kluwer Academic.
305. Amuda, O.S., A.A. Giwa, and I.A. Bello, *Removal of heavy metal from industrial wastewater using modified activated coconut shell carbon.* Biochemical Engineering Journal, 2007. **36**(2): p. 174-181.
306. Nomanbhay, S.M. and K. Palanisamy, *Removal of heavy metal from industrial wastewater using chitosan coated oil palm shell charcoal.* Electronic Journal of Biotechnology, 2005. **8**(1): p. 43-53.
307. Banerjee, S., T. Hemraj-Benny, and S.S. Wong, *Covalent surface chemistry of single-walled carbon nanotubes.* Advanced Materials 2005. **17**(1): p. 17-29.
308. Balasubramanian, K. and M. Burghard, *Chemically functionalized carbon nanotubes.* Small (Weinheim an der Bergstrasse, Germany), 2005. **1**(2): p. 180-192.
309. Choi, J.H., J. Jegal, and W.N. Kim, *Fabrication and characterization of multi-walled carbon nanotubes/polymer blend membranes.* Journal of Membrane Science, 2006. **284**(1-2): p. 406-415.
310. Baughman, R.H., et al., *Carbon Nanotube Actuators.* Science, 1999. **284**(5418): p. 1340-1344.
311. Sing, K.W., *Physisorption of nitrogen by porous materials.* Journal of Porous Materials, 1995. **2**(1): p. 5-8.
312. Salam, M.A., M.S.I. Makki, and M.Y.A. Abdelaal, *Preparation and characterization of multi-walled carbon nanotubes/chitosan nanocomposite and its application for the removal of heavy metals from aqueous solution.* Journal of Alloys and Compounds, 2011. **509**(5): p. 2582-2587.
313. Lee, S., J. Cho, and M. Elimelech, *Influence of colloidal fouling and feed water recovery on salt rejection of RO and NF membranes.* Desalination, 2004. **160**(1): p. 1-12.
314. Seidel, A. and M. Elimelech, *Coupling between chemical and physical interactions in natural organic matter (NOM) fouling of nanofiltration membranes: implications for fouling control.* Journal of membrane science, 2002. **203**(1): p. 245-255.
315. Lee, S., et al., *Determination of mass transport characteristics for natural organic matter(NOM) in ultrafiltration(UF) and nanofiltration(NF) membranes.* WATER SCIENCE AND TECHNOLOGY-WATER SUPPLY-, 2002. **2**(2): p. 151-160.
316. Jackson, D.S., *Chitosan-glycerol-water gel*. 1987, Google Patents.

317. Hudson, S. and C. Smith, *Polysaccharides: chitin and chitosan: chemistry and technology of their use as structural materials*, in *Biopolymers from renewable resources*. 1998, Springer. p. 96-118.
318. Li, Q., et al., *Applications and properties of chitosan.* Journal of Bioactive and Compatible Polymers, 1992. **7**(4): p. 370-397.
319. Liang, Z.P., et al., *Preparation and properties of urease immobilized onto glutaraldehyde cross-linked chitosan beads.* Chin Chem Lett, 2005. **16**: p. 135-138.
320. Ma, X. and Z. Yao, *[X-ray microanalysis of the activity of immobilized urease on chitosan membrane]*. Guang pu xue yu guang pu fen xi= Guang pu, 2005. **25**(3): p. 456-459.
321. Mulder, C., et al., *A Belowground Perspective on Dutch Agroecosystems: How Soil Organisms Interact to Support Ecosystem Services*, in *Advances in Ecological Research*. Academic Press. p. 277-357.
322. Mallevialle, J., P.E. Odendaal, and M.R. Wiesner, *Water treatment membrane processes*. 1996: American Water Works Association.
323. Schäfer, A.I., L.D. Nghiem, and T.D. Waite, *Removal of the natural hormone estrone from aqueous solutions using nanofiltration and reverse osmosis.* Environmental science & technology, 2003. **37**(1): p. 182-188.
324. Kargol, A., *Modified Kedem–Katchalsky equations and their applications.* Journal of Membrane Science, 2000. **174**(1): p. 43-53.
325. Koter, S., *Determination of the parameters of the Spiegler–Kedem–Katchalsky model for nanofiltration of single electrolyte solutions.* Desalination, 2006. **198**(1): p. 335-345.
326. Ahmad, A., M. Chong, and S. Bhatia, *Mathematical modeling and simulation of the multiple solutes system for nanofiltration process.* Journal of membrane science, 2005. **253**(1): p. 103-115.
327. Gilron, J., N. Daltrophe, and O. Kedem, *Trans-membrane pressure in nanofiltration.* Journal of membrane science, 2006. **286**(1): p. 69-76.
328. Wang, X.-L., A.-L. Ying, and W.-N. Wang, *Nanofiltration of L-phenylalanine and L-aspartic acid aqueous solutions.* Journal of membrane science, 2002. **196**(1): p. 59-67.
329. Bhattacharjee, C., et al., *Parameter estimation and performance study during ultrafiltration of Kraft black liquor.* Separation and purification technology, 2006. **51**(3): p. 247-257.
330. Pontie, M., et al., *Studies of halide ions mass transfer in nanofiltration—application to selective defluorination of brackish drinking water.* Desalination, 2003. **157**(1): p. 127-134.
331. Elimelech, M., W.H. Chen, and J.J. Waypa, *Measuring the zeta (electrokinetic) potential of reverse osmosis membranes by a streaming potential analyzer.* Desalination, 1994. **95**(3): p. 269-286.
332. Kim, J.H., et al., *Properties and swelling characteristics of cross-linked poly (vinyl alcohol)/chitosan blend membrane.* Journal of applied polymer science, 1992. **45**(10): p. 1711-1717.
333. Singh, D.K. and A.R. Ray, *Controlled release of glucose through modified chitosan membranes.* Journal of Membrane Science, 1999. **155**(1): p. 107-112.